Experimental and numerical investigations on compressive and tensile responses of heterogeneous soils in cold environments

Sohail Akhtar

A Thesis

In the Department

Of

Building, Civil and Environmental Engineering

Presented in Partial Fulfillment of the Requirements

for the Degree of

Doctor of Philosophy (Civil Engineering) at

Concordia University

Montréal, Québec, Canada

May 2025

CONCORDIA UNIVERSITY

SCHOOL OF GRADUATE STUDIES

This is to certify that the thesis prepared

By: Sohail Akhtar

Entitled: Experimental and numerical investigations on compressive and tensile responses of heterogeneous soils in cold environments

and submitted in partial fulfillment of the requirements for the degree of

Doctor of Philosophy (Civil Engineering)

complies with the regulations of the University and meets the accepted standards with respect to originality and quality.

Signed by the final examining committee:

_____ Chair
Dr. Nematollah Shiri

_____ External Examiner
Dr. Greg Siemens

_____ Arm's Length Examiner
Dr. Yong Zeng

_____ Examiner
Dr. Ghazanfarah Hafeez

_____ Examiner
Dr. Adel Hanna

_____ Thesis Supervisor
Dr. Biao Li.

Approved by

_____
Chair of Department or Graduate Program Director

_____
Date of Defence

_____
Dean

Abstract

Experimental and numerical investigations on compressive and tensile responses of heterogeneous soils in cold environments

Sohail Akhtar, Ph.D.

Concordia University, 2025

Climate change is profoundly affecting permafrost regions, posing significant challenges to infrastructure stability. As global temperatures rise, permafrost thaws, leading to ground subsidence and compromising structures such as roads, pipelines, and buildings. Understanding soil behavior under thermo-mechanical forces is crucial for designing resilient engineering solutions. This thesis offers a comprehensive study of the thermo-mechanical behavior of cold-region soils through experimental data and numerical analyses under compression, tension, and triaxial conditions. The research investigates temperature-dependent strength variations, effective measurement techniques for the tensile behavior of frozen soil, and the rheological and residual strength characteristics of lime-treated (L-soil) and untreated natural soil (N-soil) from northern Quebec, Canada, after freeze-thaw cycles. The key contributions of this work include: (I) identifying effective and reliable techniques for quantifying tensile strength; (II) determining the critical number of freeze-thaw cycles to predict residual strength in L-soil and N-soil; (III) analyzing failure modes and stress behavior in L-soil and N-soil under varying confining stresses and thermal conditions; (IV) accurately modeling visco-elastic, visco-plastic, and creep behavior of compressive and tensile strength using finite element methods; and (V) calibrating triaxial testing approaches against experimental data. Finally, this study simulates the damage initiation and crack propagation in uniaxial compressive test and indirect tensile test using damage XFEM model in finite element-based software package (Abaqus). Findings emphasize the importance of

considering time-dependent strength degradation, analyzing the complex behavior of frozen soil due to interactions between frozen and unfrozen water, and quantifying tensile strength with minimal local plastic deformation. The research also highlights the benefits, drawbacks, and challenges of using lime to enhance soil residual strength in cold climates.

Despite significant advancements, the research acknowledges limitations, such as the need for microscopic studies of unfrozen pore water and ice interactions, scanning electron microscopy (SEM) analyses of lime, silt, fine sand, and clay particle interactions, and broader validation efforts for real-world scenarios. Recommendations for future work include micro-level soil sample studies, dynamic and creep loading tests under various temperature and moisture conditions, modifying hyperbolic Drucker-Prager modeling to account for temperature-dependent parameters, conducting long-term studies, and integrating field data to enhance model accuracy and applicability.

Keywords: Frozen soil mechanics, Thermo-mechanical behavior, Freeze-thaw cycles, Double punch tensile strength, Lime-treated soil, Numerical modeling in geomechanics, Extended Finite Element Method (XFEM), Cold region engineering.

Acknowledgments

I would like to express my deepest gratitude to my supervisor, Professor Biao Li, for his unwavering support, invaluable guidance, and insightful advice throughout my PhD journey. His expertise and encouragement have been instrumental in shaping this research, and I feel truly privileged to have had the opportunity to learn from him. His mentorship has not only enriched my academic growth but also instilled in me a deeper appreciation for scientific inquiry.

I am also sincerely grateful to Professor Adel M. Hanna for his invaluable guidance, support, and encouragement throughout this work. His insights and expertise have been truly instrumental.

Additionally, I am profoundly thankful to my mentors, Dr. Farah Hafeez and Dr. Jassim Hassan, for their thoughtful feedback, constructive criticism, and constant support. Their encouragement has consistently motivated me to strive for excellence.

Special thanks to Mr. Mark Elie and Mr. Roberto Avila Perez, whose technical expertise and assistance in developing and modifying machines to meet the specific needs of my experiments have been invaluable. Their support in the laboratory has greatly contributed to the successful execution of this research.

Finally, my sincere appreciation goes to my friends, whose encouragement, companionship, and unwavering support have been invaluable throughout this journey. Their presence has provided joy, and much-needed motivation during this challenging yet fulfilling academic endeavor. This journey would not have been possible without the contributions of all these remarkable individuals, and for that, I am profoundly grateful.

I also would like to acknowledge the fund provided by NSERC Discovery Grant Canada (NO. RGPIN-2017-05169).

Dedication

To my beloved wife, whose unwavering love, support, and sacrifices have been the cornerstone of my success. Her confidence in me has been my greatest source of strength and motivation; she was the light through every late night and the force behind every step of this journey. You own this just as much as I do.

To my parents and siblings: Thank you for your unwavering support, tolerance, and company. This trip is not only possible but also profoundly meaningful because of your presence in my life. Thank you for always being there for me.

List of Publications

Refereed journal papers composing this thesis:

- **Akhtar, S.** and Li, B., 2024. Modeling time-dependent uniaxial compressive behaviors of an artificial frozen sandy clay at different temperatures. Geotechnical and Geological Engineering, 42: 3829-3842.
  https://doi.org/10.1007/s10706-024-02760-1
- Li, B. and **Akhtar, S.**, 2022 Characterizations of tensile yield and failure processes of frozen clay soils: laboratory testing and numerical modeling. Bulletin of Engineering Geology and the Environment, 81,429.
  https://doi.org/10.1007/s10064-022-02942-2
- **Akhtar, S.** and Li, B., 2025 Experimental study of mechanical behaviors of lime-treated Quebec silty clay soils under freeze-thaw cycles. Environmental Geotechnics. (Manuscript number: ENGE-2024-118).
  https://doi.org/10.1680/jenge.24.00118
- **Akhtar, S.** and Li, B., 2025 Experimental and numerical investigation of the mechanical behavior of lime-treated silty clay under varying stress paths and temperature conditions. Submitted to Acta Geotechnica. (Manuscript number: AGEO-D-25-00251)

Other journal papers published during the Ph.D. program

- Girgis, N., Li, B., **Akhtar, S.**, and Courcelles, B., 2020. Experimental study of rate-dependent uniaxial compressive behaviors of two artificial frozen sandy clay soils. Cold Regions Science and Technology, 180, p. 103166. https://doi.org/10.1016/j.coldregions.2020.103166.
- **Akhtar, S.** and Li, B., 2020. Numerical analysis of pipeline uplift resistance in frozen clay soil considering hybrid tensile-shear yield behaviors. International Journal of Geosynthetics and Ground Engineering, 06: 47.
- **Akhtar, S.** and Li, B., 2023. A structural state model interpreting the residual strength transition behavior of clay soils. Geotechnical and Geological Engineering, 41: 2913-2922.

Conference proceedings papers and presentation:

- Akhtar, S., Li, B. and Chen, W. 2025, May. Mitigating Freeze-Thaw Soil Damage: Lime vs. Basalt Fiber Stabilization. In 23rd Global Joint Seminar on GeoEnvironmental Engineering.
- **Akhtar, S.**, Li, B., and Chen, W. 2024, September. Experimental investigation of the mechanical behavior of frozen fine grain soil stabilized with lime. In 77th Canadian Geotechnical Conference.
- **Akhtar, S.**, Li, B., Hafeez, G., and Wang, L. 2024, September. Numerical modeling of pipeline uplifting resistance in a lime treated frozen soil. In 77th Canadian Geotechnical Conference.
- Li B., Akhter Z., Nazemi, A., and **Akhtar S.** 2023. Thermo-mechanical responses of embankments under a changing climate in a Canadian first nation community. In Canadian Geotechnique Magazine.
- **Akhtar, S.** and Li, B. 2022, October. Influence of curing time on uniaxial compression behavior of raw lime-treated clayey soil. In 75th Canadian Geotechnical Conference.
- **Akhtar, S.** and Li, B. 2022, October. Evolution of macroscopic deformation in lime stabilization of soil. In 11th Conference on Structural Health Monitoring of Intelligent Infrastructure.
- **Akhtar, S.** and Li, B. 2021, September. Numerical modeling rate-dependent tensile behavior of frozen clay soils. In 74th Canadian Geotechnical Conference.
- Akhtar, Z., Li, B., Akhtar, S., and Xu, B. 2021, November. Numerical modeling compaction and dilation induced permeability changes in a laumionite-rich tight rock in laboratory and field scales. In 13TH Asian Regional Conference.
- **Akhtar S.**, Li, B., Ma, X., Xu, B., and Yang, B. 2020**.**, June. Stress-induced permeability change in a laumontite-rich tight rock. In 54th US Rock Mechanics/Geomechanics Symposium.
- **Akhtar, S.** and Li, B. 2019, August. Numerical analysis of pipeline uplift resistance in a frozen clay at varying temperatures. In 18th International Conference on Cold Regions Engineering and the 8th Canadian Permafrost Conference

Contribution of Authors

The content of this thesis reflects the author's unique and independent contributions to the research. The candidate took primary responsibility for experimental data, Finite Element Method (FEM) calibration and implementation, and the development of innovative enhancements. These tasks were carried out under the close guidance and supervision of Professor Biao Li.

In Chapter 4, the concept for development of multitasking subframe was provided by Dr. Biao Li.

In Chapter 6 and Chapter 7, lime was provided by the local company in Montreal, named Graymont and the marine soil was extracted from the Northern Quebec, where Cree communities reside by the BluMteric Environmental Inc.

All authors have reviewed and approved the final manuscript.

Table of Contents

List of Figures

List of Tables

Chapter 1

1 Introduction

1.1 Context and Inspiration for the Study

The physio-mechanical behavior of frozen soil is highly sensitive to temperature, confining pressure, loading rate, and the presence of unfrozen bound water. As the temperature increases, the amount of unfrozen water (including bound water and pore-free water) in the soil decreases, leading to complex nonlinear mechanical behavior such as viscoelasticity, viscoplasticity, and post-peak shear softening. The residual strength of frozen soil after thawing and the effects of freeze-thaw cycles on soil stability are critical concerns, particularly in the context of climate change and infrastructure durability. Rising global temperatures accelerate permafrost thaw and seasonal frost degradation, compromising the structural integrity of frozen ground. This poses significant challenges for civil engineering, geotechnical stability, and environmental impact assessments, especially in cold regions where roads, pipelines, and buildings depend on frozen soil for stability. Repeated freeze-thaw cycles further weaken soil strength by altering its pore structure, water content, and particle bonding, resulting in settlement, erosion, and reduced load-bearing capacity. These processes necessitate a thorough understanding of residual soil strength to develop resilient infrastructure and mitigate risks associated with permafrost degradation and seasonal frost.

Recently, there has been a notable rise in construction projects involving frozen ground, including natural foundations, highways, and railways. Additionally, the use of artificial ground freezing (AGF) in mining and tunneling engineering has become increasingly common (Xu et al. 2019). However, various construction challenges have emerged both during and after project completion due to the deformation of frozen materials. Changes in the mechanical properties of these materials, influenced by climate variations and environmental factors, contribute to significant engineering and environmental issues, such as infrastructure damage, slope instability, and land subsidence (Chen et al. 2023). For example, Figure 1-1a illustrates the uplift of a pipeline by approximately 1.1 meters due to frost heave. Figure 1-1b depicts a longitudinal crack in a highway caused by tensile stresses induced by frost heaving. Additionally, Figure 1-2 shows cracks and warping in the runway and taxiways at Iqaluit International Airport resulting from permafrost thaw.

Figure 1-1 Deformation of infrastructure in cold regions; a) Pipe uplifting of norman wells (Nixon and Burgess 1999); b) longitudinal thermal crack (Doré and Zubeck 2009).

Figure 1-2 Ground settlement due to freezing-thawing action on the taxiway of Iqaluit International Airport (Natural Resources Canada 2017).

Frozen soil is widely distributed across the globe, with permafrost covering approximately 21.8% of the land area in the Northern Hemisphere (Obu et al. 2019) (Figure 1-3). During the coldest month of winter, nearly 50% of the land area is covered by frozen soil (Chen et al. 2023). Canada, as a member of the United Nations, is actively implementing decarbonization strategies to achieve the Sustainable Development Goals by 2030. Understanding the mechanical behavior and properties of frozen soils, such as strength, deformation, and creep is crucial for the investigation, design, construction, and operation of engineering projects in cold regions, particularly as these environments experience gradual degradation due to climate change and human activities.

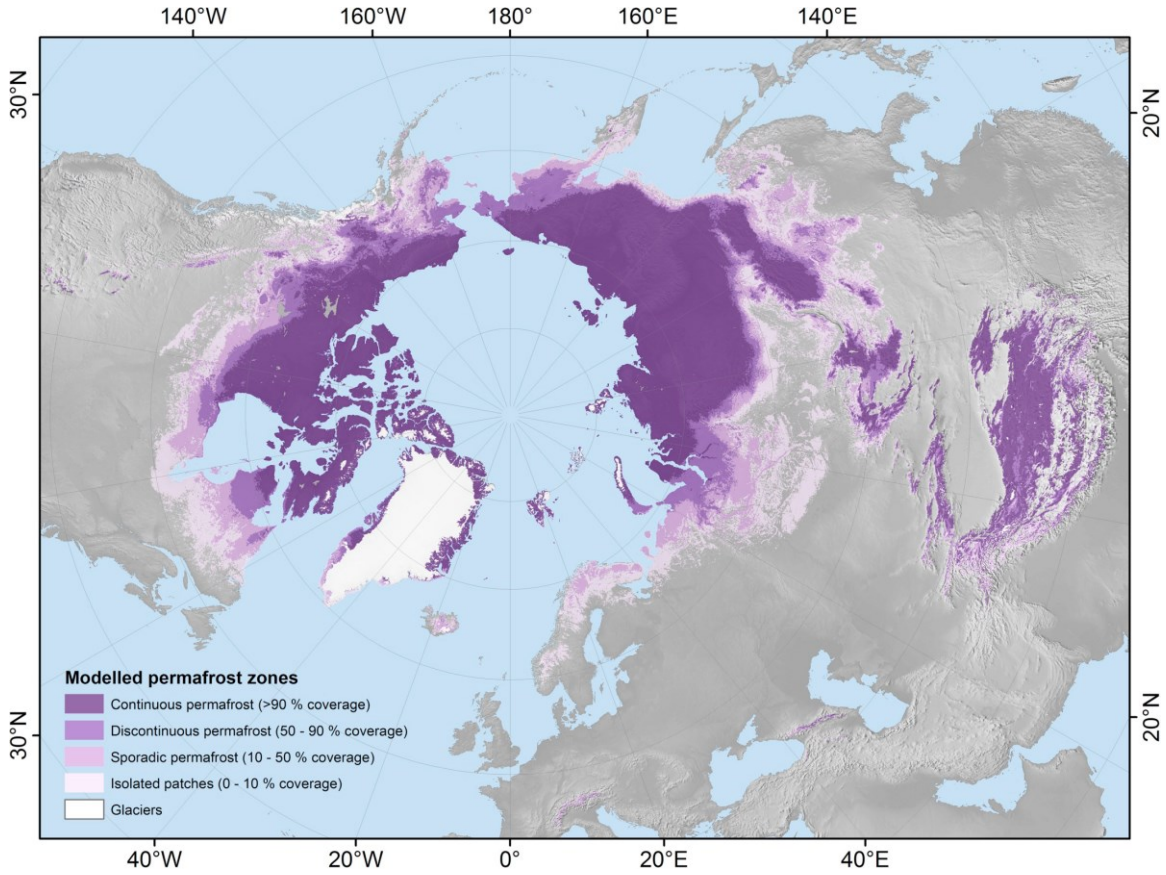

Figure 1-3 Permafrost distribution and zonation according to modeled permafrost probability, reflecting the proportion of permafrost underlying each 1 km² pixel (Obu et al. 2019).

Currently, there is a lack of comprehensive studies on the residual strength of frozen soil after thawing, as well as the threshold of bearing capacity in cold regions following freeze-thaw cycles. Additionally, existing numerical modeling tools are limited in their ability to accurately simulate deformation processes in both saturated and unsaturated frozen soils. Understanding the residual strength threshold and changes in failure patterns of soils in cold regions is crucial for engineers and the construction industry to mitigate climate-induced infrastructure damage and minimize geotechnical risks. Reliable models are essential for accurately quantifying freeze-thaw effects in soils, which are complex porous media composed of solid soil particles, ice, liquid water, and air. Therefore, a deeper understanding of frozen soil behavior is critical for improving infrastructure resilience in cold environments.

Frozen soils consist of a mixture of soil particles, water, ice, and air. They naturally occur in the seasonal frozen and permafrost layers of Arctic and subarctic regions, as well as in loess sediments. Areas such as Siberia, Canada, Greenland, Antarctica, and Alaska, located in both the Northern and Southern Hemispheres, experience prolonged freezing temperatures (Kadivar and Manahiloh 2019). Additionally, the application of artificial ground freezing in civil and mining projects has recently increased as a method to control ground and groundwater movement. Frozen soils are generally classified into two categories: saturated, where air is absent, and unsaturated, where air is present within the soil matrix.

The thermo-mechanical behavior of both untreated natural soil (N-soil) and lime-treated soil (L-soil) under freeze-thaw cycles, varying loading rates, temperatures, and confining pressures has been studied from multiple perspectives. Given that frozen soils are heterogeneous materials that retain free porewater even at low temperatures, their mechanical behavior is highly sensitive and complex under loading conditions. This study aims to develop an effective method for measuring the tensile strength of frozen soil, identify the residual strength threshold after freeze-thaw cycles, investigate the response of soil under varying temperature and confining pressure conditions, and calibrate finite element-based numerical models against experimental data for both N-soil and L-soil. These insights will contribute to a better understanding of frozen soil mechanics and improve predictive modeling for engineering applications in cold regions.

1.2 **Objectives and scope**

This study aims to address the following issues:

1- To establish an effective tensile strength testing technique for frozen soil that minimizes local plastic deformation and accurately determines the lower bound tensile strength, focusing on laboratory-based methods relevant to cold region geotechnical applications.

2- To determine the threshold number of freeze-thaw cycles required to reach residual strength in both N-soil and L-soil, using unconfined compressive strength and double punch tensile strength tests.
3- Experimental analysis of thermo-mechanical behaviour of N-soil and L-soil under temperature control triaxial tests at various temperatures, confining pressures and loading rates.
4- To calibrate the hyperbolic Drucker-Prager model using experimental data from double punch tensile, unconfined compressive strength, and triaxial tests, in order to evaluate its effectiveness in simulating the complex stress-strain behavior of frozen untreated and lime-treated soils, including instantaneous and visco-elastic responses, non-linear plasticity, peak and post-peak behavior, as well as incorporating time-dependent creep behavior under high loading rates.
5- To utilize and calibrate extended finite element method (XFEM) damage models in Abaqus against experimental data, in order to accurately capture damage patterns, crack initiation, and propagation in frozen soils under unconfined compressive strength and double punch tensile strength tests.

1.3 Original contribution

This research introduces several original contributions to the quantifying rheological behavior of frozen soil and its residual strength:

1.3.1 Numerical model for time-dependent uniaxial compression:

This study focuses on calibrating Abaqus-based numerical simulations with laboratory experiments to accurately capture the strain hardening, post-peak softening, and stress relaxation behavior of frozen sandy clay. It explicitly integrates strain rate- and temperature-dependent functions to characterize plastic hardening. Furthermore, the study distinguishes between short-

term rate-dependent behavior, governed by strain hardening, and long-term stress relaxation, controlled by creep deformation. The findings emphasize that creep deformation plays a critical role in prolonged stress relaxation scenarios, making it a key factor in understanding the long-term mechanical behavior of frozen soils.

1.3.2 **Identifying effective tensile testing technique for frozen soil:**

In this study, the Double Punch Tensile Strength Test is identified as a conservative yet reliable technique for measuring the tensile strength of frozen soil. It ensures consistent contact area throughout the test, leading to more accurate and reproducible results. Additionally, this method helps determine the effective specimen size for tensile testing, optimizing experimental accuracy. By integrating laboratory testing with finite element modeling, this study enhances our understanding of tensile failure mechanisms in frozen soils. This combined approach contributes valuable insights to both experimental and computational geomechanics, improving predictive modeling and the design of engineering structures in cold regions.

1.3.3 **Frozen soil residual strength improvement:**

This study examines the mechanical response of lime-treated silty clay under varying freeze-thaw cycles. It quantifies both the degradation and subsequent recovery of strength, which is crucial for assessing the long-term performance of stabilized soils in cold climates. A key finding is the identification of a freeze-thaw cycle threshold, representing the point of maximum strength degradation. Beyond this threshold, the soil begins to exhibit strength recovery, providing valuable insights into its resilience and long-term stability. These findings contribute to the optimization of soil stabilization techniques for infrastructure durability in cold regions.

1.3.4 **Predicting cold-region soil behavior treated with lime:**

This study investigates the compressive, tensile, and shear strength of lime-treated silty clay under varying temperature and stress conditions, providing a comprehensive understanding of its mechanical behavior. It successfully employs the Hyperbolic Drucker–Prager model to simulate the response of lime-treated silty clay under different stress paths and temperature conditions. Additionally, the study effectively models damage initiation and crack propagation, marking a significant advancement in simulating brittle failure in frozen lime-treated soil. These findings enhance the predictive capabilities of numerical models, improving the reliability of geotechnical assessments in cold regions.

1.4 **Thesis organization**

This thesis follows a manuscript-based format, with four of the seven chapters consisting of journal article manuscripts that have either been published or are under review, as outlined in the list of publications. Excluding this chapter, the thesis is organized as follows:

Chapter 2 presents a comprehensive literature review, outlining the key challenges in the field and proposing experimental and numerical approaches to address them. This chapter establishes the foundational context for the study by synthesizing existing research and identifying critical knowledge gaps.

Chapter 3 explores the development and calibration of a finite element-based numerical model using experimental data under unconfined compressive stress. It emphasizes the accuracy and effectiveness of the Hyperbolic Drucker–Prager model combined with the Singh–Mitchell creep model in capturing key mechanical behaviors, including strain hardening, post-peak softening, and

stress relaxation. This chapter demonstrates the model's capability to simulate the complex mechanical response of frozen soils under varying loading conditions.

Chapter 4 identifies the most effective testing technique for accurately capturing the tensile strength behavior of frozen soil. The study demonstrates that the Double Punch Test maintains a consistent contact area throughout the testing process, leading to more reliable results up to the complete failure stage. This chapter highlights the advantages of the method in minimizing variability and improving the accuracy of tensile strength measurements in frozen soils.

Chapter 5 examines the thermo-mechanical behavior of lime-treated soil subjected to freeze-thaw cycles. The study identifies the threshold number of freeze-thaw cycles that results in maximum deformation while ensuring reliable residual strength under both compression and tension tests. These findings contribute to a better understanding of soil stabilization techniques and their effectiveness in cold environments.

Chapter 6 evaluates both experimental and numerical investigations of the mechanical behavior of lime-treated silty clay under varying stress paths and temperature conditions. The study also focuses on the calibration of a finite element-based numerical model and damage models using experimental data to accurately replicate failure patterns. These advancements enhance the predictive capability of numerical simulations, improving the understanding and forecasting of soil behavior in cold environments.

Chapter 7 synthesizes the key findings of the research, highlighting the major contributions to the understanding of frozen soil behavior. It also identifies the limitations encountered during the study and provides recommendations for future research to further improve the understanding and modeling of frozen soils. This chapter serves as a conclusion, outlining potential directions for

advancing experimental methods and numerical simulations in geotechnical engineering for cold environments.

Chapter 2

2 Literature review

2.1 Introduction

This section provides a comprehensive review of existing literature on the behavior and applications of frozen soil. By examining various aspects of frozen soil research, it aims to establish a solid foundation for understanding the complexities involved in studying and utilizing frozen soils, particularly in the context of climate change and engineering applications. This review highlights key challenges, advancements, and knowledge gaps, guiding future research and practical implementations.

2.2 Thermo-mechanical behavior of frozen soil

Research on frozen soil dates back to the first half of the 20th century, with early studies primarily focusing on determining the bearing capacity of frozen ground while considering its long-term stability (Arenson et al. 2007). Interest in frozen soil mechanics, including seasonally frozen soil, permafrost, and artificially frozen ground, grew as construction activities expanded to support national development. Frozen soil is defined as soil that contains a fraction of ice, with the system's prevailing temperature at or below 0°C (Lai et al. 2013). This definition underscores the thermo-mechanical complexity of frozen soils, making them a critical area of study in geotechnical and environmental engineering.

Frozen soil is a complex, heterogeneous mixture composed of clay particles, non-clay particles, unfrozen water, frozen pore ice, and/or air bubbles (Figure 2-1). It occurs naturally in various

geographical regions, including seasonally frozen and permafrost layers, Arctic and subarctic zones, and loess sediments, all of which experience prolonged freezing temperatures (Kadivar and Manahiloh 2019). In addition to its natural occurrence, the use of Artificial Ground Freezing (AGF) has recently increased in civil engineering applications, such as tunneling, pipeline installation, mining, and slope stabilization. AGF is employed to temporarily enhance soil bearing capacity and control ground and groundwater movement (Vitel et al. 2015, Xu et al. 2019). However, cyclic freezing and thawing processes introduce significant risks, including infrastructure damage, land subsidence, and borehole failures. These concerns are further exacerbated by climate change, which is leading to more frequent and severe weather events, intensifying the challenges associated with frozen soil stability (Na and Sun 2017). Frozen soils are classified into two categories: saturated, which lack air, and unsaturated, where air is present within the medium. In both cases, freezing processes can lead to frost heave, causing an expansion of soil volume. Frost heave occurs due to increased water migration and crystallization during freezing, which separates soil particles. This phenomenon poses significant risks in cold regions, often resulting in engineering failures such as pipe ruptures and foundation damage. Extensive research has been conducted to quantify the mechanical behaviors of frozen soils, including tensile strength, compressive strength, modulus of elasticity, and Poisson's ratio, as well as to characterize deformation behavior. Studies have specifically investigated frozen silty soil (Ladanyi 1972, Zhu and Carbee 1984, Akagawa and Nishisato 2009, Azmatch et al. 2010, 2011, Xu et al. 2017b, Ming et al. 2017, Kadivar and Manahiloh 2019), clayey soil (Andersland and Akili 1967, Zhao et al. 2009, Kadivar and Manahiloh 2019), helin loess (Chou et al. 2013, Xu et al. 2017b), and sandy soil (Bragg and Andersland 1981, Arenson et al. 2007). These studies have consistently shown that as temperature decreases, the strength of frozen soil increases. However, the strength is highly

sensitive to water content and strain rate. Further investigations by Parameswaran and Jones (Parameswaran and Jones 1981), Ladanyi and Benyamina (Ladanyi and Benyamina 1995), Esmaeilli-Falak et al. (Esmaeili-Falak et al. 2018, 2020), Xu et al. (Xu et al. 2019), Kadivar and Manahiloh (Kadivar and Manahiloh 2019), and Zhou et al. (Zhou et al. 2020), focused on shear failure mechanisms and shear strength quantification of frozen soil using triaxial shear compression tests. These studies revealed that the ice fraction in frozen soil enhances cohesive strength and elasticity, making it highly sensitive to confining pressure. Strength increases with confining pressure up to a critical threshold, beyond which it begins to decrease due to pressure melting and the crushing of cemented bonds between ice and solid particles. For frozen loess, (Zhou et al. 2018) determined that this inflection point occurs at 7 MPa at -6°C, although it remains highly dependent on unfrozen water content and soil type. A comprehensive understanding of the mechanical behavior of frozen clay soils is crucial for assessing geological hazards, such as permafrost slumps, infrastructure damage due to seasonal freeze-thaw cycles, and artificial ground freezing applications in engineering projects (Andersland and Ladanyi 1994, Wang et al. 2016, Girgis et al. 2020, An et al. 2022, Ma et al. 2023).

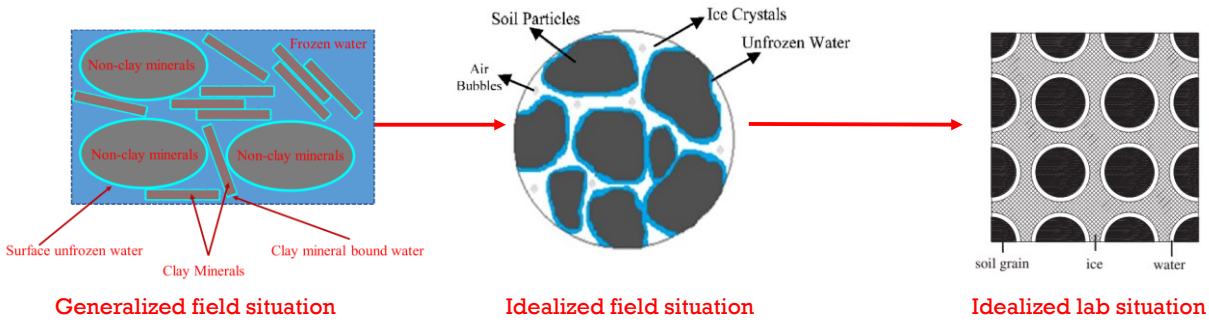

Figure 2-1 Schematic view of frozen soil matrix (Zhou and Li 2012, Kadivar and Manahiloh 2019). {The effect of air bubbles is not considerable in saturated soils}

Previous research has shown that the physio-mechanical behavior of frozen clayey soil is highly sensitive to temperature, confining pressure, loading rate, and unfrozen bound water content (Zhou

et al. 2018, Girgis et al. 2020). As temperature increases, the amount of available unfrozen water (including bound water and free pore water) in clay soil decreases, inducing complex nonlinear mechanical behavior, such as viscoelasticity, viscoplasticity, and post-peak shear softening. The brittle pre-peak and post-peak softening behavior of frozen soil is significantly influenced by temperature and deformation rate. However, clayey soils retain more unfrozen water than silty soils due to the higher water-holding capacity of clay particles, even at lower freezing temperatures (Nixon 1992, Esmaeili-Falak et al. 2018). This characteristic makes clayey frozen soils more susceptible to temperature-dependent mechanical variations. According to the studies of Kadivar and Manahiloh (Kadivar and Manahiloh 2019), and Girgis et al. (Girgis et al. 2020), pressure melting in frozen soil, caused by stress concentration and higher loading rates, leads to reduced mechanical strength and post-peak softening behavior, as illustrated in Figure 2-2 and Figure 2-3. Similarly, finding of research studies by Nixon (Nixon 1992) and Esmaeilli-Falak et al. (Esmaeili-Falak et al. 2020) confirm that clay retains a higher percentage of unfrozen water than silt, even at lower temperatures. This finding emphasizes the importance of bound water in frozen clay minerals, which cannot be treated the same way as non-clay minerals in frozen soils. Therefore, in this study, the role of unfrozen water content will be separately analyzed for clay and non-clay minerals, as illustrated in Figure 2-4. Several researchers have examined the time-dependent microstructural response of frozen soil (Zhou et al. 2018, Wang et al. 2019c). Initially, the applied load is resisted by the frozen pore ice, which, under stress, undergoes melting and fracturing. Depending on the loading rate, this behavior can be ductile or brittle. As the ice weakens, interparticle effective interactions between solid grains take over, counteracting further deformation. If the load continues to increase, it eventually leads to particle-level deformation, grain rearrangement, and finally lead to failure, as demonstrated in Figures 2-2 and 2-3. It is worth

noting that microstructural response dictates the overall deformation behavior of frozen soil. Research conducted by Ghoreishian Amiri and Grimstad (Ghoreishian Amiri and Grimstad 2017), Hou et al. (Hou et al. 2018), Li et al. (Li et al. 2018), and Wang et al. (Wang et al. 2019b) has shown that deformation in frozen soil follows a progressive sequence; Instantaneous elastic and plastic deformation, followed by viscoelastic deformation of pore ice, and viscoplastic deformation of solid grains, leading to the failure stage (Figure 8). The creep behavior of frozen soil consists of three distinct stages: (I) Primary (attenuation) stage where the strain rate decreases, while creep strain increases; (II) Secondary (steady) stage where the strain rate remains constant, and creep strain increases steadily over time; and (III)Tertiary (acceleration) stage where the strain rate and creep strain increase rapidly, leading to failure, as provided in Figure 2-5. As time progresses, the sample undergoes progressive damage, ultimately failing completely. If the loading rate is too high or the applied stress exceeds the long-term strength of the soil, a post-peak softening behavior will emerge. These findings highlight the critical role of strain rate, temperature, and unfrozen water content in the mechanical behavior of frozen soils, which must be carefully considered in geotechnical engineering applications.

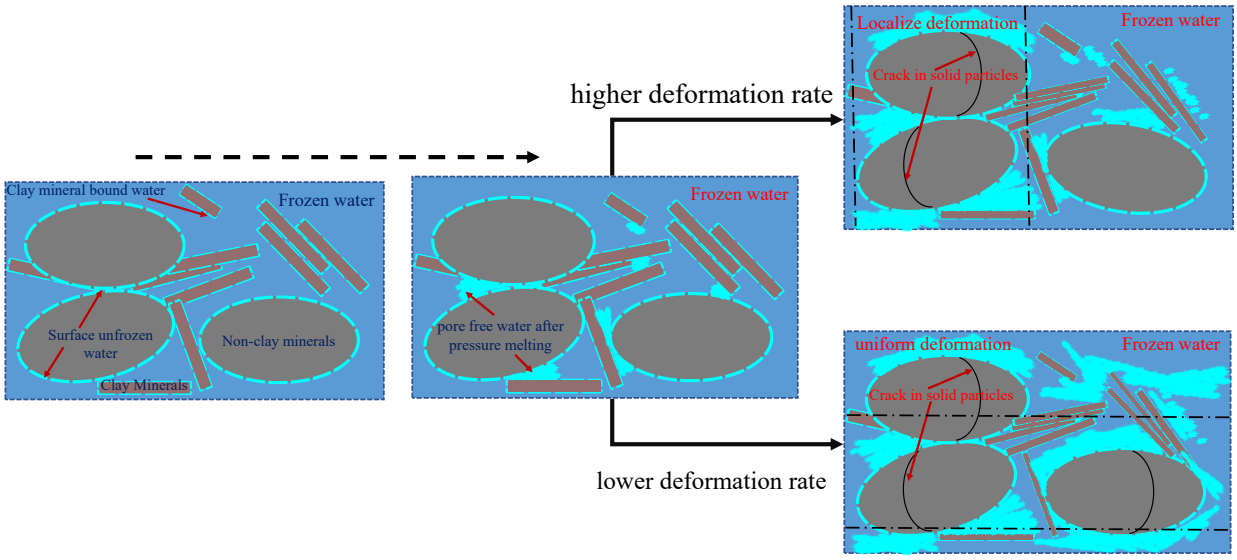

Figure 2-2 Schematic view of time-dependent micro-structural damage in frozen soil.

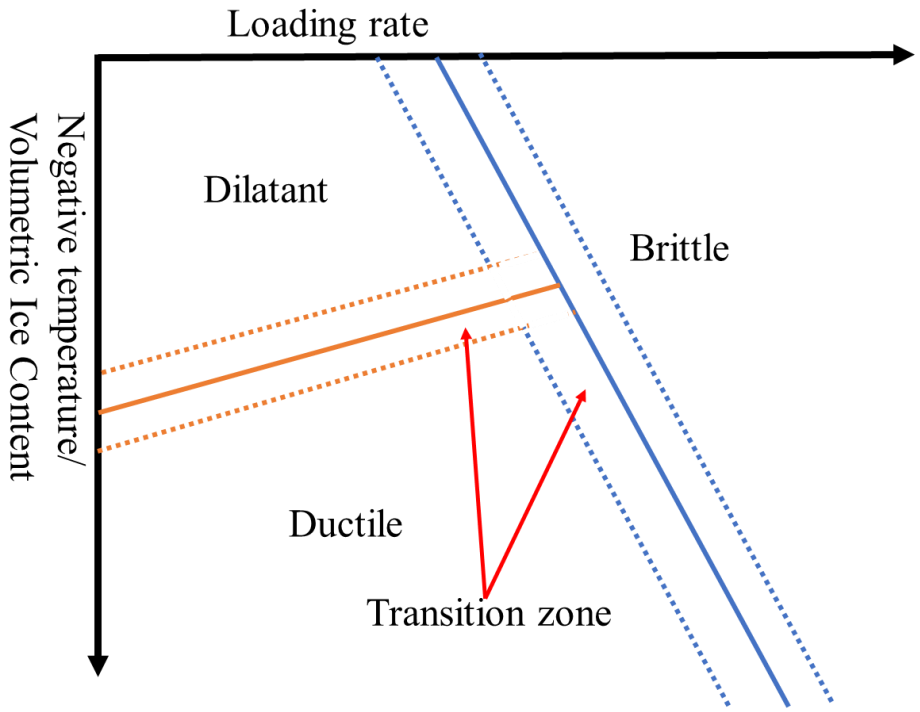

Figure 2-3 Schematic view of The response of frozen soil during the shearing stage as influenced by ice content and strain rate, after (Kadivar and Manahiloh 2019).

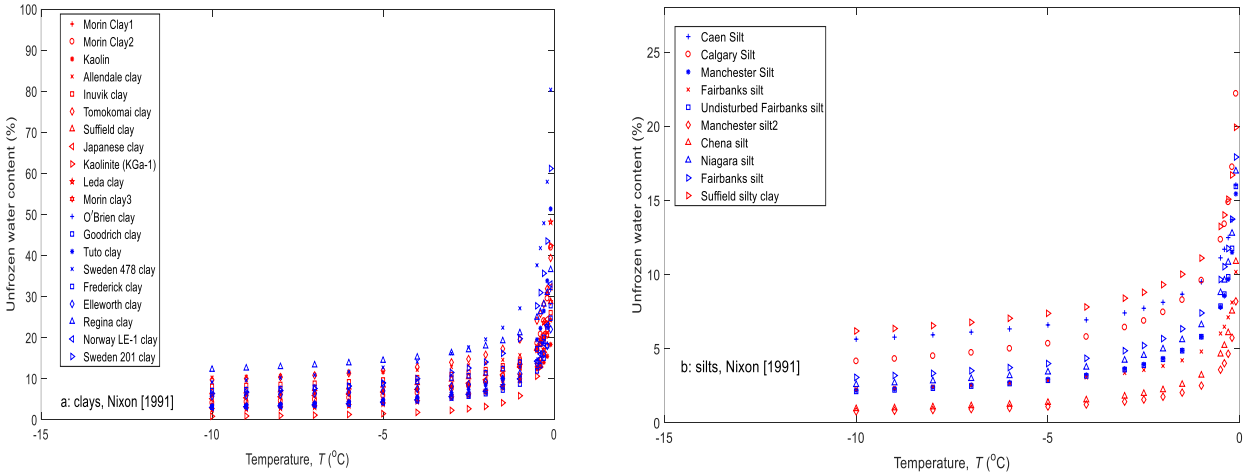

Figure 2-4 Plots for showing phase transition between unfrozen and frozen water content with respect to temperature, after (Nixon 1991).

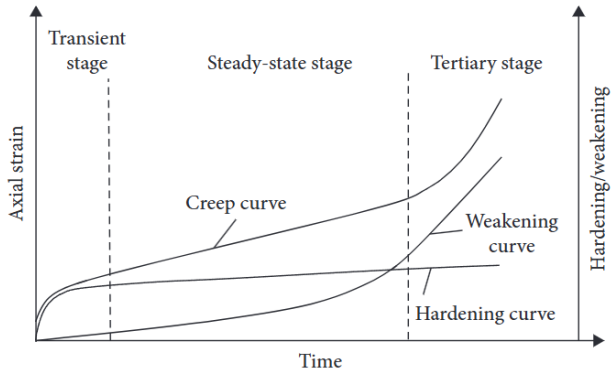

Figure 2-5 Schematic view of creep deformation (Li et al. 2018) .

2.3 Numerical modeling in cold region

Achieving a comprehensive understanding of the rate-dependent behavior of frozen clay soils and its correlation with temperature requires a large number of specimens with similar compositions and microstructures. However, obtaining in-situ frozen soil samples presents significant challenges due to complex procedures, which hinder theoretical studies of their behavior. Furthermore, laboratory tests provide limited characterization, and uncertainties persist regarding the intrinsic anisotropic properties of frozen soil samples with varying mineralogy. To overcome these challenges, researchers have increasingly turned to finite element-based numerical modeling to determine the equivalent properties of heterogeneous media like frozen soils. These models consider key variables such as loading rate, time, stress history, and temperature. Numerical modeling serves as a powerful tool in soil mechanics, complementing experimental laboratory work by enhancing our ability to analyze, predict, and optimize soil behavior under diverse conditions. Additionally, it reduces material costs and minimizes the need for extensive trial-and-error experiments. Several studies have been conducted to model frozen soil behavior using numerical approaches (Puswewala and Rajapakse 1990, Zhang et al. 2016a, Akhtar and Li 2020b, 2024b, Shastri et al. 2021, Sweidan et al. 2022, Suh and Sun 2022, Li and Akhtar 2022). Additionally, significant research has focused on frozen soil-structure interactions (Selvadurai et

al. 1999a, 1999b, Liu et al. 2008b, Akhtar and Li 2019, 2020b, Wang et al. 2023, Bian and Wang 2024). These studies have contributed to advancing numerical modeling techniques, improving the predictive accuracy of frozen soil behavior, and enhancing the design and performance of infrastructure in cold regions.

Furthermore, numerical modeling is a powerful and effective approach for capturing the complex nonlinear thermo-hydro-mechanical behavior of frozen soil. Several studies have demonstrated the capability of numerical models to accurately simulate stress behavior, deformation patterns, and environmental influences in frozen geomaterials. For instance, Shastri et al. (Shastri et al. 2021) investigated the mechanical behavior of natural frozen soils from Alaska, covering a wide temperature range ($-6°C < T < -26°C$) and confining pressures ($0 \leqslant \sigma_3 \leqslant 54.6$ MPa). They applied an elastoplastic model within a coupled thermo-hydro-mechanical finite element framework to analyze experimental data from natural frozen soil samples (Figure 2-6). Their results indicate that the numerical model effectively captures stress behavior and deformation paths, particularly at very low temperatures. Similarly, Xu et al. (Xu et al. 2022) developed a coupled numerical model to simulate seepage and temperature fields in frozen soils. Their study identified four key factors affecting the freezing temperature field; (I) Groundwater flow rate; (II) Frozen pipe spacing; (III) Frozen pipe diameter; and (IV) Initial ground temperature. They concluded that while groundwater flow rate influences the frozen temperature field, its impact can be mitigated under controlled conditions.

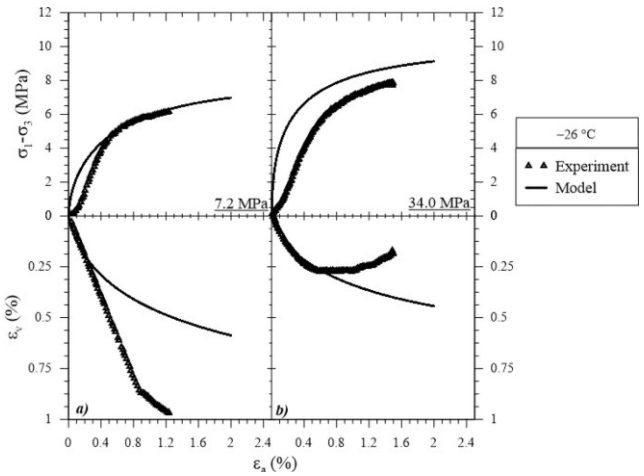

Figure 2-6 Comparison of validation, model, and experimental results for deviatoric stress (top) and volumetric strain (bottom) as functions of axial strain. Triaxial tests conducted at T = -26 °C under two confining pressures: (a) σ_3 = 7.2 MPa and (b) σ_3 = 34 MPa (Shastri et al. 2021).

For frozen geomaterials, a numerical homogenization approach is required to accurately account for the interfacial effects between frozen and unfrozen media. Woo and Go (Woo and Go 2024) numerically evaluated the mechanical behavior of a retaining wall subjected to frost heave in frost-susceptible soil. Their study included a comparative analysis of the interaction between frost-heaved soil and the retaining wall structure, considering factors, such as initial groundwater level in the backfill and presence or absence of drainage material. Their numerical model successfully captured frost heave and frost depth (Figure 2-7), demonstrating the importance of hydrothermal effects in geotechnical structures. In another study, Zhang et al. (Zhang et al. 2016a) conducted numerical simulations of frozen soil under impact loading. They validated their model by comparing numerical analysis outputs against experimental data (Figure 2-8), demonstrating the effectiveness of numerical approaches in capturing impact-induced deformations. Additionally, Akhtar and Li (Akhtar and Li 2020b) performed numerical analysis of a laboratory experiment by Liu et al. (2008) on pipeline uplift resistance in frozen soil. Their study identified complex tensile and shear deformation mechanisms under uplift loading conditions, further emphasizing the necessity of accurate numerical modeling (Figure 2-9). More recently, Akhtar and Li (Akhtar and

Li 2024b) conducted numerical model calibration using experimental data on the time-dependent behavior of frozen clay soils over a temperature range of 0°C to -15°C. Their study (Figure 2-10) highlights the significance of incorporating time-dependent material properties to improve numerical predictions of frozen soil behavior.

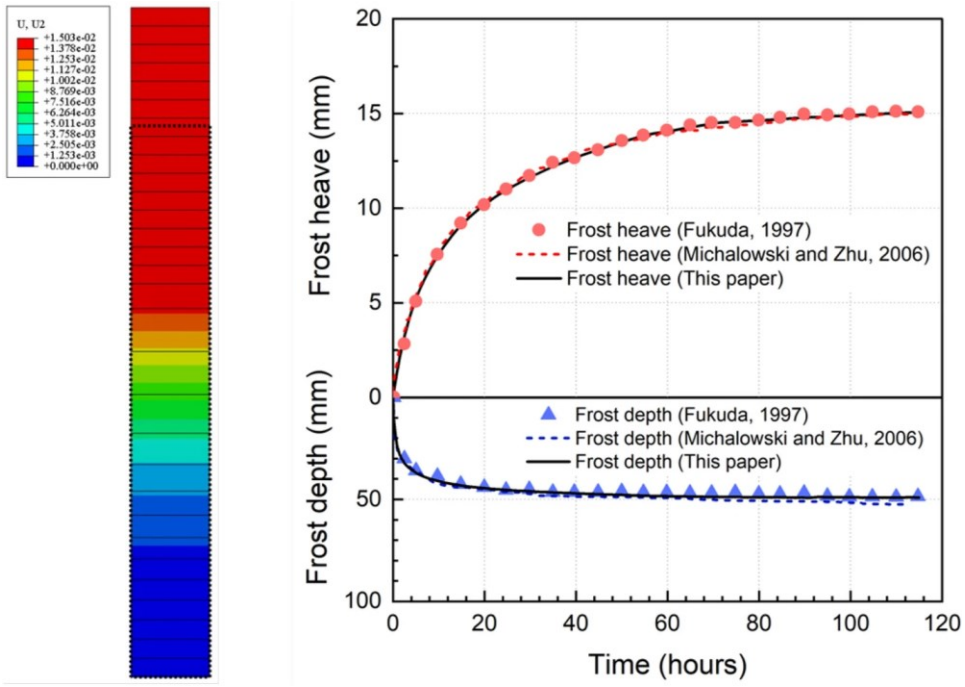

Figure 2-7 Comparison of results from the one-dimensional frost heave test under stepwise freezing conditions (Woo and Go 2024).

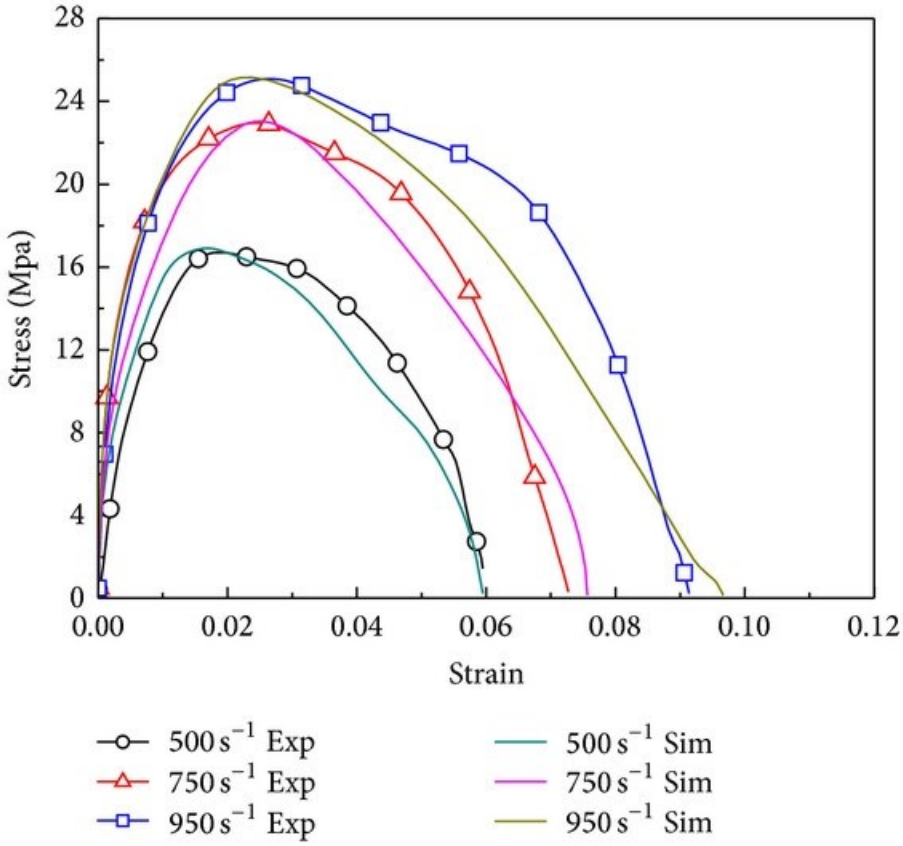

Figure 2-8 Comparison of experimental and numerical simulation curves at different strain rates (Zhang et al. 2016a).

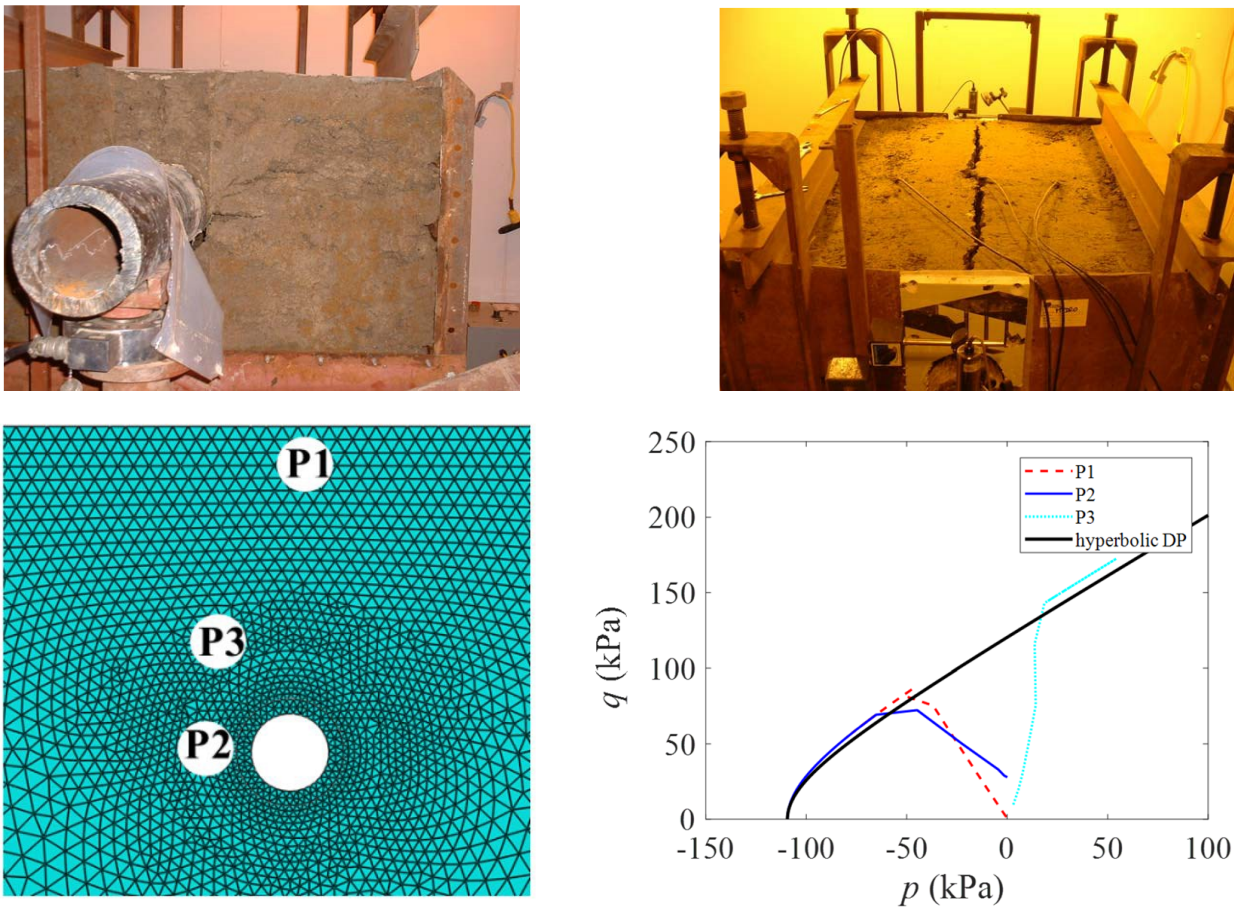

Figure 2-9 Comparison of experimental and numerical simulation (Liu et al. 2008a, Akhtar and Li 2020b).

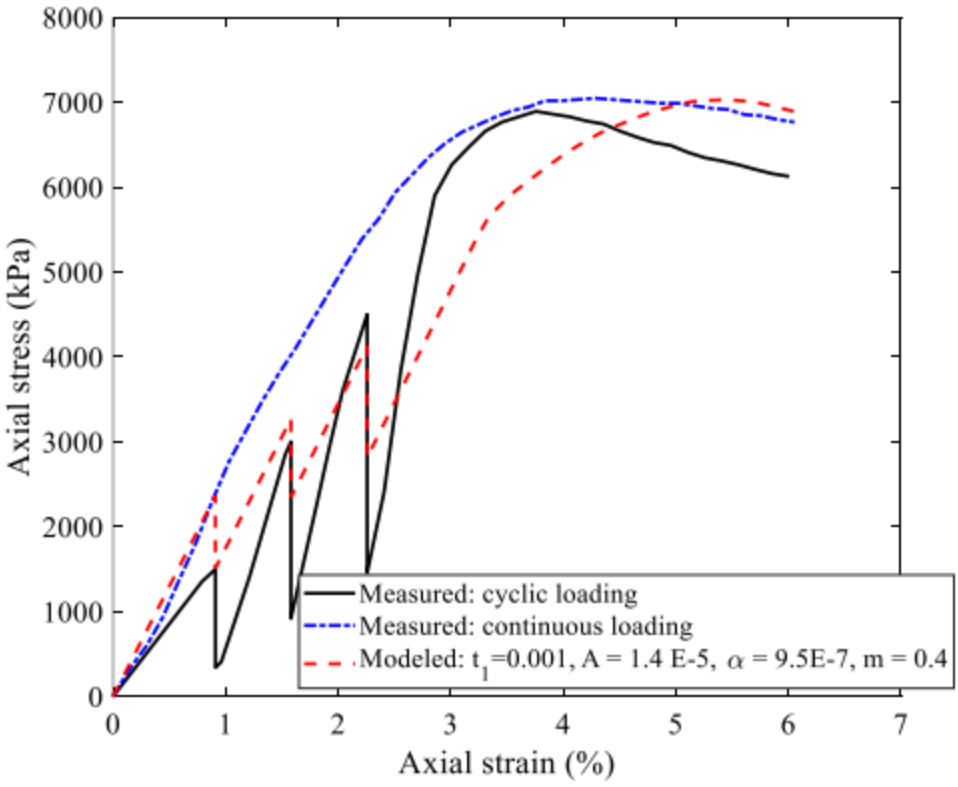

Figure 2-10 Measured and modeled stress–strain curves under cyclic loading and stress relaxation conditions (T= −15 °C, loading rate =9 mm/min (Akhtar and Li 2024b).

Overall, these studies demonstrate that numerical modeling is an essential tool for simulating the multi-physics interactions in frozen soils, enabling better prediction, design, and optimization of geotechnical systems in cold regions.

2.4 Utilization of lime for soil stabilization

Lime stabilization is one of the most widely used soil improvement techniques globally. This process causes clay particles to bond together, forming larger aggregates (Broderick and Daniel 1990). Today, lime stabilization is extensively applied in various infrastructure projects, including highways, railways, airports, embankments, foundation bases, slope protection, canal linings, and more (Wilkinson et al. 2010). The effectiveness of lime treatment depends on various factors, including soil granulometry (Broms 1991, Cabane 2004), clay mineralogy (specifically the type

and proportion of minerals in the fine fraction) (Mitchell and Hooper 1961, Bell 1996, Al-Mukhtar et al. 2014), the silica-to-alumina structure, and related properties such as specific surface area and cation exchange capacity (Mitchell and Soga 2005). Additionally, lime stabilization significantly reduces environmental impacts during both construction and the operational phase of access road pavements. It minimizes excavation and compaction requirements while preserving visual aesthetics during construction. Furthermore, the reduced cut-and-fill volumes during construction help mitigate damage to rock quarries. In studies conducted by Kavak (Kavak 1996), lime stabilization was applied to pure bentonite and kaolinite clays, and their unconfined compressive strengths were analyzed. The results indicated that the unconfined compressive strength increased by six times for bentonite and twelve times for kaolinite within one month. Long-term curing further enhanced the strength of these samples. Similarly, research by Kavak and Akyrli (Kavak and Akyarlı 2007) demonstrated that the compressive strength of lime-stabilized brown clay increased by 3.8 times within seven days and by 4.7 times after one year. Additionally, the deformation at failure was reduced from 3% to 1%, as illustrated in Figure 2-11.

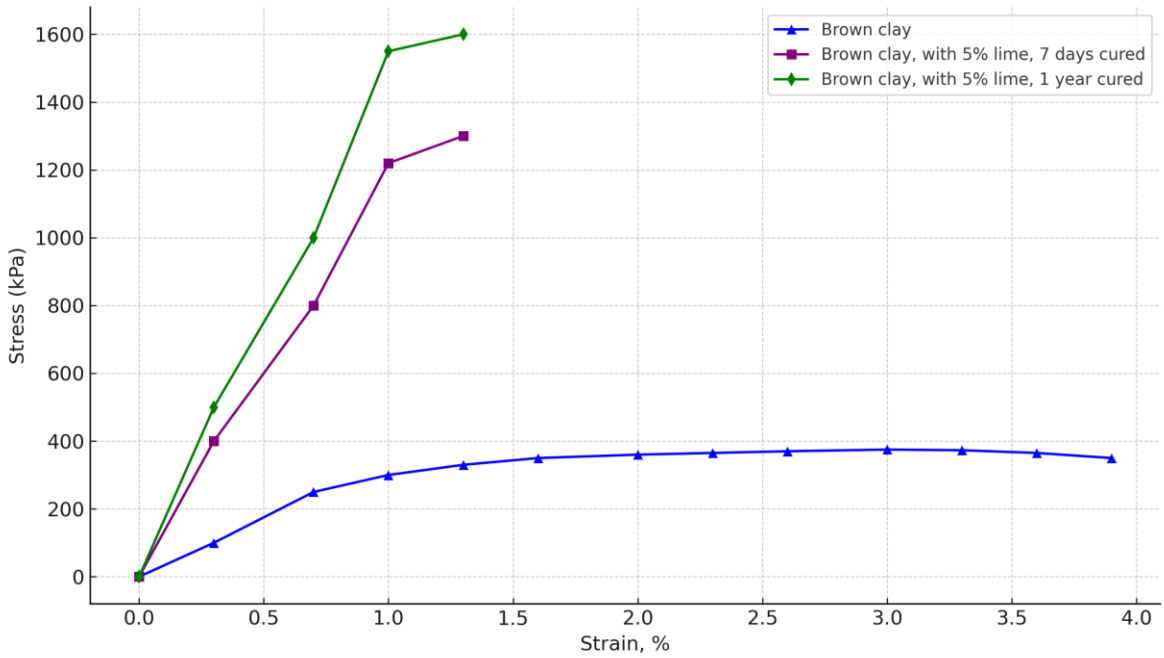

Figure 2-11 Axial stress vs axial strain plot for treated and untreated soil (Kavak and Akyarlı 2007).

Laboratory studies indicate that the number of freeze-thaw (F-T) cycles, freezing rates, and stress conditions have the most significant impact on changes in hydraulic conductivity. As the rate of freezing and the number of F-T cycles increase, and as the overburden pressure decreases, hydraulic conductivity tends to rise. Other factors, such as the ultimate temperature, dimensionality of freezing, and availability of an external water supply, appear to have minimal influence on changes in hydraulic conductivity (Yıldız and Soğancı 2012). It is well established that extreme ground temperature fluctuations, such as those caused by F-T cycles, significantly affect the geotechnical properties of soil. Previous research has consistently demonstrated that freeze-thaw cycles lead to a noticeable reduction in soil stability (Simonsen and Isacsson 1999, Xu et al. 2019). The behavior of clay materials under F-T conditions is complex and depends on various parameters, including the type of clay mineral (kaolinite, illite, or montmorillonite), degree of saturation, duration, and amplitude of the F-T cycles (Wang et al. 2007, Svensson and Hansen 2010, Cui et al. 2014). Pousette et al. (Pousette et al. 1999) reported that F-T cycles adversely affect strength gain in various types of peat with moisture contents around 200%. Their study

revealed that stabilized peat samples subjected to eight F-T cycles (−10 °C/+20 °C) lost approximately 30% of their strength compared to samples that were not exposed to these cycles. Similarly, Thompson and Dempsey (Thompson 1968) found that if sufficient lime is available, pozzolanic reactions continue under favorable conditions.

In cold regions, the mechanical properties of soils are severely impacted by ice lens formation between particles during freezing and the excess water produced during thawing (Konrad 1989). These effects can significantly weaken the strength and bearing capacity of foundation soils (Wang et al. 2007, Kamei et al. 2012, Aldaood et al. 2014). According to Lee et al. (Lee et al. 1995), cohesive soils with a uniaxial compressive strength (UCS) below 55 kPa exhibit negligible effects from F-T cycles, whereas soils with a UCS exceeding 103 kPa experience a reduction of more than 50% in resilient modulus due to the freeze-thaw process.

Parsons and Milburn (Parsons and Milburn 2003) observed that soil samples subjected to 12 F-T cycles exhibited weight losses ranging from 2% to 41%, primarily due to microscale soil-particle separation caused by ice pressure within soil pores. The volume expansion of freezing water increases pore pressure, reducing particle cohesion and soil strength, ultimately making the soil more susceptible to erosion. Among various soil stabilization methods, cement-treated soils exhibited the least weight loss (2%–7%), while lime-treated samples, particularly those with lean clay, experienced the greatest losses. Fly ash-treated soils exhibited intermediate losses, ranging from 7% to 19%.

Given the uncertainty in the mechanical response observed in the aforementioned studies, it is crucial to explore existing research gaps and identify key missing variables related to lime-soil interactions, which this study aims to investigate.

2.5 Climate change and permafrost degradation in north of Quebec

Climate change-induced permafrost degradation presents a significant environmental and geological challenge in Arctic and subarctic regions, as exemplified by areas such as Umiujaq and Nunavik in Quebec, Canada. Rising temperatures accelerate permafrost thaw, leading to profound impacts on slope stability, hydrology, and local ecosystems. In steep bedrock areas, permafrost thaw can trigger slope instability, resulting in sudden and severe destabilization (Gruber and Haeberli 2007). Permafrost degradation also threatens infrastructure, particularly roads and airstrips, which were designed and constructed without accounting for the long-term effects of climate warming. In many cases, permafrost was assumed to be stable at the time of construction, but increasing temperatures now compromise the structural and functional integrity of these facilities. For instance, settlement and cracking patterns observed at Iqaluit Airport in Iqaluit, Nunavut, Canada, illustrate the impact of underlying permafrost degradation on the runway (Fortier et al. 2011, Natural Resources Canada 2017). Structural distress, including thaw settlement and cracking, is commonly observed in areas where permafrost is deteriorating (Figure). On the Qinghai-Tibet Plateau (QTP), the damage ratio (the proportion of damaged road sections relative to the total length) exceeded 30% for existing roads before the construction of the Qinghai-Tibet Railway (Cheng and Wu 2007, Zhang et al. 2016b). These cases highlight the critical challenges that permafrost degradation poses to infrastructure design, construction, and maintenance in permafrost-affected regions. The ongoing degradation of permafrost due to rising temperatures is evidenced by the thickening of the active layer and the northward retreat of permafrost extent, both of which are strongly influenced by climatic factors (Vasiliev et al. 2020). Beyond its impact on infrastructure, permafrost degradation significantly alters regional hydrology and groundwater dynamics (Dagenais et al. 2020). The loss of permafrost is expected to continue throughout the

21st century, posing an escalating threat to the stability of Arctic infrastructure and the sustainable development of Arctic communities (Hjort et al. 2018, Minsley et al. 2022). Additionally, permafrost thaw contributes to climate change by releasing stored carbon into the atmosphere, further exacerbating global warming (Miner et al. 2022). Thawing permafrost also influences vegetation growth by altering the timing of surface thaw onset, which affects various stages of the Arctic growing season (Young et al. 2020, Chen and Jeong 2024). Moreover, the release of plant-available nitrogen from thawing permafrost in subarctic peatlands drives changes in vegetation composition and biomass production (Keuper et al. 2012, 2017). Given the widespread and multifaceted consequences of permafrost degradation, the implementation of effective stabilization measures is imperative to mitigate foreseeable geohazards and ensure the resilience of Arctic and subarctic ecosystems and infrastructure.

2.6 **Summary**

The study of frozen soil behavior, particularly in Arctic and subarctic regions, is crucial due to its profound implications for geotechnical engineering, environmental sustainability, and climate change adaptation. A comprehensive review of existing literature and research findings highlights that permafrost degradation, exacerbated by climate warming, presents complex challenges, including slope instability, hydrological changes, and disruptions to ecosystem dynamics. The thawing of permafrost not only threatens infrastructure stability, such as roads, airstrips, and buildings, but also alters groundwater flow, accelerates soil erosion, and releases greenhouse gases, further intensifying global warming. Additionally, the loss of permafrost can impact vegetation patterns and biodiversity, affecting local communities that rely on permafrost-stabilized landscapes for transportation and resource extraction. Addressing these challenges requires interdisciplinary approaches, including advanced soil stabilization techniques, improved

engineering design for infrastructure resilience, and climate-adaptive policies that mitigate environmental and socioeconomic impacts.

To address these challenges, researchers have increasingly adopted finite element-based numerical modeling approaches. These models integrate factors such as rate dependency, temperature effects, and compression behavior into existing constitutive models for unfrozen soils, allowing for a more accurate simulation of frozen soil behavior under freezing and thawing conditions. By incorporating these complexities, numerical models can effectively capture the mechanical and thermal responses of permafrost. Validated through field data and experimental studies, these models offer valuable insights into permafrost dynamics, ground stability, and infrastructure performance in response to climate-induced changes. They play a crucial role in predicting soil deformation, thaw settlement, and slope stability, aiding in the development of mitigation strategies for engineering projects in permafrost-affected regions. Furthermore, ongoing advancements in computational techniques and material characterization continue to enhance the precision and applicability of these models in addressing the challenges posed by permafrost degradation.

Furthermore, alternative approaches such as lime stabilization techniques are increasingly being applied in the field to enhance soil stability and mitigate the adverse effects of permafrost thaw. These methods help improve the mechanical properties of thawing soils by reducing moisture susceptibility, increasing shear strength, and enhancing long-term residual strength in previously frozen slopes. Field studies have demonstrated its effectiveness in stabilizing thaw-weakened ground, preventing excessive settlement, and improving load-bearing capacity. As a result, lime stabilization is emerging as a practical and sustainable technique for mitigating geotechnical challenges associated with permafrost degradation and climate change-induced ground instability.

Preface to Chapter 3

The study of frozen soil mechanics has gained increasing attention in geotechnical engineering, particularly due to the growing infrastructure developments in cold regions. The mechanical behaviour of frozen soils is complex, influenced by temperature variations, loading conditions, and time-dependent deformation mechanisms such as creep and stress relaxation. However, while extensive experimental research has been conducted, there is still a gap in numerical modelling approaches that accurately capture the time-dependent stress-strain behaviours of frozen clay soils across different subzero temperatures. This chapter presents a comprehensive numerical investigation into the uniaxial compressive behavior of artificial frozen sandy clay. This study provides a finite element-based approach to simulate both instantaneous and long-term deformation characteristics. The results contribute valuable insights into the strain hardening, post-peak softening, and stress relaxation behaviour of frozen soils, bridging the gap between experimental findings and practical numerical modelling. This research will serve as a valuable resource for geotechnical engineers, researchers, and practitioners involved in cold-region infrastructure development. By improving the predictive accuracy of frozen soil behavior, this work contributes to the broader understanding and safe construction of engineering projects in permafrost and seasonally frozen environments.

Chapter 3

3 Modeling time-dependent uniaxial compressive behaviors of an artificial frozen sandy clay at different temperatures [1]

3.1 Abstract

Extensive experimental studies have demonstrated the time-dependent mechanical behaviors of frozen soil. Nonetheless, limited studies are focusing on the constitutive modeling of the time-dependent stress-strain behaviors of frozen clay soils at different subzero temperatures. The objective of this study is to numerically investigate the time-dependent behavior of frozen clay soils at a temperature range of 0^{o}C to -15^{o}C. The Drucker-Prager model is adopted along with the Singh-Mitchell creep model to simulate time-dependent uniaxial compression and stress relaxation behaviors of frozen sandy clay soil. The numerical modeling is implemented through the finite element method based on the platform of Abaqus. The constitutive modeling is calibrated by a series of experimental results on laboratory-prepared frozen sandy clay soils, where the strain hardening, the post-peak softening, and stress relaxation behaviors are captured. Our results show that both the rate-dependent model and creep model should be adopted to characterize a comprehensive time-dependent behavior of frozen soils. The rate-dependent stress-strain

[1] A version of this manuscript has been published in *Journal of Geotechnical and Geological Engineering* (2024).

behaviors heavily rely on the rate- and temperature-dependent hardening functions, where the creep strain provides a very limited contribution. Nevertheless, the creep strain should also be adopted when a long-term analysis or stress relaxation behavior is involved.

Keywords: Uniaxial compression tests, rate-dependent behavior, Drucker-Prager model, Singh-Mitchell creep model, frozen soils, finite element method

3.2 Introduction

The continuous economic development requires massive investment in various construction industries (i.e. roads, tunnels, high-rise buildings, pipelines, railways). To accommodate this requirement, the utilization of land in cold regions and the use of the artificial ground freezing technique for soft grounds expanded a lot in the last few decades (Andersland and Ladanyi 2003, Chen et al. 2011, Tang et al. 2012, 2015, Liu et al. 2019, Evirgen and Tuncan 2019, Shastri et al. 2021). As a multiphase porous media, frozen soils are comprised of solid particles, pore ice, unfrozen water, and possibly some air. Thus, the mechanical responses of frozen soils are sensitive to loading conditions and the applied temperature. Infrastructures built on frozen soil foundations in cold regions encounter deformation and heavy uneven settlement due to the influence of continuous loading over time (Lai et al. 2013), as well as freeze-thaw actions (Ishikawa et al. 2015, Wang and Liu 2015, Li et al. 2019a, Akhtar and Li 2020a, 2020b, Li and Akhtar 2022, Ghazavi et al. 2023). Execution of a uniaxial compression test is proficient in studying the mechanical properties of frozen soil (Christ and Park 2010, Yang et al. 2015, 2016, Yugui et al. 2016), and can efficiently be applied to frozen ground engineering practices. It is mostly applicable for shallowly buried frozen soils mainly contained in the active layer of the ground, where the magnitude of confining pressure is limited (Baker et al. 1982, Xu et al. 2017b). Numerous research studies have been conducted to study the uniaxial compressive strength and deformation behaviors of frozen soils. Bragg and Andersland (Bragg and Andersland 1981) studied the impact of loading rate and temperature on frozen sand samples under compression and tension stress conditions. They concluded that the impact from loading rates on the compressive strength is not significant. It is not consistent with the studies on clay soils, which hold considerable unfrozen water even at very low temperatures (Chen et al. 2011). Zhu and Carbee (Zhu and Carbee 1984) carried out a

number of uniaxial compression tests on Fairbanks silts with a constant rate of deformation and examined the impact of temperature, dry density, and strain rate. They develop a nonlinear empirical relation between peak strength, strain rate and negative temperature. Hu et al. (Hu et al. 2013) conducted compression and tensile tests on marine soils under very low temperature conditions, and they generated a series of temperature-dependent mechanical relations (e.g., strength, elastic modulus, and Poisson ratio), where the loading rate effect is not considered. Fei and Yang (Fei and Yang 2019) proposed to describe the unconfined compressive strength of silts as a function of negative temperature, strain rate, and density. Empirical relations were developed to model the relation between the key parameters and temperature. Additionally, a new power law relation was produced for relating strength, negative temperature, and strain rate. Li et al. (Li et al. 2004) investigated the role of negative temperature, strain rate and dry density on the compressive strength of frozen saturated clay. They found a linear relation between the frozen temperature and compressive strength. However, the increase in strain rate leads to an increase in strength exponentially. Zhao et al. (Zhao et al. 2009) evaluated the compressive strength of saturated frozen clay and investigate the effects of temperature gradients on elastic modulus. Linear empirical relations were developed to predict the elastic modulus and peak strength as function of negative temperature. Girgis et al. (Girgis et al. 2020) conducted a series of uniaxial compression and stress relaxation tests on artificially prepared frozen sandy clay soils. A nonlinear power law empirical relation as a function of negative temperature was produced to predict the mechanical properties of frozen clay soils under different loading rates.

As most projects in cold regions are expected to maintain their safety for a lifelong term and the cold regions infrastructure largely relies on the long-term stability of frozen ground. Another important aspect of time-dependent responses of frozen soils is the creep behavior. Initially,

various creep models were proposed to study the time-dependent properties of frozen soil (Ladanyi 1972, Wang et al. 2014, Xu et al. 2017a, Hou et al. 2018). Alternatively, stress relaxation tests, being more efficient, have also been considered to study the time-dependent rheological behavior of frozen soils (Ladanyi and Benyamina 1995, Wang et al. 2011). Nevertheless, the developed models are not suitable to numerically simulate the time-dependent compressive behaviors of frozen soil at different constant temperatures. Under different strain rates or temperatures, frozen soils tend to display very different stress-strain behaviors (Li et al. 2004, Xu et al. 2017b, Girgis et al. 2020). A high deformation rate tends to generate brittle failure with post-peak softening behavior, and a low deformation rate results in a diffuse failure associated with strain hardening. Most previous constitutive modeling is mainly based on analytical or semi-analytical approaches, where a strain rate or temperature condition should be pre-defined to generate matched stress-strain curves. However, such an approach is not well implemented using a general numerical method like FEM. Therefore, an extension of laboratory-scale constitutive modeling to the field practice is problematic since the deformation rate and temperature conditions vary geometrically and change with time steps.

In this study, finite element modeling was performed using the linear Drucker-Prager model combined with the Singh-Mitchell creep model, to investigate the temperature and strain-rate-dependent deformation behaviors. The simulation was calibrated by a series of measured results on laboratory-prepared sand clay soil samples at different subzero temperatures.

3.3 Modes of failure, constitutive models, and temperature-dependent parameters

3.3.1 Modes of failure in frozen soil

The degradation behavior of mechanical strength parameters in frozen sandy clay soil during uniaxial compression depends on the pore-ice, temperature, and loading rates. Wang et al. (Wang et al. 2019b) showed that the characteristics of strength degradation are controlled by the microstructural deformation (i.e. instantaneous elastic, viscoelastic deformation in pore-ice, and viscoplastic deformation in solid elements of frozen soil). As shown in Figure 3-1, the schematic views of stress-strain curves under the uniaxial compression loading condition are characterized by two deformation modes. Major features are summarized as follows:

1. At a lower temperature (i.e. -15ºC,) and a higher loading rate (i.e. 9 mm/min), the frozen soil encounters three distinctive phases during deformation (i.e. linear elastic, non-linear plastic hardening, and shear softening) as shown in Figure 3-1 (a). The shear softening portion (b-c) is a unique function of the loading rate. Higher loading rates produce distinctive shear softening which diminishes or disappears under the lower loading rate.

2. At a warmer temperature (i.e. -2ºC) and a low deformation rate (i.e. 1 mm/min.), the frozen soil yields only two modes of deformation (i.e. linear elastic and plastic hardening) as shown in Figure 3-2 (b).

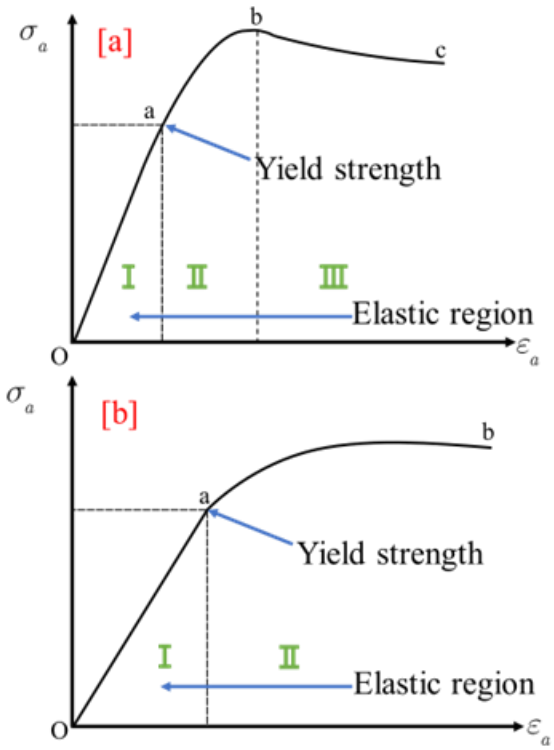

Figure 3-1 Schematic diagram of stress-strain modes in frozen clay soils under the uniaxial compression testing condition.

3.3.2 **Constitutive model**

In this study, the finite element-based software package Abaqus (Dassault Systèmes 2016) was used to simulate instantaneous elastic and rate-dependent elastic and plastic deformation in a frozen soil. The linear Drucker-Prager model along with the Singh-Mitchell creep model, are used to calibrate the experimental data and numerically analyze the frozen soil deformation behaviors. Some user-defined field programming is conducted to make the simulation possible for field practice by leveraging the varied temperature and strain rate conditions.

Drucker-Prager model

The Drucker-Prager model has been widely used in the numerical analysis of geomaterials and geotechnical problems (Helwany 2007). The linear Drucker-Prager yield criterion is given by Equation 3.1:

$$F = q - p' \tan\beta - d \tag{3.1}$$

where p' is the mean effective stress given by the effective stress tensor $\boldsymbol{\sigma}'$ as $p' = \frac{1}{3} trace(\boldsymbol{\sigma}')$; q is the von Mises equivalent stress given by $q = \sqrt{\frac{3}{2}\mathbf{S}:\mathbf{S}}$. The deviatoric stress tensor is defined as $\mathbf{S} = \boldsymbol{\sigma}' - p'\mathbf{I}$; where $\mathbf{I}$ is the identity matrix; and d is the Drucker-Prager cohesive parameter which can be defined as $d = \left(1 - \frac{1}{3}\tan\beta\right)\sigma_c$; σ_c is the uniaxial compression yield stress; and β is the angle of friction in the p' -q space. An unassociated plastic flow potential function can be applied as:

$$G = q - p' \tan\psi \tag{3.2}$$

where G is the flow potential; and ψ is the dilation angle. Additionally, since the strength of frozen soil is both loading rate and temperature dependent, the strain hardening can be expressed as functions of strain rate and temperature as:

$$\bar{\sigma} = \sigma_c(\bar{\varepsilon}^{pl}, \dot{\bar{\varepsilon}}^{pl}, T) \tag{3.3}$$

where σ_c is the uniaxial compression yield stress; $\dot{\bar{\varepsilon}}^{pl}$ is the equivalent plastic strain rate; $\bar{\varepsilon}^{pl} = \int_0^t \dot{\bar{\varepsilon}}^{pl} dt$ is the equivalent plastic strain; T is temperature. The strain rate-dependent plastic hardening behavior can be quantified by applying the rate and temperature-dependent strain hardening function. In this study, the hardening behavior is defined by giving the uniaxial compression yield stress (σ_c) as a function of uniaxial compression plastic strain (Dassault Systèmes 2016) as is shown in Equation 3.4:

$$\bar{\varepsilon}^{\mathrm{p}} = |\bar{\varepsilon}^{\mathrm{p}}_{11}| \tag{3.4}$$

Singh-Mitchell creep model

As another important aspect of time-dependent behavior, the creep deformation should be characterized using a separate creep model. We adopt the Singh-Mitchell creep model for the present study. There are two separate and independent creep mechanisms. One is shear creep which is controlled by the cohesion mechanism ($d\varepsilon_s^{cr}$), and the second is consolidation creep which is attributed to the consolidation mechanism ($d\varepsilon_c^{cr}$). The total creep strain is a combination of these two components:

$$d\varepsilon^{cr} = d\varepsilon_s^{cr} + d\varepsilon_c^{cr} \tag{3.5}$$

In this study, only the shear creep needs to be considered since our tests on frozen soils do not consider the drainage induced volumetric consolidation behavior. Therefore, the consolidation creep can be neglected ($d\varepsilon_c^{cr} = 0$).

According to the documentation of Abaqus (Dassault Systèmes 2016), the Singh-Mitchell creep model for the shear creep takes the form:

$$\dot{\varepsilon}_1 = A^s e^{\alpha^s \sigma_{cr}^s} \left(\frac{t_1}{t} \right)^{m^s} \tag{3.6}$$

where A^s , α^s , and m^s are the three creep parameters. t_1 is the initial time (given in minutes). σ_{cr}^s is the equivalent creep stress, determined from the intersection of the equivalent creep surface with the uniaxial compression curve by the following expression:

$$\sigma_{cr}^s = \frac{q - p' \tan\beta}{\left(1 - \frac{1}{3}\tan\beta \right)} \tag{3.7}$$

The creep potential function for calculating creep strains in multidimensional directions is given by:

$$g_s^{cr} = \sqrt{\left(0.1\frac{d}{(1-\frac{1}{3}\tan\beta)}\tan\beta\right)^2 + q^2} - p' \tan\beta \tag{3.8}$$

3.3.3 **Temperature-dependent mechanical properties**

The deformation behavior of frozen soil is highly dependent on the applied temperature and loading deformation rates (Arenson and Springman 2005). The unfrozen water present in the frozen soil contributes to the complex mechanical behaviors. The research study by Nixon (Nixon 1992) presents an empirical relation between unfrozen water and temperature using ($W_u = A(-T)^B$), in which T is the negative temperature while A and B are soil parameters. Similarly, experimental data demonstrates that a non-linear power law relation, given by Equation 3.9, controls the relation between temperature and peak strengths of frozen soil (Girgis et al. 2020):

$$\sigma_c = M\left(\frac{T}{T_0}\right)^N + Q \tag{3.9}$$

where M, N, and Q are the dimensionless curve fitting parameters to be determined, and T_0 is a reference temperature (-1°C is applied herein).

Table 3-1 Elastic properties of soil, rock and interface stiffness parameter applied to current numerical model

Parameters	**Units**	**Value**
Bulk Density	(g/cm3)	1.53
Water content	(%)	59
Specific gravity	(%)	2.63
Liquid limit	(%)	97
Plastic limit	(%)	34
Plastic Index	(%)	63
Sand	(%)	50
Clay	(%)	50

To capture the constitutive behavior of clay soils effectively at different strain rates and under varying applied temperature conditions, we carried out a series of uniaxial compressive and stress relaxation tests on laboratory-prepared sandy clay samples to maintain repeatability. The tests were conducted on artificially frozen sandy clay soil samples composed of silica sand 7030 (50 % by weight) and Bentonite Western 325M (50% by weight). According to ASTM D4083-2016, the prepared soil is classified as high plastic inorganic sandy clay. Atterberg limits and other physical properties of this soil mixture are given in Table 3-1. More detailed information on sample preparation and testing conditions are included in our published article by Girgis et al. (Girgis et al. 2020).

Different post-failure modes were observed for samples as shown in Figure 3-2. Three different loading rates (i.e. 1mm/min, 3mm/min, and 9mm/min) were used to observe the time-dependent strength degradation at various frozen temperatures. At lower temperatures, less external disintegration is observed compared to cases with higher temperatures. This difference is insignificant at a higher loading rate. Post failure samples for tests at -15°C, -10°C, -5°C, and -2°C are displayed in Figure 3-2 to demonstrate the gradual transition of shear failure to compaction

type failure when the temperature is getting warmer. The significant sample end enlargement only happens to the samples at T = -2°C.

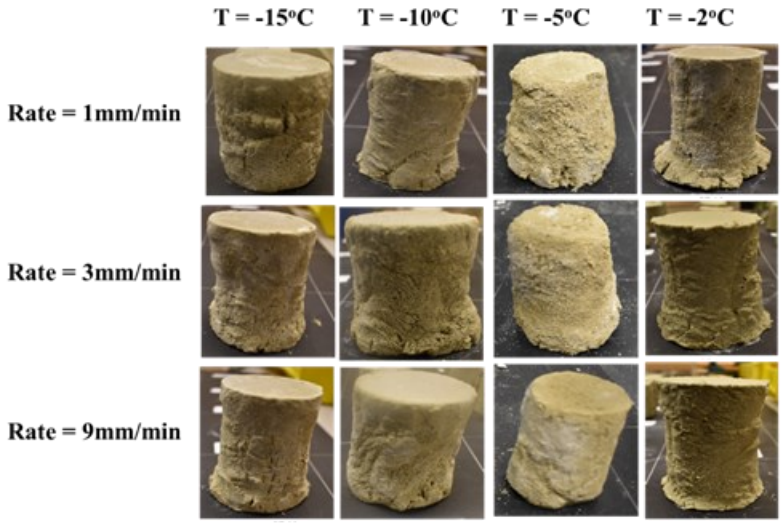

Figure 3-2 Post-failure photos of UCS test samples at different applied temperatures and deformation rates.

Our experimental data also yields temperature-dependent mechanical properties (Young's modulus, Poisson ratio, and uniaxial compressive strength) covering a temperature range from 0°C to -15°C. The nonlinear relations are summarized in Table 3-2.

Table 3-2 Nonlinear equations for temperature-dependent mechanical properties of the frozen clay sandy soils

No.	Strength Parameter	Equation	Loading rate	M	N	Q	R^2
1	Young's modulus	$E = M\left(\frac{T}{T_0}\right)^N + Q$	9 mm/min	12.85	1.082	16.952	0.999
			3 mm/min	7.235	1.261	12.621	0.999
			1 mm/min	4.468	1.31	9.594	0.999
2	Poisson's ratio	$\mu = M\left(\frac{T}{T_0}\right)^N + Q$	9 mm/min	-0.069	0.3	0.340	0.986
			3 mm/min	-0.065	0.3	0.361	0.979
			1 mm/min	-0.069	0.3	0.399	0.980
3	Uniaxial compression Strength	$C_0 = M\left(\frac{T}{T_0}\right)^N + Q$	9 mm/min	0.41	0.996	0.547	0.998
			3 mm/min	0.28	1.082	0.547	0.999
			1 mm/min	0.206	1.11	0.307	0.999

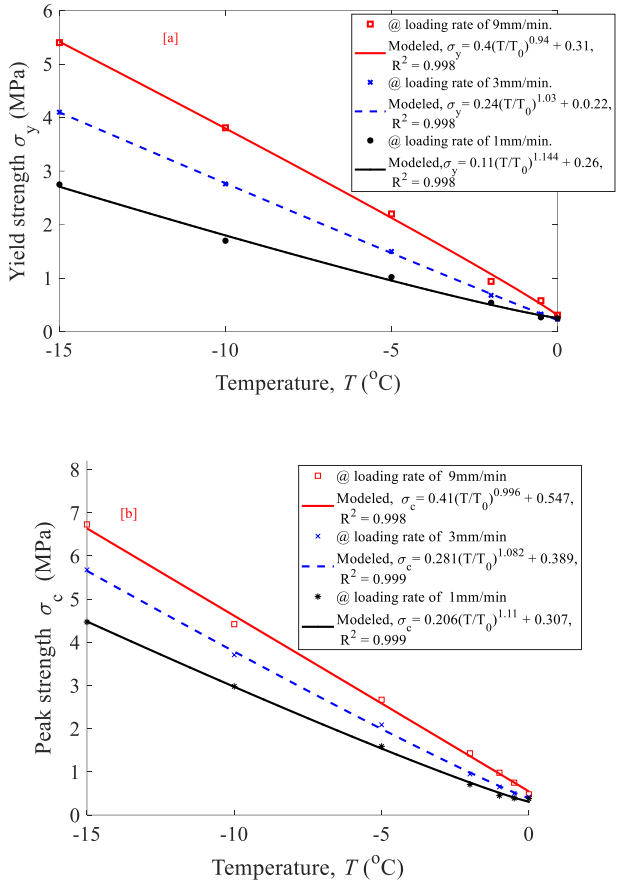

Figure 3-3 Relations between temperature, (a) yield strength and (b) uniaxial compressive peak strength for studied frozen sandy clay samples.

Figure 3-3 illustrates that both yield strength and peak strength increase with the decrease of temperature and increase of loading rates. Nevertheless, the temperature parameter is more dominant regarding the increase of the yield strength and peak strength when the temperature is between 0oC and -5°C, while the loading rate becomes dominant when the temperature is between -5°C and -15°C. At the highest loading rate (i.e. 9mm/min.), the elastic limit and peak strength increase 5.7 times and 4.7 times respectively when the frozen temperature decreases from -2°C to -15°C. At the lowest loading rate (i.e. 1mm/min.), the elastic limit and peak strength increase 6 times and 6.31 times respectively. Similarly, at the lower temperature (i.e. -15°C), the elastic limit and peak strength increase 2 times and 1.5 times respectively when the loading rate increases from

1mm/min. to 9mm/min. At a higher temperature (-2°C), the elastic limit and peak strength increase 1.74 times and 2 times, respectively.

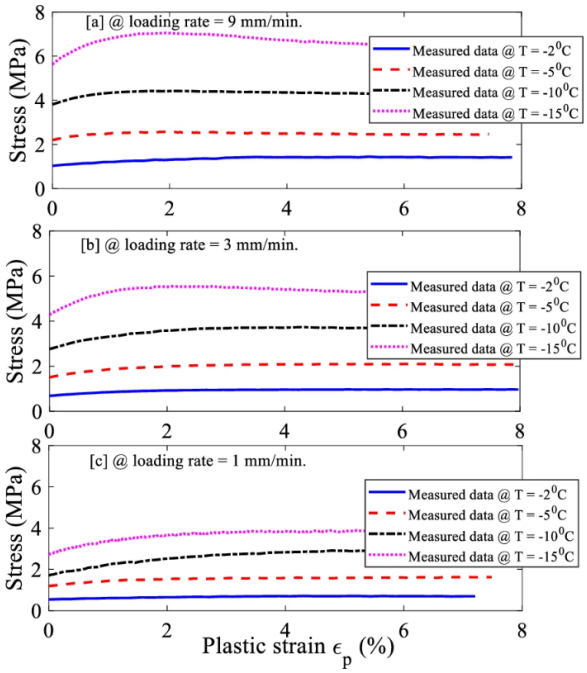

Figure 3-4 Temperature-dependent hardening relations applied for FEM modeling.

The obtained temperature and rate-dependent hardening relations for the uniaxial compression stress as a function of plastic strain are demonstrated in Figure 3-4. The relations were programmed as an input file in Abaqus. In this study, separate yield function is not developed but the available constitutive model (i.e., Drucker-Prager) was utilized by explicitly considering the plastic strain as temperature and rate dependent. The data is coded as a table of values that are linearly interpolated. The value of friction angle (26.1°) is obtained using the approach proposed by Li and Wong (Li and Wong 2016) based on the sample's clay fraction and minerology. The applied dilation angle (7°) was derived based on the equation given by Bolton (Bolton 1986). Additionally, both dilation angle and frictional angle are used as constant values, thus the temperature dependency of friction angle is neglected.

3.4 Numerical modeling and analyzing uniaxial compressive behaviors

3.4.1 Finite element configuration and material parameters

We used Abaqus (Dassault Systèmes 2016) to conduct finite element modeling of uniaxial constitutive behaviors. The linear Drucker-Prager model was used along with the Singh-Mitchell creep law to characterize the time-dependent behavior. It should be noted that the rate-dependent plastic behavior and creep behavior using stress relaxation approach are accounted for separately. A displacement-controlled condition is applied on the top of the soil sample and the bottom is kept fixed while the temperature is held constant as an analogy to the condition in laboratory tests (Girgis et al. 2020). The 8-node linear brick (C3D8R) element was utilized in our finite element modellings, where a reduced integrated scheme was adopted. The Newton method was used to solve the nonlinear equations with the unsymmetric matrix storage approach. For the numerical analysis, the required mechanical parameters are based on the equations presented in Table 3-2. Parameters of frictional angles are from our recent publications (Akhtar and Li 2020b, 2023). The creep parameters are based on the result by Girgis et al. (Girgis et al. 2020). The finite element model along with the generated mesh and the location of monitoring points (i.e. Point 1 is for vertical stress and axial strain and Point 4 is for lateral strain) are illustrated in Figure 3-5. The size of the simulated sample is according to those used in laboratory tests (4 inches in height and 2 inches in diameter). The mesh is kept small enough that a further increase in mesh numbers does not affect the overall results. Thus, a mesh convergency was calibrated. It should be noted that the selected monitoring point (Point 4) for the lateral strain is at the maximum intensity of the strain location.

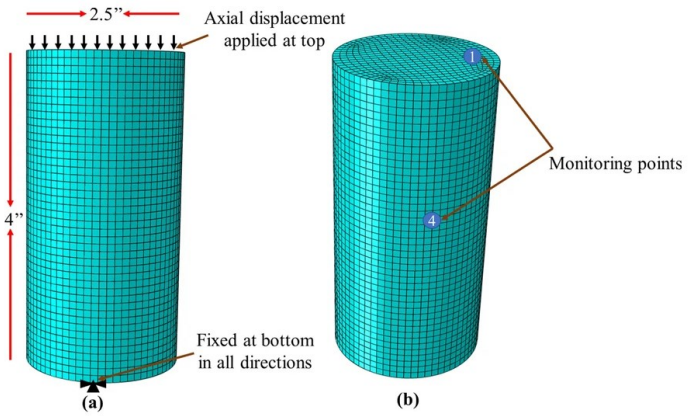

Figure 3-5 Sketch showing the (a) FEM mesh with geometry dimensions and (b) key monitoring points.

3.4.2 **Simulation results and analysis**

Monotonic compression behaviour

Using the above-mentioned approach, we were able to perform a numerical analysis of the time-dependent deformation behaviors of frozen soil under the uniaxial compression loading. It should be noted that the hardening relations were programmed as a user-defined input file in Abaqus. The hardening behavior was explicitly made temperature and rate dependent which can capture the yield behavior of frozen soil under uniaxial compression effectively. Given considerable laboratory data on the stress-strain relations at different temperatures, values are linearly interpolated to cover a broad range of temperature and strain rate conditions. Thus, for a specific simulation, there is no need to set up separate yield function and hardening relations at different applied temperatures or deformation rates. Such an approach can be considered applicable for a field case since the exact temperature and strain rate condition is changing during the modeling process.

Contours of Mises equivalent stress distribution in the samples are given in Figure 3-6, which shows the stress dependency of two selective strain rates at a constant temperature of -15ºC. The stress is deducted from the integration points. At this stage, numerical analysis contours are not

able to show the brittle cracks in the sample. However, the increase in equivalent stress intensity can be visualized from these contours at different loading rates.

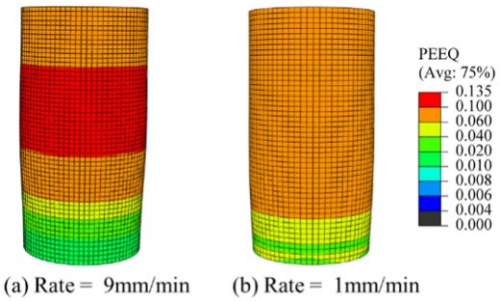

Figure 3-6 Modeled PEEQ distributions in frozen sandy clay soil at constant temperature (T= -15 oC) using deformation rates of (a) 1mm/min, and (b) 9mm/min.

Figure 3-7 shows the stress-strain relationships between the modeled results and experimental data at various frozen temperatures under different loading rates. The curves indicate that the peak strength of frozen soil increases with the decrease in temperature and the increase in loading rates. The strength degradation characteristics change from ductile behavior to brittle with the increase in loading rates. This brittle mechanical strength behavior is more dominant at lower temperatures (i.e. -5^{o}C, -10^{o}C, and -15^{o}C). This is because the strength of pore-ice increases at these temperatures, which increases the incorporative rate-dependent characteristics in frozen soil. Figure 3-7(a)-(b) shows that the post-peak shear softening vanishes with a decrease in temperature under constant loading rates, while Figure 3-7(c) displays curves without a post-peak softening behavior. Figure 3-7 also calibrates that measured stress-strain relations are properly modeled using the proposed approach, where the Drucker-Prager plastic model combined with rate- and temperature-dependent hardening is applied. All three deformation stages (i.e. linear elastic, hardening, and softening behaviors) were captured. However, it should be noted that some deviations between measured and modeled curves for the cases of lower temperatures and higher loading rates are also reflected in Figure 3-7. The differences are mainly due to the adopted programmed temperature- and rate-dependent hardening laws. The data for hardening is coded as

a table of values that are linearly interpolated, the generated hardening function cannot perfectly capture the hardening behavior of all the cases with different strain rates and temperatures. Our previous approach of adopting separate hardening function in numerical modeling for cases with different temperatures and strain rates has generated better fitting between measured and modeled results (Akhtar and Li 2020a). However, that approach requires a manual update of hardening function at a given temperature and strain-rate condition. A theoretical development of temperature- and rate-dependent hardening law with the consideration of pore ice responses should be conducted to generate more comprehensive modeling results.

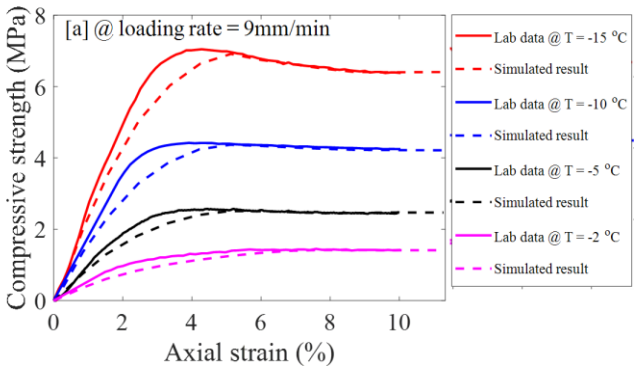

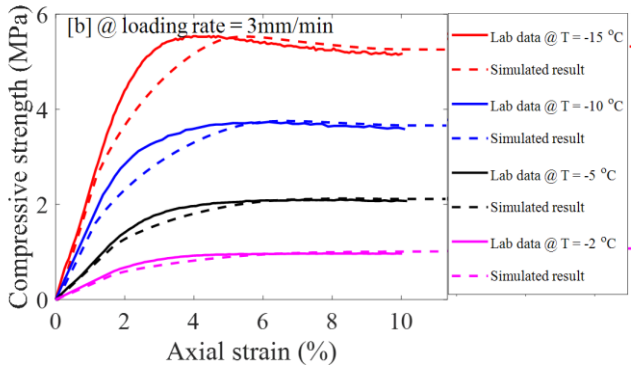

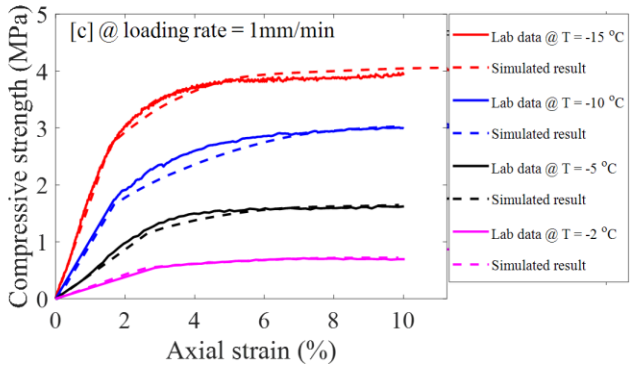

Figure 3-7 Measured and modeled stress-strain curves at various strain rates and temperatures: (a) T = -15oC, (b) T = -10oC, (c) T = -5oC, and (d) T = - 2oC.

The axial strain vs. volumetric strain relationship illustrates the deformation characteristics of frozen soil and determines the critical deformation characteristic. Figure 3-8(a) and (b) illustrate the measured and modeled axial-volumetric strain relations at various temperatures and under different loading rates. These plots show that volumetric strain increases with the decrease of loading rate; however, this phenomenon is more dominant at lower temperatures (i.e. -5°C, -10°C, and -15°C). The simulation results obtained from the numerical analysis are reasonably promising with the experimental data before the post-peak strength. Once the peak of strength is achieved, the simulated axial-volumetric strain plots fall apart from the experimental data. This is because of major cracks and fractures that occur on the surface of the soil sample during lab testing, which cannot be captured in the numerical analysis at this stage. However, as is shown in Figure 3-6, the equivalent plastic strain contours predict the intensity of deformation in the frozen soil at different loading rates. In addition, it depends on the position of strain gauges on the soil sample. In numerical analysis, we simply selected the area where the maximum lateral strain was produced. This systemic problem will be illustrated and discussed in the discussion section.

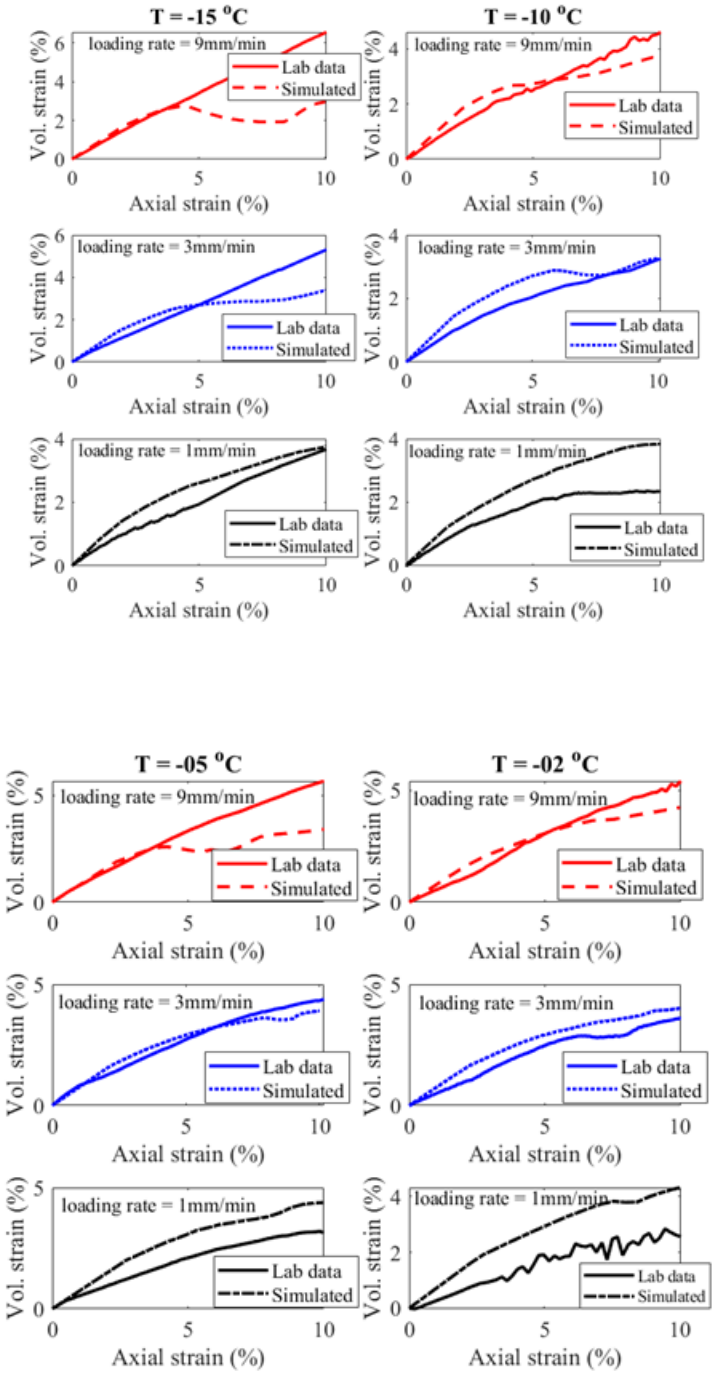

Figure 3-8 Measured and modeled axial-volumetric strain curves at various strain rates and temperatures: (a) T = -15oC and -10oC, (b) T = -5oC and -2oC.

Cyclic loading with stress relaxation

The uniaxial compression behavior under cyclic loading with stress relaxation is also simulated using the proposed approach. Shown in Figure 3-9, it is presented that the time-dependent model (Singh Mitchell model) used for simulating the creep deformation in frozen soil can generally capture the trend of deformation characteristics. In particular, the stress-strain relation tends to recover as a state comparable to the monotonic loading condition after three cycles of relaxations. However, Figure 3-9 shows that the simulated curves could not capture the magnitude of stress degradation during stress relaxation. The reason can be due to the significant strain localization due to stress concentration near the contact area between the loading ram and the sample's tops as reflected in Figure 3-2, which cannot be captured in our simulation. A better experimental set up should be used in the future to mitigate such sample end effect.

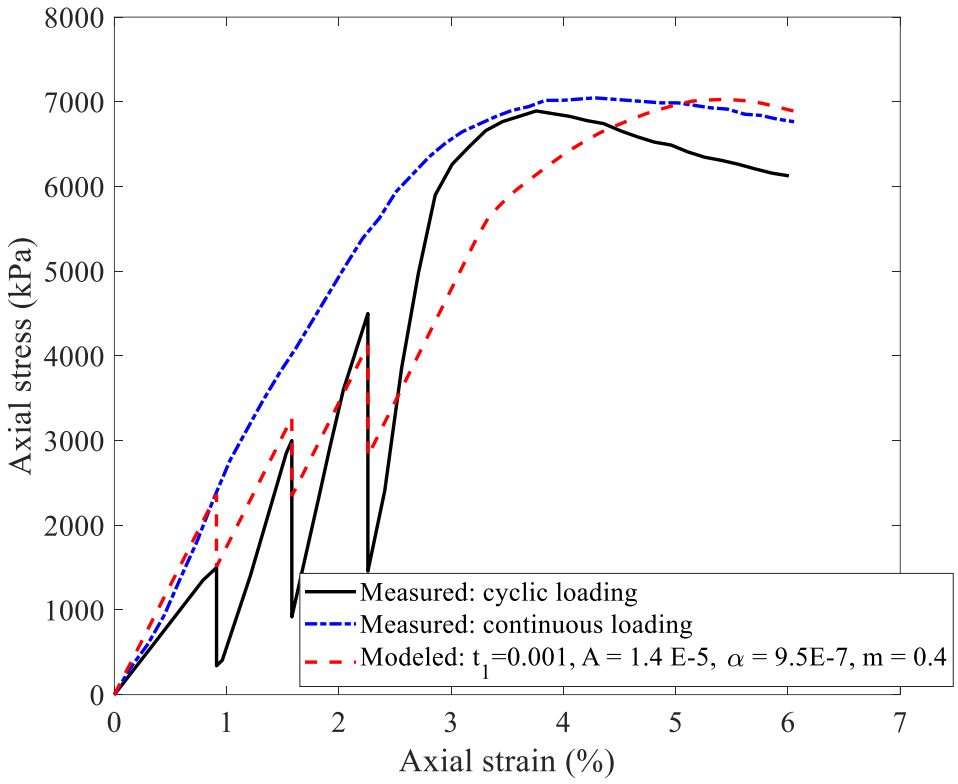

Figure 3-9 Measured and modeled stress-strain curves under cyclic loading and stress relaxation conditions (T = -15oC , loading rate = 9mm/min).

3.5 Discussions

3.5.1 Volumetric deformation behavior

The selected constitutive model is generally effective in quantifying the deformation characteristics of the studying frozen sandy clay soil. Measured axial-volumetric strain relations can generally be simulated for the part before the peak strength (Figure 3-10). However, measured post-peak dilation behavior for the case with the high deformation rate cannot be simulated (Figure 3-10b). At a lower loading rate, the simulated result is closely following the measured curve because there is no dilation behavior or post-peak softening behavior (Figure 3-10c and Figure 3-10d).

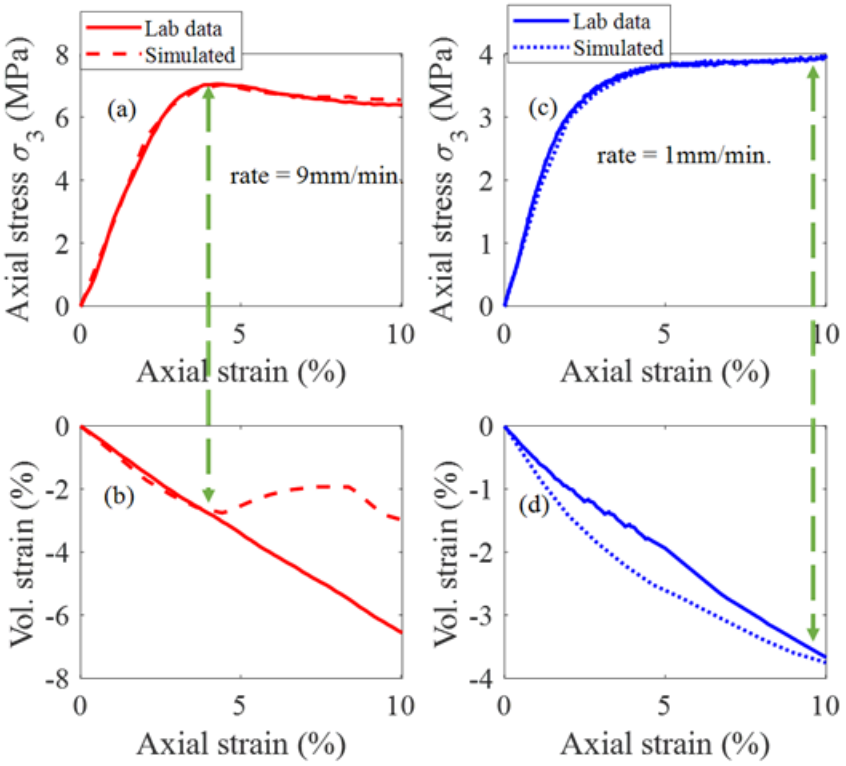

Figure 3-10 Measured and modeled stress-strain and volumetric-axial strain relations at T = -15oC.

The difference in characterizing the volumetric deformation behavior can be due to the pressure-induced melting behavior. During laboratory testing, we noticed some cracks at sample ends when the applied load is beyond the sample's strength (Figure 3-2). Some extra laboratory tests are required to examine the pressure-induced melting behavior. The enlarged sample ends were contributed by the shrinkage of the body part. The lateral strain gauge will always indicate that the sample is under compaction. Thereby, the post-peak dilation cannot be captured by the lateral strain gauge (Figure 3-11). The impact of such a deformation characteristic is not incorporated in the numerical model. It is also recommended to try different plastic potential functions to produce better axial-volumetric strain relations for a future study.

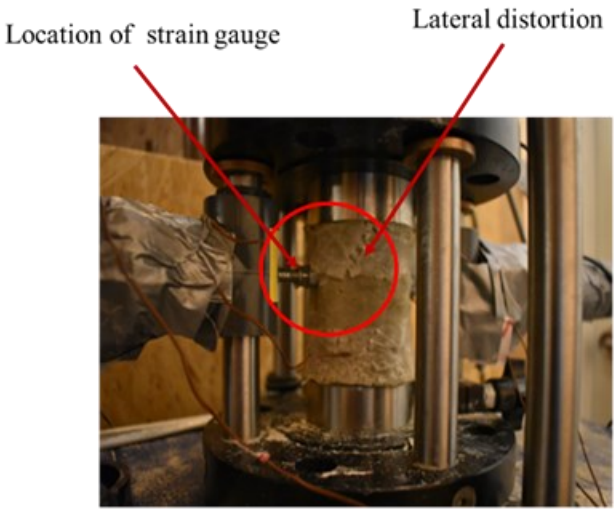

Figure 3-11 Diagram showing the position of strain gauges and a soil sample at failure.

3.5.2 **The contribution from creep deformation**

The present simulation considers rate-dependent deformation and creep deformation separately. The reason can be demonstrated by showing the strain components from the strain development curves (Figure 3-12). The results indicate that creep deformation contributes to a very small strain when compared with the plastic part under such a short testing period. Thus, the creep itself cannot

generate the short-term rate-dependent stress-strain relation. A rate-dependent hardening model is needed to quantify the rate-dependent stress-strain relation. Nevertheless, the necessity of applying the creep model is justified in the cyclic loading results (Figure 3-9). The creep should be considered in the long-term deformation analysis or stress relaxation analysis.

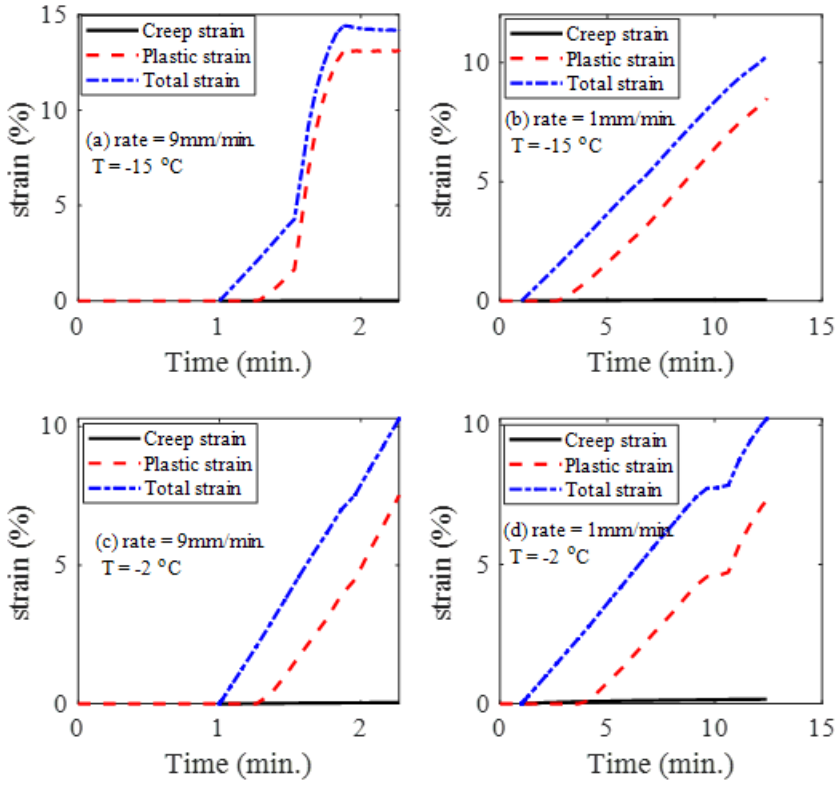

Figure 3-12 Curves showing the simulated deformations from different components for samples at different loading rates and temperatures.

3.6 Concluding remarks

The numerical modeling of the time-dependent uniaxial compressive behaviors of an artificial frozen sandy clay has provided valuable insights into the mechanical response under different sub-zero temperature conditions. The complex stress-strain behaviors of frozen sandy clay soils can be modeled using the Drucker-Prager model combined with a rate- and temperature-dependent hardening function. Both the strain hardening followed by post-peak softening and pure strain

hardening behaviors can be characterized using the proposed FEM modeling approach. The user-defined program embedded in the simulation makes it applicable for field practice by leveraging the varied temperature and strain rate conditions. Both a rate dependent model and a creep model should be applied to carry out a comprehensive time-dependent analysis of the uniaxial compressive behavior of frozen soils. For a short-term study, the creep deformation makes little contribution to the strain behavior and has a limited impact on the rate-dependent stress-strain relations. However, the creep deformation is essential for the stress relaxation process and a creep model should be applied in the constitutive modeling.

Preface to Chapter 4.

Frozen clay soils play a critical role in the stability of infrastructure in cold regions, yet their tensile strength and failure mechanisms remain challenging to quantify accurately. With climate change accelerating permafrost thaw, understanding these materials' mechanical behavior is essential for predicting and mitigating geological hazards such as ground settlement and thaw-induced slumps. Despite extensive research on frozen soils, limited studies have focused on the tensile yield and failure characteristics, particularly at temperatures close to freezing. This chapter presents a comprehensive investigation into the tensile strength of frozen clay soils through laboratory testing and numerical modeling. A hyperbolic Drucker-Prager model is employed in finite element simulations to explore the tensile yield behavior and validate the experimental findings. The results provide valuable insights into the rate- and temperature-dependent characteristics of frozen clay soils, contributing to the advancement of geotechnical engineering in permafrost regions. By bridging the gap between laboratory testing and numerical simulations, this study offers a more reliable approach to evaluating the tensile strength of frozen clay soils. The findings will support engineers and researchers in designing safer infrastructure and improving risk assessments for projects in cold environments.

Chapter 4

4 Characterizations of tensile yield and failure processes of frozen clay soils: laboratory testing and numerical modeling.[2]

4.1 Abstract

An accurate characterization of the tensile failure processes of frozen soils under a warming environment is critical for predicting geological disasters such as thawing-induced slumps. In this study, the approaches of rod bar splitting test and double punch test are applied to measure the tensile strength of artificially prepared frozen sandy clay samples with the same clay fraction. The tests are conducted in a temperature-controlled cold room, and the applied temperature ranges from -15°C to 0°C. Our laboratory tests demonstrate that the rod bar splitting tests tend to overestimate frozen clay soil's strength, which is owing to the increase in the contact area between loading strips and samples. By contrast, the double punch tests keep the same contacting area and provide more reliable results. The tensile strength-temperature relationships covering a temperature from -15°C to 0°C are modeled using an updated power law function. Our results show that the measured tensile strengths are highly dependent on the applied deformation rates. Finite element numerical simulations are conducted to investigate the tensile yield and failure processes in the studied frozen

[2] A version of this manuscript has been published in the journal of *Bulletin of Engineering Geology and the Environment* (2022).

soil samples. The stress paths at key monitoring points are retrieved to demonstrate the tensile yield behavior. Impacts from the sample size and experimental conditions on estimated tensile strengths are analyzed, and optimized sample and puncher sizes are determined. Our numerical results confirm that the double punch test is an effective and reliable approach in measuring the tensile strength of frozen clay soils.

Keywords: Double punch test; frozen clay soil; tensile yield; hyperbolic Drucker-Prager model; laboratory tests; stress paths

4.2 Introduction

The tensile strength characteristics of frozen clay soils have potential influences on ice lens initiation and the growth that are closely associated with the stabilities of engineering structures in cold regions (Akagawa and Nishisato 2009, Zhou et al. 2015, Ji et al. 2019). Numerous infrastructures (e.g., foundations and pipelines) are already, or will soon be, constructed in permafrost regions (Jin et al. 2008, Le et al. 2018). Long-term records indicate that the ongoing global warming has resulted in the thawing of some permafrost regions, which leads to extensive geological disasters including slumps and ground settlements causing damage to infrastructures (Andersland and Ladanyi 2003, Wang et al. 2019a). The characterization of mechanical properties of frozen clay soils is indispensable for projects in cold regions. Since the tensile strength of clay-related geomaterials is closely related to the tensile yielding or cracking behavior involved in theoretical analysis of slope stabilities (Park and Michalowski 2017) or soil-structure interactions (Liu et al. 2008a, Akhtar and Li 2020b), the experimental investigations on the tensile strengths of clay or frozen clay soils increasingly draw the attention of researchers all over the world (Akagawa and Nishisato 2009, Zhou et al. 2015, Li et al. 2019b). Frozen clay soils displayed significant plastic behaviors, which are affected by the moisture content, clay mineralogy, clay contents, loading rate, and applied temperature. Thus, there are unavoidable uncertainties in the tensile strength measurements.

Bragg and Andersland (Bragg and Andersland 1981) conducted split cylinder tests on frozen sand and indicated that the tensile strength results appear to be independent of deformation rates. They also reported that split cylinder tests might not be feasible for warm frozen soils due to the sample's localized compression in the area of the loading strips (Bragg and Andersland 1981). Zhou et al. (Zhou et al. 2015) applied split cylinder tests on warm frozen clay soils under various temperatures

warmer than -2°C. Their results indicated that the relationship between the tensile strength of frozen clay soils and corresponding negative temperatures can be described by a power law function. They also observed that the measured peak tensile strength is independent of the applied loading rate, which varies from 1mm/min to 4 mm/min. Clay contents of soil samples used in the study by Zhou et al. (Zhou et al. 2015) range from 12% to 20%. Christ and Kim (Christ and Kim 2009) studied the tensile strength of frozen silt using the direct tensile method on dumbbell shape samples. Their results show that the tensile strength of frozen silt increases with an increase in the sample's moisture content and a decrease in temperature. However, the strain rate impact was not studied. Akagawa and Nishisato (Akagawa and Nishisato 2009) investigated the tensile strength of Fairbanks silt with a specially designed dumbbell, which facilitated frozen sample preparation and tensile strength testing using a single apparatus. The measured relationship between tensile strength and negative temperature displays a nonlinear increasing trend. However, the results are sparsely scattered, which resulted in a low coefficient of determination. The impact of the strain rate was not explored in their study either. Their method would not be appropriate for measuring the tensile strength of frozen clay soils, because the sample preparation procedure would require a long time to complete given the low consolidation coefficients of clay soils. Haynes et al. (Haynes et al. 1975, Zhu and Carbee 1984) both studied the relationship between strain rate and tensile strength of frozen silts and reported that a lower strain rate leads to ductile failure and will result in a lower tensile strength. Azmatch et al. (Azmatch et al. 2011) applied a four-point bending test to study the tensile strength of frozen Devon silt samples under a temperature near freezing (0°C to -1.5°C) at different deformation rates (0.08 mm/min to 8.0 mm/min). Their results show that the temperature, the deformation rate, and the unfrozen water content all affect the tensile strength of the soil, particularly at temperatures close to 0°C. The four-point bending method may not be

effective in measuring the tensile strength of frozen clay soils. The highly plastic nature of warm frozen clay soils can induce large strain localization at sample-tool contact surfaces like what is involved in split cylinder tests.

Shen et al. (Zhongyan et al. 1995) was the first to apply the double punch test (DPT) to study the tensile strength of frozen soils at temperatures varying from -2°C to -15°C and determined that the axial splitting method was more feasible and reliable for undisturbed frozen soils. Limited data from the literature were found regarding the effectiveness and efficiency of using the double punch method to measure the strength of frozen clay soils at temperatures close to the ice melting point (0 to -2°C). In addition, the yield and failure processes in different parts of a frozen soil sample during a double punch test was never examined. A comparison between results from double punch test and direct tension test was not investigated. The double punch test has been used extensively to measure the tensile strength of concrete and clay soils at the room temperature condition (Chen and Yuan 1980, Fang et al. 2006, Wen et al. 2013). However, a comprehensive study on its effectiveness of being used in a cold environment is very necessary.

In summary, there are various experimental approaches for studying the tensile strength of frozen soils, and different observations are recorded (e.g., the effect of strain rates on peak tensile strength). A reliable characterization of the tensile strength of frozen soils is critical for site selections and designs of engineering infrastructures, early warning of slumps in permafrost regions due to climate change, and the stability analysis of artificially frozen ground. A thorough understanding of the tensile mechanical behavior and its relationship with temperature requires a large number of specimens with similar compositions and micro-structures. The challenges in obtaining in-situ frozen clay soils have affected the theoretical development in this field. In addition, previous measurements on the tensile strength of frozen soils were most conducted on

soils with low clay contents and the samples were treated as brittle material. The investigation on the tensile yield and failure behaviors of high clay content frozen soils is limited. In this study, a series of laboratory tests were performed on high clay content artificial frozen sandy clay samples to measure the tensile strengths using multiple self-designed approaches. Finite element modeling was conducted to examine the effectiveness of using the double punch test to measure the tensile strength of frozen clay soils.

4.3 Experimental investigations

4.3.1 Artificial frozen clay soil samples used

To permit control and repeatability, a large quantity of artificial frozen clay soils with the same mineralogy compositions and stress history were prepared for the laboratory tests. Sand clay samples were prepared by using a specially designed consolidation equipment (Girgis et al. 2020). The materials used in this research were silica sand 7030, Bentonite Western 325M, and saline water as the pore fluid. According to ASTM (ASTM D2488-17e1 2017), the prepared bentonite-sand mixture was classified as grey, inorganic sandy clay of high plasticity, and well-bonded soil. All mixtures were composed of 50% sand and 50% clay by dry weight. The specific gravity value of the mixture was measured as 2.63. Saline water with a concentration of 1 g/L (NaCl solution) was used to prepare the mixtures. The reason of using saline water is to simulate the saline pore fluid present in some clay soils (L'Heureux et al. 2014). Liquid limit (%) and Plastic Limit (%) of bentonite-sand mixtures were measured as 97 and 34, respectively. The bentonite-sand mixtures were consolidated under a pressure of 60 kPa to replicate a shallowly buried field condition. After consolidation, the soil was ejected, and placed in a freezing mold. Basic physical properties including bulk density and water content of samples were measured on five selected samples and included in Table 4-1. Clay soil samples with a bulk density of 1.53 and moisture content of 59%

were obtained upon the completion of consolidation. The sandy clay soil samples were then placed into a fast freezer with a minimum temperature of -40°C to produce frozen soil samples. A vacuum seal has been applied to prevent the generation of ice lenses (Girgis et al. 2020). All the prepared frozen clay soils sample hold a dimension of 50.8 mm (2 inches) in height and 50.8 mm in diameter.

Table 4-1 Physical properties of prepared bentonite-sand samples before freezing

Dimension		Bulk density (g/cm^3)	Water content (%)
Height (mm)	Diameter (mm)		
50.8	50.8	1.53	59

4.3.2 **Experimental setup and procedures**

All tensile strength tests were carried out in an environmental chamber in the Building Envelope Performance Laboratory (BEPL) at Concordia University. For a comparison purpose, we applied two approaches to conduct indirection tension tests. The setups for the rod bar splitting test (RST), and double punch test (DPT) are displayed in Figure 4-1. Among two different approaches, RST is a typical splitting test using a loading strip for measuring the tensile strength of brittle materials (ASTM D3967-16 2008, Abrishambaf et al. 2015). The application of DPT in frozen soil strength measurement traces back to 1995 (Zhongyan et al. 1995), but there is very limited follow-up research on the effectiveness of using DPT to measure the tensile strength of frozen clay soils. We designed a special sub-loading frame that can handle two different tensile strength tests while only changing loading strips and sample orientations (Figure 4-1). The sub-frame was provided with two pairs of loading tools made from stainless steel of grade 420. The loading strip of the RST was a rod with a diameter of 8 mm (Figure 4-1a) while a pair of cylindrical punchers with a diameter of 12.7 mm (½ inch) was used for DPT (Figure 4-1b).

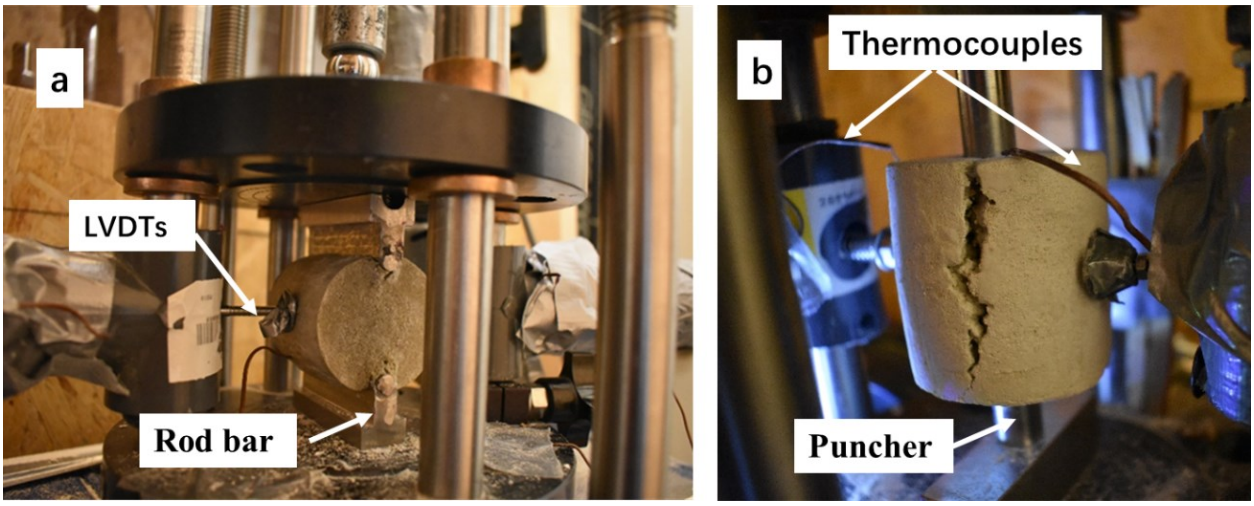

Figure 4-1 Picture showing the setup of (a) rod bar splitting test (RST), and (b) double punch test (DPT).

The vertical load was provided with a motorized, automatic loading system. The axial displacement was measured by using a high accuracy linear variable displacement transducer (LVDT) with a range of 50 mm. The lateral deformations were obtained with two high accuracy LVDTs with a range of 50 mm manufactured by Solartron Metrology. All LVDTs were placed into a polyvinyl chloride (PVC) tube with the same external diameter and the back ends were closed using a threaded cap. The tubes were then placed in a PVC sleeve and the space between them was filled with a dense spray foam to ensure proper insulation. All LVDTs were calibrated at a temperature ranging from -20°C to +20°C before starting the experimental work. Two thermocouples (type T) were used in measuring the temperature of the frozen soil sample and the ambient temperature, respectively. The first thermocouple was adjusted to be in contact with the sample, and the second one was fixed close to the sample to measure the ambient temperature (Figure 4-1). All thermocouples were calibrated with a resistance temperature detector. Samples were placed in BEPL with the required temperature for a minimum of 24 hours. The applied temperature ranges from -15°C to 0°C. During tests, displacement-controlled loadings with different deformation rates (1 mm/min, 3 mm/min, and 9 mm/min) were applied to soil samples until failure, and a data acquisition system was used to record all the measurements. The data of

vertical loads, vertical displacements, horizontal displacements, and post-failure pictures of samples were obtained.

4.3.3 **Results and analysis**

Different failure modes were noticed for samples at different applied temperatures and strain rates. Taking samples after loading at T = -10°C (Figure 4-2a) and T = -1°C (Figure 4-2b) for example, the contact area between loading strips and samples for RST is larger for the case with a low strain rate (1 mm/min) than that with a high strain rate (9 mm/min). At a temperature close to the freezing temperature (-1°C), Figure 4-2b shows that there is not any tensile cracking behavior in samples when the loading is applied at a slow rate (1mm/min) using RST. By contrast, the puncher-soil contacting area is consistent during a double punch test, and samples always display tensile cracks after DPTs at different temperatures. At a high strain rate (9 mm/min), the sample for DPT displays a double-fracture failure mode. However, the sample only displays a single failure plane when the applied strain rate is 1 mm/min.

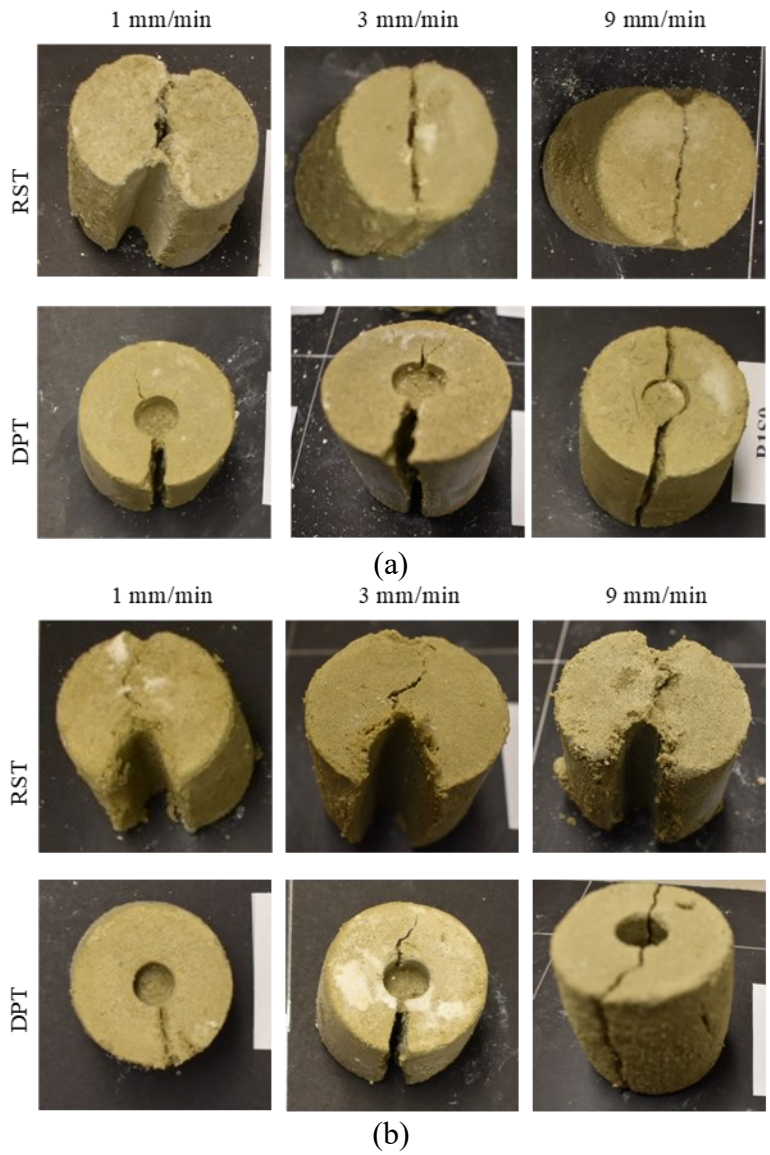

Figure 4-2 Bentonite-sand samples after indirect tensile tests at (a) T =- 10 °C and (b) T = -1°C.

Typical load-displacement curves of an RST and a DPT are displayed in Figure 4-3. The tensile strength of each tested sample is calculated at two different load levels. As shown in Figure 4-3, the load at the end of the linear portion of the load-displacement curve is used to calculate the yield tensile strength. The maximum applied load is selected to determine the peak tensile strength. According to ASTM (ASTM D3967-16 2008), the tensile strength obtained from RST is determined using:

$$\sigma_t = \frac{2P}{\pi LD} \tag{4.10}$$

where σ_t is the tensile strength; P is the applied load at yield or failure; D is the diameter of the sample, and L is the thickness of the sample. Equation 4.10 assumes that a line load is applied to the sample, and tensile failure occurs at the center of the disk where the maximum tensile stress is located.

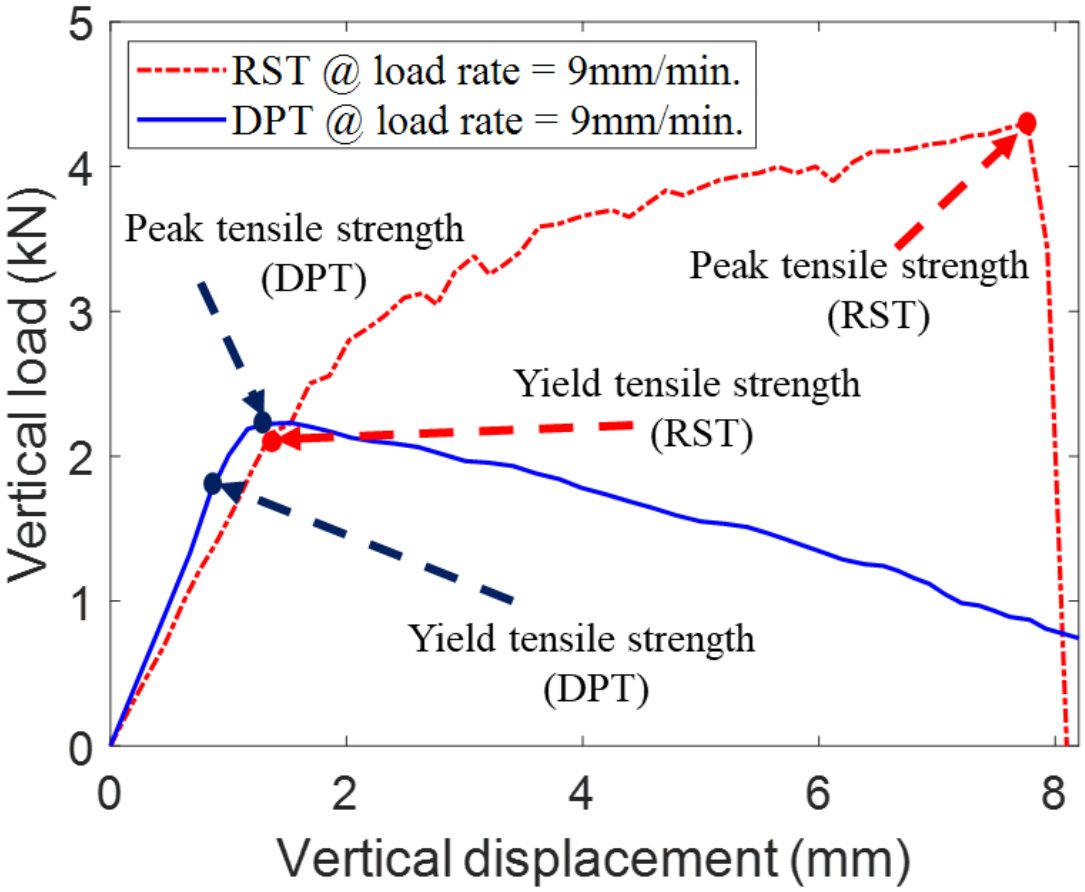

Figure 4-3 Graph showing the yield and peak tensile strengths for bentonite-sand samples tested by different approaches (T= -10°C).

In a DPT, a cylindrical sample is compressed concentrically and vertically through two cylindrical steel punchers on the sample's top and bottom surfaces. The tensile strength from DPT can be calculated using (Fang and Daniels 2017):

$$\sigma_t = \frac{P}{\pi\left(KbL - a^2\right)} \tag{4.11}$$

where σ_t is the tensile strength; P is the punch load at yield or failure points; b is the sample radius; a is the punch radius; L is the specimen length; K is a material constant which is given a value of 1.0 for soil (Fang and Daniels 2006). It should be noted that the tensile strength calculation is based on the theory of perfect plasticity. Fang and Chen (Fang and Chen 1971) indicated that a height-to-diameter ratio of the specimen varying from 0.8 to 1.2 and a ratio of diameter of the specimen to the diameter of the punch varying from 0.2 to 0.3 are suitable for DPTs on soils.

Shown in Figure 4-4, the tensile strength results show remarkable differences between different approaches. The yield tensile strengths measured by RST and DPT are comparable (Figure 4-4a). However, the peak tensile strength values measured by RST are almost twice the values obtained by DPT under the same temperature and loading conditions. This difference should be owing to the increase in the contact area between loading strips and samples in RST (Figure 4-2). In a successful rod bar splitting test, a line load is supposed to be generated along the disc. However, due to the local plastic deformation, there is a huge increase in the contact area between the rod bar and the soil sample. Thus, the chance of creating a maximum tensile stress in the center of the disc is affected. By contrast, the DPT keeps the same loading area and holds the chance of generating maximum tensile stress along the annulus region of samples. The DPT results will be examined to illustrate the dependency of tensile strength on temperatures and applied deformation rates. It should also be noted that an appropriate sample size is also important in obtaining a reliable tensile strength result. Related justifications will be presented in the discussion section.

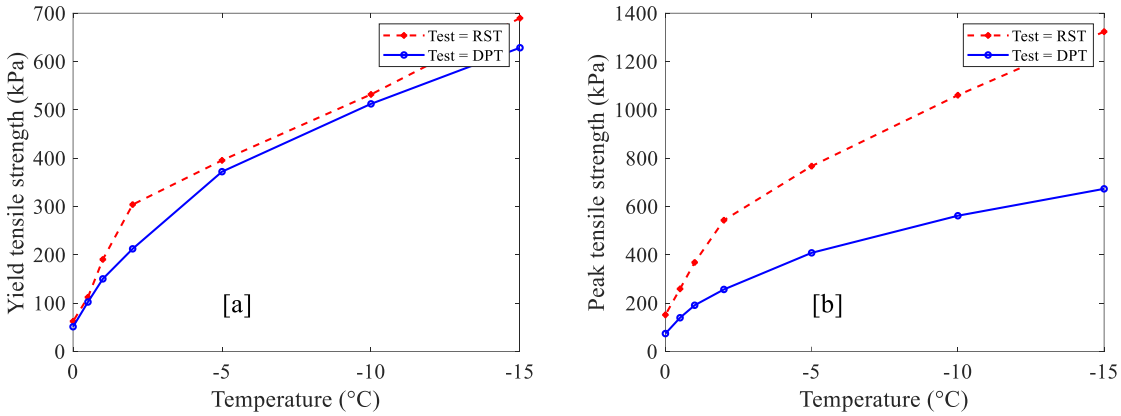

Figure 4-4 Derived yield and peak tensile strength-temperature curves for bentonite-sand samples (deformation rate=9 mm/min).

Load-displacement curves of all DPT results for samples at the deformation rate of 9 mm/min are displayed in Figure 4-5. Significant differences in vertical load-vertical displacement relationships are found at different temperatures. At temperatures lower than -5°C, there is a clear post-peak softening behavior. At temperatures close to the freezing point (-2°C to 0°C), a single hardening behavior is noticed.

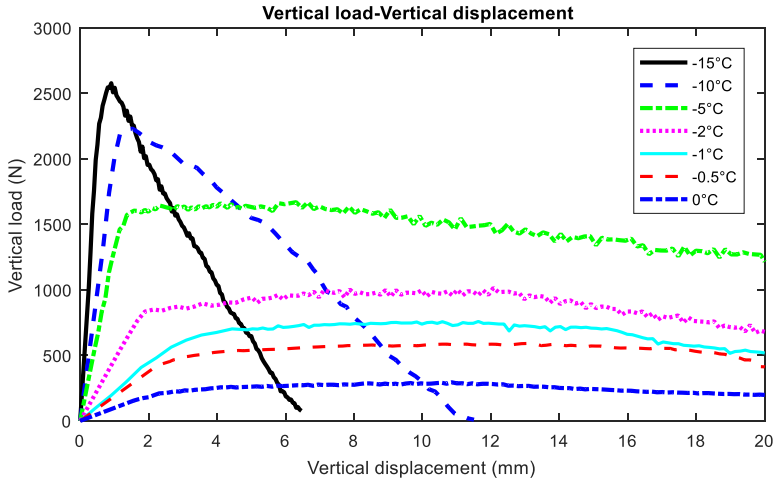

Figure 4-5 Derived yield and peak tensile strength-temperature curves for bentonite-sand samples (deformation rate=9 mm/min).

Previous studies show that frozen soil strengths vary nonlinearly with temperature (Hu et al. 2013, Zhou et al. 2015). Such nonlinear correlation should be closely related to the temperature-

dependent unfrozen water content in the frozen soil. The tensile strength of frozen soil is mainly contributed from pore ice cementation. When the temperature decreases from 0 oC to -5 oC, there is a significant decrease in unfrozen content in frozen soil (Nixon 1992). Upon a further decrease in temperature, there is little change in unfrozen water content. However, the tensile strength of ice keeps on increasing with the decrease in temperature (Haynes 1978). The research by Nixon (Nixon 1991) provides a relationship between unfrozen water content and temperature as a non-linear power law equation. To quantify the tensile strength-temperature relations, we applied a modified power law function (Equation 4.12) to properly consider the strength at T = 0°C:

$$\sigma_t = A\left(\frac{T}{T_0}\right)^B + C \tag{4.12}$$

where , and are parameters to be determined, and is a reference temperature (-1°C is applied herein). Solid correlations between the tensile strength and temperature are developed and plotted in Figure 4-6, where the tensile strength has a remarkable increase with a decrease in temperature. This power law function is effective for the broad temperature range from -15°C to 0°C. The significant impact from deformation rates is indicated with the difference between the curve fitting parameters. In order to demonstrate the sensitivity of parameters in Eq. (3) to frozen clay soils with different clay contents, we summarize results of clay soil samples with different clay contents and present in Figure 4-7. The results for soils with low clay contents (12.3% and 20%) were retrieved from Zhou et al (2015) who carried out splitting tests on Qinghai–Tibetan Plateau clay soils. Since their soils contain lower amount of clay minerals, samples tend to have brittle behavior. Thus, they were successful in conducting splitting tests to generate line load along discs and obtain reliable tensile strength. In addition, they have applied different loading rates but found that their results are not dependent on the applied loading rates. It should also be due to reason that samples

contain lower amount of clay minerals. As is displayed in Figure 4-7, parameter B has little variations. Even though there is some difference in clay mineralogy, a general trend is noticed that parameter A has a higher value for samples with a lower clay content. The parameter C standing for the tensile strength at T = 0°C increases with the increase in clay content.

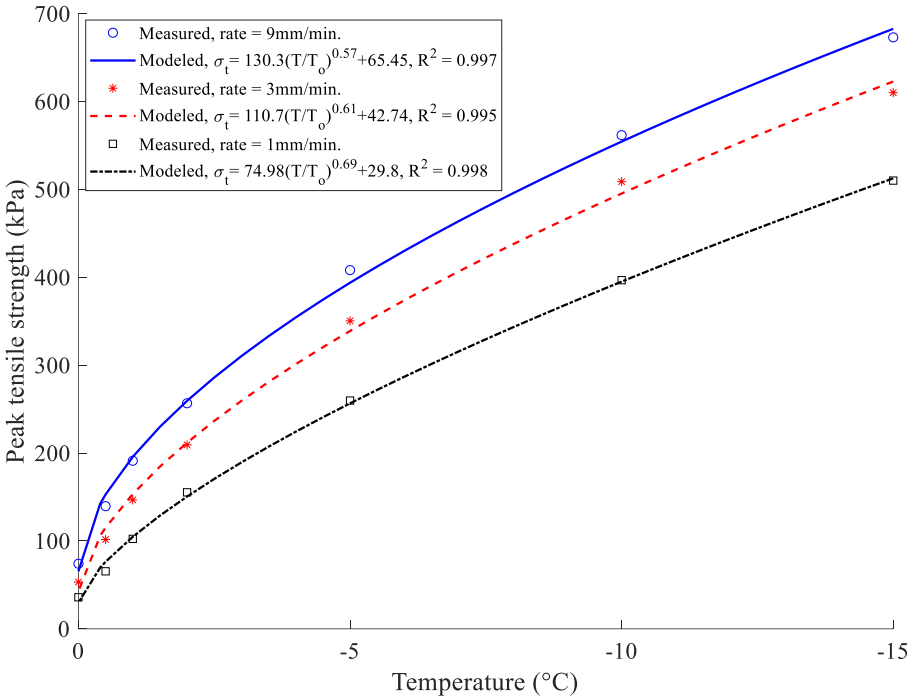

Figure 4-6 Curves showing measured peak tensile strength values versus temperautres at different loading rates (T0 = -1°C).

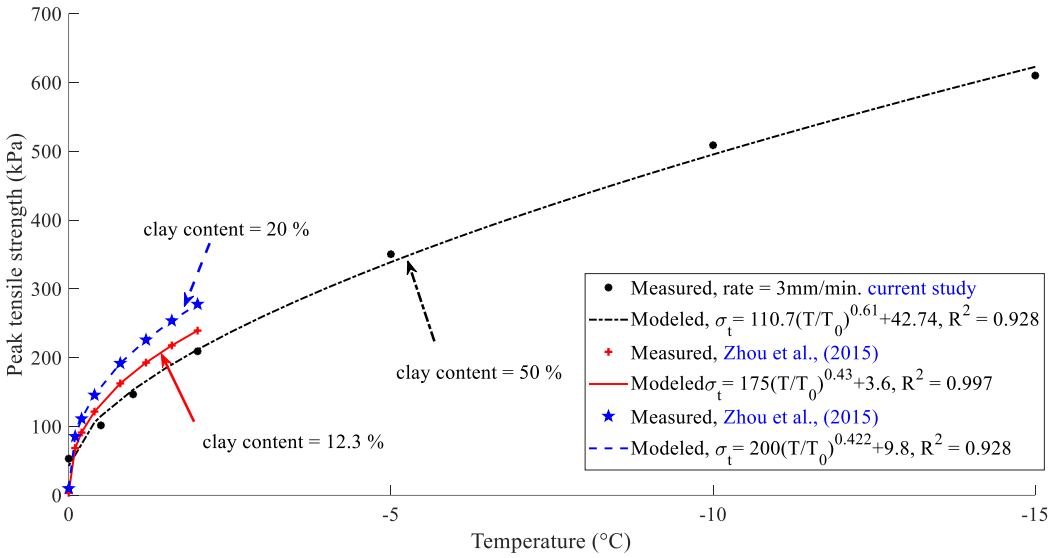

Figure 4-7 Plots of measured and modeled load-displacement curves for samples with different clay contents.

4.4 Numerical analysis

In this study, finite element modeling is conducted to simulate the deformation and tensile yield behavior of frozen soils under different test conditions. We assumed an associated flow rule and applied the hyperbolic Drucker-Prager model, in which the tensile yield behavior is integrated. The hyperbolic Drucker-Prager model has been found effective in simulating both brittle and post peak ductile behaviors of frozen soil (Akhtar and Li 2020b). According to the Abaqus manual (Dassault Systèmes 2016), the hyperbolic Drucker-Prager yield function is given by:

$$F = \sqrt{\left(d' - \sigma_t \tan\beta\right)^2 + q^2} - p\tan\beta - d' = 0 \tag{4.13}$$

where σ_t is the tensile strength; p is the mean effective stress ($p = \frac{1}{3} trace(\sigma)$). Since pore pressure is not considered in the present study, the total stress equals to the effective stress; q is the von Mises equivalent shear stress ($q = \sqrt{\frac{3}{3}(\mathrm{S}:\mathrm{S})}$); S is the deviator stress ($\mathrm{S} = \sigma - p\mathrm{I}$); β

and d are Drucker-Prager model's angle of friction and cohesion strength parameter in the $p-q$ space, respectively; d' is related to d by the following equation:

$$d' = \sqrt{(d - \sigma_t \tan\beta)^2 + \sigma_t^2} + \frac{\sigma_t}{3}\tan\beta \tag{4.14}$$

and,

$$d = (1 + \frac{1}{3}\tan\beta)\sigma_t \tag{4.15}$$

According to Puzrin (Puzrin 2012), the Drucker-Prager friction angle parameter , is related to the Mohr-Coulomb friction angle by:

$$\beta = \tan^{-1}(\frac{6\sin\phi}{3-\sin\phi}) \tag{4.16}$$

Numerical models were created only for laboratory experiments on samples at T= -1oC and T = -10°C. The input parameters required for this analysis were included in Table 4-2. The peak friction angle data was based on published shear test results on sand-bentonite mixtures with similar mineralogy compositions (Tanaka et al. 2001, Saffer and Marone 2003). The elastic deformation parameter was based on our published uniaxial compression test results on the same type of artificial frozen sandy clay samples (Girgis et al. 2020). It should be noted that the creep behavior is not considered in the present simulation, thus our numerical modeling will only be validated using DPT measurements at a high deformation rate (9 mm/min).

Table 4-2 Physical properties of prepared bentonite-sand samples before freezing

Parameters	Value	Reference
Peak friction angle, ϕ_{max} (degrees)	34	(Tanaka et al. 2001; Saffer and Morone 2003)
Drucker-Prager angle of friction, β (degrees)	54	-
Initial tensile strength, $\sigma_t\|_o$ (kPa) at T = -1°C	103.9	-
Initial tensile strength, $\sigma_t\|_o$ (kPa) at T =-10°C	443.9	-
Poisson ratio, v at T =-1°C	0.25	(Girgis et al. 2020)
Poisson ratio, v at T =-10°C	0.18	(Girgis et al. 2020)
Modulus of elasticity, E (MPa) at T =-1°C	28	(Girgis et al. 2020)
Modulus of elasticity, E (MPa) at T =-10°C	180	(Girgis et al. 2020)

The finite element model is idealized in terms of boundary conditions to make an analogy to the conditions in laboratory tests (Figure 4-8a). The frozen soil sample and steel puncher were modeled using a small sliding, surface-to-surface contact pair technique. The top puncher contact surface was considered a master while the soil top and bottom contact surfaces were considered a slave.

A finite element model along with the mesh distribution and location of monitoring points are displayed in Figure 4-8b. The dimensions of the soil sample and the puncher are the same as our laboratory test. The bottom puncher was kept restrained in all directions, and the top puncher was restrained in x-y directions, respectively. The C3D8R type of element was used for both soil

samples and punchers, and the sensitivity of mesh convergence has been examined utilizing different element sizes. The steel puncher was treated as a rigid body during the simulation.

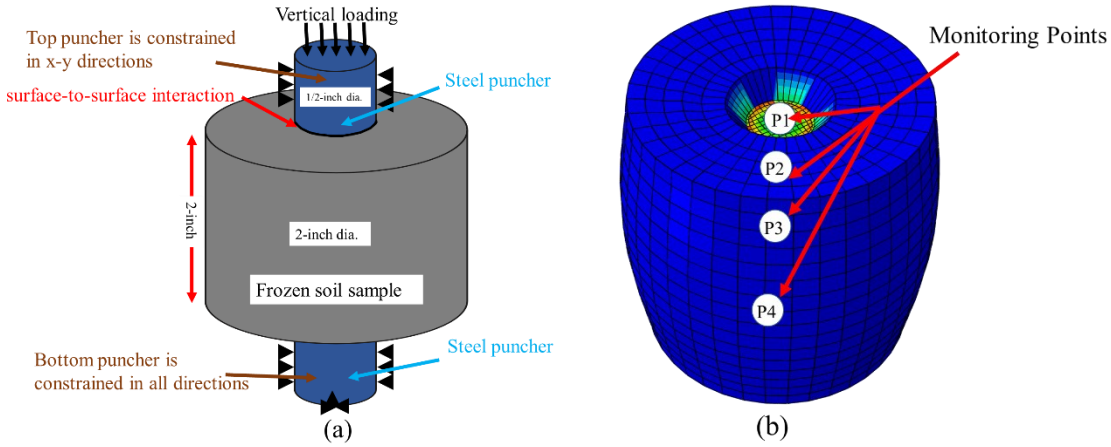

Figure 4-8 Sketch showing (a) the sample dimension, boundary condition, and puncher positions (b) FEM mesh distribution and locations of monitoring points.

Simulated principal stress path curves in the meridional (p - q) plane of four monitoring points (P1, P2, P3, and P4) of two frozen soils during double punch tests are obtained and displayed in Figure 4-9. In general, the trends for the case of T = -10oC (Figure 4-9a) and T = -1°C (Figure 4-9b) were comparable. The point P1 located under the puncher displayed a compression yielding behavior. By contrast, the other three monitoring points (P2, P3, and P4) showed a significant tension trend and ended up with a tensile yield while touching the hyperbolic Drucker-Prager failure yield envelop.

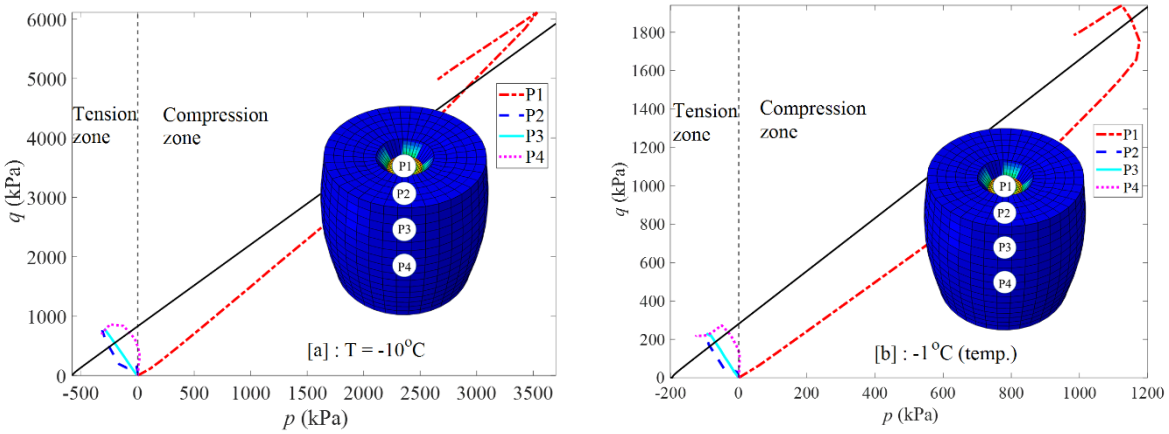

Figure 4-9 Simulated stress paths of four monitoring points in soil samples during double punch tests in the meridional plane at (a) T = -10°C, and (b) T = -1°C.

Simulated contours of equivalent plastic strains (PEEQs) of samples after DPT at T = -10°C and T = -1°C were displayed in Figure 4-10, where the PEEQ was given by:

$$\bar{\varepsilon}^{pl} = \int \frac{\sigma : d\varepsilon^{pl}}{d'} \tag{4.17}$$

Not like the punching splitting failure behaviors observed in Figure 4-2, our simulated plastic strains were uniformly distributed along samples' cylindrical sides. However, the circular yield along the cylindrical side indicated the large induced tensile stress. Compared with the result for T = -1°C (Figure 4-10b), the case with T = -10°C (Figure 4-10a) displayed much less amount of plastic strain. The difference in yield behavior was more clearly indicated in load-displacement curves (Figure 4-11). At T = -10°C, the sample tended to have a brittle failure behavior. By contrast, strain hardening behavior was displayed for the case with T = -1°C.

The simulated load-displacement curve had a good match with the measured result for the test at T = -1°C. However, the simulated result was a little lower than the measured result for the test at T = -10°C. It could be due to the difference in failure behavior between the simulated result and the measured one since the brittle slitting failure behavior of the sample at T = -10°C was highly significant (Figure 4-2). Further studies are required to simulate the brittle splitting failure behavior of frozen soils.

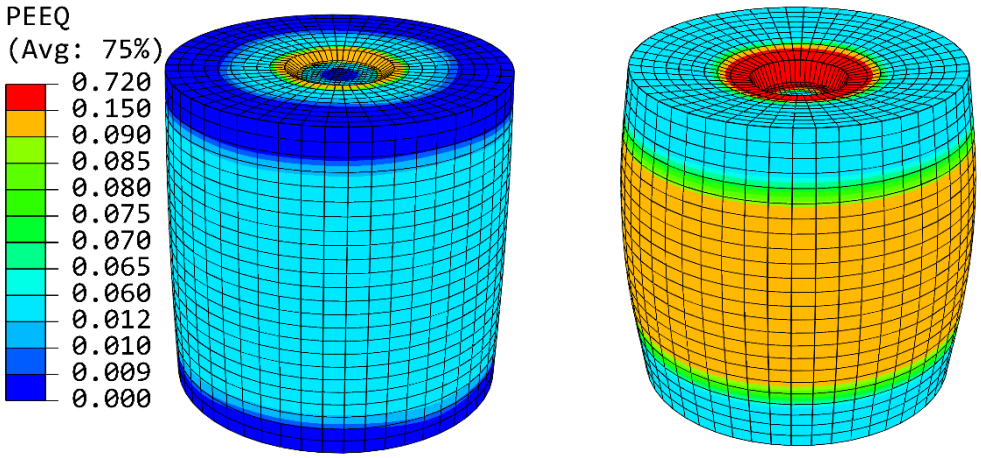

(a) T = -10ºC (b) T = -1ºC

Figure 4-10 Simulated equivalent plastic strain distribution in the frozen soil sample at (a) T = -10ºC with vertical displacment = 0.003 m, and (b) T = -1ºC with vertical displacement = 0.01 m (PEEQ = equivalent plastic strain).

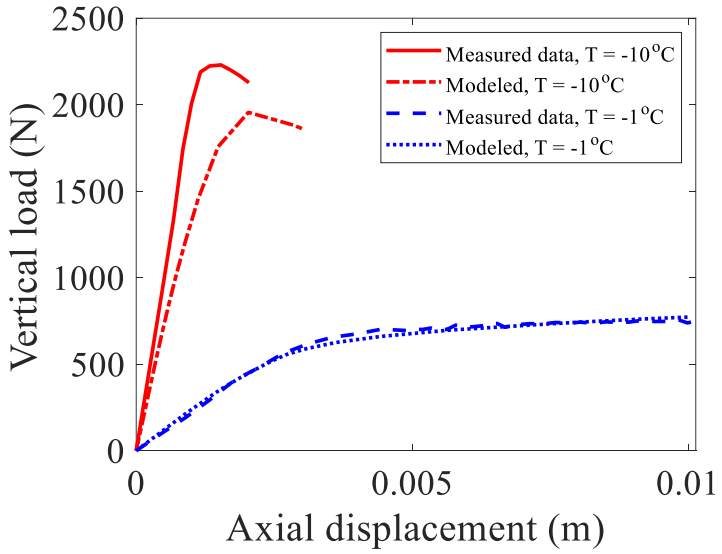

Figure 4-11 Plots of measured and modeled load displacement curves for samples at different temperatures.

4.5 Discussions

4.5.1 Sample size effect

Currently, there is no standard for determining the sizes of samples and punch for the DPT of frozen soils. A change in a sample's dimensions or the diameter of the punch will affect the stress distribution and result in a different plastic zone or failure mode. Given the difficulty of preparing the frozen soil samples in different diameters, we only applied a single sample size for DPTs, and therefore the effect of size could not be considered experimentally. Instead, we carried out 3D

numerical tests to investigate the effect of sample size on the stress and strain distributions during DPTs to determine the optimum sample size for a DPT test.

We conducted numerical tests for cases of T = -10°C and T = -1°C on simulated samples, which had diameters of 1 inch, 2 inches, 3 inches, and 4 inches, respectively. Simulated vertical load-axial displacement relations of numerical tests on samples with different diameters were displayed in Figure 4-12. A sample diameter of D = 2 inches corresponded to the sample size used in our laboratory tests. It was noticed that peak vertical loads were very sensitive to sample sizes both for cases at T = -10°C and at T = -1°C. At T = -10°C, brittle failure turned to be a plastic strain hardening when the sample diameter was increased from D = 1 inch to D = 4 inches (Figure 4-12a). At T = -1°C, the plastic strain hardening was enhanced with the increase in sample diameter (Figure 4-12b). Using Eq. 2, the peak tensile strength values of these numerical tests were obtained and displayed in Figure 4-13. At T = -10°C, the peak strength showed a slight increase when D was increased from 1 inch to 2 inches, but a slightly decreasing trend was noticed with a further increase in D (Figure 4-13a). In general, the peak tensile strength was not sensitive to the sample's diameter for cases with T = -10°C. By contrast, a decreasing trend was noticed for cases with T = -1°C (Figure 4-13b). When a sample's diameter is not appropriate, DPT is not effective because of the generated high amount of plastic strain and the chance of inducing splitting punch failure is low. As is demonstrated in Figure 4-14, when the size of a puncher is comparable to the sample's diameter (e.g., D = 1 inch), the plastic yield behavior is more like that from a uniaxial compression test. When the puncher size is much smaller than the sample's diameter (e.g., D = 4 inches), plastic strain tends to generate locally instead of creating tensile yielding along the sample's annulus region. Based on our numerical tests, a sample diameter of D = 2 inches can be treated as a representative size for the DPT test with a puncher size of ½ inch.

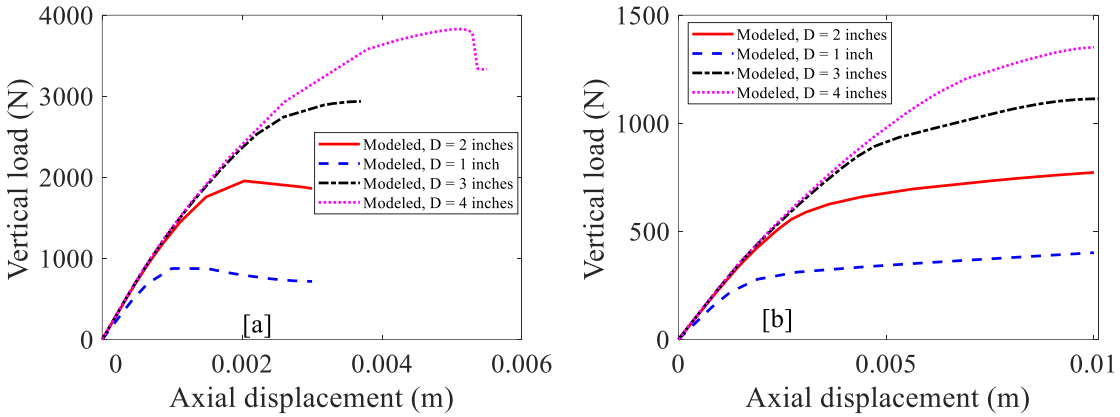

Figure 4-12 Simulated vertical load-axial displacement relations of numerical tests on samples with different diameters at (a) T = -10°C, and (b) T = -1°C.

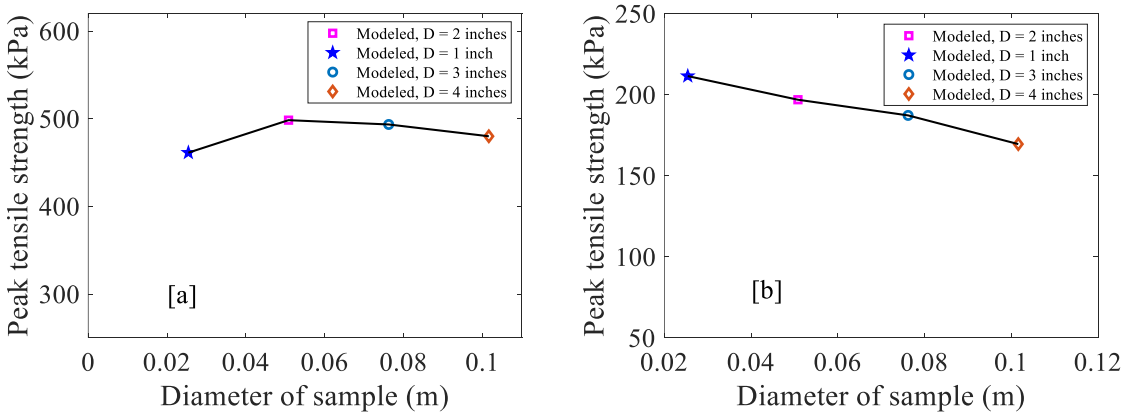

Figure 4-13 Simulated relations between peak tensile strength and sample diameter at (a) T = -10°C, and (b) T = -1°C.

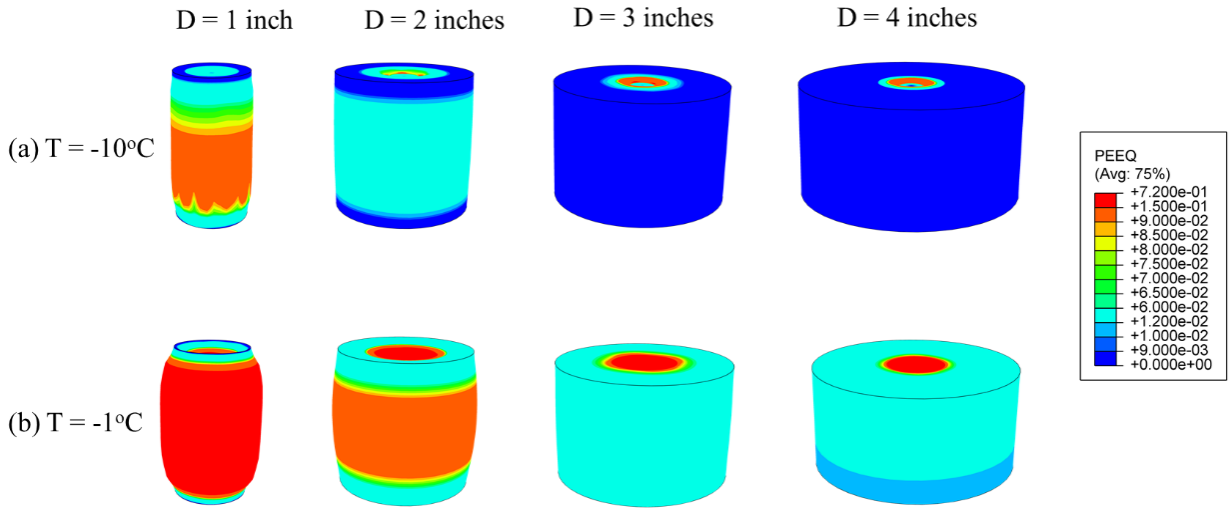

Figure 4-14 Simulated equivalent plastic strain distributions in the frozen soil samples with different sizes at (a) T = -10 ºC, and (b) T = -1 ºC.

4.5.2 A comparison with numerical results of direction tension tests

Direction tension tests were treated as a reliable approach for measuring tensile strength of clay soil or concrete in the ambient temperature condition (ASTM C307-18 2003, Li et al. 2019b). However, it is extremely difficult to carry out direct tension tests on frozen clay soil samples due to the complexity in sample preparation and loading conditions in a cold environment. Instead, numerical modeling applies an efficiency way by changing the boundary condition. Since the mechanical parameters have been validated by the DPT results, we conducted FEM numerical modeling of direct tension tests using the same parameters as indicated that used in DPT numerical tests (Table 4-2). The sample size is based on the ASTM recommended standard test method for tensile strength of chemical-resistant mortar (ASTM C307-18 2003), where briquet gang shaped samples were used for direct tension tests. The FEM mesh, boundary condition, and three monitoring points of the direct tension numerical tests are displayed in Figure 4-15. Horizontal displacement controlled numerical tests were simulated and the stress paths of three monitoring points in soil samples during direct tension tests were shown in Figure 4-16. During direction tension loading, the stresses at three monitoring parts were always located in the tension zone. Among the three monitoring points, P3 (located in the center of the sample) displayed the most significant trend in tensile stress. Plots of modeled load displacement curves and related equivalent plastic strain distributions for direct tension tests at different temperatures are displayed in Figure 4-17. Similar to the DPT results, post peak softening with small area of plastic zone was observed for the numerical test at T = -10ºC. By contrast, the curve for the numerical test at T = -1ºC displayed a strain hardening behavior accompanied by a large plastic deformation. Based on the horizontal force and the cross-section area of the sample, the simulated tensile strength values were

derived and included in Table 4-3. Even though the applied mechanical parameters are the same, estimated tensile strengths values from direct tension numerical tests are 35% more than these from DPT numerical tests (samples with D = 2 inches), which confirms that DPT is conservative in estimating tensile strength of frozen clay soils.

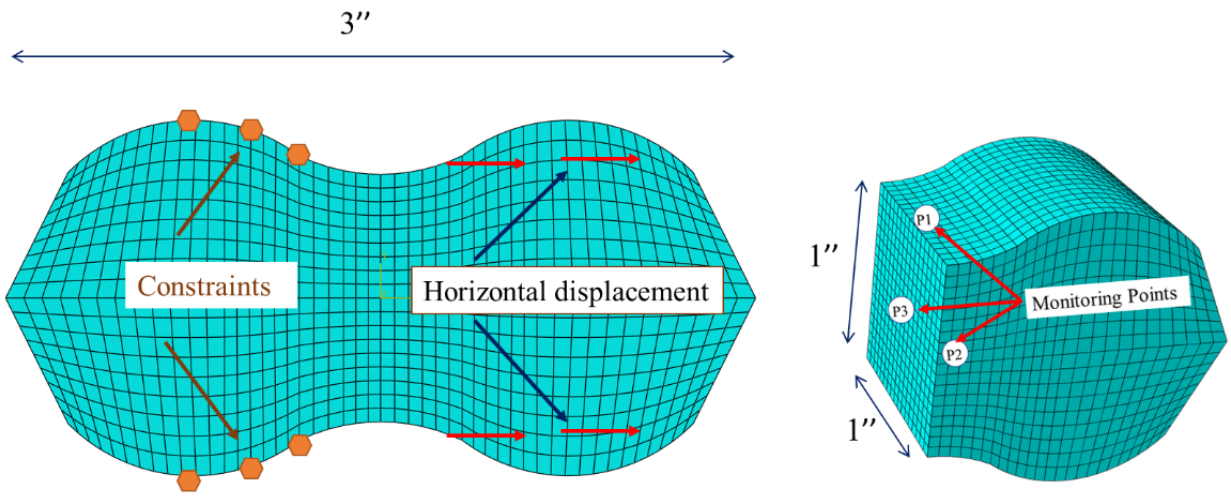

Figure 4-15 Sketch showing FEM mesh, boundary condition, and three monitoring points of the direct tension numerical test.

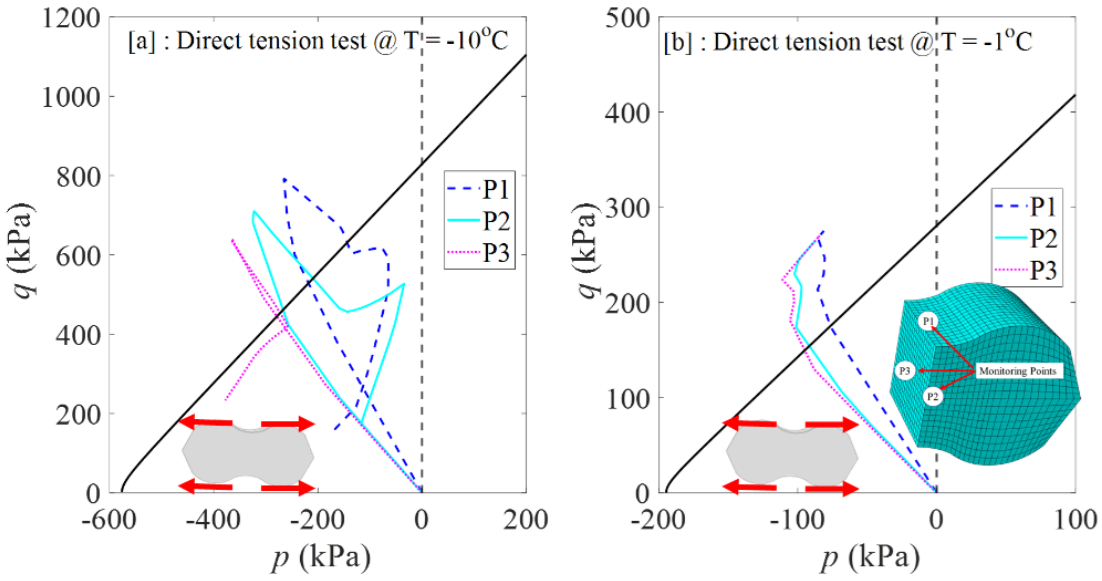

Figure 4-16 Simulated stress paths of monitoring points in soil samples during direct tension tests at (a) T = -10 ºC, and (b) T = -1 ºC.

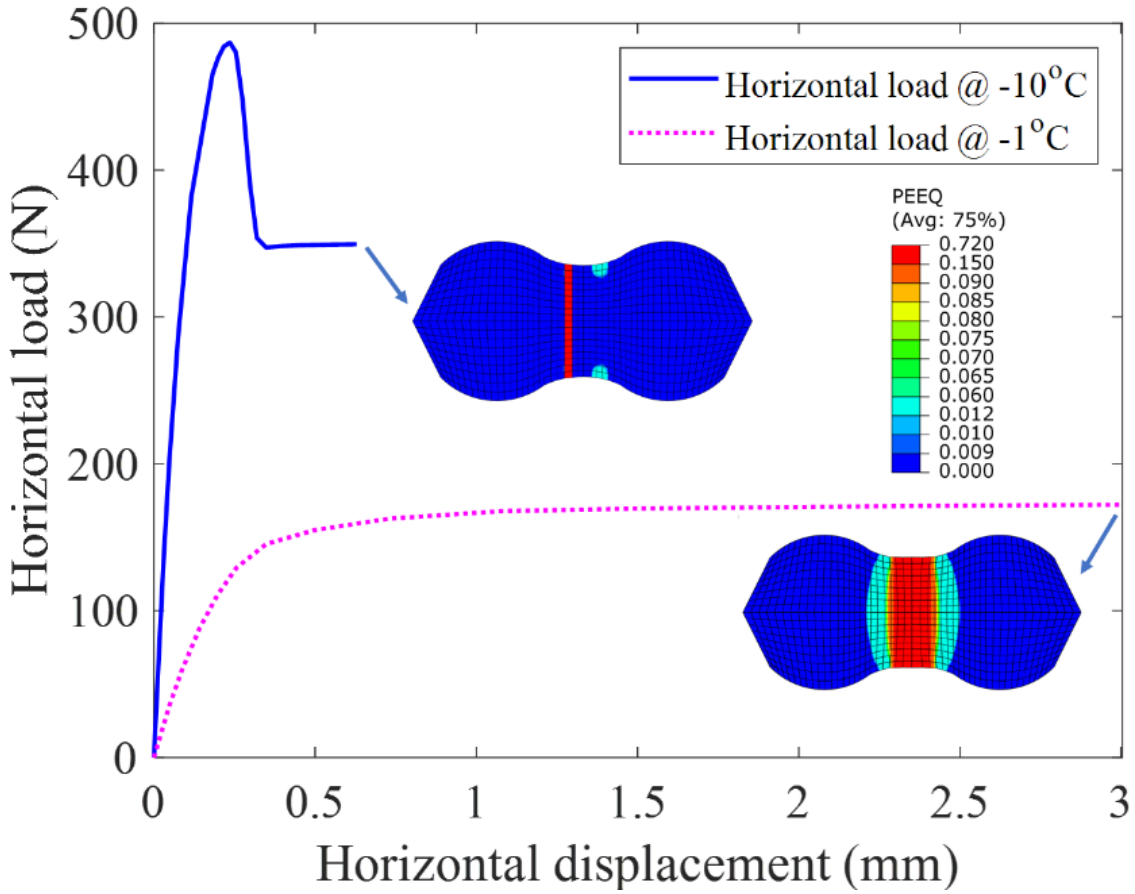

Figure 4-17 Plots of modeled load-displacement curves and related equivalent plastic strain distributions for direct tension tests at different temperatures.

Table 4-3 Summary of estimated tensile strength values of frozen clay soils from different numerical tests

Test	Temperature (ºC)	Peak tensile strength (kPa)
Double punch test	-1	191.1
Direct tension test	-1	266.9
Double punch test	-10	567.9
Direct tension test	-10	754.6

4.6 Conclusions

A series of laboratory tests were performed on artificially prepared frozen sandy clay samples to measure tensile strengths. The effects of experimental approaches, applied temperatures, and

loading rates on tensile failure behaviors were examined. Finite element modeling was conducted to investigate the effectiveness of using DPT to estimate the tensile strength of frozen clay soils. Several conclusions can be drawn as the following:

- The DPT approach is more effective in measuring the tensile strength of frozen clay soil when compared with the rod bar splitting test (RST). Due to the plastic characteristic of frozen soils at temperatures close to freezing, an increase in the contact area between loading strips and samples for RST will overestimate a sample's tensile strength.
- Our experimental results show that the effects of temperature and deformation rates on the sample's tensile strength are significant. A low temperature and a high deformation rate tend to generate brittle failure with post-peak softening behavior. A temperature close to the freezing temperature and a low deformation rate result in a diffuse failure associated with strain hardening. The tensile strength-temperature relationship for the artificial frozen clay soils can be modeled by using a power law function, which covers a broad temperature range from -15°C to 0°C. The parameters for the modeling function are highly dependent on the applied deformation rates.
- The hyperbolic Drucker-Prager model can be used in finite element modeling to simulate deformation and yield behavior in DPT on frozen clay soils. Our results demonstrate that DPT is an effective approach to create tensile stress in a cylindrical sample. Our simulation results also confirm that the applied sample and puncher sizes in our laboratory tests are representative. A comparison between simulated results of DPT and direct tension tests indicates that DPT is conservative in estimating tensile strength of frozen clays soils.

Preface to Chapter 5

As infrastructure development expands into colder environments, understanding soil stabilization methods is essential to ensuring long-term structural integrity. One widely used approach is the application of lime treatment, which enhances soil strength and durability. However, the impact of repeated freeze-thaw cycles on the mechanical properties of lime-treated soils remains an area of ongoing research, with significant implications for construction practices in subarctic and arctic regions. This chapter investigates the mechanical behavior of lime-treated silty clay soils subjected to freeze-thaw cycles, focusing on strength degradation and recovery mechanisms. Through a series of laboratory experiments, including unconfined compressive strength and double punch tensile tests, the study evaluates the effects of curing periods, loading rates, and moisture exposure. The findings reveal critical insights into the resilience of lime-treated soils, shedding light on their potential application in stabilizing infrastructure foundations, highway subgrades, and embankments in cold regions. By advancing our understanding of how lime treatment interacts with freeze-thaw cycles, this research contributes to the ongoing development of sustainable and resilient geotechnical solutions. We hope this study will be a valuable resource for engineers, researchers, and policymakers striving to improve soil stabilization techniques for infrastructure projects in challenging climatic conditions.

Chapter 5

5 Experimental study of mechanical behaviors of lime-treated Quebec silty clay soils under freeze-thaw cycles [3]

5.1 Abstract

In cold regions, environmental factors significantly affect infrastructure such as roads, highways, and pipelines. Although lime and limestone products have been used to stabilize soil and enhance its engineering properties, their application in subarctic regions has been limitedly investigated. This study examines the effect of freezing and thawing on the mechanical responses of lime-treated soils retrieved from northern Canada. Samples were stabilized with lime and subjected to a curing period of up to 28 days to ensure consistent humidity and temperature. The cured samples were evaluated for unconfined compressive strength (UCS) and indirect tensile strength using a custom-designed measurement facility considering the number of freeze-thaw (F-T) cycles, loading rates, and curing duration. The double punch test is shown to be effective in capturing samples' brittle tensile behavior. Our results demonstrate that both the UCS and tensile strength are significantly improved by adding lime to the soil. Both strengths generally degrade during the first ten F-T cycles. However, lime-treated soils begin to regain strength after ten F-T cycles. Additionally, our

[3] A version of this manuscript has been submitted to the *Journal of Environmental Geotechnics* (2025).

test results show that the lime-treated soil is sensitive to exposure to ambient moisture. Nevertheless, the lime-treated soil still retains a much higher UCS compared to the natural soil.

Keywords: Lime, clayey soil, compressive strength, tensile strength, double punch test, curing period, freeze-thaw cycles

5.2 Introduction

Growing urbanization and technological improvements are creating a greater need for sustainable civil infrastructure development in colder climates. These locations, which were once thought to be isolated, uninhabitable, and nearly uninhabited, are now seen as potentially productive areas of the future. Sustainable civil infrastructure systems, such as roads, runways, water and wastewater treatment plants, electricity grids, pipelines for the transportation of natural resources, mineral extraction, and communications, are also necessary for the social and economic activities that take place in cold climates. Urban places cannot flourish and develop without these mechanisms. Nevertheless, weak soil conditions are always present when building these types of structures in these places, mainly because of permafrost degradation, which causes thawing effects as a result of climate change (Akhtar and Li 2020b, 2024b, Norouzi and Li 2024, Li et al. 2024). Roughly 23% of the world's total land area is made up of the distribution area of permafrost and seasonal frozen soil regions (Zhou et al. 2018). The performance and durability of embankments and roadway projects are greatly impacted by weathering conditions known as freeze-thaw cycles in cold climates (Kamei et al. 2012). The ability of permafrost to support the structural stresses placed on it by buildings and other structures can be significantly reduced by changes in the ground thermal regime brought about by outside influences (Streletskiy et al. 2015). The thawing of ice-rich soil alters the engineering properties of soils, including compactness, strength, permeability, compressibility, and load-bearing capacity (Qi et al. 2006). This also causes ground subsidence

and uneven deformation, which compromises the stability of engineered structures (Nelson et al., 2001). Mechanical and physical properties of the soil, such as porosity, moisture content, and soil type, play an important role in the degree of damage from freeze–thaw cycles (Kamei et al. 2012).

Road networks, highways, and pipelines are examples of infrastructure projects that often traverse diverse terrains. However, local soils frequently exhibit low strength, poor workability, and reduced bearing capacity, which are deficient engineering characteristics. Effective management of natural resources, such as soil, is essential in any land development project. The high costs of excavating and replacing problematic soils with suitable materials, along with stringent legislative controls governing the use of these limited resources for earthworks construction, exacerbate these engineering challenges. Soft and weak soils are often the only option available to the construction industry. To address this issue, stabilization and reinforcement methods are employed to improve the mechanical behavior of these soils, enabling their use in construction without the need for expensive, premium soil. However, to mitigate temperature-dependent failures, it is crucial to investigate potential in-situ soil modifications and enhance residual soil strength after thawing, given the weak mechanical response of subsoil and the financial constraints associated with soil replacement.

Currently, to improve the physio-mechanical response of weak soil and enhance over all bearing capacity, research use various approaches and techniques among which hydraulic binders such as cement, lime and fibers are most commonly utilized in real field (Bell 1988, Asgari et al. 2015, Khajeh et al. 2020, 2021, Meziani and Gadouri 2023, MolaAbasi et al. 2024). Lime has been widely employed as an addition for many different projects over the course of history in the construction industry (McDowell 1959). In modern infrastructure, lime is employed to enhance ground stability in projects such as highways, airports, embankments, lime piles, and pavement

subgrades (Bell 1989, Little 1995, Vorobieff and Murphy 2003, Wilkinson et al. 2010, Notman 2011, Herrier et al. 2012, Abiodun and Nalbantoglu 2015, Das et al. 2021). However, the historical use of lime in construction was not well documented until the mid-1900s when proper specifications and procedures were established (Herrin and Mitchell 1961). A research study by Kelley (Kelley 1988) identified lime-stabilized layers that have performed exceptionally well, maintaining excellent strength properties for over 40 years.

Hydrated lime, also known as calcium hydroxide, is produced through a controlled process in which quicklime reacts with water (Li et al. 2023), as shown in Equation 5.18. When lime is mixed with soil and water, a series of chemical reactions occur. The lime interacts with clay minerals, and the presence of soluble silica (particles smaller than 5 microns) in the soil enhances this reaction. This reaction is more pronounced when three-layer clay minerals are present, as their exposed silica faces on both sides are more reactive than those of two-layer clay minerals (Bell 1989). The calcium ions (Ca++) replace existing cations in the clay (K+, Na+, H+, etc.), leading to the rearrangement of particles into flocculated/aggregated structures. This process increases intra-particle porosity and produces larger aggregates (Di Sante 2020). The immediate reaction also reduces the double-layer thickness of clays by increasing the electrolyte concentration in the pore water (Mitchell and Soga 2005). The presence of these ions, which initiate chemical reactions, plays a crucial role in disturbing the interlayer unfrozen water content, further influenced by cation self-diffusion. With the addition of lime, calcium ions replace sodium ions in clayey soil. This process reduces the thickness of the diffuse double layer around the clay minerals, leading to a reduction in the moisture content film (Dash and Hussain 2012). Consequently, the decrease in moisture content lowers the soil's susceptibility to freezing. Additionally, time-dependent pozzolanic reactions produce cementitious compounds, such as calcium silicate hydrates (CSH)

and calcium aluminate hydrates (CAH), which further limit interlayer water (Federico et al. 2015). The presence of calcium ions from lime also replaces weaker ions on the clay surface, forming stronger bonds with the clay particles. This phenomenon limits the movement of water and ions (Diamond and Kinter 1965, de Brito Galvão et al. 2004, Lasledj 2009) during thermal fluctuations, thereby improving soil stability and mitigating frost heave effects (Arabi, et al. 1989). However, its effectiveness is highly dependent on the curing duration and lime content. This development within the soil system reduces plasticity, increases workability, and typically requires 1-3% lime (Bell 1996). Following this, long-term pozzolanic reactions can occur over weeks to years. These reactions involve silica and alumina from the soil reacting with calcium ions from the lime, forming gels that harden over time (Bell 1989). Maintaining the soil pH at 12.4 is crucial for dissolving silica and alumina, allowing them to react with calcium ions from the lime to form calcium silicate hydrates (CSH) and calcium aluminate hydrates (CAH), as shown in Equation 5.19 and Equation 5.20. These hydrates eventually create cementitious materials similar to calcium and aluminate hydrates (Eades and Grim 1960).

$$CaO+H_2O \rightarrow Ca(OH)_2 \quad (5.18)$$

$$Ca(OH)_2+SiO_2 \rightarrow CaO\text{-}SiO_2\text{-}H_2O \quad (5.19)$$

$$Ca(OH)_2+Al_2O_3 \rightarrow CaO\text{-}Al_2O_3\text{-}H_2O \quad (5.20)$$

Lime has been utilized in various forms, including hydrated lime (calcium and/or calcium-magnesium hydroxide), quicklime (calcium and/or calcium-magnesium oxide), and industrial waste lime. The widespread use of lime in light construction work can be attributed to its affordability, ready availability, and minimal skill requirements. Research on the use of lime in soil stabilization under warm conditions is well-documented (Khattab et al. 2007, Wilkinson et al.

2010, Verbrugge et al. 2011, Dash and Hussain 2012, Federico et al. 2015, Gelder and Fowmes 2016, Afrin 2017, Chen et al. 2021, Khajeh et al. 2022, 2023, 2024, Padmaraj and Arnepalli 2024, Jia n.d.).

Research studies related to the use of lime in cold regions, particularly under freeze and thaw action, are very limited. Previous studies have investigated the impact of freeze-thaw cycles on the shear strength of various soils, including loess, expansive soil, soft clay, and saline soil (Khoury and Zaman 2007, Kamei et al. 2012, Zhou et al. 2018, Mahedi et al. 2019) revealed that the intensity of freeze-thaw effects depends on factors such as the number, type, duration, and depth of frost penetration cycles. Little (Little 1995) noted that the rate of strength loss due to moisture cycling and freeze-thaw cycling in soils and aggregates can be substantially reduced through lime stabilization. Yao et al. (Yao et al. 2020) studied the impact of freeze and thaw on the shear strength of lime-solidified dispersion soils and found that the strength parameters (cohesion and frictional angle) increased by 9% with the addition of lime. They also observed that the effect of freeze-thaw cycles on the strength of saline soil mixed with lime is less pronounced compared to saline soil alone, a finding consistent with Liu et al. (Liu et al. 2019). Overall, the addition of lime to the soil enhances resistance to freeze-thaw impacts. Yildiz and Soganci (Yıldız and Soğancı 2012) found that mixing lime with clay substantially increased the hydraulic conductivity due to flocculation. However, after three freeze-thaw cycles, the strength of the mixtures decreased by 15%.

Wei et al. (Wei et al. 2022) analyzed the influence of 15 freeze-thaw cycles on stabilized silty clay through triaxial tests. They observed that freeze-thaw cycles affected cohesion more than friction angle and the size and volume of internal pores. Moreover, the failure pattern of lime-soil mixture changed from peak post-softening to indistinctive softening. Ismeik and Shaqour (Ismeik and Shaqour 2020) investigated the role of lime in fine soil under unconfined compressive strength,

considering the impact of freeze-thaw on strength degradation. They found that the strength of the soil increased considerably with the addition of 6% lime. Although freeze-thaw cycles adversely affected the strength of the soil-lime mixture, the effect was less than on untreated soil. Liu et al. (Liu et al. 2010) conducted dynamic triaxial tests on lime-modified clays subjected to 10 freeze-thaw cycles. In addition to increasing optimum water content and decreasing maximum dry density, their study found that adding lime to soil improved resistance to freeze-thaw cycles. However, the dynamic stress decreased due to freeze-thaw cycles. Tebaldi et al. (Tebaldi et al. 2016) investigated the effect of up to 20 freeze-thaw cycles on the mechanical strength of clayey soil modified with quicklime, using unconfined compressive strength and direct shear tests. They found that the strength of the modified soil decreased by 35% due to freeze-thaw cycles. Despite previous research on using lime to enhance the longevity and strength of soil, there has been limited investigation into the combined effects of curing time, lime concentration, and soil mineralogy on the resilience of fine-grained soils. Additionally, there is a lack of data on the tensile failure behavior of lime-treated soils. Further studies are needed in this field to enhance our understanding. In particular, as part of the sustainable development initiatives in northern Quebec, Canada, extensive construction activities are underway in the local Cree communities, where the ground consists of marine clay deposits (Royer 2016). Without a comprehensive investigation into the geotechnical behavior of these soils, the safety of both existing and future infrastructure may be jeopardized.

The purpose of this study is to enhance our understanding of the physio-mechanical response of silty clay soils treated with lime under varying freeze-thaw (F-T) cycles. This study investigates soil strength improvement using lime for applications such as shallow foundations, highway subgrades, and natural slopes. A unique marine soil, collected from a site in northern Quebec,

Canada, at a depth of one to three meters, was subjected to various tests, including uniaxial compressive strength and double punch tensile strength tests. The experiments were conducted under varying loading rates and curing durations, incorporating up to 16 freeze-thaw (F-T) cycles. This study aims to identify the threshold number of F-T cycles that cause maximum strength degradation in lime-treated soil and to evaluate the effectiveness of the indirect tensile test (i.e., double punch test) for characterizing tensile behavior without excessive plastic deformation at the contact area. However, this study does not consider aspects such as microstructural analysis, the impact of external moisture contact, or the pore water redistribution pattern during F-T cycles.

5.3 Materials properties and sample preparation procedure

The primary objective of adding lime is to enhance the hydro-mechanical behavior of the soil. The response of the soil to lime treatment is influenced by factors such as the chemical composition of the lime, the soil type, and its mineralogical properties. The following sections offer a detailed discussion on soil characteristics, lime's chemical composition, soil preparation methods, and sample preservation techniques for freeze-thaw (F-T) cycle testing.

5.3.1 Physical properties of soil

Soil samples for this study were excavated from the town of Waskaganish in northern Quebec, on the southeast shore of James Bay, at a depth up to three meters. The particle size distribution of the soil was obtained using standard sieve analysis methods (ASTM D422-63 2007) and sedimentation analysis (ASTM D7928-21e1 2017), as shown in Figure 5-1(a). According to the Unified Soil Classification System (USCS), the soil is classified as fine sands or clayey silts (ML) and silty clays or sandy clays (CL) with low plasticity. To prepare the soil for lime mixing and testing, it was first air-dried and then hand sieved to 2.36 mm. Silt, clay, and fine size sand particles affect the mechanical response and soil characteristics, as shown in Figure 5-1(b). Table 5-1 lists

the specific physical characteristics of the soil. The values provided for the physical parameters represent the average values for the same soil. However, the variability in the results was less than 1%. The bulk density, specific gravity, water content, and Atterberg limits were determined using ASTM D698, ASTM D854, and ASTM D4318 (ASTM D854-23 2006, ASTM D4318-17e1 2017, ASTM D698-12 2021), respectively. The sieve analysis results showed the following particle size distribution: silt fraction (41.15%), clay fraction (13.95%), sand fraction (22.97%), and gravel fraction (21.9%).

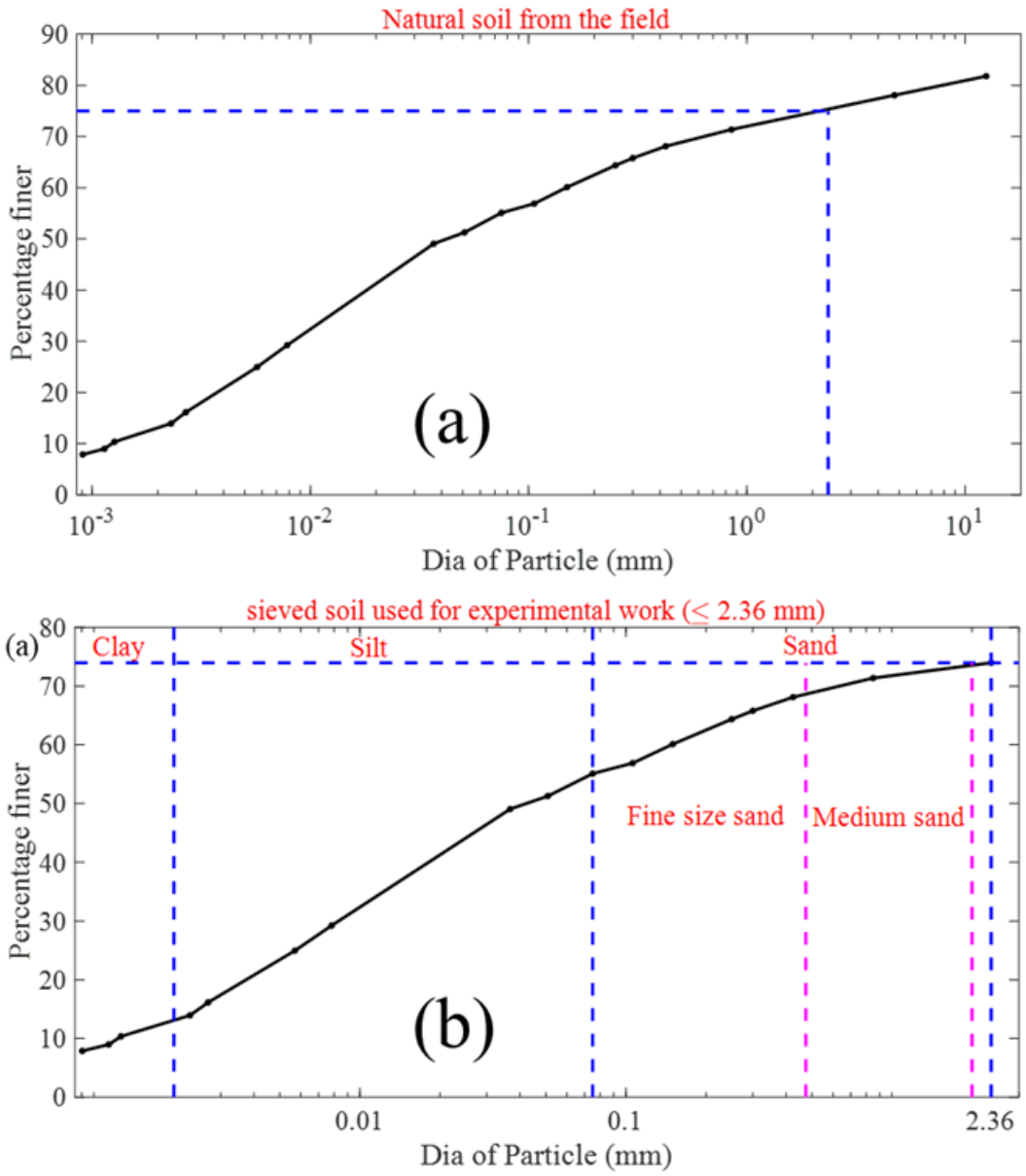

Figure 5-1 Grain size distribution of soil used for this research work.

Table 5-1 Atterberg limits and other physical properties of natural soil

$w_{natural}$ (%) of field soil	Bulk density (kg/m^3) of fine soil	Specific gravity	w_{opt} (%) of fine soil	LL (%)	PL (%)	PI (%)
29.2	2030	2.66	11.2	22.8	16.8	6.3

Note: $w_{natural}$ =natural water content; w_{opt} =optimum water content; LL = liquid limit; PL = plastic limit; PI = plastic index

5.3.2 **Physical and chemical properties of lime**

The hydrated lime used in this study is a locally available product, typically utilized for construction purposes, and was provided by Graymont in Montreal, Canada. The soil basic characterization is presented in Table 5-2, indicating the quartz is the predominant mineral, with a notable presence of albite, as determined by X-ray diffraction (Babanas and Courcelles 2025). The physical and chemical properties of the lime-treated soil mixture and the hydrated lime are presented in Table 5-3 and Table 5-4, respectively. Here the optimum moisture content and optimum lime content is derived from study by Hamza and Benoit (Babanas and Courcelles 2025).

Table 5-2 Basic characterization of natural soil

Mineralogy	Relative density	pH	Clay Activity	Saturation Degree	Reference
Quartz predominates, with noticeable albite	2.812	8.6	17.3 %	81.3	(Babanas and Courcelles 2025)

Table 5-3 Physical properties of lime treated soil (LS)

w_{opt} (%)	Bulk density (kg/m^3)	Optimum lime content (%)	Lime bulk density(kg/m^3)	Lime Specific gravity	pH of lime (25 °C)
14.5	2141.6	2.66	445-530	2.24	12.454

Note: w_{opt} =optimum water content of modified soil; Bulk density of modified soil is based on 28 days of curing.

Table 5-4 Chemical composition of the used hydrated lime

Calcium hydroxide (lime index %)	Available Calcium oxide (lime index %)	Silica (SiO_2) %	Carbonates ($CaCO_3$) %

95.9	72	1.1	1.4

5.3.3 Sample preparation for testing

The sieved, pulverized, and air-dried soil was mixed with the optimum amount of water, mentioned in Table 1, for each sample and stored in an airtight container for 24-hours curing to achieve maximum moisture homogenization. Following this, the wet soil was blended with the specified quantity of hydrated lime for 5 minutes. After mixing, the lime-treated soil mixture was maintained under hermetic conditions for an additional 2 hours to ensure thorough homogenization and ambient equilibrium. For the compaction phase, a scaled-down procedure consistent with the standard Proctor compaction method (ASTM D698) was employed, achieving 98.5% of the optimum density. During preparation for the compaction test, the modified soil was compacted in three layers within a mold measuring 4 inches in height and 2 inches in diameter. For the double punch tensile test, the modified soil was compacted in two layers within a mold measuring 2 inches in both dimensions. Following compaction, the samples were secured in their molds and kept in a hermetic environment for the designated curing times, which are covered in detail in section 3.

5.3.4 Sample preservation for freezing and thawing

Once the curing period ended, the samples were removed from the aluminum molds using a manual vertical extruder. They were then covered with plastic to maintain moisture levels, followed by aluminum foil, and finally placed in vacuum-sealed bags to prevent moisture leakage and protect against environmental moisture effects. The samples were transferred to an industrial-grade freezer set to -30°C for 12 hours to ensure uniform freezing without the formation of ice lenses, followed by thawing at room temperature for another 12 hours, as shown in Figure 5-2. This procedure aligns with the findings of Zheng et al. (Zheng et al. 2021), which indicate that samples freeze and thaw completely within 12 hours. The quick-freezing method was employed to avoid the

development of ice lenses during freezing, which could alter the thermo-mechanical response of the samples and is not considered in this study.

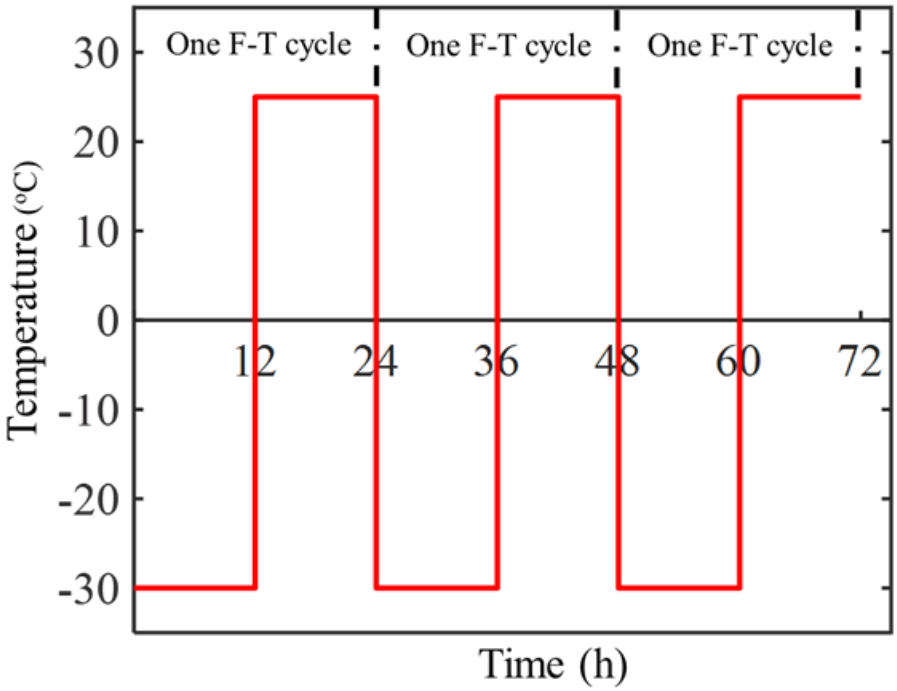

Figure 5-2 Temperature variation pattern during freeze-thaw cycles.

5.4 Experimental setup and test program

This section provides an overview of the experimental setup and presents the post-failure images of samples from both the unconfined compressive strength test and the double punch tensile strength test. A summary of the test program is illustrated in Figure 5-3.

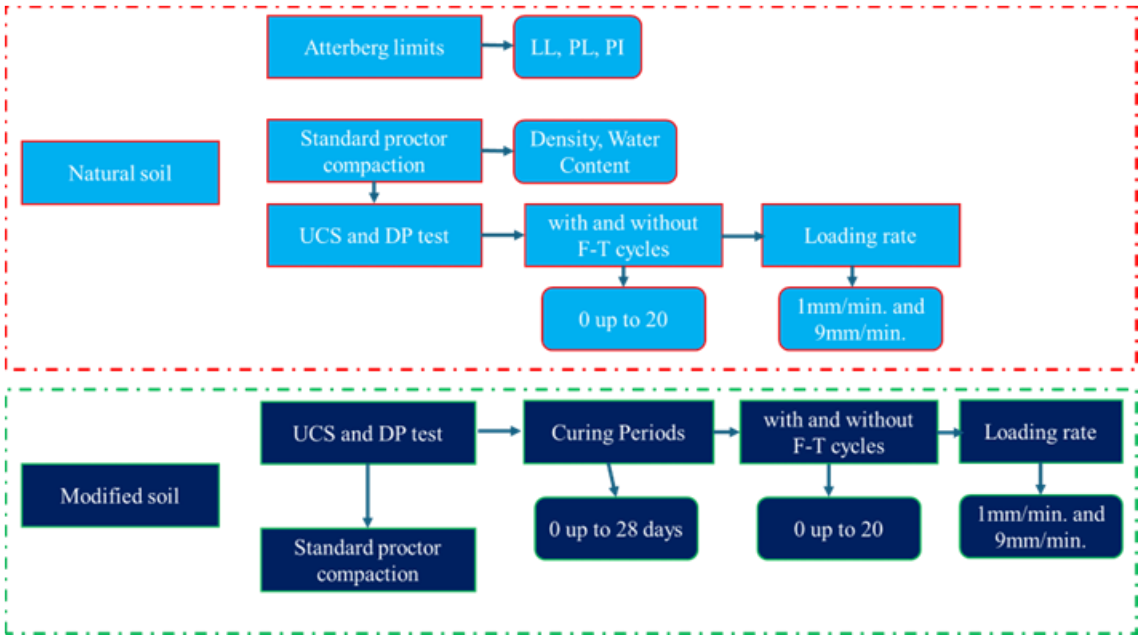

Figure 5-3 Temperature variation pattern during freeze-thaw cycles.

In this study, we use our self-designed uniaxial compression subframe to carry out unconfined compressive strength tests and indirect tensile strength tests. The indirect tensile strength tests are conducted using the double punch subframe, which was demonstrated to be effective in measuring the tensile strength of clay soils under the cold environment by producing minimum deformation around the contact area (Li and Akhtar 2022). A special subframe was developed to accommodate the switch from unconfined compressive strength (UCS) test (Figure 5-4a) to the indirect tensile strength test (Figure 5-4b). One linear variable displacement transducer was vertically installed to measure vertical displacements due to the vertical load.

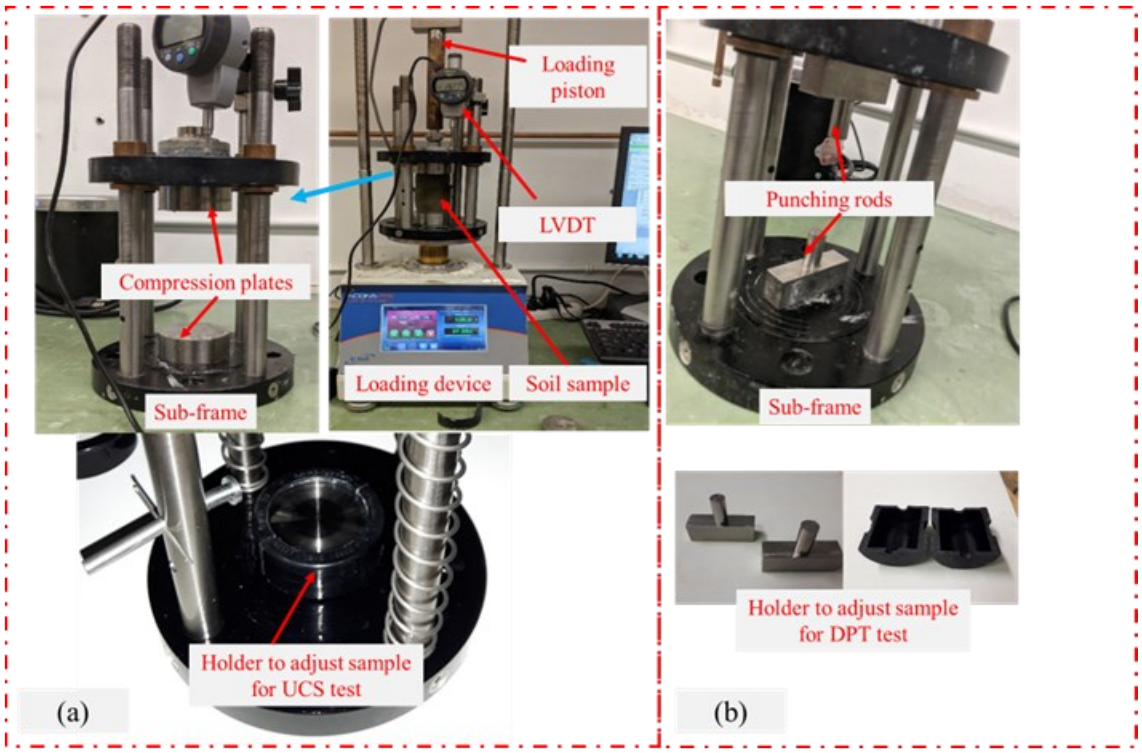

Figure 5-4 Experimental setup for (a) unconfined compressive strength (UCS) test and (b) indirect tensile strength test.

5.5 Experimental results

This section details the experimental setup, post-failure images of the samples, and the experimental results based on the outlined test procedures. The post-failure images are presented in the first subsection, preceding the discussion of the physio-mechanical response of lime-treated soil. This arrangement allows for an analysis of changes in failure paths and patterns, which can later be validated against the experimental results.

5.5.1 Post-failure samples

Figures 5-5 and 5-6 present images of deformed samples subjected to F-T cycles after reaching peak strength limits in unconfined compressive strength and double punch tensile strength tests, respectively. The deformation patterns observed in the compression test samples indicate that the failure path and characteristics of both natural and lime-treated soils are influenced by F-T cycles. Particularly, the failure patterns are more pronounced in the lime-treated soil samples. In the

absence of F-T cycles, the lime-treated soil exhibited cracks traversing the entire section of the sample. However, after exposure to F-T cycles, the crack pattern shifted to a cap-crack configuration, where deformation and cracking were concentrated in the top one-third of the sample, near the loading plate. This change not only indicates strength degradation due to thermal variations induced by F-T cycles but also highlights that large pore developed during the coagulation process resulted in localized failure without effective load transfer across the sample section. Similarly, post-failure images from the double punch tests (Figure 5-6) reveal that localized deformations around the loading rod diminish with F-T cycles, a pattern observed in both treated and untreated soils. This behavior aligns with the findings from the compression tests. The lime-induced flocculation of soil particles creates larger pores. During freezing, the expansion of pore water further disrupts particle arrangements and coagulant formations, leading to increased pore sizes. This phenomenon will be explored in greater detail in the subsequent sections.

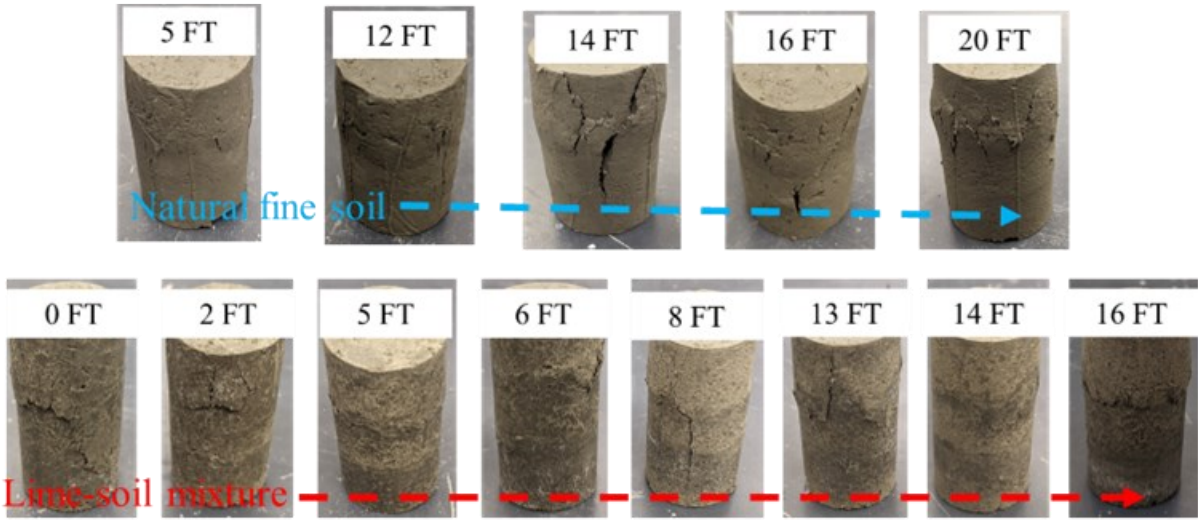

Figure 5-5 Post-failure images of soil samples after unconfined compressive strength tests, highlighting the fracture patterns and failure modes.

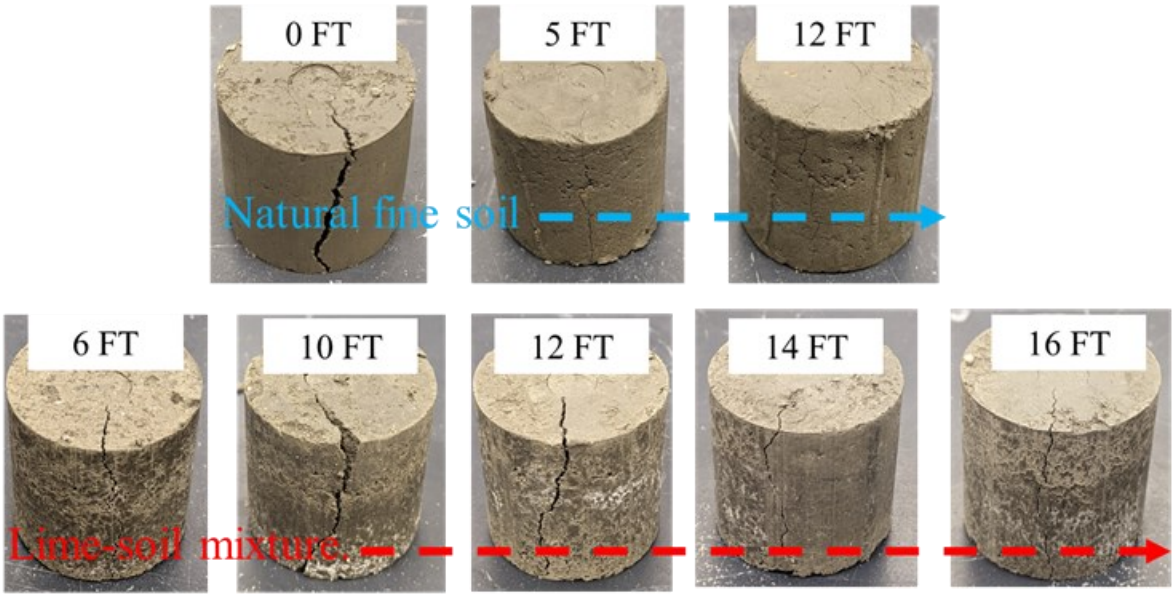

Figure 5-6 Post-failure images of soil samples following double punch tests, highlighting the central failure zone and radial crack pattern.

5.5.2 **Role of curing period and basic index properties**

As shown in Figure 5-7a, the moisture content of the lime-treated soil mixture decreases over the curing period. This reduction is likely due to the ongoing exothermic reaction and water leaching. The most substantial decrease occurred within the first 24 hours, where the moisture content dropped from 14.5% at the time of mixing to 11.6%, representing a rate of 2.9% per day. However, in the subsequent 28 days, the moisture content decreased at a much slower rate of only 0.06% per day. This trend aligns with Szendefy's findings (Szendefy 2008), which indicate that most changes in lime-treated soil occur within the initial 28 days, with the pozzolanic reaction contributing to time dependent strength enhancement. Similarly, the most significant reduction in the bulk density of the lime treated soil occurred within the first 48 hours of curing, with further curing having a negligible effect on density. The impact of F-T cycles on the dry density of the modified soil is also illustrated in Figure 5-7b. The figure shows that the maximum drop in density took place during the first three F-T cycles, with subsequent thermal changes due to these cycles having little impact on the soil's density. Figure 5-7b also shows that cycles 5, 6, and 7, as well as cycles 9 and

10, have the same bulk density up to three decimal points. This could be attributed to the closed test setup, where the sample was preserved to prevent any external interference and to stop ice heave formation during freezing. Additionally, the quick freezing at -30°C and the short thawing period of only 12 hours likely resulted in reduced pozzolanic reactions that could affect the density. These effects are further corroborated by the post-failure images of lime-treated soil (LS) samples shown in Figure 5-5. The failure pattern shifts from failure across the section to top-cap failure. This localized deformation occurs because the addition of lime forms coagulates (lime, clay, silt, and fine sands), leaving large inter-particle pores. As curing progresses, the system's moisture content decreases, and moisture may also drain downward due to gravity. Initially, the increased load is resisted by modified friction, but as the load exceeds the limit, cracks begin to propagate, connecting with nearby micro-cracks. This leads to the formation of larger cracks and a transition in the mechanical response from ductile to brittle behavior.

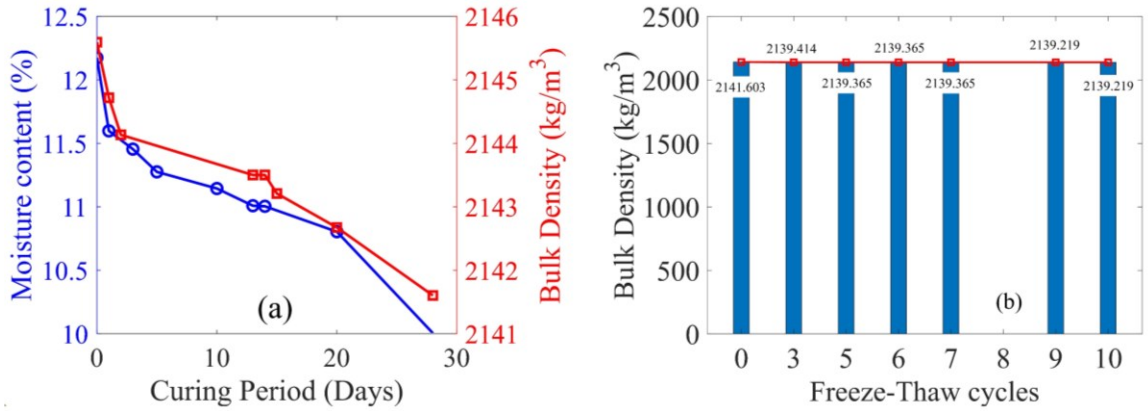

Figure 5-7 Graphical representation of the evolution of water content and density during curing and after successive freeze-thaw cycles.

The results indicate that the majority of changes in moisture content and dry density of lime-treated soil occur within the first 48 hours of curing, with subsequent changes being relatively minor. Freeze-thaw cycles also impact dry density, particularly during the first three cycles. Lime treatment induces coagulation, creating large pores that influence failure patterns. As curing

progresses and moisture levels decrease, crack propagation under increased loads leads to a transition in the soil's behavior from ductile to brittle.

5.5.3 Unconfined compressive strength test

Figures 5-8a and 5-8b present the compressive strength and deformation behavior of natural soil and lime-treated soil, respectively. It can be observed that in up to 10 freeze-thaw (F-T) cycles, the strength of the natural soil (Figure 5-8a) remains relatively unchanged. However, with additional F-T cycles, a slight increase in soil strength is noted, likely due to changes in interparticle orientation. Despite the careful preservation of the samples, the presence of sand and the formation of large inter-particle pores during freezing caused the displacement of pore water during thawing. This displacement improved interparticle contact among coarse particles, leading to a marginal increase in strength. Additionally, it is evident that with ongoing F-T cycles, the peak strength is reached at higher deformation levels. This suggests that the initial load compresses the soil, reducing the larger pores formed during freezing, after which the load is more effectively transmitted to the soil particles.

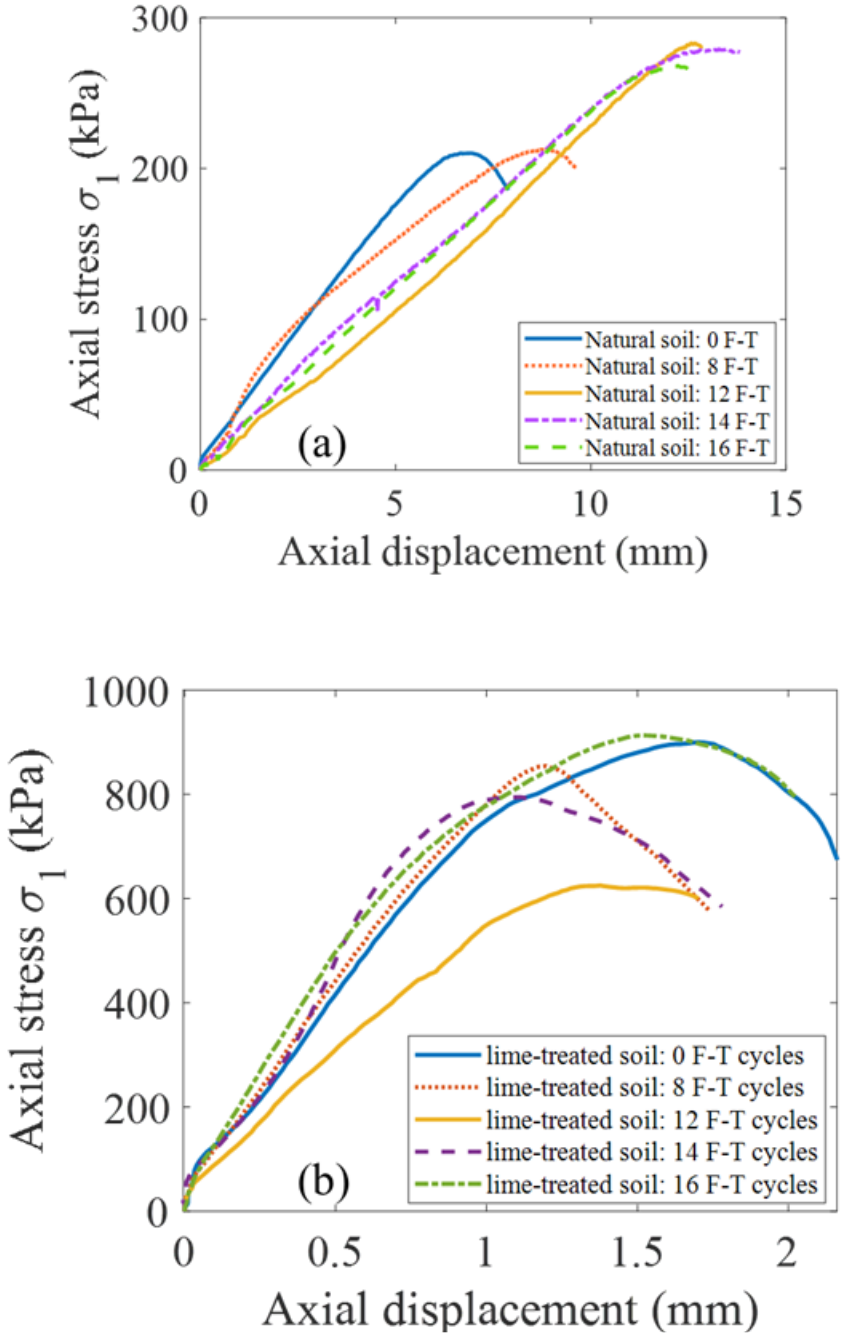

Figure 5-8 Stress-displacement curves for (a) natural soil and (b) lime-treated soil from unconfined compressive strength tests (deformation rate =1 mm/min).

The behavior of lime-treated soil under freeze-thaw (F-T) cycles differs significantly from that of natural soil, as depicted in Figure 5-8b. The strength of lime-treated soil increases from 208 kPa to 880 kPa, demonstrating an enhancement of nearly four times with the addition of lime. Moreover, Figure 5-9 shows that although the strength initially degrades under the influence of F-

T cycles, recovery begins after 12 cycles. This occurs because, during the freezing stage, the lime-soil reaction slows down, while the water in the system expands. The expanding pore ice exerts pressure on and crushes the agglomerates, leading to an initial reduction in strength. However, during the thawing process, the lime-soil reaction resumes, aided by the drainage of free pore water due to the presence of sand and the larger intra-particle pores formed during freezing. Unlike natural soil, the peak strength of lime-treated soil is achieved at a lower deformation. This is because the primary strength of lime-treated soil arises from agglomerate formation. Once the friction within the structure is overcome by the load, nearby cracks begin to coalesce, leading to significant deformation, as illustrated in Figure 5-5. This behavior of lime-treated soil can be further validated through energy absorption capacity and secant modulus, as shown in Figures 5-10 and 11. Figure 5-10 illustrates the amount of energy required to induce deformation in the lime-treated soil sample, which is determined by calculating the area under the stress-strain curve. The figure shows that at low strain values (i.e., <0.5%), there is no significant change in energy absorption capacity across all F-T cycles. However, at higher strain values, the energy absorption capacity initially decreases below that of lime-treated soil with 0 F-T cycles for up to 12 F-T cycles. With further F-T cycles, the energy absorption capacity increases, eventually surpassing that of the 0 F-T cycles. Additionally, for a specific strain value, the energy absorption capacity for 12 and 14 F-T cycles appears to be the same. This behavior can be attributed to the fact that the stiffness of lime-treated soil decreases up to 12 F-T cycles but recovers beyond 12 F-T cycles.

Figure 5-11 presents the secant modulus of natural and lime-treated soil. The results indicate that lime-treated soil at 0 F-T cycles exhibits a higher elastic secant modulus than natural soil. However, the modulus decreases during the initial F-T cycles (up to 12 cycles) before recovering with further F-T cycles. This behavior aligns with the peak strength trends shown in Figure 5-9. It

can be explained by the transition in the soil's behavior from ductile to brittle due to the addition of lime. During the first 12 F-T cycles, the redistribution of pore water and micro-damage caused by the freeze-thaw process reduces the modulus, resulting in ductile behavior. With more F-T cycles, secondary pozzolanic reactions and the role of cation exchange dominate, leading to an increase in stiffness and a return to brittle behavior.

The experimental data indicates that the strength of natural soil remains stable through up to ten freeze-thaw (F-T) cycles, with a slight increase attributed to improved interparticle interactions resulting from pore water redistribution during thawing. In contrast, lime-treated soil exhibits a significant strength increase (from 208 kPa to 880 kPa) due to the development of agglomerations caused by lime treatment. While the initial F-T cycles weaken the material, recovery begins after 12 cycles as lime-soil reactions resume following thawing. When cracks coalesce under load, leading to significant deformation, lime-treated soil, unlike natural soil, achieves its peak strength at a lower deformation rate.

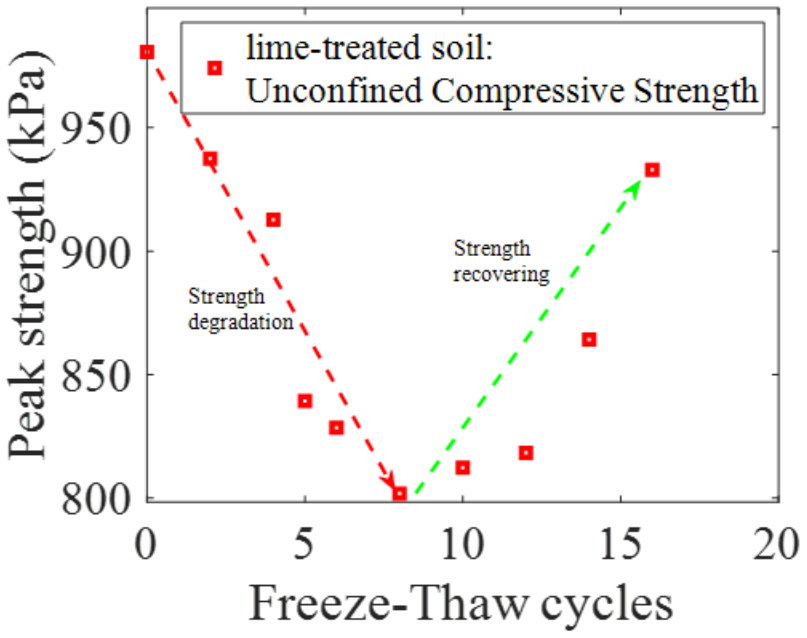

Figure 5-9 Plot showing the peak uniaxial compressive strength versus freeze-thaw cycles for lime-treated soil (deformation rate = 1 mm/min).

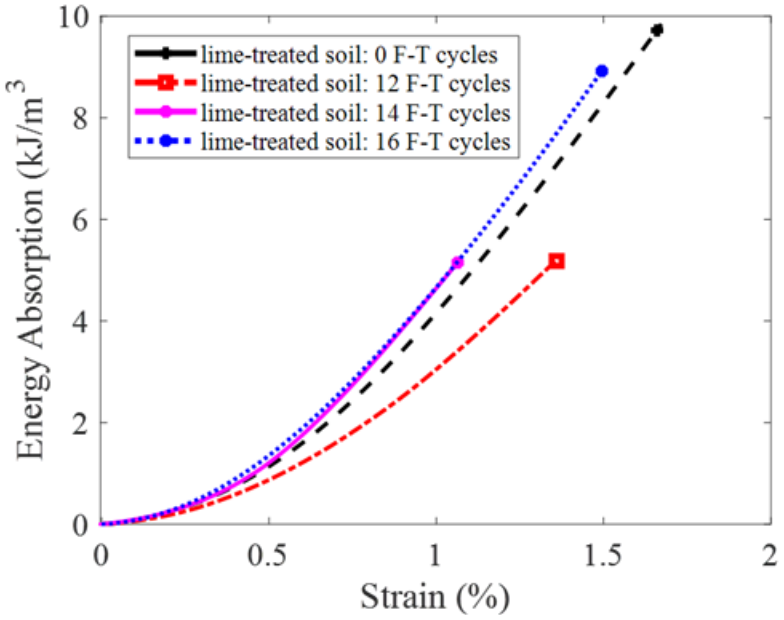

Figure 5-10 Variation of the absorbed energy with axial strain for lime treated soil with different F-T cycles (deformation rate = 1 mm/min).

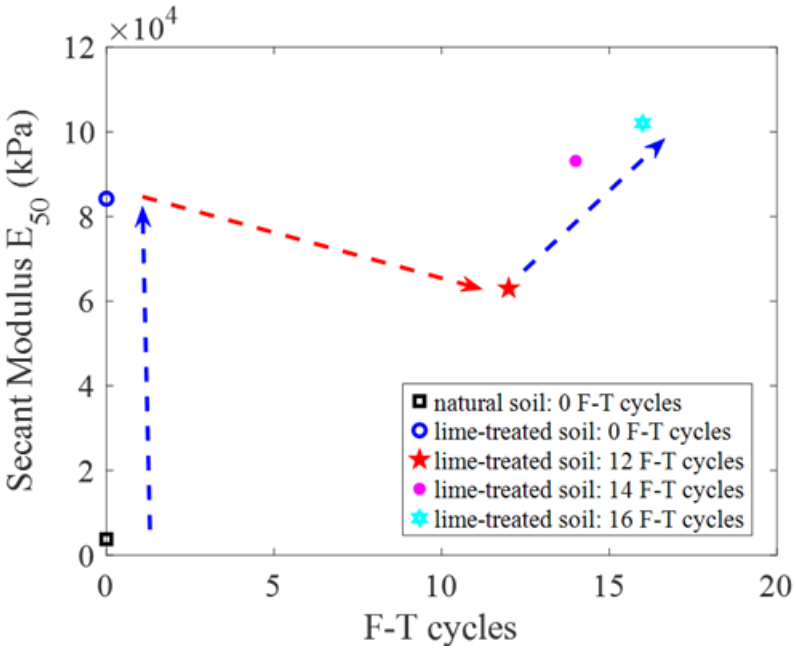

Figure 5-11 Plot showing the secant modulus versus freeze-thaw cycles for lime-treated soil (deformation rate = 1 mm/min).

5.5.4 **Double punch tensile strength**

The double punch test is employed to determine the tensile strength of soil and has been shown to be effective in capturing brittle tensile behavior (Li and Akhtar 2022). This test indirectly estimates tensile strength by accumulating the strength yields resulting from excessive distortion (Figure 5-12). Unlike conventional tensile tests, which develop local plastic deformation under the contact area and often overestimate the strength, the double punch test proved to be a non-destructive method that accurately captures tensile strength by minimizing localized plastic deformation. This approach has proven particularly effective for materials with a large number of porous media. The mathematical relation used to determine tensile strength from the double punch test is provided in Equation 5.21.

$$\sigma_t = \frac{P}{\pi\left(KbL - a^2\right)} \tag{5.21}$$

where σ_t is the tensile strength; P is the punch load at failure on specimen; b is the sample radius; a is the punch radius; L is the specimen length; K is a material constant which is given a value of 1.0 for soil (Fang and Daniels 2017).

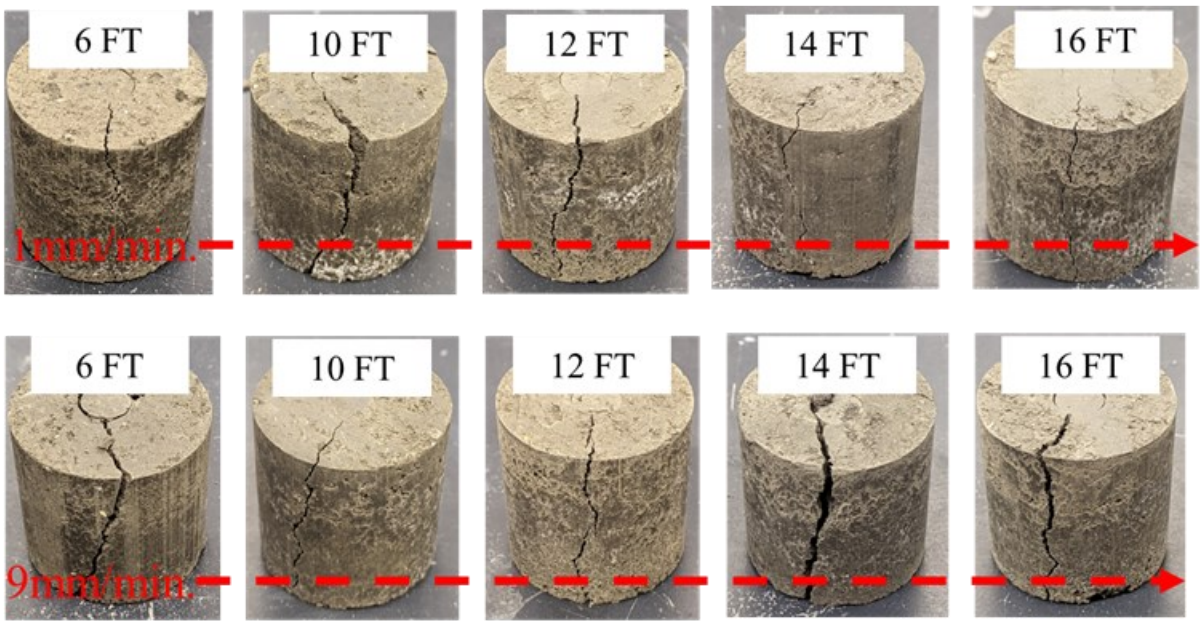

Figure 5-12 Post-failure images of lime-treated soil samples following double punch tests on samples after different F-T cycles and loading rates.

Figure 5-13a and 5-13b illustrate the thermo-mechanical changes in natural soil and lime treated soil induced by freeze-thaw (F-T) cycles, as observed through the double punch tensile test. The plots confirm that the tensile strength of natural soil was not significantly impacted by the F-T cycles. However, failure occurred at lower deformation levels due to the F-T cycles, with a notable reduction observed up to 5 F-T cycles, after which the strength stabilized despite additional F-T cycles. This behavior can be attributed to the nature of the double punch testing method, where the punch primarily impacts the center of the sample without affecting the surrounding area, thereby preventing an overestimation of tensile strength. Additionally, the freezing process induces internal deformation, while thawing promotes pore water drainage, enhancing effective interparticle interaction. This results in a shift in the tensile response from ductile behavior to brittle failure.

Similar to unconfined compressive strength, the tensile strength of lime-treated soil increases from 20 kPa to 135 kPa, indicating an enhancement of nearly seven times with the addition of lime, as

shown in Figure 5-13. Despite this increase, deformation at the failure stage remains largely unaffected. However, the tensile behavior shifts from ductile to brittle with freeze-thaw (F-T) cycles. Additionally, Figure 5-14 demonstrates that, although tensile strength initially decreases due to F-T cycles, recovery begins after 10 cycles, similar to the trend observed in unconfined compressive strength.

The experimental data demonstrates that the double punch test is an effective method for evaluating the tensile strength of soil. This technique minimizes localized plastic deformation, effectively captures brittle behavior, and performs well with porous materials. For natural soil, tensile strength is not significantly affected by freeze-thaw (F-T) cycles; however, failure occurs at lower deformation levels and stabilizes after five cycles. When soil is treated with lime, its tensile strength increases significantly, improving sevenfold from 20 kPa to 135 kPa. The behavior transitions from ductile to brittle with F-T cycles, although the failure deformation remains constant. After ten F-T cycles, the tensile strength begins to recover, mirroring trends observed in unconfined compressive strength.

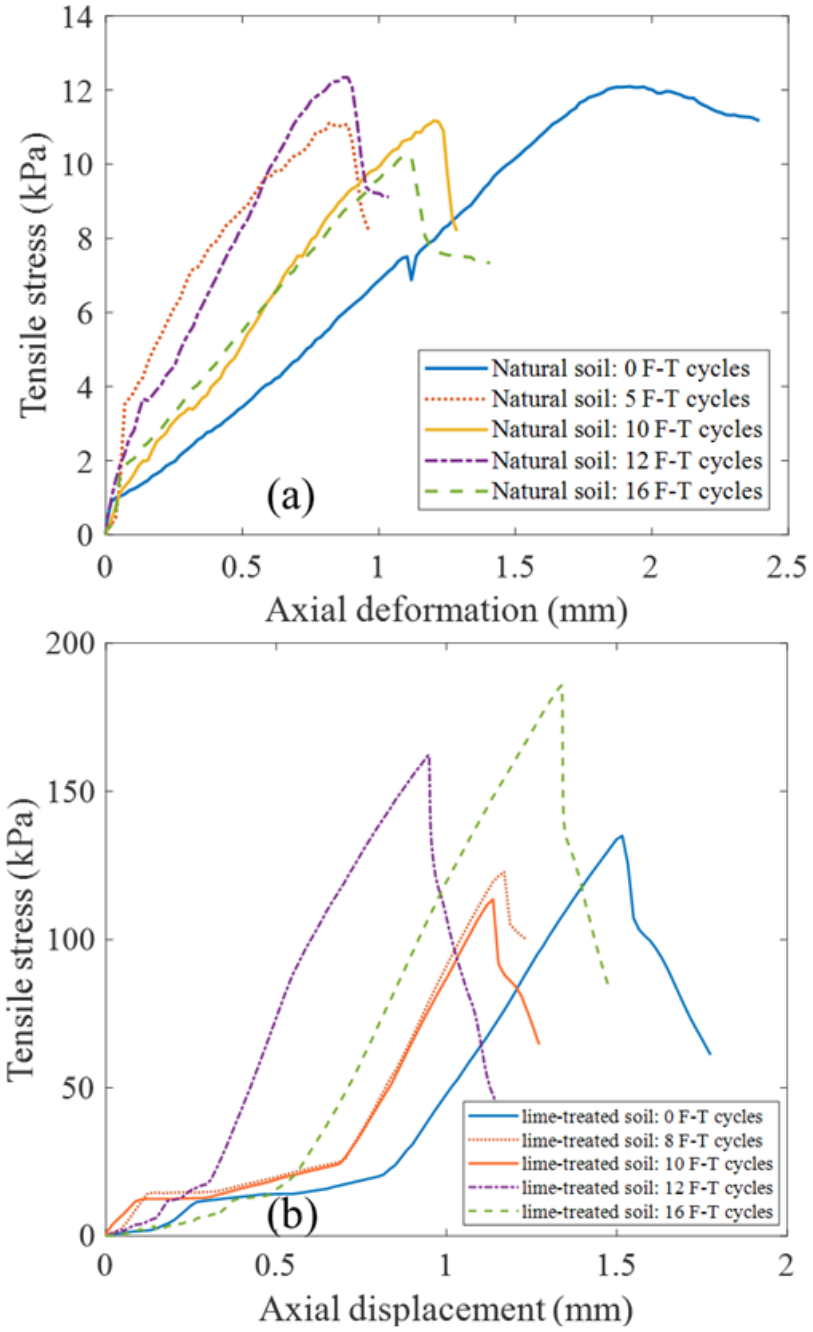

Figure 5-13 Stress-displacement curves for (a) natural soil and (b) lime-treated soil based on double punch tensile tests (deformation rate = 1 mm/min).

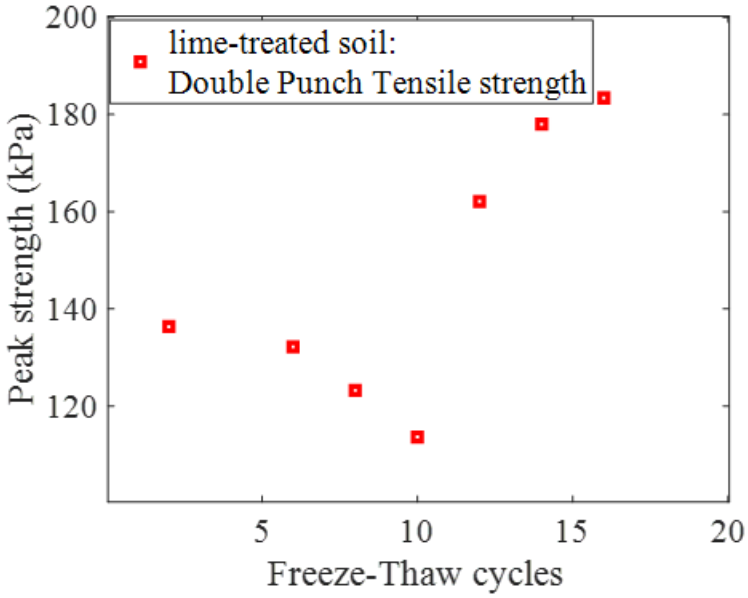

Figure 5-14 Plot showing the peak tensile strength versus freeze-thaw cycles for lime-treated soil (deformation rate = 1 mm/min).

5.6 Discussion and critical remarks

In this research, the optimum moisture content increases, consistent with the findings of Herrin and Mitchell (Herrin and Mitchell 1961). Meanwhile, the density increased from 2030 kg/m³ to 2141.6 kg/m³. This section discusses the key sensitive parameters identified in the laboratory experiments. The data showed that lime treated soil is highly sensitive to curing period, loading rates, freeze-thaw cycles, ambient moisture, and the exposure of lime treated soil to external moisture.

5.6.1 Role of curing period and loading rate in lime-treated soil strength

Figures 5-15 and 5-16 show the effects of curing period and loading rate on unconfined compressive strength and double punch tensile strength, respectively. At a slow loading rate (1 mm/min), the strength of the modified soil increases with the curing period. The failure occurred at lower deformation levels, while the failure mode shifts from a ductile style to the brittle style. This change is attributed to the decrease in moisture content over time, resulting from initial

chemical reactions and the evaporation of pore water. As moisture content reduces, the friction between soil particles and agglomerates improves, which leads to an enhanced strength. As loading continued, small cracks form and gradually coalesce with surrounding micro-cracks. This occurrence eventually leads to the formation of major cracks, as depicted in the post-failure images (Figure 5-17). In samples cured for 7 days, the deformation is distributed across the sample, whereas samples cured for 28 days exhibited top-cap failure. However, this phenomenon is less pronounced in the double punch test due to the relatively smaller area under compression. Additionally, at a higher loading rate (9 mm/min), the strength enhancement is less significant compared to the 1 mm/min rate, and failure occurred at lower deformation. This is because, at higher loading rates, minor cracks formed due to agglomeration quickly coalesced into major cracks without effectively transferring the load across the section (Figure 5-17).

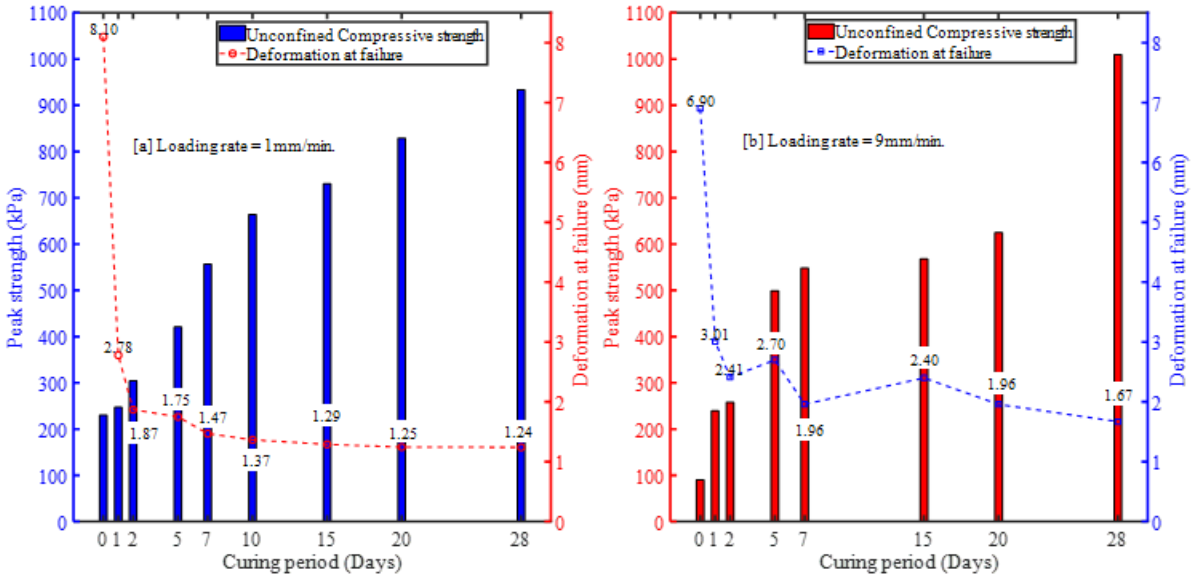

Figure 5-15 Curves showing peak stress and failure deformation as a function of curing period for lime-treated soil in unconfined compressive strength tests, comparing the impact of deformation rates of (a) 1 mm/min and (b) 9 mm/min.

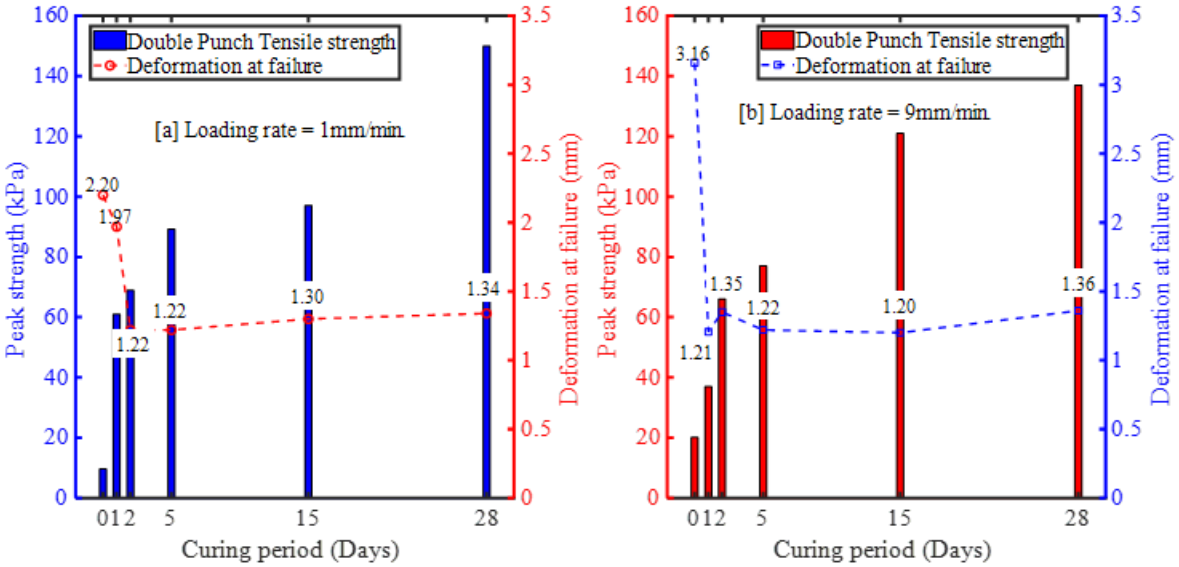

Figure 5-16 Curves showing peak stress and failure deformation as a function of curing period for lime-treated soil in double punch tensile test, comparing the impact of deformation rates of (a) 1 mm/min and (b) 9 mm/min.

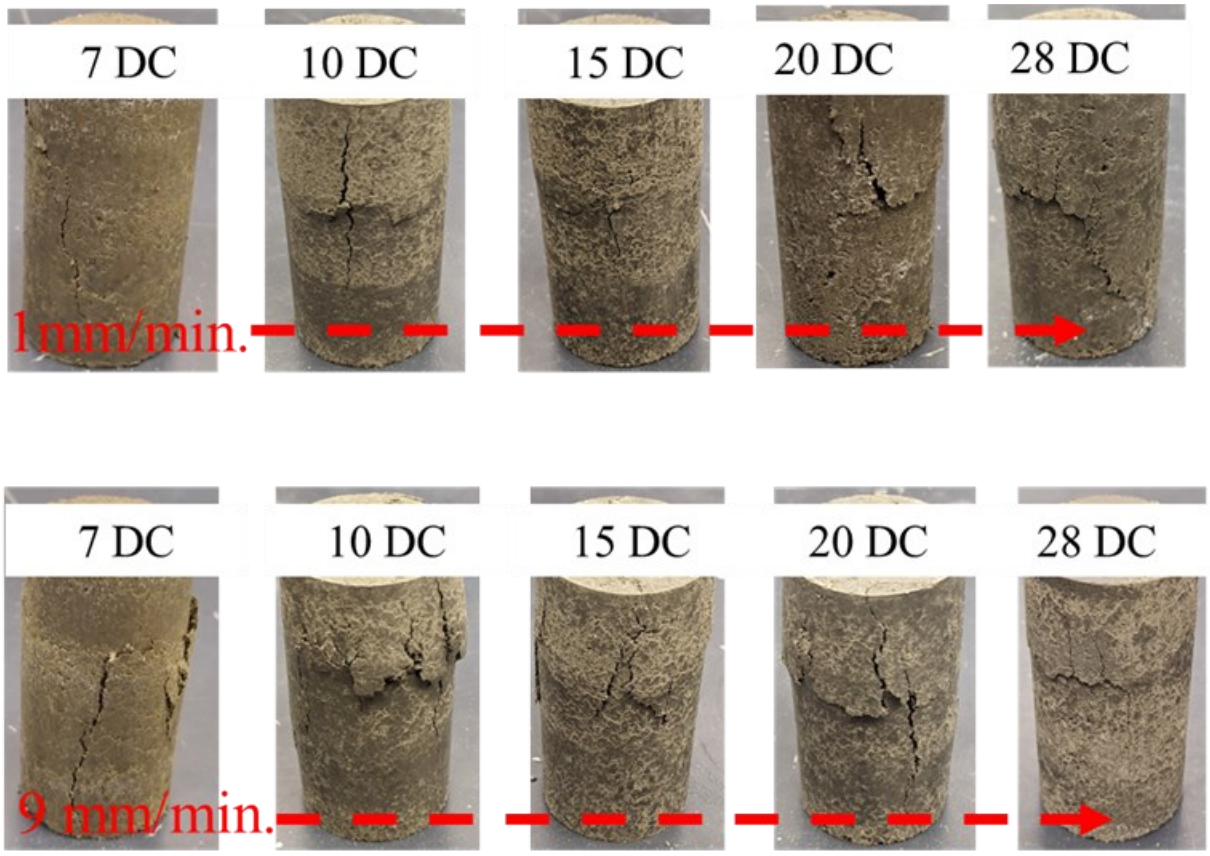

Figure 5-17 Post-failure images of lime-treated soil after unconfine compressive strength testing at loading rates of (a) 1 mm/min and (b) 9 mm/min, showing the effects of different curing periods in days (DC) on failure patterns.

5.6.2 **Role of long-term curing period**

Consistent with numerous previous studies, we assumed that a 28-day curing period would be representative of achieving maximum soil stability. However, earlier research has also investigated the long-term strength gain of lime-stabilized clayey soil. Figure 5-18 illustrates the evolution of unconfined compressive strength in lime-treated soils over an extended curing period. The plot demonstrates that the strength of the lime-treated soil increases from 890 kPa to 1900 kPa, representing more than a twofold enhancement over 155 days of additional curing. This improvement is attributed to secondary pozzolanic reactions and modifications in interparticle interactions. It can also be seen that that the strength increases 13.1 kPa/day from 20 to 28 days of curing, but the strength increases only 6 kPa/day for 28 days and 183 days. This trend shows that the secondary pozzolanic reaction in lime treated soil with water is extremely slow beyond 28 days. Additionally, the plot shows only a negligible difference in deformation at peak strength, indicating that significant changes in index properties occur primarily within the first 28 days of curing.

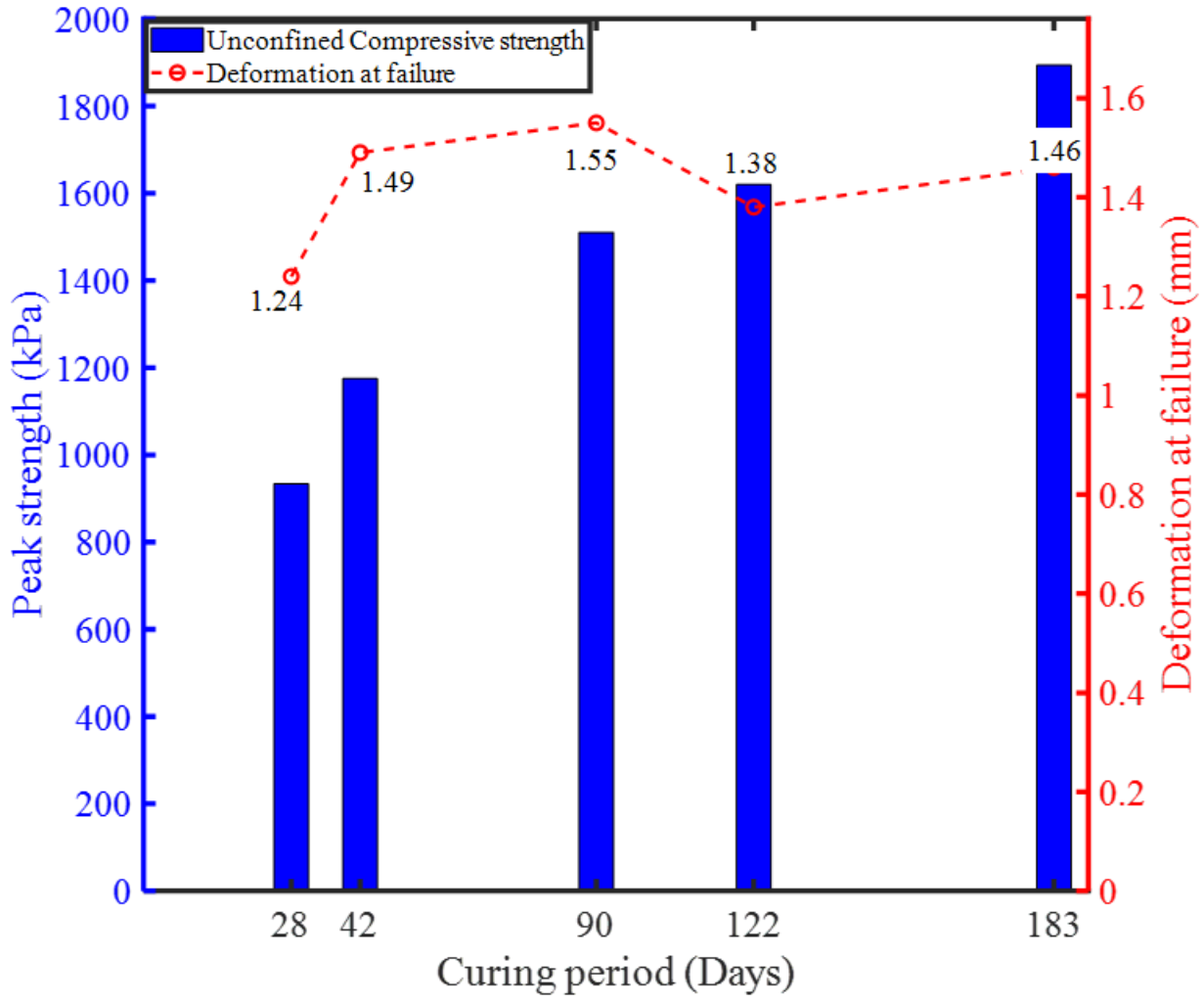

Figure 5-18 Plots showing the relation among unconfined peak strength and failure deformation versus curing period for lime-treated soils (deformation rate = 1 mm/min).

5.6.3 **Role of loading rate during freeze-thaw cycles**

The loading/deformation rate significantly affects the mechanical response of viscoelastic and viscoplastic materials. Figures 5-19 and 5-20 illustrate the strength curves for natural soil and lime-treated soil under the combined effects of loading rate and freeze-thaw (F-T) cycles. While F-T cycles had minimal impact on natural soil at a loading rate of 1 mm/min, a higher loading rate of 9 mm/min resulted in approximately 30% strength degradation during the first 6 F-T cycles. This was followed by a strength recovery with additional F-T cycles (Figure 5-19). This degradation

occurs because, at higher loading rates, microcracks coalesce into larger local cracks. This effect is exacerbated by F-T cycles, which create larger pores during freezing. Additionally, it is observed that the strength recovery after 6 F-T cycles is greater at higher loading rates compared to lower ones. This is likely due to the rearrangement of particles, particularly sand, which enhances resistance but leads to a more brittle response.

In contrast to natural soil, lime-treated soils exhibit greater strength and ductile behavior under higher loading rates. However, its response to freeze-thaw (F-T) cycles is similar to that at lower loading rates, showing initial strength degradation followed by recovery (Figure 20). This behavior is further illustrated in Figure 5-21, which plots peak strength against F-T cycles. The strength degrades up to 12 F-T cycles before the modified soil begins to regain strength. Although the effect of loading rate combined with F-T cycles is not clearly observed in the double punch test, the changes in failure mode support our findings from previous sections. Specifically, the deformation pattern in modified soil samples subjected to F-T cycles shifts to a cap-failure mode, which becomes more pronounced in cases with higher loading rates and more F-T cycles. Additionally, this phenomenon is more apparent in Figure 5-22 where damage factor is plotted against the F-T cycles. It can be seen that under compression test, strength continuously degraded till 12 F-T cycles but with further F-T cycles the lime treated soil started regain strength after this threshold F-T cycles, however, at lower loading rate the strength degradation is more than higher loading rate but the strength regain is slower. In contrast to compression test during double punch test, the strength degradation continued till 5 F-T cycles and it degraded more at higher loading rate while the strength recovery reach to almost same percentage at 16 F-T cycles.

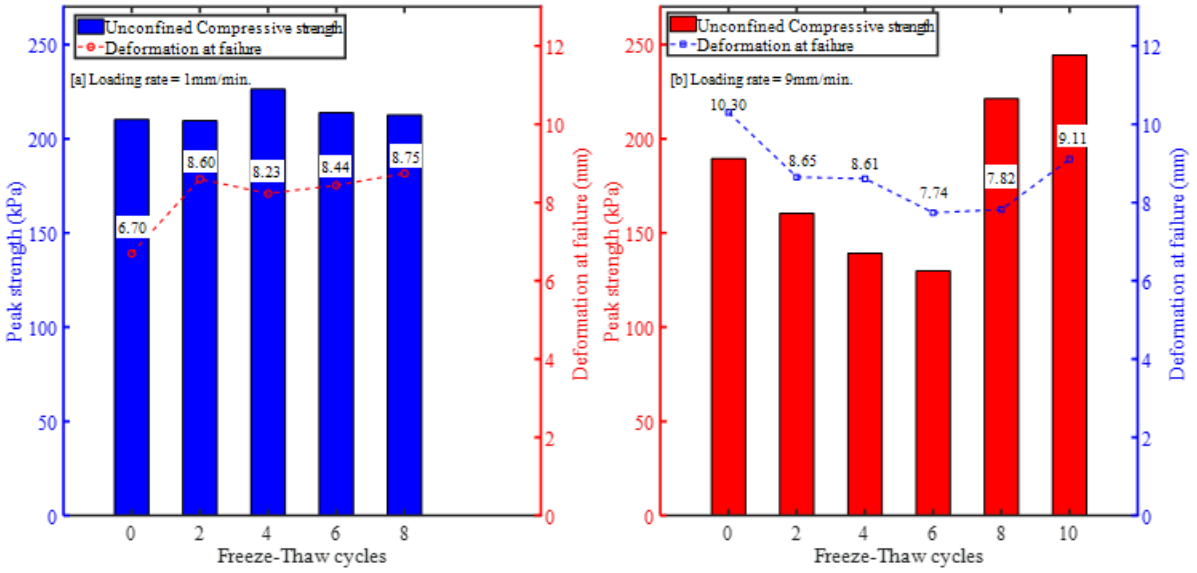

Figure 5-19 Curves illustrating peak stress and failure deformation as a function of freeze-thaw cycles for natural soil (NS) under unconfined compressive strength testing at (a) 1 mm/min and (b) 9 mm/min deformation rates, demonstrating the influence of freeze-thaw cycles on soil performance.

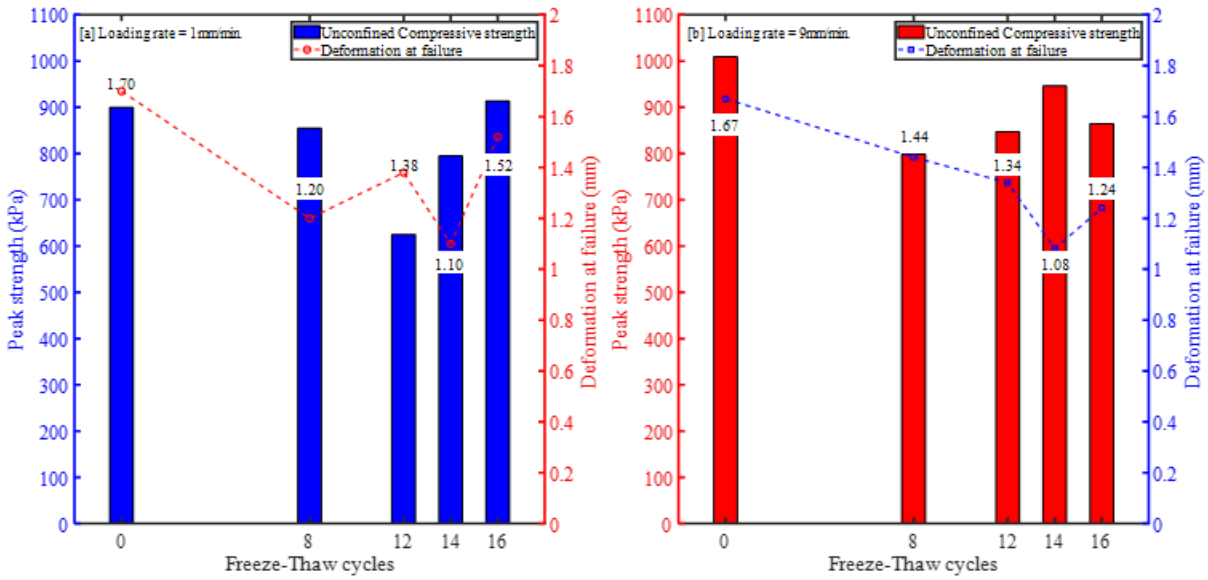

Figure 5-20 Curves illustrating peak stress and failure deformation as a function of freeze-thaw cycles for lime treated soil (LS) under unconfined compressive strength testing at (a) 1 mm/min and (b) 9 mm/min deformation rates, demonstrating the influence of freeze-thaw cycles on soil performance.

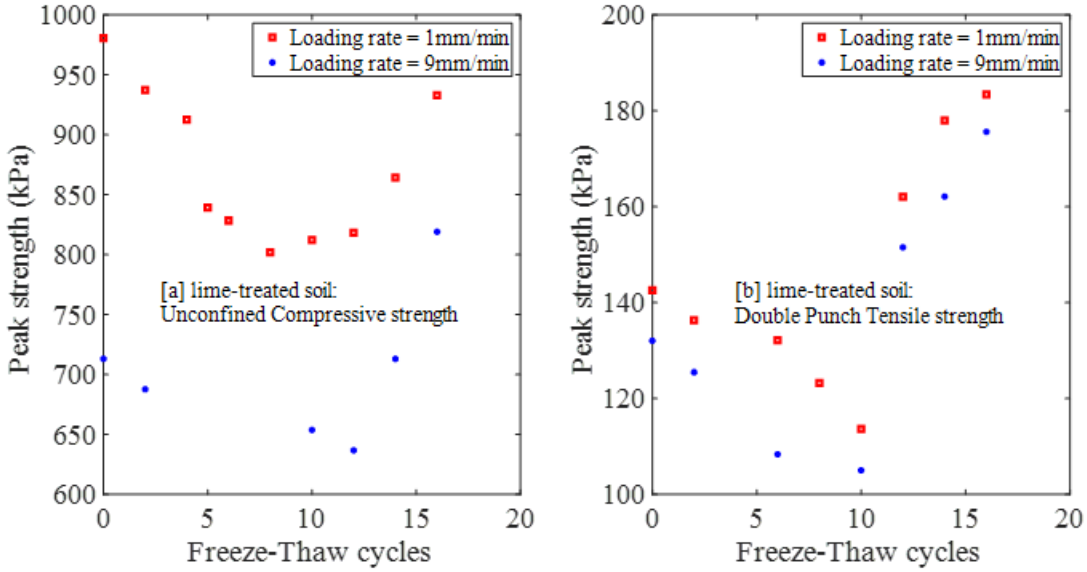

Figure 5-21 Peak stress versus freeze-thaw cycles for lime-treated soil under different deformation rates: (a) Unconfined compressive strength test at 1 mm/min and 9 mm/min, and (b) Double punch tensile strength test at 1 mm/min and 9 mm/min.

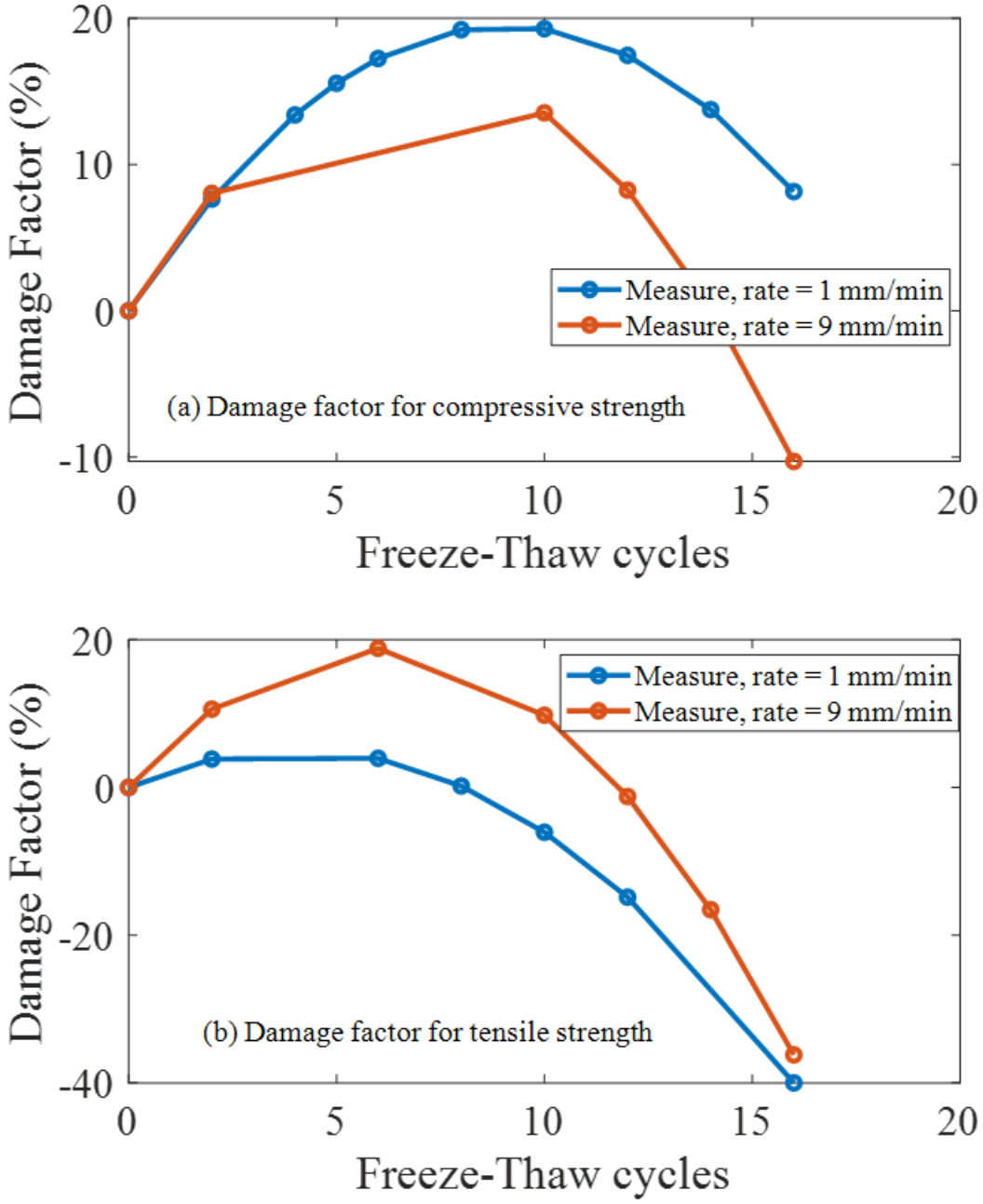

Figure 5-22 Damage factor versus freeze-thaw cycles for lime-treated soil under different deformation rates: (a) Unconfined compressive strength test at 1 mm/min and 9 mm/min, and (b) Double punch tensile strength test at 1 mm/min and 9 mm/min.

5.6.4 **Role of moisture on post-curing strength**

This section examines the effect of external moisture contact on lime-treated soil cured for 28 days. In this study, 10 grams of water were sprayed onto the entire surface of the lime-treated soil

sample following the completion of the 28-day standard curing period. The sample was then preserved using the same method as for freeze-thaw (F-T) cycles to prevent moisture evaporation. As shown in Figure 5-23, the strength of the water-treated modified soil sample decreases by nearly 200 kPa when tested 15 days after the post-curing treatment. In contrast, the plot indicates that lime-treated soil, despite being exposed to moisture, retains higher strength than natural soil. Moreover, lime-treated soil demonstrates limited deformation at failure for the sample with extra moisture treatment.

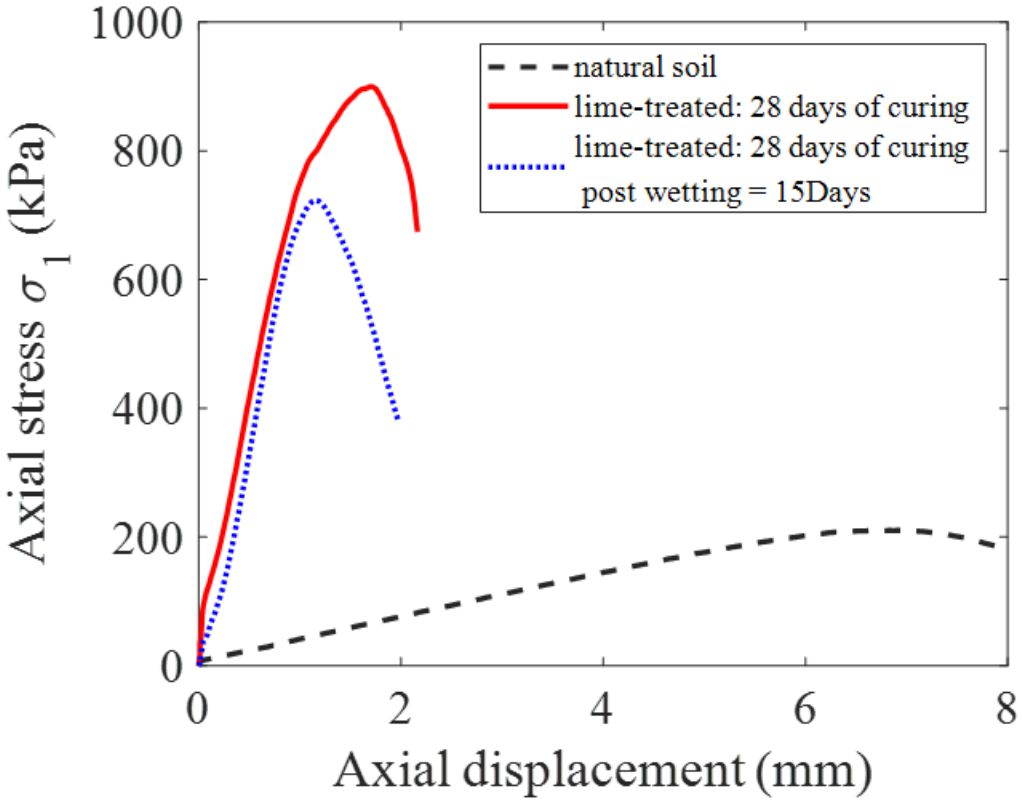

Figure 5-23 Stress-displacement curve for natural soil and lime-treated soil during unconfined compressive strength testing at 1 mm/min., showing the effect of external moisture content on lime-treated soil.

5.7 Conclusions and findings

This paper investigated the effects of hydrated lime, F-T cycles, curing periods, and loading rates on the mechanical response and physical properties of silty clay/sandy silt soil retrieved from a

northern Quebec construction site. The underlying stabilization mechanism was analyzed, and the unexpected response soil was explored and discussed. The conclusions are drawn as follows:

- Adding hydrated lime increased the optimum moisture content of the soil from 11.2 % to 14.5 % and decreased its bulk density from 2030 kg/m3 to 2141.6 kg/m3. The enhancement in strength is more pronounced at lower loading rates. Regardless of the loading rate, the strength of the modified soil improves with longer curing periods. Notably, the deformation required to reach peak strength is significantly reduced up to 28 days of curing. Although further curing continued to enhance strength, it has minimal impact on deformation beyond this period.
- Monitored air temperature data at the Umiujaq site shows significant fluctuations, with ambient temperatures contributing to permafrost thawing. Our study compared three different GSHP operation scenarios and concluded that to effectively control ground settlement, it is preferable to maintain GSHP operation year-round rather than shutting it down during the summer months. Our numerical results also quantify the potential plastic deformation in the ground surrounding the borehole due to GSHP operations.
- Freeze-thaw cycles not only affect the strength of natural soil but also alter the deformation at the peak strength. For natural soils, the strength increases due to the reorganization of coarse particles, resulting in failure at larger deformations. Similarly, the mechanical response of lime-treated soil (under both UCS and DPT tests) is highly sensitive to F-T cycles. The strength of lime-treated soil decreases up to 12 F-T cycles, accompanied by a reduction in deformation at peak strength. However, the strength begins to recover with additional cycles, with peak strength being achieved at higher deformation levels. The double punch test proves effective and efficient in capturing the brittle tensile response without causing unnecessary damage or localized accumulation of plastic deformation near the contact area.

- The loading rate, lime content, curing period, and freeze-thaw (F-T) cycles significantly influence the failure modes in soils. Under UCS loading conditions with a loading rate of 1 mm/min, the addition of lime and the application of a curing period led to a change in failure modes. This behavior is more pronounced with the combination of F-T cycles and higher loading rates. However, this effect is less evident in the double punch tests due to the nature of the test.
- The formation of agglomerates (clay, silt, and fine sands), combined with the effects of freeze-thaw (F-T) cycles and loading rates, play a crucial role in strength degradation and failure modes, highlighting the need for further investigation. Additionally, the impact of long-term curing, surrounding moisture on modified soil and determination of threshold moisture level that would make the treatment ineffective requires a detailed long-term curing and micro-level study, given the complex and inconsistent outcomes observed during long-term curing and external moisture contact.

Preface to Chapter 6

The stabilization of silty clay soils is a critical challenge in geotechnical engineering, especially in cold regions where varying stress paths and temperature conditions significantly impact soil behavior. Lime stabilization has been widely adopted as an effective method to enhance soil strength and durability. However, the interaction of lime-treated soils with freeze-thaw cycles and different loading conditions remains an area requiring further exploration. Understanding these influences is essential for designing long-lasting infrastructure in permafrost and seasonally frozen environments. This chapter presents an experimental and numerical investigation into the mechanical behavior of lime-treated silty clay under different stress paths and temperature variations. Through comprehensive laboratory testing, including unconfined compressive strength, double punch tensile strength, and temperature-controlled triaxial tests, this research quantifies the effects of lime treatment on strength characteristics and deformation responses. Additionally, finite element modeling (FEM) is employed to simulate strain hardening and post-peak softening behaviors, providing a predictive framework for soil performance under real-world conditions. By bridging experimental findings with numerical simulations, this research contributes to the development of improved soil stabilization techniques. The insights gained will aid engineers and researchers in optimizing lime treatment strategies, ensuring safer and more resilient infrastructure in cold climates.

Chapter 6

6 Experimental and numerical investigation of the mechanical behavior of lime-treated silty clay under varying stress paths and temperature conditions [4]

6.1 Abstract

Lime-stabilized soil is widely used in slopes, foundations, and roadway construction, necessitating an evaluation of its strength characteristics under varying temperature conditions. This study investigates the tensile, compressive, and shear strengths of natural and lime-treated marine soils from a northern Canadian community. Experimental tests, including the double punch tensile strength test, unconfined compressive strength test, and consolidated undrained triaxial test, were conducted at varied loading rates and temperatures ranging from 25°C to -13.5°C. Results indicate that lime treatment alters the soil's ductile behavior and post-peak hardening response into brittle behavior. A nonlinear relationship between strength (friction angle and cohesion) and temperature in the studied soil is obtained based on the temperature-controlled triaxial test results. Finite element modeling, validated against laboratory data, effectively captures strain hardening and post-peak softening behaviors. The FEM analysis with the hyperbolic Drucker–Prager model accurately represents frozen soil deformation under compressive, tensile, and shear loading, while

[4] A version of this manuscript has been submitted to the *Journal of Acta Geotechnica* (2025).

the damage XFEM model successfully simulates damage initiation and crack propagation in uniaxial compressive and indirect tensile tests. These models reliably replicate failure patterns, enhancing the predictive capability for soil behavior in cold environments.

Keywords: Lime stabilization, frozen soil, strength characterization, finite element modeling, damage

6.2 Introduction

In cold regions, there is an increasing need for sustainable civil infrastructure development due to urbanization and technology improvements. The existence of crucial infrastructures like roads, runways, water and wastewater treatment plants, electricity grids, pipelines for the transportation of natural resources, networks for mineral extraction, and communication systems are crucial to the development and prosperity of metropolitan communities in these locations. However, unstable soil conditions, mostly brought on by permafrost degradation and melting impacts made worse by climate change, frequently make construction in these areas difficult (Doré et al. 2016, Akhtar and Li 2020b, Zhang et al. 2023). Changes in the ground's temperature regime brought on by environmental factors can drastically reduce permafrost's ability to tolerate the structural loads imposed by infrastructure and structures (Streletskiy et al. 2015). Reduced compactness, strength, permeability, compressibility, and load-bearing capacity are among the engineering characteristics of ice-rich soils that alter as they thaw (Qi et al. 2006). The stability and integrity of engineered structures are put at risk by these changes, which frequently cause uneven deformation and ground subsidence (Nelson et al. 2001, Lu et al. 2024).

Artificially frozen ground engineering in soft soil formations is another issue related to the thermo-mechanical responses of clay soils under freezing actions (Akhtar and Li 2025). Such poor and

soft soils are often the only feasible option for construction due to limited space in urban planning. To address this challenge, stabilization and reinforcement techniques are applied to enhance their mechanical properties, enabling their effective use without relying on costly, high-quality alternatives. However, reducing temperature-induced failures requires a focus on in-situ soil modification techniques and improving the residual strength of soils after thawing. This approach balances the need to address the weak mechanical behavior of subsoil with the financial limitations associated with full soil replacement. Several strategies are used in the field to address this problem and maintain consistent and dependable residual soil strength. Broadly, the soil stabilization strategies are divided as chemical, biological, and physical/mechanical (Prusinski and Bhattacharja 1999, Nelson et al. 2001, Shukla et al. 2009, Bo et al. 2009, Das 2010, Ghazavi and Roustaei 2013, Kanchi et al. 2015, Ozdemir 2016, Triantafyllidis and Kimmig 2019, GhavamShirazi and Bilsel 2021, Ying et al. 2022, Lu et al. 2024, Akhtar and Li 2025). While mechanical stabilizing methods like reinforcing and compaction are frequently employed, they are generally expensive and prone to instability. Although biological stabilization techniques, including microbially generated calcium carbonate precipitation, have been thoroughly studied, it is still unclear how they will be put into practice. Comparatively, chemical stabilization techniques are more dependable, less expensive, and the most used for stabilizing soil at the moment. It has been demonstrated that conventional chemical stabilizers, such as cement and lime, greatly increase the strength of soil (Wei et al. 2023). Throughout history, lime has been widely utilized in a variety of construction projects (McDowell 1959). It is frequently used in modern infrastructure to increase ground stability in projects like pavement subgrades, embankments, airports, highways, and lime piles (Little 1995, Bell 1996, Vorobieff and Murphy 2003, Wilkinson et al. 2010, Notman 2011, Herrier et al. 2012, Abiodun and Nalbantoglu 2015, Das et al. 2021).

Previously, various researchers studied the role of lime in cold region soil and the impact of thermally induced changes in strength of various soil includes loess, expansion soil, soft clays and saline soil (Herrier et al. 2012, Aldaood et al. 2014, Abiodun and Nalbantoglu 2015, Güllü 2015, Streletskiy et al. 2015, Bozbey et al. 2018, Das et al. 2021). Zhang et al. (Zhang et al. 2020) studied the impact of temperature and curing period periods on unconfined compressive strength, thermal conductivity and pH value of lean clay, silt and elastic silt soils. Their study determined that with the drop in temperature (2 ^{o}C), the compressive strength drops twice as much as at 21 ^{o}C because of the reduction of pozzolanic activities at lower temperature. Ghobadi et al. (Ghobadi et al. 2014) studied effect of pH variations and curing period of unconfined compressive strength and shear strength parameters of clay soil at room temperature. Unconfined compressive strength increased with the increase in curing period up to 30 days, after which it stabilized. However, both cohesion and friction angle drop initially but shows recovery once the pH value reaches 5. Kan and Fancois (Kan and François 2023) studied the behaviour of lime treated plastic clay under both consolidated undrained triaxial tension and compression tests at room temperature and different confining pressures (up to 540 kPa). They determined that shear strength parameters (e.g. cohesion and friction angle) increased considerably with the addition of lime and curing periods. Wang et al. (Wang et al. 2013) investigated the geotechnical properties of lime treated Dunkirk sediments under unconfined compressive strength test, oedometers test, direct shear test and triaxial shear test at room temperature with the addition of lime in 3 % and 6 % by weight of dry sediments. According to their test results, adding lime significantly increased the unconfined compressive and shear strengths. As the lime concentration rises, failure shifts from plastic to brittle, accompanied by increased failure strength and lower failure strains. Through pozzolanic interactions with clay minerals, lime improves shear strength metrics including cohesiveness and internal friction angle

and the pre-consolidation pressure raised. Additionally, Both the untreated and lime-treated Dunkirk sediments have almost no cohesiveness, but the internal friction angle is greatly increased by lime treatment. Song et al. (Song et al. 2020) studied the impact of wetting and drawing cycles on lime treated soil under triaxial test at room temperature. Song et al. concluded from their experiments that the strength and permeability properties of lime-stabilized specimens improved significantly. After undergoing cyclic wet-dry cycles, the shear strength, strength parameters, and shear moduli decreased notably for lime treated and untreated specimens but gradually increased for lime-stabilized ones. Baldovino et al. (Baldovino et al. 2018) studied the mechanical strength response of lime-stabilized soil under unconfined compressive strength test and split tensile strength test at room temperature considering role of lime contents and curing period. They concluded that the split tensile and compressive strength increase proportionally with lime content (up to 9%), curing time, and sample porosity. Importantly, they determined that suction has minimal impact on strength when specimens are molded at optimal water content with saturation levels above 80%. Furthermore, besides studies focusing on the physio-mechanical response of lime-treated soil subjected to freeze-thaw cycles and temperature-dependent curing periods, extensive research has also been conducted on the instantaneous and time-dependent strength behavior of untreated frozen soil. These investigations have employed various testing methods, including uniaxial compression tests (Bragg and Andersland 1981, Zhu and Carbee 1984, Girgis et al. 2020), tensile strength tests (Akagawa and Nishisato 2009, Zhou et al. 2015, Li et al. 2019b, Li and Akhtar 2022), and triaxial tests (Chamberlain et al. 1972, Nassr et al. 2018, Staszewska et al. 2024). Additionally, numerical modeling of frozen soil has also been utilized to simulate laboratory experiments (Selvadurai et al. 1999b, Liu et al. 2008b, Li and Akhtar 2022, Akhtar and Li 2024b).

Prior research has examined the impact of freeze-thaw on cold-weather soils and the application of lime to strengthen soil. The temperature-dependent mechanical behavior of fine-grained soils treated with lime, however, has received little study. Additionally, comprehensive investigations of lime-treated soil behavior under compression and tension stress paths are lacking. Furthermore, there is a substantial data gap concerning the numerical modeling of soils treated with lime. To fill in these gaps and advance our knowledge of this area, more study is necessary. For sustainable development projects in northern Quebec, Canada, where massive building is taking place in Cree villages, this need is especially important. There are particular difficulties because to the local ground conditions, which are primarily composed of marine clay deposits (Royer 2016). The safety of existing and future infrastructure may be jeopardized if the geotechnical behavior of these soils is not thoroughly investigated.

This study investigates the effectiveness of lime treatment in enhancing the strength of marine silty clay soils for geotechnical applications, including natural slopes, highway subgrades, and foundations, where varying stress path conditions—compression, tension, and shear—may be encountered. A series of laboratory tests were performed on soil samples retrieved from northern Quebec, Canada, utilizing specially designed experimental facilities. The experimental program included temperature-controlled triaxial tests, double-punch tensile strength tests (DPTs), and unconfined compressive strength tests (UCS). The resulting data were subsequently incorporated into finite element modeling to establish a comprehensive database for practical engineering applications in the field.

6.3 **Lime stablization**

The distribution of interior voids and the interaction between internal particles determine a material's mechanical properties. The kind and amount of soil and binder utilized have a significant

impact on the particle interaction in stabilized soils that are subjected to particular curing conditions. In the meantime, the compactness of the soil is directly related to the distribution of voids (Guo et al. 2022). Beginning in the early 1900s, lime was used to stabilize soil (Johnson 1949, Bell 1996). In the United States, it was initially used as a soil stabilizer on a small section of highway in 1924 (McCaustland 1925). The stabilization of soils using lime as an addition has gradually risen with the expansion of highways and railroads in the contemporary era. This is mostly because of its affordability and notable stability features over the long and short term (Rogers and Glendinning 2000).

The main affecting processes include carbonation, pozzolanic reactions, flocculation and agglomeration, and cation exchange (Arabi and Wild 1986, Prusinski and Bhattacharja 1999). According to Boardman et al. (Boardman et al. 2001), these response mechanisms fall into two primary processes: modification to reduce plasticity and solidification. According to Salehi and Sivakugan (Salehi and Sivakugan 2009), flocculation and cation exchange activity lead to modification, whereas pozzolanic processes cause solidification. Significant changes in treated soils' physical, chemical, mineralogical, and microstructural characteristics result from these interactions (Khattab et al. 2007). The following phases are involved in the transformation of lime-treated soil:

a. adding water to hydrated lime causes an exothermic reaction that splits the lime into OH- and Ca2+ ions (Equation 6.22).
b. To address the charge deficiency in the crystal structure of clay, cations and dipolar water molecules are attracted to the negatively charged cleavage surfaces. This interaction creates a diffused separation between two charged surfaces, commonly referred to as the "diffuse double layer." The double layer acts as a lubricant, with its thickness determining the soil's activity

and plasticity (i.e. the thicker the layer, the more active and plastic the soil becomes). Monovalent cations, such as sodium (Na^+) and potassium (K^+), along with water molecules, primarily form this double layer. When calcium ions (Ca^{2+}) are introduced, they replace the monovalent cations in the soil minerals. This substitution increases the inter-particle attractive forces, significantly reducing the thickness of the diffuse double layer (Rogers and Glendinning 2000). If the attractive forces exceed repulsion, the negative charges on the clay faces interact with the positive charges on the edges, leading to flocculation and agglomeration. Calcium-based soil stabilizers provide a sufficient supply of calcium ions to facilitate this ion exchange. The higher charge density of di- or trivalent ions reduces the double layer thickness significantly. This ion-exchange process occurs rapidly, typically within a few hours, as illustrated in Figure 6-1.

c. In the second stage, the hydroxide ions (OH^-) that are produced from hydrated lime make the soil matrix more alkaline, which results in a high pH environment ($pH \geqslant 12.4$) that makes it easier for silica and alumina to dissolve from the soil (Thompson 1968). Cementitious compounds like calcium silicate hydrate (CSH) and calcium aluminate hydrate (CAH) are created when silica and alumina from clay lattices dissolve and react with calcium ions (Ca^{2+}) and hydroxide ions (OH^-) under these circumstances (Federico et al. 2015). Equations 6.23 and 6.24 describe these reactions, which are referred to as pozzolanic reactions. The resulting cementitious compounds, such as CSH and CAH, strongly bond clay particles together, leading to long-term improvements in soil properties. These improvements include increased shear strength, enhanced stability, and higher bearing capacity (Eades and Grim 1960, Petry and Little 2002, Rosone et al. 2020).

d. Carbonation is another reaction that takes place between lime and ambient carbon dioxide. The amount of lime accessible for pozzolanic reactions is decreased by this process, which yields comparatively weak cementing agents such calcium carbonate (Goldberg and Klein 1953, Eades and Grim 1960). These weak cementing agents prevent the pozzolanic interactions between silica, alumina, and lime, but they only slightly increase strength because of the setting or solidification of lime. Thus, the potential for long-term strength development is limited by the decrease in accessible lime (Arman and Saifan 1967).

The primary factor influencing the rate of dissolution of lime is particle size; finer gradations dissolve more quickly due to their larger exposed surface area (Prusinski and Bhattacharja 1999). The maximum dry density of a flocculated soil structure decreases because it defies compaction attempts and takes up more space in the soil matrix. Furthermore, the dissociation of lime raises the water requirement of the soil, which in turn raises the optimal moisture content (Bell 1996). Until the lime content reaches about 3%, the density decreases, and moisture content rises continues. After this point, additional lime content increases result in a slower density rise and a slower optimum moisture content decrease (Hussain and Dash 2014). After 3% of lime is added, the concentration of Ca2+ ions at the clay surfaces rises, and because the pore fluid's Ca2+ concentration differs, free water molecules tend to move towards the clay surface to balance the charge concentration difference. Hydration force opposes the attractive forces in this process, and eventually, the resulting forces have a tendency to turn repulsive. As a result, clay particles tend to separate, and the soil structure becomes more dispersive. This makes it easier for soil particles to slide over one another, which increases the density (Mitchell and Soga 2005, Hussain and Dash 2014).

$$CaO+H_2O \rightarrow Ca(OH)_2 \rightarrow Ca^{2+} + 2OH^- \quad (6.22)$$

$$Ca^{2+} + 2OH^{-} + SiO_2 \rightarrow CaO\text{-}SiO_2\text{-}H_2O\ (CSH) \quad (6.23)$$

$$Ca^{2+} + 2OH^{-} + Al_2O_3 \rightarrow CaO\text{-}Al_2O_3\text{-}H_2O\ (CAH) \quad (6.24)$$

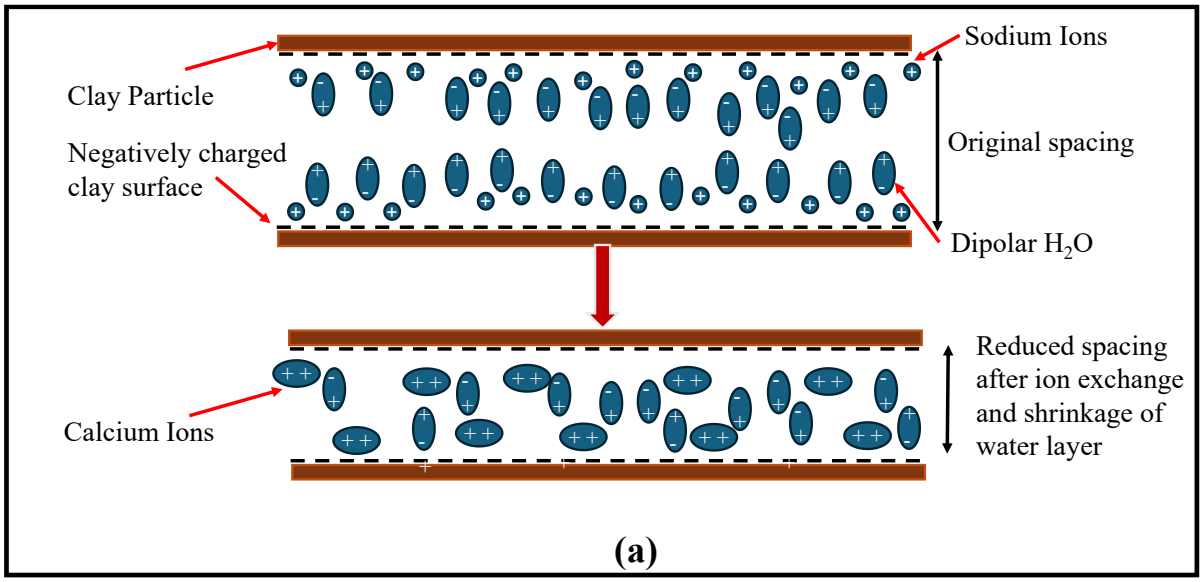

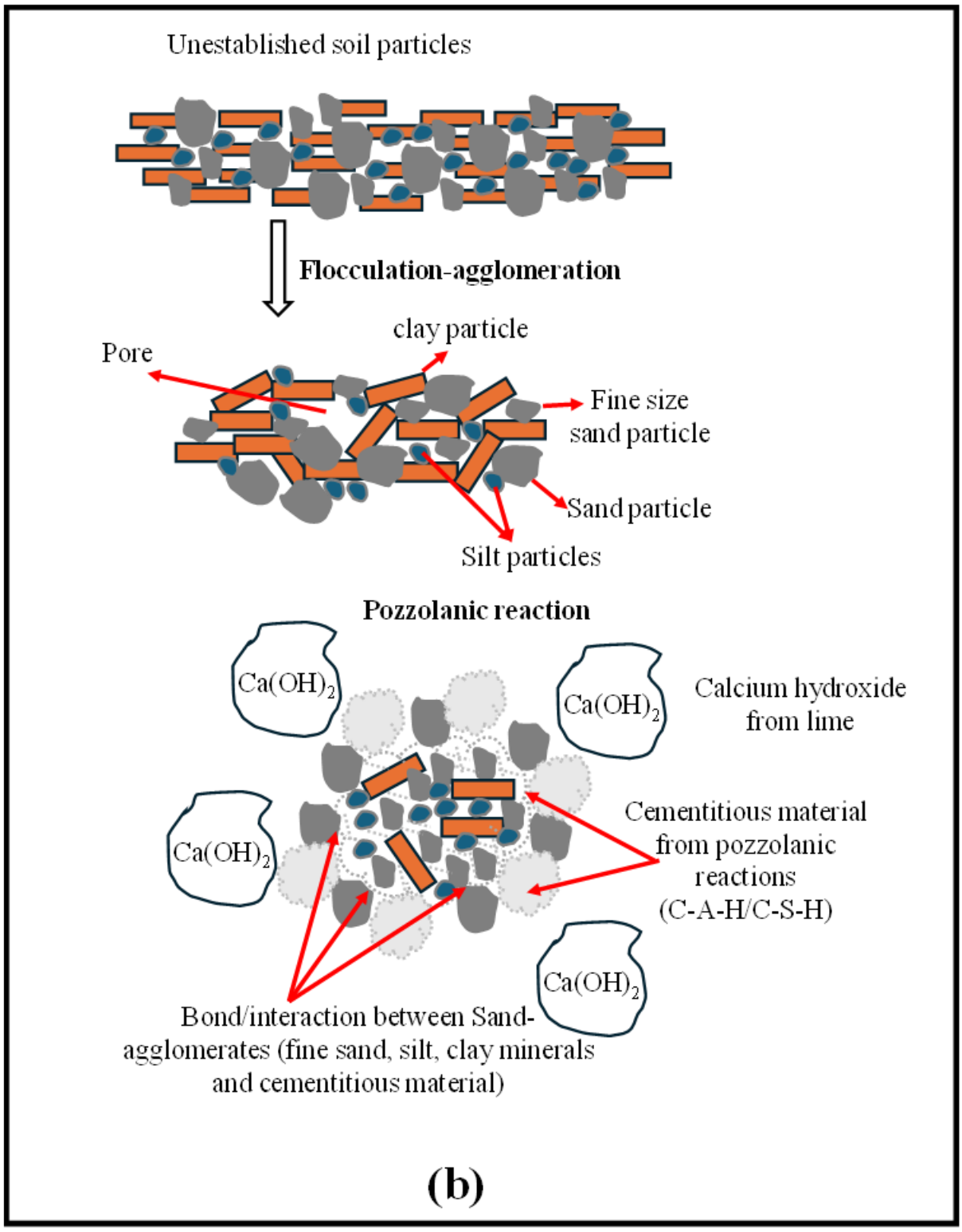
Unestablished soil particles
Flocculation-agglomeration
clay particle
Pore
Fine size sand particle
Sand particle
Silt particles
Pozzolanic reaction
Ca(OH)2
Ca(OH)2
Calcium hydroxide from lime
Ca(OH)2
Cementitious material from pozzolanic reactions (C-A-H/C-S-H)
Ca(OH)2
Bond/interaction between Sand-agglomerates (fine sand, silt, clay minerals and cementitious material)
(b)

Figure 6-1 a) Cation exchange in lime treated soil, b) Flocculation, agglomeration, and Pozzolanic reaction in lime treated soil.

6.4 Experimental program

This section presents the physio-mechanical properties of the tested soil, the chemical composition of the lime used, the experimental setups, and the results from various strength tests, including unconfined compressive strength tests (UCS), double-punch tensile strength tests (DPTs), and the temperature-controlled consolidated undrained (CU) triaxial test. The behavior of both natural soil (N-soil) and lime-treated soil (L-soil) is analyzed under varying loading conditions, temperatures, and confining pressures.

6.4.1 Material

In this study, soil was excavated to a depth of approximately three meters in the town of Waskaganish, located in northern Quebec on the southeastern shore of James Bay, Canada. The collected soil underwent several preparation steps, including air-drying, pulverization, and sieving using a 2.36 mm sieve. Detailed information on the physical properties of the soil can be found in (Akhtar and Li 2024a). The soil is classified as clayey silts (ML) with low plasticity. The particle size distribution is reconstructed and presented in Figure 6-2, while the key physical and mechanical properties are summarized in Table 6-1.

The lime was provided by the chemical company in Quebec Province, Canada. The chemical compositions of provided lime were also provided by the manufacturer. The important chemical composition of lime and soil is listed in Table 6-2.

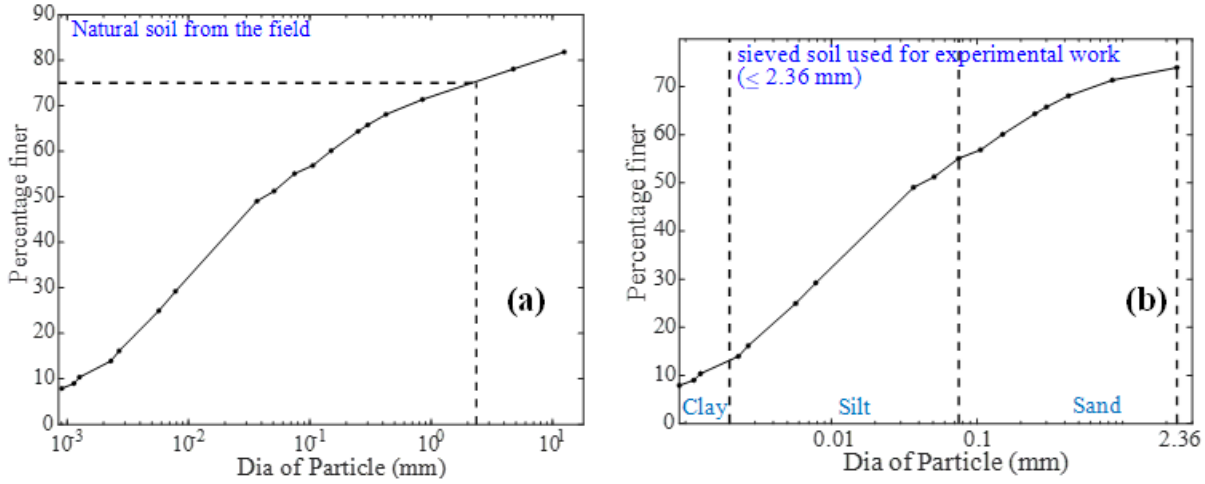

Figure 6-2 Grain size distribution of soil used for this research work: (a) natural soil from the field and (b) sieved soil used for experimental work.

Table 6-1 Physical and mechanical properties of silty clay

Property	**Value**
Particle size	≤ 2.36 mm
Liquid limit, *LL*	22.8 %
Plastic limit, *PL*	16.8 %
Plastic Index, *PI*	6.3 %
Specific gravity, *Gs*	2.66
Soil classification	ML
Cohesion (kPa)	65
Internal friction angle (°)	35

Table 6-2 Chemical composition of the used hydrated lime

Compounds	$Ca(OH)_2$	CaO	SiO_2	$CaCO_3$
Value (%)	95.9	72	1.1	1.4

6.4.2 **Experimental setup and test layout**

The soil specimens used in this study were categorized into two types: (I) specimens prepared for unconfined compression and triaxial tests, with dimensions of 50.8 mm in diameter and 101.6 mm in height; and (II) specimens for double punch tensile strength tests, with dimensions of 50.8 mm in both diameter and height. Details regarding sample preparation and preservation are available in (Akhtar and Li 2024a). Unconfined compression and double punch tensile strength tests are performed using our specially designed sub-loading frame, which enables both uniaxial compression and indirect tensile testing within a single setup by utilizing different loading frames (Girgis et al. 2020, Li and Akhtar 2022). Key technical aspects of the unconfined compressive strength test, double punch tensile strength test, and temperature-controlled triaxial tests include the following: (1) the applied loading rates were 1 mm/min, 3mm/min., and 9mm/min. for the unconfined compression test, triaxial test, and double punch test; and (2) the confining pressures in the triaxial test ranged from 100 kPa to 1800 kPa, with the testing temperatures varying between +25°C and -13.5°C. The experimental setup for the triaxial test is illustrated in Figure 6-3. To minimize thermally induced pore pressure and prevent the formation of air bubbles within the system, a small backup pressure was applied before setting the cell to the required temperature. Once the temperature was adjusted, the designated confining pressure was applied and maintained for at least 7 hours to ensure maximum consolidation. An external temperature control unit was used to achieve and stabilize the required temperature in the sample. Initially, the system took approximately 3.5 hours to reach the target temperature, which

was then maintained for an additional 12 hours to ensure the entire sample was at a uniform and stable temperature, with the confining pressure kept constant. Subsequently, the shearing stage was carried out using a strain-controlled approach. For the unconfined compressive strength test and double punch tensile strength test, the endpoint of the test was defined as either the post-peak failure stage or the strength at 15% strain in cases where strain hardening was observed. In contrast, the triaxial test was concluded when either the deviator stress stabilized, or the axial strain reached 20%.

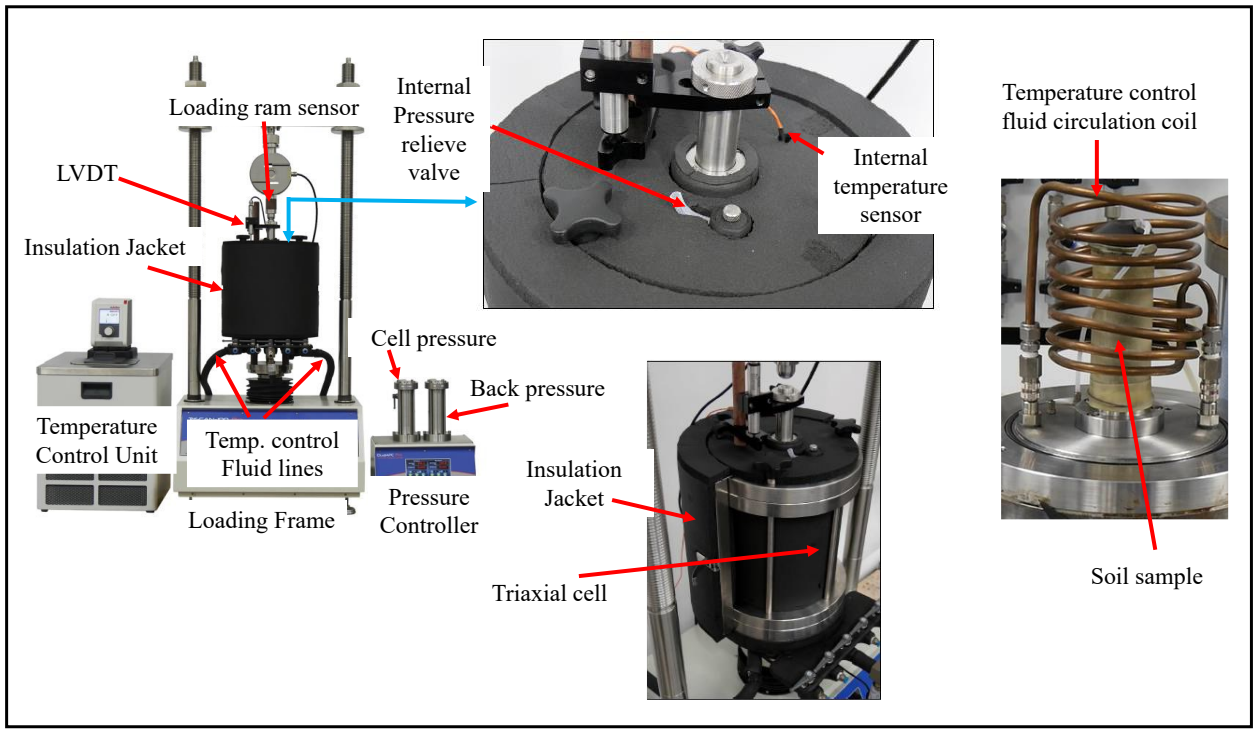

Figure 6-3 Pictures showing the applied temperature-controlled triaxial testing system.

6.4.3 **Results**

6.4.3.1 **Unconfined compressive strength and tensile strength**

The experimental laboratory results from the UCS test, DPT strength test, and temperature-controlled CU triaxial tests are presented and analyzed in terms of stress-strain behavior, shear strength parameters, secant modulus during the early loading phase, and the failure patterns.

These comparisons also examine the influence of lime stabilization and temperature-induced strength variations. Due to the difficulty of sample preparation and the special facility requirements, we did not conduct temperature-controlled DPT tests.

The stress-axial strain relationships for N-soil and L-soil under UCS tests and DPT tests are illustrated in Figures 6-4 and Figure 6-5. It is important to note that these stress-strain curves are derived using a single loading rate (1 mm/min), as the effect of loading rate on both soils has been detailed in a prior study (Akhtar and Li 2025). Under both UCS and DPT loading conditions, the N-soil exhibited ductile behavior initially, transitioning to brittle behavior as the test progressed. This transformation from ductile to brittle behavior are more distinct and pronounced under compression loading, as illustrated in Figure 6-4. The addition of lime introduced flocculation and agglomeration, resulting in the formation of secondary solid particles that enhanced interaction with sand particles but also increased void sizes. Consequently, during loading, the L-soil resisted the applied load due to these new interactions, but as deformation approached the failure stage, a sudden brittle failure occurred.

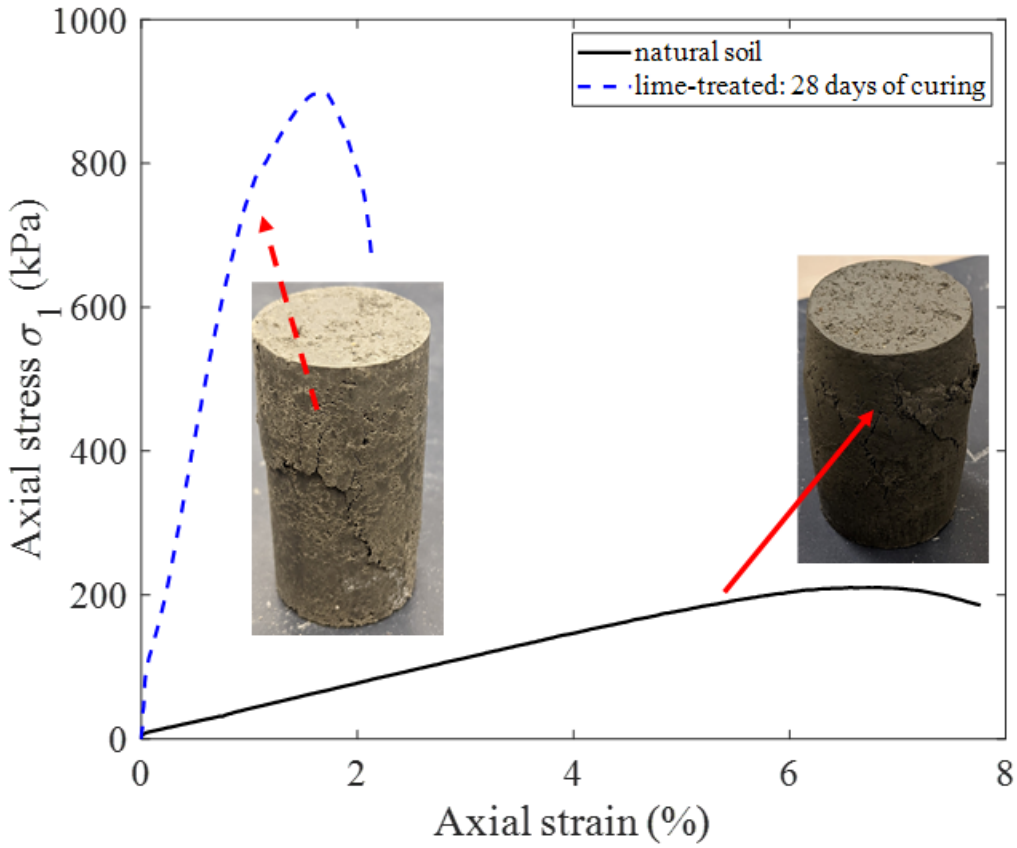

Figure 6-4 Measured stress-displacement curves of: (a) natural soil and (b) lime-treated soil from unconfined compressive strength tests (deformation rate = 1 mm/min).

A similar phenomenon can be observed in the DPT test (Figure 6-5). However, since deformation in the DPT test is applied through a puncher over a smaller area, the brittle behavior is less pronounced. Lime treatment significantly improved the strength of the soil, the compressive strength increasing from 210 kPa to 900 kPa (a 4.3-fold improvement) and tensile strength increasing from 12 kPa to 135 kPa (an 11.2-fold improvement). Furthermore, the ratio of compressive to tensile strength decreased from 17.5 in N-soil to approximately 7 in L-soil, indicating a relative improvement in tensile strength compared to compressive strength.

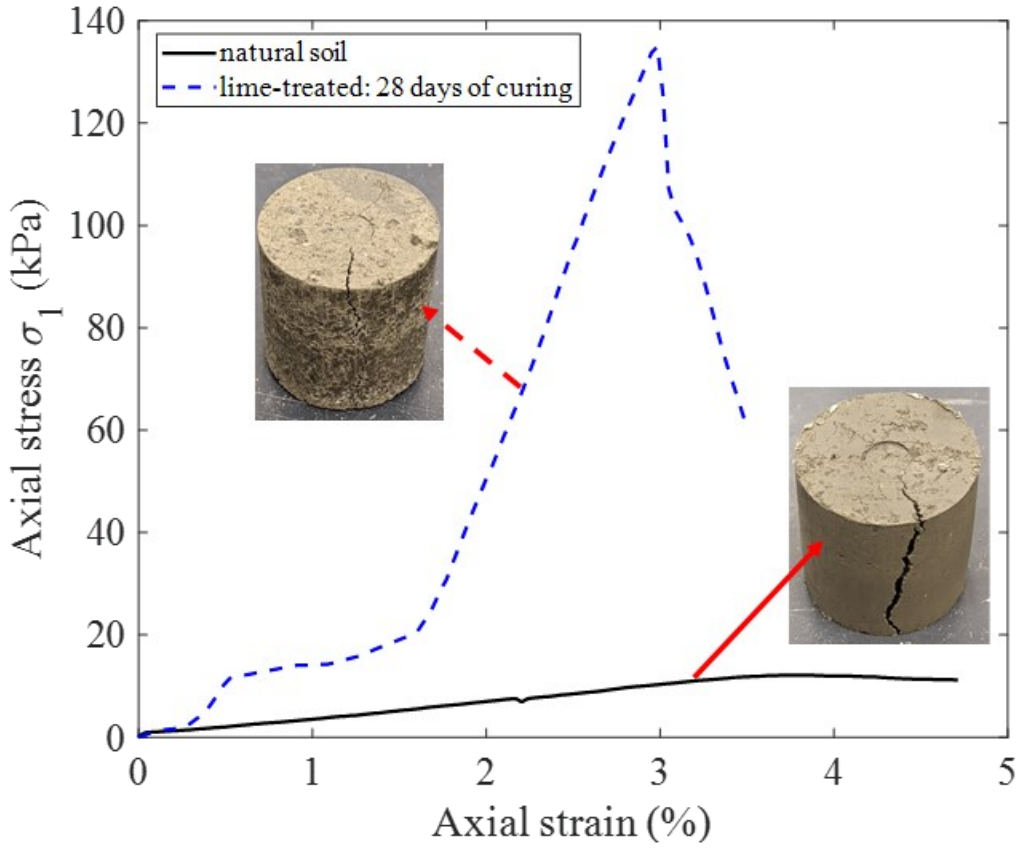

Figure 6-5 Stress-displacement curves of: (a) natural soil, and (b) lime-treated soil based on double punch tensile strength tests (deformation rate = 1 mm/min).

6.4.3.2 **Triaxial test outcomes**

The deviatoric stress-axial strain relationships for N-soil and L-soil at both room temperature and -6°C are presented in Figure 6-6. These stress-strain curves correspond to a single confining pressure of 100 kPa under varying temperature conditions. For N-soil, stress-strain behavior exhibits strain hardening at room temperature, transitioning to post-peak softening behavior when subjected to lime treatment or lower temperatures (Figure 6-6a). In contrast, L-soil (Figure 6-6c) initially displays post-peak softening behavior at room temperature, which transitions to strain hardening at lower temperatures. However, as the temperature decreases further, the post-peak softening behavior re-emerges, characterized by a steeper slope in the stress-strain curve.

Lime treatment significantly enhances the shear strength of the soil, increasing it from 0.36 MPa to 1.17 MPa, indicating the strengthening effect of lime stabilization. This behavior reflects the interplay between temperature, soil stabilization, and the resulting changes in soil microstructure and mechanical properties. The results also revealed that the deviatoric strength of N-soil increases significantly from 0.36 MPa to 5.25 MPa (approximately 15-fold) as the temperature decreases from +25°C to -6°C. Similarly, the deviatoric strength of L-soil increases from 1.17 MPa to 7.25 MPa (approximately 6.2-fold) under the same temperature change. This disparity in strength enhancement aligns with the findings discussed in Section 2, which attribute the strength increase in lime-treated soil to flocculation and agglomeration, as well as time-dependent pozzolanic reactions. Additionally, the presence of lime triggers exothermic reactions that reduce the amount of free water in the soil by evaporation and other chemical reactions. This reduction in free water results in a relatively smaller increase in strength at sub-zero temperatures (-6°C) compared to N-soil. This is because frozen soil strength is directly influenced by the amount of free water that freezes into pore ice as temperatures drop that implies more available water leads to more pore ice formation and, consequently, greater strength.

As illustrated in Figures 6-6b and 6-6d, the failure strain of L-soil initially increases with a temperature decrease down to 0°C but then declines as the temperature further drops from 0°C to -6°C. A similar trend is observed for N-soil, although the reduction in failure strain is less pronounced in L-soil. However, with continued temperature reduction below -6°C, the failure strain begins to increase again. This behavior is attributed to the dynamics of free water within soil pores, which freezes into pore ice as temperatures drop. The relationship between temperature, free water availability, and resulting mechanical behavior has been previously highlighted in various studies (Nixon 1992, Kadivar and Manahiloh 2019, Akhtar and Li 2020b).

This phenomenon will be further elaborated in the discussion section. At 0 ºC, the free water within the soil begins to transition into ice. However, the initial ice formed at this stage is relatively weak, and the presence of remaining free water results in the frozen soil exhibiting dilatant behavior. This occurs due to early ice breakage under applied forces and interactions between pore ice and solid particles. As the temperature decreases further, the free water progressively converts to pore ice, with the majority of this phase change occurring around -6 ºC. At temperatures below -6 ºC, the pore ice starts to gain strength, significantly contributing to the overall soil strength. This progression highlights a key behavior of pore ice: while decreasing temperatures enhance soil strength, the material exhibits brittle behavior up to -6 ºC. Beyond this threshold, as the temperature continues to drop, the soil's behavior transitions into a more ductile state, indicating a shift in the mechanical response of the material due to the strengthening and restructuring of pore ice.

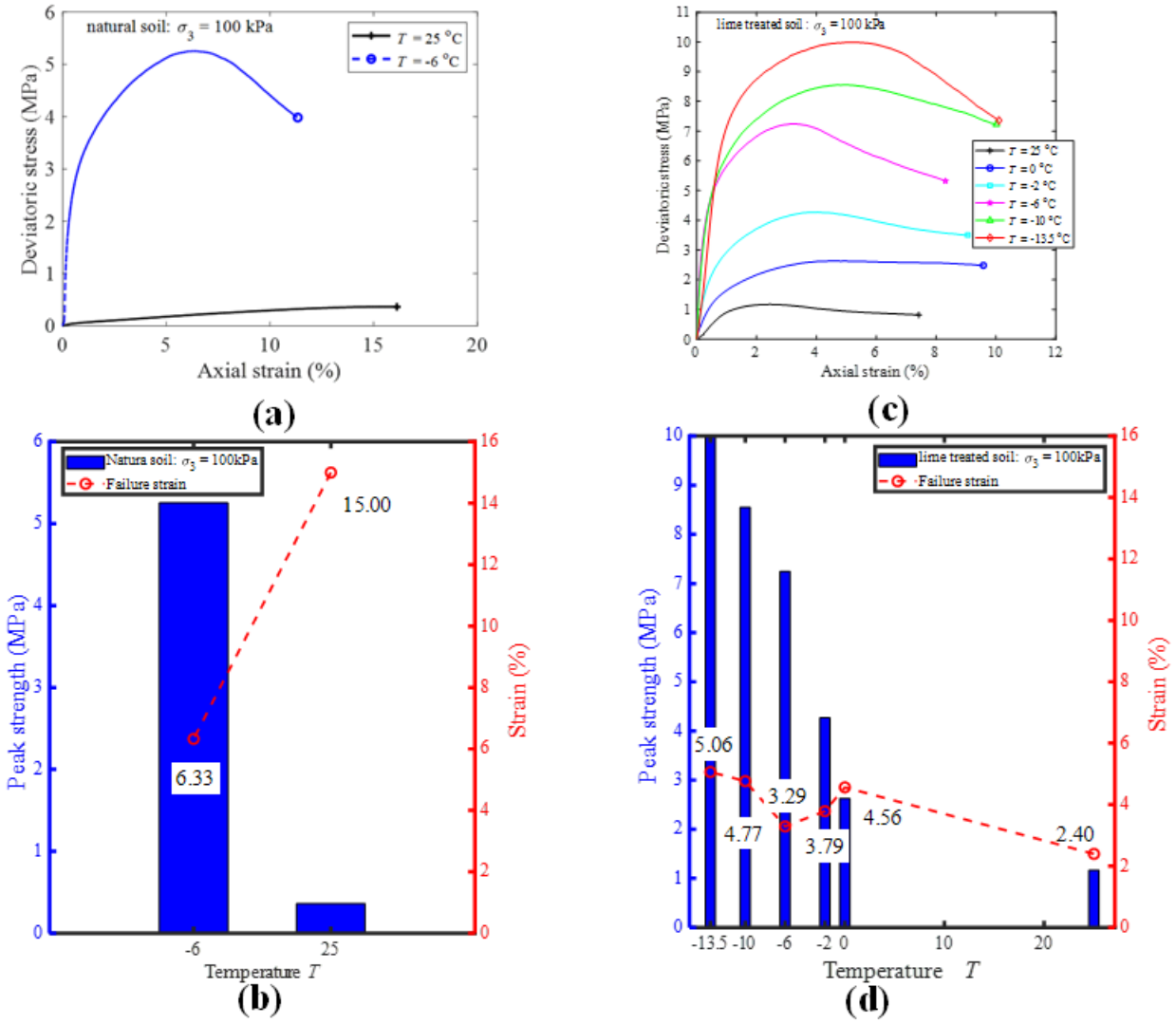

Figure 6-6 Typical results from temperature-controlled triaxial tests: (a) natural soil, (b) Peak strength of natural soil vs failure strain, (c) lime-treated soil, and (d) peak strength of lime treated soil vs failure strain (deformation rate = 1 mm/min, confining pressure = 100 kPa).

6.5 Numerical analysis

6.5.1 Layout for finite element numerical modeling

In this study, both finite element modeling (FEM) and extended finite element modeling (XFEM) were employed to simulate the mechanical responses of N-soil and L-soil under the following testing conditions: (a) unconfined compressive strength (UCS) test at room temperature, incorporating a damage model; (b) double punch tensile strength (DPT) test at room temperature,

with a focus on crack formation modeling; and (c) consolidated undrained (CU) triaxial tests at various temperatures and confining pressures.

Previous research has demonstrated that the hyperbolic Drucker-Prager model effectively captures both the brittle and post-peak ductile behavior of frozen soils (Akhtar and Li 2020b). According to the Abaqus documentation, the hyperbolic Drucker-Prager yield function is defined by Equation 6.25. When hardening behavior is characterized under both compression and tension, it is represented by Equation 6.26 and Equation 6.27.

$$F = \sqrt{\left(d' - \sigma_t \tan\beta\right)^2 + q^2} - p' \tan\beta - d' = 0 \tag{6.25}$$

$$d' = d_t' = \sqrt{\left(d_{ot}' - \sigma_t \tan\beta\right)^2 + d_t^2} + \frac{\sigma_t}{3}\tan\beta \tag{6.26}$$

$$d_{ot}' = \left(1 + \frac{1}{3}\tan\beta\right)\sigma_t$$

$$d' = d_c' = \sqrt{\left(d_{oc}' + \sigma_c \tan\beta\right)^2 + d_t^2} - \frac{\sigma_c}{3}\tan\beta \tag{6.27}$$

$$d_{oc}' = \left(1 - \frac{1}{3}\tan\beta\right)\sigma_c$$

where σ_c is compressive strength; σ_t is the tensile strength; and p is the mean effective stress ($p = \frac{1}{3} trace(\sigma)$). Since the pore pressure is not considered in this study, the total stress equals to the effective stress; q is the von Mises equivalent shear stress ($q = \sqrt{\frac{3}{3}(\mathrm{S}:\mathrm{S})}$); S is the deviatoric stress ($\mathrm{S} = \sigma + p\mathrm{I}$); β and d are Drucker-Prager model's angle of friction and cohesion strength parameter in space, respectively. According to Puzrin (Puzrin 2012), these parameters are related to the Mohr–Coulomb friction angle as:

$$d = \frac{6c\cos\phi}{3-\sin\phi} \tag{6.28}$$

$$\beta = \tan^{-1}\left(\frac{6\sin\phi}{3-\sin\phi}\right) \tag{6.29}$$

Additionally, the Concrete Damage Model in Abaqus was employed to calibrate the finite element model against the experimental data from the UCS test, ensuring accurate representation of damage and failure under compressive loading. For the DPT test, the Ductile Damage Model was utilized to calibrate the simulation, effectively capturing crack initiation and propagation under tensile loading conditions. These modeling approaches provided a robust framework for aligning the numerical simulations with the experimental observations. The mathematical relations for concrete damage model are provided as:

$$d_{c/t} = 1 - \frac{\sigma_i}{\sigma_{cu/tu}} \tag{6.30}$$

$$\varepsilon_0^{elastic} = \frac{\sigma_{c/t}}{E_0} \tag{6.31}$$

$$\varepsilon_{c/t}^{inelastic} = \varepsilon_{c/t} - \varepsilon_0^{elastic} \tag{6.32}$$

where the term $d_{c/t}$ is the damage parameter in compression/ tension ($0 \geq d_{c/t} \leq 1$); $\sigma_{cu/tu}$ is the ultimate stress in compression/tension.

Similarly, mathematical relations for ductile damage parameters (η and D) are provided given below:

$$\eta = \frac{p}{\sigma_{eq}} \tag{6.33}$$

$$D = \frac{\varepsilon_i^{plastic} - \varepsilon_0^{plastic}}{\varepsilon_f^{plastic} - \varepsilon_0^{plastic}} \tag{6.34}$$

where stress triaxiality ($\eta = 0.33$) in axial loading condition; D is damage parameter; $\varepsilon_f^{plastic}$ is fracture strain. In this model, damage evolution was considered displacement control and the crack initiates after peak strength achieved where ($D = 0$). The finite element model was developed as an analogy to the laboratory experimental tests in terms of boundary conditions (Figure 6-7).

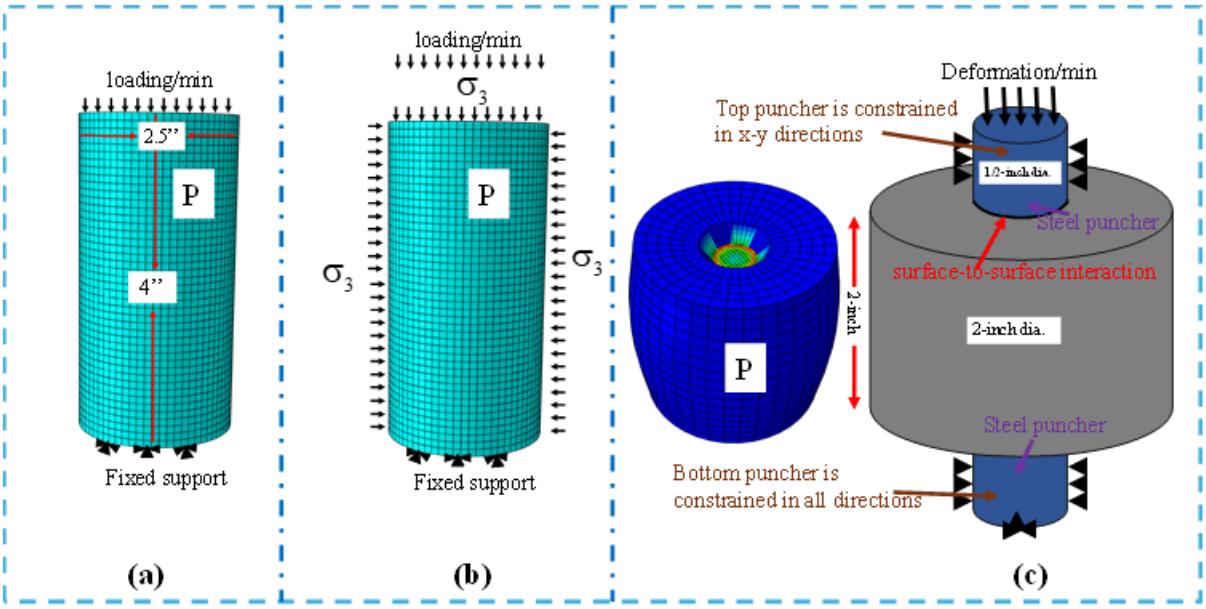

Figure 6-7 Sketch showing the sample dimension, boundary condition, and FEM mesh: (a) unconfined compression test, (b) triaxial test, and (c) double punch test.

6.5.2 Numerical outcomes

As illustrated in Figure 6-8, the finite element model utilizing the hyperbolic Drucker-Prager model effectively captures both the peak and post-peak behavior of lime-treated soil. Additionally, the damage model demonstrates its capability to predict the ultimate strength of the soil accurately. Notably, due to the inherent non-linearity in the elastic range of lime-treated soil, the secant modulus (E_{50}) was identified as a more suitable alternative to Young's modulus for characterizing

its behavior. Similarly, the finite element numerical models prove effectively capture the peak strength of L-soil during the double punch test (Figure 6-9). The ductile damage model used for the DPT also successfully captures the ultimate strength of the sample.

In the numerical analysis of the triaxial test, as shown in Figures 6-10 and 6-11, the numerical model based on the hyperbolic Drucker-Prager model effectively captured the key mechanical responses of both N-soil and L-soil samples under various confining pressures and temperatures. These included the instantaneous elastic range, plastic range, peak strength, post-peak strain hardening, and post-peak softening behavior. The use of the secant modulus (E_{50}) proved to be an effective parameter for capturing the non-linear response of lime-treated soil and soil at lower temperatures. However, for N-soil at room temperature, the secant modulus failed to adequately represent the linear elastic range, indicating limitations in its application under these specific conditions. This highlights the necessity for careful parameter selection tailored to the material type, temperature, and treatment condition when modeling soil behavior numerically.

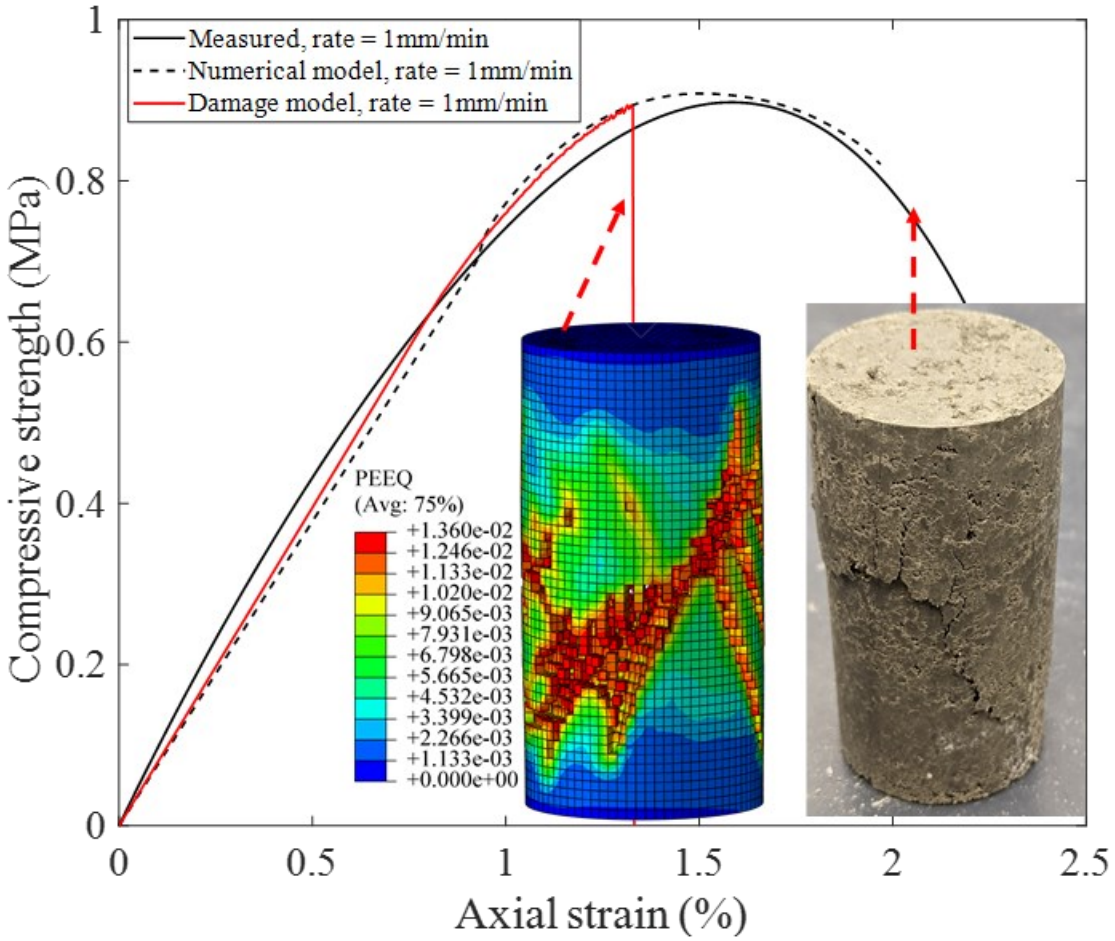

Figure 6-8 Plots of measured and modeled stress-strain curves for lime treated soil samples under the unconfined compressive strength test.

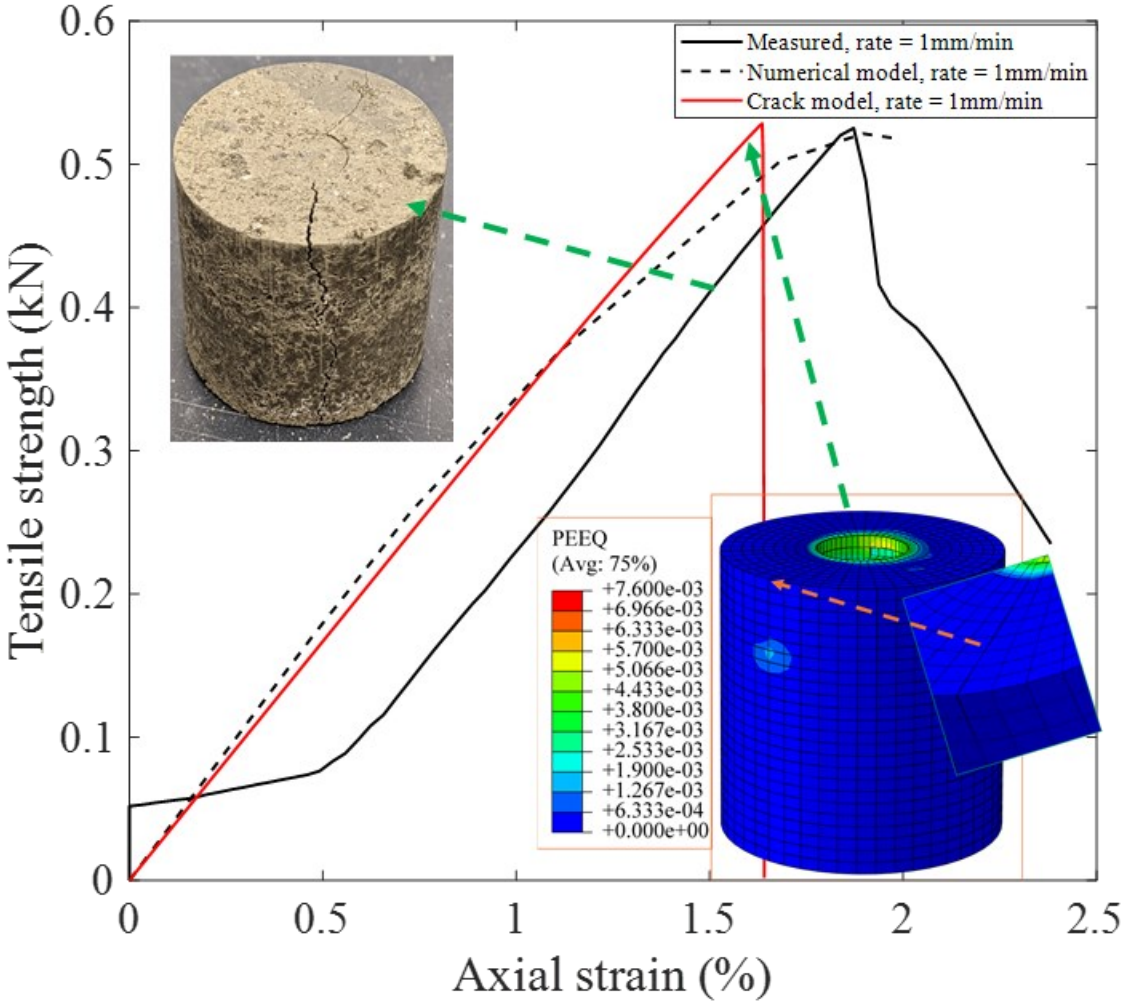

Figure 6-9 Plots of measured and modeled stress-strain curves for samples under the double punch tensile strength test.

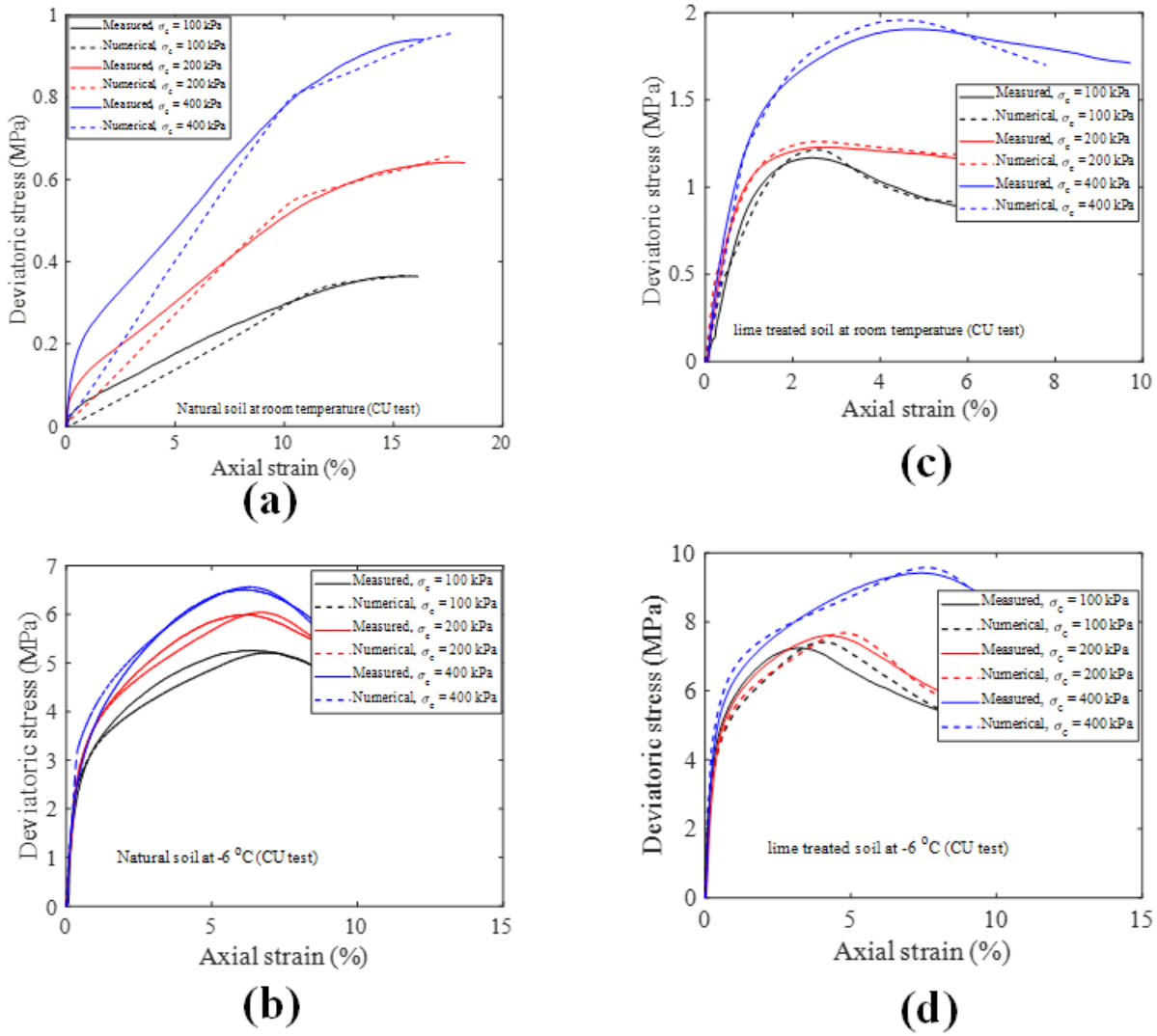

Figure 6-10 Plots of measured and modeled stress-strain curves for both untreated natural soil and lime-treated soil samples under triaxial test at different temperatures and confining pressures.

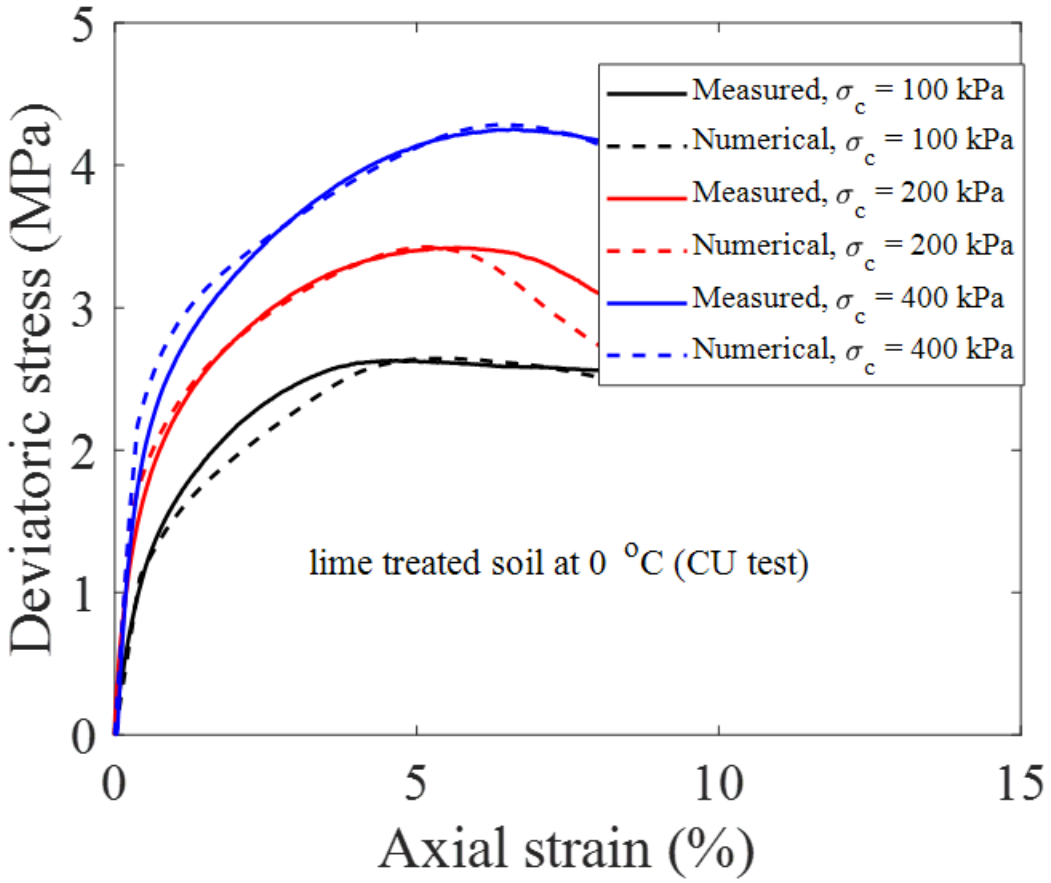

Figure 6-11 Plots of measured and modeled stress-strain curves for lime-treated soil samples under triaxial test at T = 0 °C and different confining pressures.

6.6 Discussions

This section examines the changes in shear strength parameters, elastic modulus, and energy absorption capacity of tested soils (i.e., N-soil and L-soil) under different temperature conditions. It presents an experimental analysis comparing the strength of lime-treated soil (L-soil) and untreated natural soil (N-soil) through consolidated drained and consolidated undrained triaxial tests, while also evaluating the influence of shear rate. Additionally, the study explores the impact of confining pressure on the failure behavior of tested soils.

6.6.1 **Shear strength parameters**

The shear strength parameters, specifically cohesion and the angle of internal friction, of N-soil and L-soil are influenced by temperature, as they govern the balance between unfrozen free water and frozen water in the soil samples.

Figure 6-12a compares the friction angles of N-soil and L-soil under different conditions. At room temperature, N-soil exhibits a higher friction angle compared to L-soil. This difference is attributed to the increase in pore volume caused by agglomeration in the L- soil, as previously illustrated in Figure 6-1. As the temperature decreases, the friction angle increases for both N-soil and L-soil. However, the rate of increase is significantly greater in L-soil than in N-soil. This enhanced response in L- soil is associated with the interaction among coarse sand particles, pore ice, and the secondary coarse material generated by flocculation. These secondary materials, which include fine sand, silt, and clay, contribute to an improved interparticle bonding and enhanced strength as the temperature drops. This behavior highlights the temperature-dependent strengthening mechanisms in lime-treated soils.

Similarly, as shown in Figure 6-12b, the cohesion of both N-soil and L-soil increases with decreasing temperature, ranging from 65 kPa to 1350 kPa for N-soil and from 285 kPa to 1351 kPa for L- soil as the temperature drops from +25 °C to -13.5 °C. Unlike the friction angle, L- soil consistently exhibits higher cohesion compared to N- soil, starting at 285 kPa for L-soil versus 65 kPa for N-soil at room temperature. Furthermore, at -6 °C, the cohesion of N- soil approximately matches the cohesion of L- soil at -13.5 °C. This behavior is attributed to the temperature-induced phase change of water into ice. N-soil retains more water compared to L- soil, as L-soil undergoes exothermic reactions during curing (up to 28 days), which reduces its water content. The increase in cohesion with decreasing temperature is largely due to the cementitious properties of ice, which

contributes to stronger interparticle bonding as more water transitions into pore ice at sub-zero temperatures.

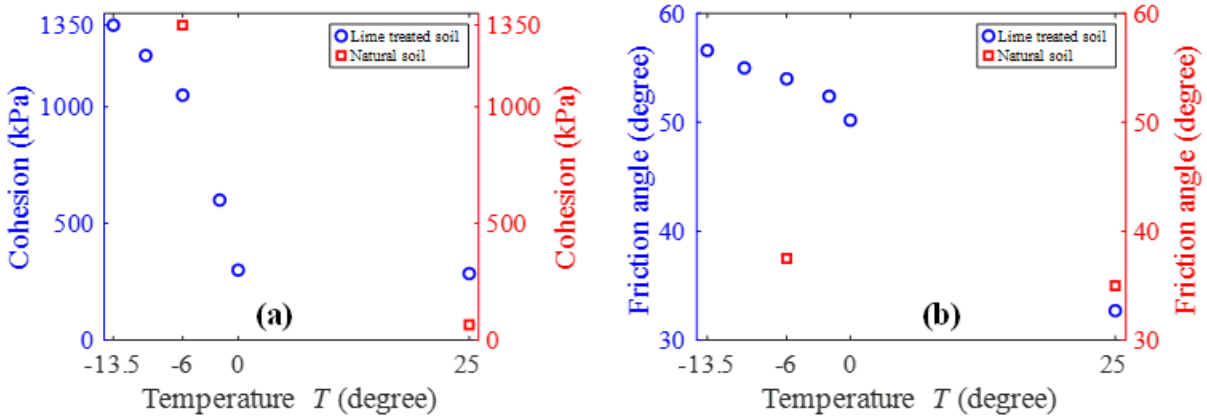

Figure 6-12 Plots for both untreated natural soil and lime treated soil at different temperatures: (a) cohesive parameters vs temperature, (b) friction angle vs temperature.

6.6.2 **Secant modulus**

The secant modulus is a key indicator of sample hardness and plays a crucial role in estimating soil deformation. In this study, the secant modulus was calculated for both N-soil and L-soil at 50% of the peak strength, defined as the ratio of deviatoric stress to the corresponding axial strain at that specific point on the stress-strain curve.

Figure 6-13 illustrates the variation in secant modulus for N-soil compared to L-soil at room temperature (Figure 6-13a) and the variation in secant modulus for N-soil at +25ºC and -6°C (Figure 6-13b) under different confining pressures. It can be observed that L-soil generally exhibits a higher stiffness in terms of the secant modulus compared to N- soil. This increased stiffness is attributed to the strengthening effects of flocculation, agglomeration, and pozzolanic reactions introduced by lime treatment. Additionally, as confining pressure increases, the stresses acting on the inter-particle bonds within the soil mixture also increases, leading to an overall rise in soil stiffness and the secant modulus. However, an anomaly was observed for L- soil at a confining

pressure of 800 kPa, where the secant modulus dropped. This reduction indicates that the internal stresses induced by the high confining pressure caused damage to the inter-particle bonds formed during the flocculation process and early-stage pozzolanic reactions. This highlights the potential vulnerability of L-soils to bond damage under excessive confining pressures, which may require further investigation to optimize their mechanical performance.

Figure 13b illustrates that the secant modulus of N-soil at -6°C exhibits a high negative sensitivity to confining pressure. Initially, the secant modulus increases due to the enhanced cementitious bonding caused by the formation of pore ice. However, at a confining pressure of 400 kPa, the secant modulus begins to decrease at room temperature. As the confining pressure increases further, the secant modulus drops below the level observed in N-soil at room temperature. This behavior in frozen soil can be attributed to confining-induced pore-ice melting and the subsequent reorientation of soil particles, which weakens the interparticle bonds. This observation is consistent with the trends presented in Figure 6-6.

A similar phenomenon of confining-induced pressure melting and associated damage to flocculation bonds formed by lime reactions is evident in Figure 6-14 for L-soil. While decreasing temperature generally results in an increase in secant modulus due to the strengthening effects of frozen pore ice, this effect is reversed at 400 kPa, where the secant modulus begins to decline. This reduction is more pronounced at lower temperatures, particularly at -13.5°C, where frozen soil becomes increasingly sensitive to confining pressure. It is also noteworthy that the reduction in secant modulus at higher confining pressures is more severe in N-soil compared to L-soil. This difference can be attributed to the additional structural integrity provided by the flocculation and pozzolanic reactions in L-soil, which render it less susceptible to bond damage caused by confining pressures.

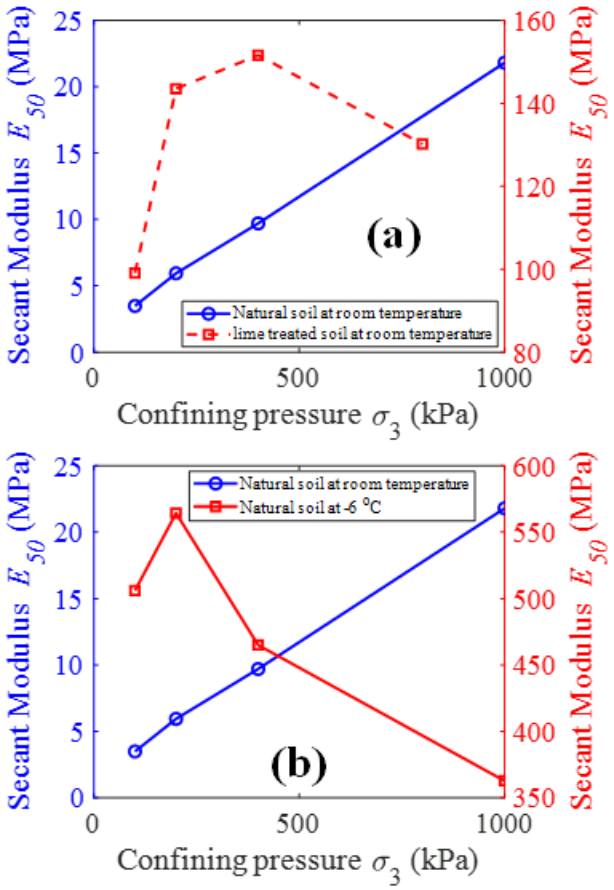

Figure 6-13 Plot showing the secant modulus versus confining pressures: (a) natural untreated soil vs lime-treated soil to room temperature and (b) natural untreated soil at room temperature vs natural untreated soil at -6ºC.

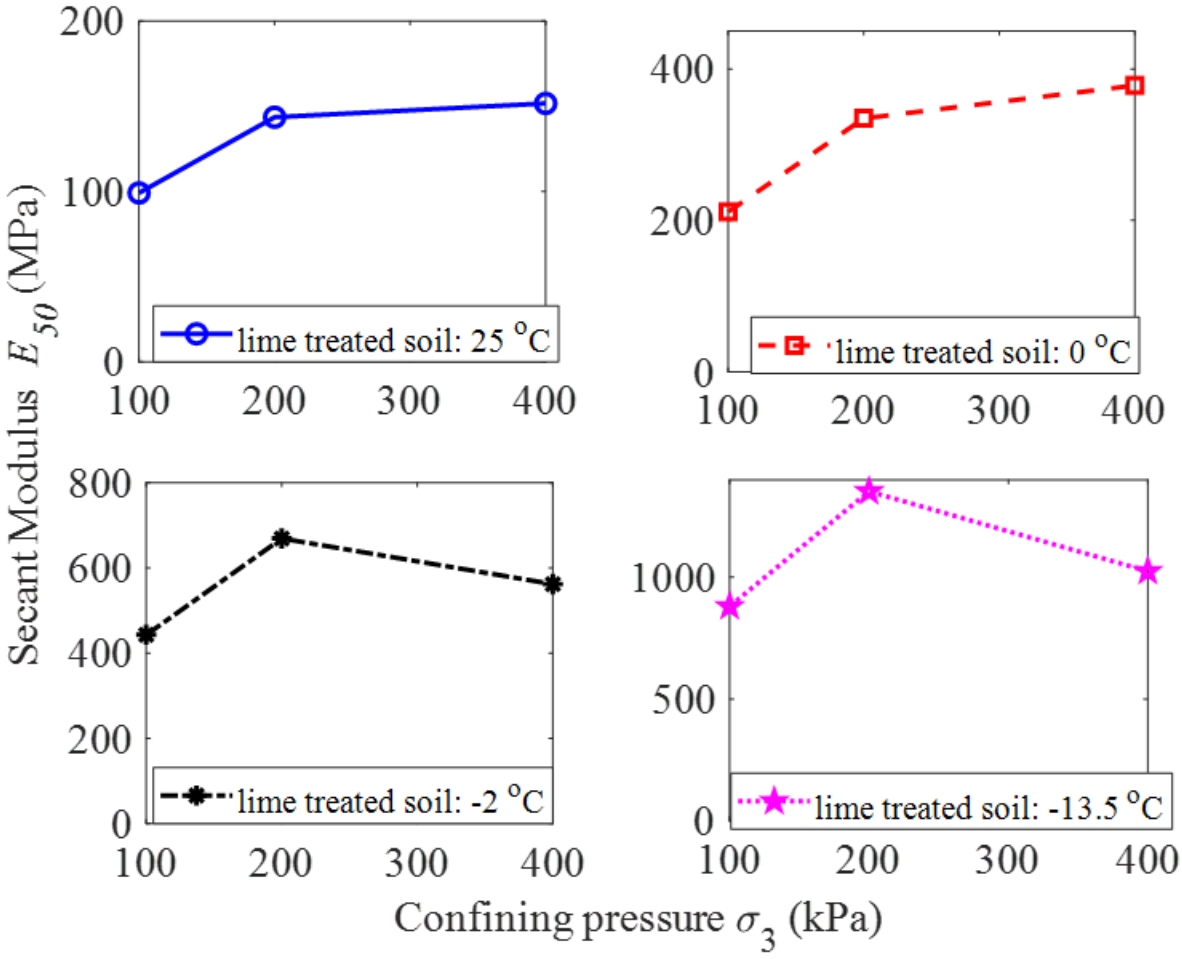

Figure 6-14 Plot showing the secant modulus versus confining pressure for lime-treated soil at different temperatures.

6.6.3 **Energy Absorption Capacity**

Energy absorption capacity represents the amount of energy required to induce deformation in soil samples and is calculated as the area under the stress-strain curve. As shown in Figure 6-15, the energy absorption capacity increases with increasing confining pressure for both N-soil and L-soil. However, this increase is more pronounced for N-soil, primarily due to particle reorientation and the closing of gaps between particles under pressure.

Additionally, the energy absorption capacity of both N-soil and L-soil increases as the temperature decreases from +25 °C to -6 °C. This is attributed to the strengthening effects of pore water

transforming into pore ice, which enhances the soil's resistance to deformation. At lower strain levels (approximately 4%), the energy absorption capacity shows minimal differences across the tested samples, except for N-soil at room temperature. This is due to the brittle behavior induced by pore ice in frozen soil and the rigid behavior caused by lime stabilization in L-soil. These factors limit energy dissipation at lower strains, resulting in similar energy absorption capacities across most conditions, except where N-soil at room temperature retains more ductile characteristics.

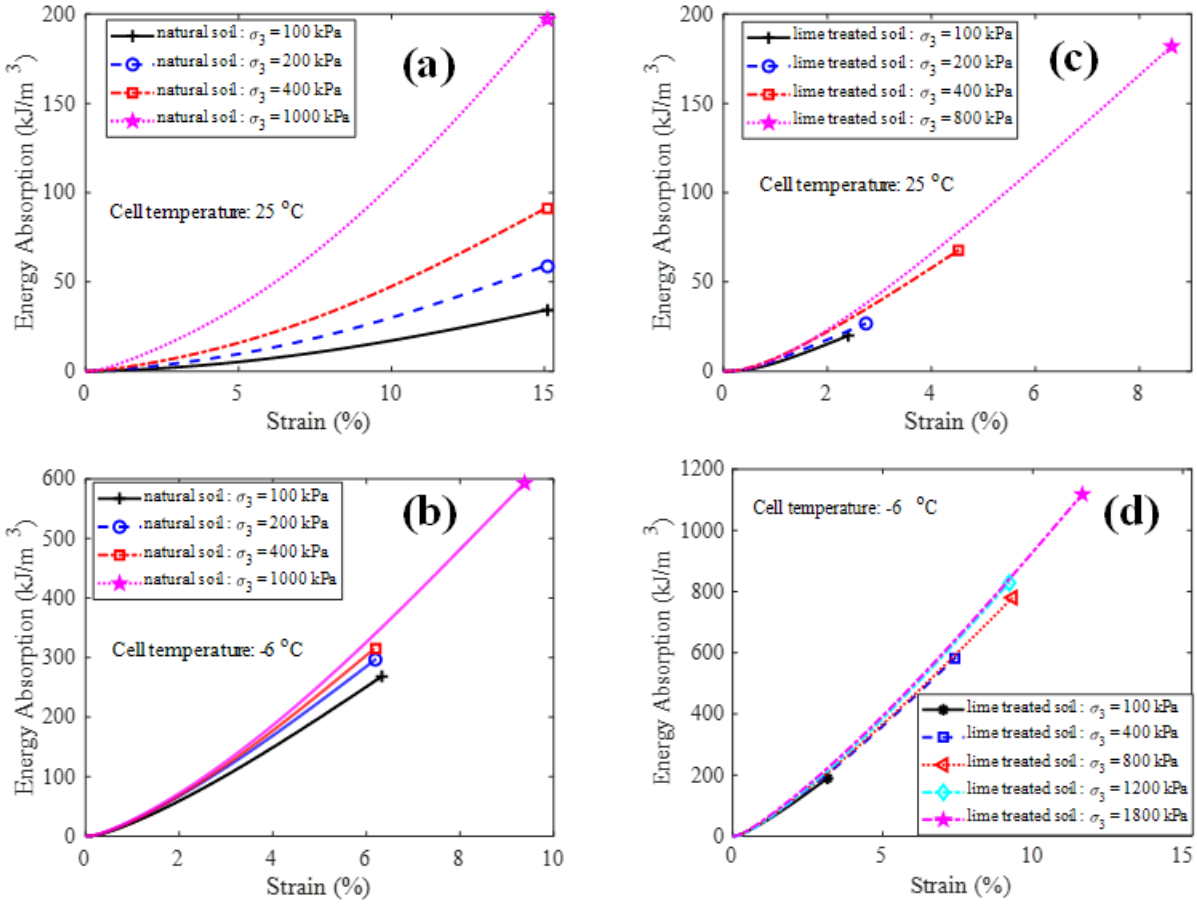

Figure 6-15 Variation of the absorbed energy capacity with axial strain for untreated natural soil and lime treated soil at room temperature and -6 ºC temperature loading under different confining pressure.

6.6.4 **Consolidated drained and Consolidated undrained triaxial condition**

For comparison, we also carried out some tests under the consolidated drained (CD) stress path condition in some triaxial tests. As shown in Figure 6-16, for both CU (Consolidated Undrained)

and CD (Consolidated Drained) triaxial tests at room temperature, there is no significant difference in the deviatoric stress and failure pattern under varying confining conditions for both N-soil and L-soil. This behavior suggests that under high loading rates (1 mm/min.), the available free water in the soil system is unable to escape during loading. This inability of free water to migrate results in the soil behaving in a manner similar to a fully frozen and undrained system, where the presence of trapped free pore water dominates the stress response, minimizing the influence of different confining pressures. Consequently, the soil's mechanical response under these conditions becomes largely dependent on the water within the pores and interparticle interaction, rather than the applied drainage or confining conditions.

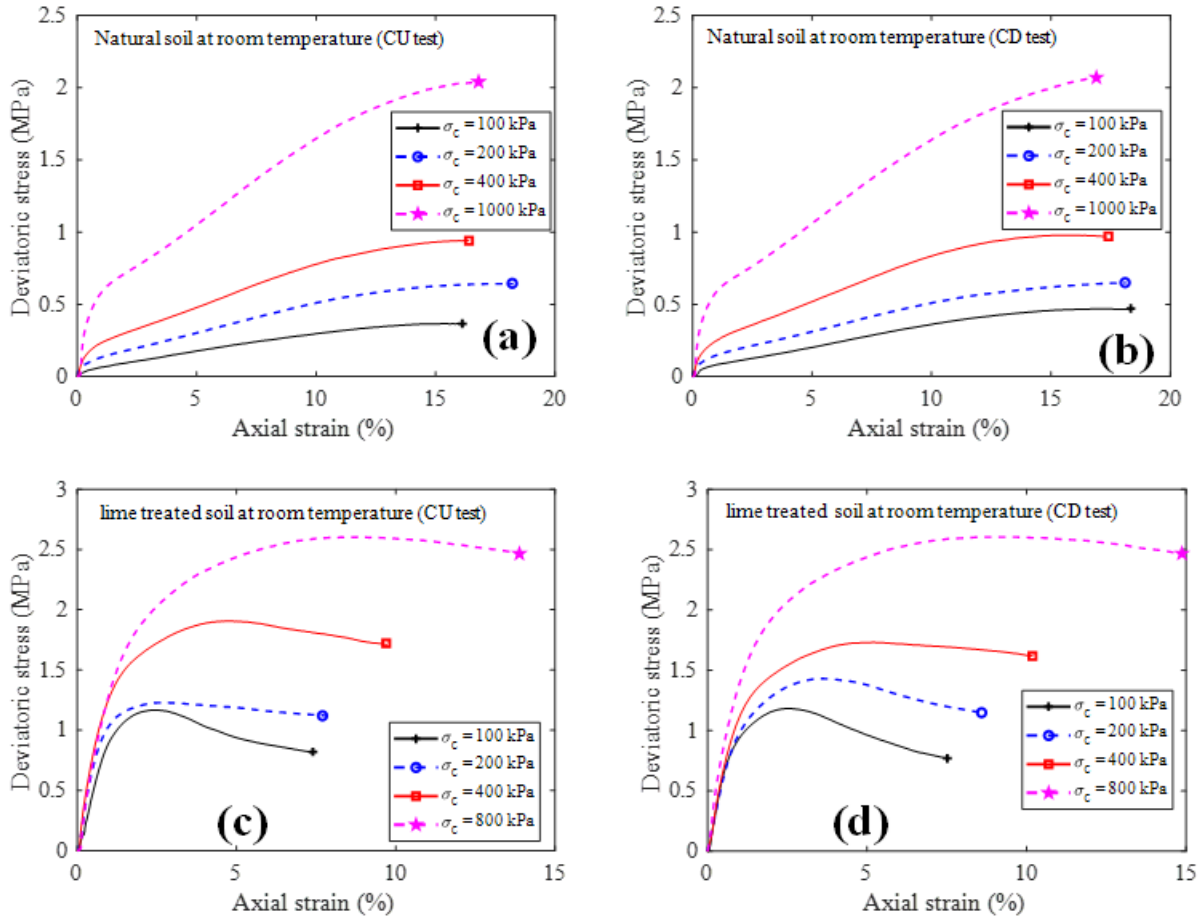

Figure 6-16 Stress-strain curves for untreated natural soil and lime treated soil under consolidated undrained and consolidated drained triaxial test conditions.

6.6.5 **Loading rate**

As illustrated in Figure 6-17, the consolidated undrained (CU) triaxial testing results show no significant differences in the mechanical response of both N-soil and L-soil under varying loading rates (1 mm/min, 3 mm/min, and 9 mm/min) during the shear stage. While there is a slight increase in peak strength with increasing loading rates, the overall mechanical behavior, including the elastic region, plastic region, peak location, and post-peak behavior, remains consistent. This indicates that the soil's deformation and failure mechanisms are largely unaffected by variations in loading rates within this range. The observed increase in peak strength with higher loading rates can be attributed to strain rate effects, where higher loading rates provide less time for microstructural adjustments and bond rearrangements, resulting in slightly higher resistance to shear. However, this does not translate into a noticeable change in the overall mechanical behavior of the soil.

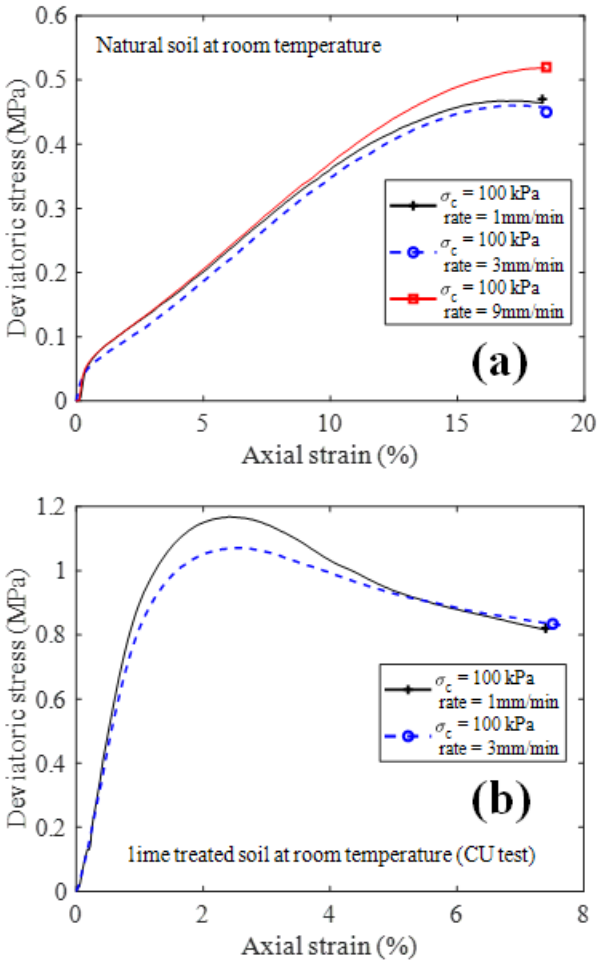

Figure 6-17 Stress-strain curve at room temperature under different shearing rate: (a) natural untreated soil and (b) lime treated soil.

6.6.6 **Failure behavior**

The response of both N-soil and L-soil to changes in confining pressure and temperature is evident in their peak strength and deformation behavior during failure, as demonstrated in Figures 6-18 and 6-19. Both soil types display high sensitivity to these factors: (1) At room temperature (+25°C), the peak strength increases significantly with rising confining pressure, from 210 kPa at 0 kPa (UCS test) to 1992 kPa at 1000 kPa. Across all confining pressures, the sample exhibits strain-hardening behavior, with 15% strain being identified as the strain at failure due to the continuous deformation without a distinct peak. (2) At frozen conditions (-6°C), the peak strength increases from 5192 kPa at 100 kPa to 8027 kPa at 1000 kPa, a

substantial rise compared to room temperature. The failure strain, however, shows a non-linear trend as initially decreases to a minimum at 200 kPa confining pressure and it then recovers at 400 kPa and increases to approximately 9% at 1000 kPa, compared to 6% at 100 kPa. This behavior suggests that higher confining pressure brings soil particles closer together, improving interparticle contact and increasing effective strength. However, at frozen conditions, pressure-induced pore-ice melting occurs. This melting, combined with interactions between pore ice and soil particles, transitions the behavior from brittle to ductile as confining pressure rises.

In contrast to N-soil, at room temperature (+25°C), the L-soil exhibits a steady increase in peak strength with increasing confining pressure, accompanied by an increase in failure strain. This highlights the improved interparticle bonding and enhanced resistance to deformation due to lime-induced flocculation, agglomeration, and pozzolanic reactions. At Frozen Conditions (-6°C), while the peak strength of lime-treated soil also increases with confining pressure at frozen conditions, the rate of increase is less pronounced compared to N-soil. It is worth noting that beyond a confining pressure of 1000 kPa, there is no significant increase in peak strength, indicating that the soil has reached its maximum effective interaction. This plateau occurs because the structural changes induced by lime stabilization (e.g., flocculation and pozzolanic bonding) have already optimized the soil's strength capacity, leaving limited room for further improvement under frozen conditions.

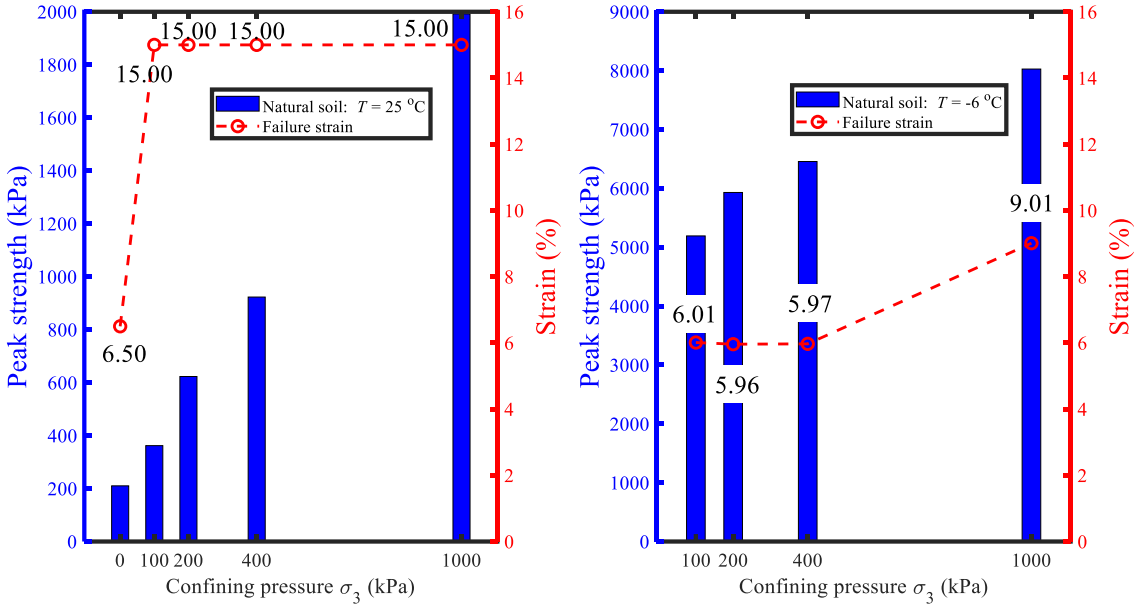

Figure 6-18 Plots of Peak strength and failure strain under different confining pressures (deformation rate = 1 mm/min): (a) natural untreated soil at room temperature and (b) natural untreated soil at -6ºC.

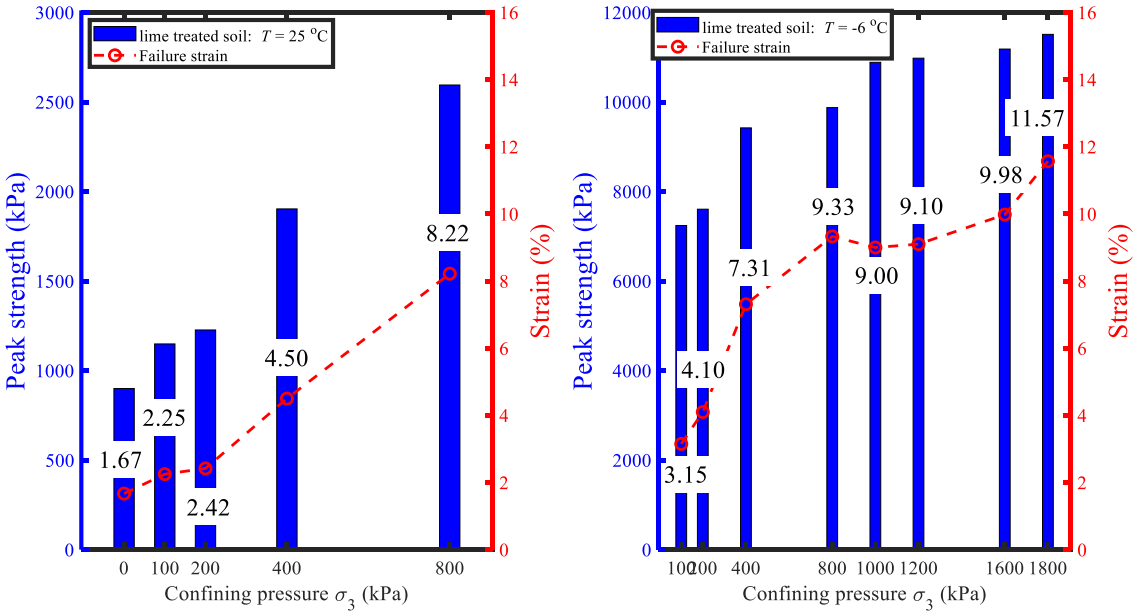

Figure 6-19 Plots of peak strength and failure strain under different confining pressures (deformation rate = 1 mm/min): (a) lime-treated soil at room temperature and (b) lime-treated soil at -6ºC.

6.7 Conclusion

This study investigates the mechanical behavior of lime-treated silty clay under different stress paths and temperature conditions, focusing on its application in cold-region infrastructure. It

evaluates the strength characteristics of both untreated and lime-treated soil through various laboratory tests, including unconfined compressive strength (UCS), double punch tensile strength (DPT), and triaxial tests at temperatures ranging from +25°C to -13.5°C. Several conclusions are drawn below:

- Lime treatment significantly enhances the mechanical properties of the studying silty clay, altering its behavior from ductile with post-peak hardening to brittle with post-peak softening. The compressive strength increases by 4.3 times (from 210 kPa to 900 kPa), while the tensile strength improves by 11.2 times (from 12 kPa to 135 kPa).
- The deviatoric strength of untreated soil increases approximately 15-fold (from 0.36 MPa to 5.25 MPa) as the temperature drops from +25°C to -6°C, whereas lime-treated soil exhibits a 6.2-fold increase (from 1.17 MPa to 7.25 MPa) under the same conditions. This strengthening effect results from both lime-induced reactions and the formation of pore ice. Additionally, variations in shear rate have negligible effects on the peak strength and deformation behavior.
- Both the friction angle and cohesion strength of the studied soil increase with decreasing temperature. At -13.5°C, cohesion reaches 1350 kPa for untreated soil and 1351 kPa for lime-treated soil, primarily due to the freezing of free water in soil pores. The friction angle increases more significantly in lime-treated soil, benefiting from enhanced particle bonding.
- The FEM analysis with the hyperbolic Drucker–Prager model effectively captures the deformation behavior of both untreated and lime-treated frozen soils under compressive, tensile, and shear loading. Furthermore, the damage XFEM model accurately simulates failure patterns in unconfined compressive and double-punch tensile strength tests.

Chapter 7

7 Conclusions, limitations, and recommendations for future work

7.1 Conclusions

This thesis has explored various aspects of soil mechanics and thermal-hydro-mechanical (THM) interactions in frozen and freezing soils. Through detailed numerical simulations and computational models, several key findings have been identified:

7.1.1 Modeling time-dependent uniaxial compressive behaviors of an artificial frozen sandy clay at different temperatures (Chapter 3):

- The mechanical behavior of frozen sandy clay is significantly influenced by both temperature and strain rate. At higher strain rates, the material exhibits brittle failure characterized by post-peak softening, whereas lower strain rates result in a more ductile response with strain hardening. As the temperature decreases, the mode of volumetric deformation transitions from shear failure to compaction failure. Notably, when the temperature drops from −2°C to −15°C, the elastic limit and peak strength increase by factors of approximately 5.7 and 4.7, respectively.
- The study effectively modeled the behavior of frozen sandy clay using the Drucker–Prager plasticity model in combination with the Singh–Mitchell creep model to account for long-term deformation and stress relaxation. Finite Element Method (FEM) simulations were carried out in Abaqus. Results showed that while creep deformation is minimal in short-term tests, it becomes significant over the long term, particularly for stress relaxation. Although stress relaxation tests indicated partial recovery of stress after multiple cycles, the numerical models slightly underestimated the magnitude of relaxation.

7.1.2 Characterizations of tensile yield and failure processes of frozen clay soils: laboratory testing and numerical modeling (Chapter 4):

- Rod Split Test overestimates tensile strength due to increased contact area between loading strips and samples, however Double Punch Test provides more accurate results because the contact area remains constant. Also, the numerical simulations calibrated against the experimental data confirm that DPT is a reliable and conservative method for measuring tensile strength in frozen clay soils.
- Tensile strength is temperature and loading rate dependent. Higher strain rates (9 mm/min) lead to brittle failure with post-peak softening while Lower strain rates (1 mm/min) lead to ductile failure with strain hardening.
- The study determined the effect size for double punch tensile strength test using numerical modeling approach. The use of Hyperbolic Drucker–Prager model effectively simulated tensile failure behavior and successfully captured the tress paths, failure modes, and temperature-dependent strength variations.

7.1.3 Experimental study of mechanical behaviors of lime-treated Quebec silty clay soils under freeze-thaw cycles (Chapter 5):

- The addition of hydrated lime significantly improves unconfined compressive strength (UCS) and tensile strength of silty clay soil. UCS increased fourfold, from 208 kPa to 880 kPa while the tensile strength improved sevenfold, from 20 kPa to 135 kPa. Most strength gain occurs within the first 28 days, with moisture content dropping from 14.5% to 11.6% due to hydration reactions. Beyond 28 days, strength gain continues slowly, reaching 1900 kPa after 155 days while the soil stiffness and transforms failure behavior from ductile to brittle.
- The study identified the threshold number of freeze-thaw cycles that can produce maximum strength degradation and beyond which strength recovery starts. The first 10–12 F-T cycles degrade strength, but beyond 12 cycles, strength recovery begins. Strength degradation occurs due to micro-damage and expansion of pore ice, but subsequent pozzolanic reactions help recover strength
- Exposure to external moisture (after curing) reduces soil strength by 200 kPa. However, even after moisture exposure, lime-treated soil retains higher strength than untreated soil.

- Under UCS test, failure shifts from uniform cracking (without F-T cycles) to localized top-cap cracking (after F-T cycles). While under DPT test, failure shifts from ductile to brittle as F-T cycles increase.

7.1.4 Experimental and numerical investigation of the mechanical behavior of lime-treated silty clay under varying stress paths and temperature conditions (Chapter 6):

- This study found that lime treatment improves strength and alters failure mode. The strength of untreated soil increases 15-fold as temperature drops from +25°C to -6°C (from 0.36 MPa to 5.25 MPa) while the strength of lime-treated soil increases 6.2-fold under the same temperature drop (from 1.17 MPa to 7.25 MPa). At -6°C, untreated soil sees a larger strength increase than lime-treated soil, due to greater free water availability forming more ice bonds while at -13.5°C, cohesion reaches 1350 kPa (untreated soil) and 1351 kPa (lime-treated soil), mainly due to the formation of pore ice.
- The friction angle increased with decreasing temperature, but more significantly for lime-treated soil due to improved interparticle bonding, however, the cohesion of lime-treated soil maintains higher cohesion across all temperatures.
- This study determined that finite element modeling (FEM) can effectively predicts soil behavior. The Drucker–Prager model accurately captures frozen soil deformation under compressive, tensile, and shear loading, while the XFEM damage model successfully simulates crack initiation and propagation in UCS and indirect tensile tests.

7.2 Limitations

Despite the valuable insights provided by this research, several limitations must be acknowledged:

7.2.1 Micro-scale study of frozen soil:

This study primarily investigates the macrostructural behavior of frozen, unfrozen, and lime-treated soils under static loading conditions. However, microstructural and mineralogical analyses—such as Scanning Electron Microscopy (SEM) and X-ray Diffraction (XRD), were not performed. Incorporating such techniques could yield important insights into internal structural

transformations and assist in establishing correlations between external factors (e.g., temperature, confining pressure, loading rate, and time) and internal responses (e.g., pore water pressure, ice pressure and melting, unfrozen water migration, and interactions among ice, water, and soil particles). These analyses would enhance the understanding of soil behavior at the microscopic level and support the development of more comprehensive predictive models.

7.2.2 **Ambient environmental effects:**

The tests were conducted in a controlled and enclosed environment, effectively isolating the samples from external moisture fluctuations and environmental exposure. While this setup ensures consistency and repeatability, it also limits the simulation of real-world conditions, particularly the influence of moisture ingress and pore water redistribution during freeze–thaw (F–T) cycles. In natural settings, these processes can significantly impact soil structure, strength, and durability. Moisture migration during F–T cycles often leads to ice lens formation, increased heave potential, and weakening of soil bonds, especially in fine-grained or lime-treated soils. Therefore, excluding these effects may underestimate long-term degradation or overestimate the stabilizing performance of lime treatment in field conditions. Future studies should consider incorporating variable moisture conditions to better capture the coupled hydro-thermal-mechanical behavior of soils under realistic environmental loading.

7.3 **Recommendations for Future Work**

To address the limitations and build upon the findings of the thesis, the following recommendations for future research are proposed:

1. Conduct additional experiments to investigate pressure-induced melting and its influence on the deformation behavior of frozen soils. Such studies would help to better understand the role

of ice phase transitions under varying stress conditions, particularly at high confining pressures. This phenomenon can significantly affect strength, stiffness, and long-term stability, especially in permafrost and engineered frozen ground applications.

2. Conduct microstructural and mineralogical analyses to complement mechanical testing in evaluating the effects of external moisture and pore water movement during loading and freeze–thaw cycles. Techniques such as Scanning Electron Microscopy (SEM), X-ray Diffraction (XRD), and Mercury Intrusion Porosimetry (MIP) can provide insights into soil fabric, mineral changes, and pore structure evolution. These investigations are essential for understanding how moisture ingress and redistribution influence the mechanical behavior and long-term durability of both treated and untreated soils under freeze–thaw conditions.
3. Enhance existing plasticity models to incorporate the effects of temperature, loading rate, confining pressure, and thermally induced damage in order to accurately capture stress-induced melting, rate-dependent failure modes, and temperature-driven strength degradation. Current constitutive models often lack the ability to fully represent the coupled thermo-mechanical behavior observed in frozen soils. Modifications should include temperature-dependent yield criteria, softening laws linked to ice melting and pore pressure evolution, and damage mechanics to reflect microstructural breakdown. These enhancements would improve the predictive capability of models in simulating peak strength loss and progressive failure under varying environmental and loading conditions.
4. Develop long-term curing protocols and adopt open-system testing methods that account for moisture exchange to better simulate field conditions for lime-treated soils. Laboratory testing often overlooks the prolonged curing durations and environmental moisture variations that occur in real-world applications. Incorporating extended curing periods and exposure to

ambient humidity or controlled wetting–drying cycles can more accurately reflect the long-term performance and durability of lime-treated soils. This approach is essential for evaluating strength gain, durability, and susceptibility to environmental degradation under realistic field scenarios.

5. Perform creep, stress relaxation, and dynamic loading tests on both lime-treated and untreated natural soils to accurately assess long-term strength degradation in frozen conditions. These time-dependent and cyclic loading tests are essential for understanding the delayed deformation behavior and mechanical response of soils under sustained or fluctuating loads. Creep and stress relaxation tests reveal the progressive loss of stiffness and internal resistance, while dynamic loading simulates real-world conditions such as traffic, seismic activity, or vibrations. Including both treated and untreated soils in such studies will provide a comprehensive understanding of how stabilization affects long-term performance under freezing conditions.

By addressing these recommendations, future research can enhance our understanding of frozen soil mechanics, improve predictive numerical models, and contribute to the development of effective engineering solutions in cold regions. The advancements in modeling techniques and practical applications will ultimately support the sustainable and resilient development of infrastructure in permafrost-affected areas.

Bibliography

Abiodun, A.A., and Nalbantoglu, Z. 2015. Lime pile techniques for the improvement of clay soils. Canadian Geotechnical Journal, **52**(6): 760–768. NRC Research Press. doi:10.1139/cgj-2014-0073.

Abrishambaf, A., Barros, J.A.O., and Cunha, V.M.C.F. 2015. Tensile stress–crack width law for steel fibre reinforced self-compacting concrete obtained from indirect (splitting) tensile tests. Cement and Concrete Composites, **57**: 153–165. doi:10.1016/j.cemconcomp.2014.12.010.

Afrin, H. 2017. A review on different types soil stabilization techniques. International Journal of Transportation Engineering and Technology, **3**(2): 19–24. Science Publishing Group. doi:10.11648/j.ijtet.20170302.12.

Akagawa, S., and Nishisato, K. 2009. Tensile strength of frozen soil in the temperature range of the frozen fringe. Cold Regions Science and Technology, **57**(1): 13–22. doi:10.1016/j.coldregions.2009.01.002.

Akhtar, S., and Li, B. 2019. Numerical analysis of pipeline uplift resistance in a frozen clay at varying temperatures. : 345–353. American Society of Civil Engineers. doi:10.1061/9780784482599.040.

Akhtar, S., and Li, B. 2020a. Constitutive modeling uniaxial compressive behaviors of an artificial frozen sandy clay at different temperaturesIn: 73th Canadian Geotechnical Conference,.

Akhtar, S., and Li, B. 2020b. Numerical analysis of pipeline uplift resistance infrozen clay soil considering hybrid tensile-shear yield behaviors. International Journal of Geosynthetics and Ground Engineering, **6**(4): 47. doi:10.1007/s40891-020-00228-9.

Akhtar, S., and Li, B. 2023. A structural state model interpreting the residual strength transition behavior of clay soils. Geotechnical and Geological Engineering, **41**(5): 2913–2922. doi:10.1007/s10706-023-02436-2.

Akhtar, S., and Li, B. 2024a. Experimental investigation of the mechanical behavior of frozen fine grain soil stabilized with lime. In: 77th Canadian Geotechnical Conference,. Montreal, Canada.

Akhtar, S., and Li, B. 2024b. Modeling time-dependent uniaxial compressive behaviors of an artificial frozen sandy clay at different temperatures. Geotechnical and Geological Engineering, **42**(5): 3829–3842. doi:10.1007/s10706-024-02760-1.

Akhtar, S., and Li, B. 2025. Experimental study of mechanical behaviours of lime-treated Quebec silty clay soils under freeze-thaw cycles. submitted to Environmental Geotechnics. doi:10.1680/jenge.24.00118.

Aldaood, A., Bouasker, M., and Al-Mukhtar, M. 2014. Impact of freeze–thaw cycles on mechanical behaviour of lime stabilized gypseous soils. Cold Regions Science and Technology, **99**: 38–45. doi:10.1016/j.coldregions.2013.12.003.

Al-Mukhtar, M., Lasledj, A., and Alcover, J.F. 2014. Lime consumption of different clayey soils. Applied Clay Science, **95**: 133–145. doi:10.1016/j.clay.2014.03.024.

An, R., Zhang, X., Wang, Y., Liu, X., Chen, C., and Gong, J. 2022. Freeze–thaw impact on sandy clay in artificial frozen walls: An investigation of shear strength and pore-size distribution. International Journal of Geomechanics, **22**(12): 04022230. American Society of Civil Engineers. doi:10.1061/(ASCE)GM.1943-5622.0002489.

Andersland, O.B., and Akili, W. 1967. Stress effect on creep rates of a frozen cay soil. Géotechnique, **17**(1): 27–39. ICE Publishing. doi:10.1680/geot.1967.17.1.27.

Andersland, O.B., and Ladanyi, B. 1994. An introduction to frozen ground engineering. Springer US, Boston, MA.

Andersland, O.B., and Ladanyi, B. 2003. Frozen ground engineering,. *In* 2nd Edition. Wiley.

Arabi, M., and Wild, S. 1986. Microstructural development in cured soil-lime composites. Journal of Materials Science, **21**(2): 497–503. doi:10.1007/BF01145514.

Arabi, M., Wild, S., and Rowlands, G.O. 1989. Frost resistance of lime-stabilized clay soil. **1219**: 93–102.

Arenson, L.U., and Springman, S.M. 2005. Mathematical descriptions for the behaviour of ice-rich frozen soils at temperatures close to 0 °C. Canadian Geotechnical Journal, **42**(2): 431–442. NRC Research Press. doi:10.1139/t04-109.

Arenson, L.U., Springman, S.M., and Sego, D.C. 2007. The rheology of frozen soils. Applied Rheology, **17**(1): 12147–14. De Gruyter Open Access. doi:10.1515/arh-2007-0003.

Arman, A., and Saifan, F. 1967. The effect of delayed compaction on stabilized soil-cement. Highw. Res. Rec, **198**.

Asgari, M.R., Baghebanzadeh Dezfuli, A., and Bayat, M. 2015. Experimental study on stabilization of a low plasticity clayey soil with cement/lime. Arabian Journal of Geosciences, **8**(3): 1439–1452. doi:10.1007/s12517-013-1173-1.

ASTM C307-18. 2003. Test method for tensile strength of chemical-resistant mortar, grouts, and monolithic surfacings. ASTM International.

ASTM D422-63. 2007. Test method for particle-size analysis of soils. ASTM International.

ASTM D698-12. 2021. Test methods for laboratory compaction characteristics of soil using standard effort. ASTM International.

ASTM D854-23. 2006. Test methods for specific gravity of soil solids by water pycnometer. ASTM International.

ASTM D2488-17e1. 2017. Practice for description and identification of soils. ASTM International.

ASTM D3967-16. 2008. Test method for splitting tensile strength of intact rock core specimens. ASTM International.

ASTM D4318-17e1. 2017. Test methods for liquid limit, plastic limit, and plasticity index of soils. ASTM International.

ASTM D7928-21e1. 2017. Test method for particle-size distribution (gradation) of fine-grained soils using the sedimentation (hydrometer) analysis. ASTM International.

Azmatch, T.F., Sego, D.C., Arenson, L.U., and Biggar, K.W. 2010. Tensile strength of frozen soils using four-point bending test. Calgary, Canada. pp. 436–442.

Azmatch, T.F., Sego, D.C., Arenson, L.U., and Biggar, K.W. 2011. Tensile strength and stress–strain behaviour of Devon silt under frozen fringe conditions. Cold Regions Science and Technology, **68**(1): 85–90. doi:10.1016/j.coldregions.2011.05.002.

Babanas, H., and Courcelles, B. 2025. Enhancing lime dosage determination for lean clay soil improvement: significance of plasticity limit and interpretation approach. Geotechnics, **5**(1): 9. Multidisciplinary Digital Publishing Institute. doi:10.3390/geotechnics5010009.

Baker, T.H.W., Jones, S.J., and Parameswaran, V.R. 1982. Confined and unconfined compression tests on frozen sands. pp. 387–393.

Baldovino, J.A., Moreira, E.B., Teixeira, W., Izzo, R.L.S., and Rose, J.L. 2018. Effects of lime addition on geotechnical properties of sedimentary soil in Curitiba, Brazil. Journal of Rock Mechanics and Geotechnical Engineering, **10**(1): 188–194. doi:10.1016/j.jrmge.2017.10.001.

Bell, F.G. 1988. Stabilization and treatment of clay soils with lime - some applications. Ground Engineering, **21**(2): 22–30.

Bell, F.G. 1989. Lime stabilisation of clay soils. Bulletin of the International Association of Engineering Geology - Bulletin de l'Association Internationale de Géologie de l'Ingénieur, **39**(1): 67–74. doi:10.1007/BF02592537.

Bell, F.G. 1996. Lime stabilization of clay minerals and soils. Engineering Geology, **42**(4): 223–237. doi:10.1016/0013-7952(96)00028-2.

Bian, X., and Wang, G. 2024. Study of structural seismic damage considering seasonal frozen soil–structure interaction. Buildings, **14**(6): 1493. Multidisciplinary Digital Publishing Institute. doi:10.3390/buildings14061493.

Bo, M.W., Na, Y.M., Arulrajah, A., and Chang, M.F. 2009. Densification of granular soil by dynamic compaction. Proceedings of the Institution of Civil Engineers - Ground Improvement, **162**(3): 121–132. ICE Publishing. doi:10.1680/grim.2009.162.3.121.

Boardman, D.I., Glendinning, S., and Rogers, C.D.F. 2001. Development of stabilisation and solidification in lime–clay mixes. Géotechnique, **51**(6): 533–543. ICE Publishing. doi:10.1680/geot.2001.51.6.533.

Bolton, M.D. 1986. The strength and dilatancy of sands. Géotechnique, **36**(1): 65–78. ICE Publishing. doi:10.1680/geot.1986.36.1.65.

Bozbey, I., Kelesoglu, M.K., Demir, B., Komut, M., Comez, S., Ozturk, T., Mert, A., Ocal, K., and Oztoprak, S. 2018. Effects of soil pulverization level on resilient modulus and freeze and thaw resistance of a lime stabilized clay. Cold Regions Science and Technology, **151**: 323–334. doi:10.1016/j.coldregions.2018.03.023.

Bragg, R.A., and Andersland, O.B. 1981. Strain rate, temperature, and sample size effects on compression and tensile properties of frozen sand. Engineering Geology, **18**(1): 35–46. doi:10.1016/0013-7952(81)90044-2.

de Brito Galvão, T.C., Elsharief, A., and Simões, G.F. 2004. Effects of lime on permeability and compressibility of two tropical residual soils. Journal of Environmental Engineering, **130**(8): 881–885. American Society of Civil Engineers. doi:10.1061/(ASCE)0733-9372(2004)130:8(881).

Broderick, G.P., and Daniel, D.E. 1990. Stabilizing compacted clay against chemical attack. Journal of Geotechnical Engineering, **116**(10): 1549–1567. American Society of Civil Engineers. doi:10.1061/(ASCE)0733-9410(1990)116:10(1549).

Broms, B.B. 1991. Stabilization of soil with lime columns. *In* Foundation Engineering Handbook. *Edited by* H.-Y. Fang. Springer US, Boston, MA. pp. 833–855.

Cabane, N. 2004. Sols traités à la chaux et aux liants hydrauliques : Contribution à l'identification et à l'analyse des élèments perturbateurs de la stabilisation. phdthesis, Université Jean Monnet - Saint-Etienne.

Chamberlain, E., Groves, C., and Perham, R. 1972. The mechanical behaviour of frozen earth materials under high pressure triaxial test conditions. Géotechnique, **22**(3): 469–483. ICE Publishing. doi:10.1680/geot.1972.22.3.469.

Chen, H., Gao, X., and Wang, Q. 2023. Research progress and prospect of frozen soil engineering disasters. Cold Regions Science and Technology, **212**: 103901. doi:10.1016/j.coldregions.2023.103901.

Chen, L., Chen, X., Wang, H., Huang, X., and Song, Y. 2021. Mechanical properties and microstructure of lime-treated red clay. KSCE Journal of Civil Engineering, **25**(1): 70–77. doi:10.1007/s12205-020-0497-0.

Chen, W.F., and Yuan, R.L. 1980. Tensile strength of concrete: Double-punch test. Journal of the Structural Division, **106**(8): 1673–1693. doi:10.1061/JSDEAG.0005493.

Chen, X., and Jeong, S. 2024. Asymmetric impacts of surface thaw onset change on seasonal vegetation growth in Arctic permafrost. Global Ecology and Biogeography, **33**(1): 131–140. doi:10.1111/geb.13769.

Chen, Y., Azzam, R., Wang, M., Xu, S., and Chang, L. 2011. The uniaxial compressive and tensile tests of frozen saturated clay in Shanghai area. Environmental Earth Sciences, **64**(1): 29–36. doi:10.1007/s12665-010-0813-y.

Cheng, G., and Wu, T. 2007. Responses of permafrost to climate change and their environmental significance, Qinghai-Tibet Plateau. Journal of Geophysical Research: Earth Surface, **112**(F2). doi:10.1029/2006JF000631.

Chou, Y., Xingqiang, C., and Xiangang, J. 2013. Experimental study on strength characteristics of artificial structured frozen loess. Electronic Journal of Geotechnical Engineering, **18**: 6135–6152.

Christ, M., and Kim, Y.-C. 2009. Experimental study on the physical-mechanical properties of frozen silt. KSCE Journal of Civil Engineering, **13**(5): 317–324. doi:10.1007/s12205-009-0317-z.

Christ, M., and Park, J.-B. 2010. Laboratory determination of strength properties of frozen rubber–sand mixtures. Cold Regions Science and Technology, **60**(2): 169–175. doi:10.1016/j.coldregions.2009.08.013.

Cui, Z.-D., He, P.-P., and Yang, W.-H. 2014. Mechanical properties of a silty clay subjected to freezing–thawing. Cold Regions Science and Technology, **98**: 26–34. doi:10.1016/j.coldregions.2013.10.009.

Dagenais, S., Molson, J., Lemieux, J.-M., Fortier, R., and Therrien, R. 2020. Coupled cryo-hydrogeological modelling of permafrost dynamics near Umiujaq (Nunavik, Canada). Hydrogeology Journal, **28**(3): 887–904. doi:10.1007/s10040-020-02111-3.

Das, B.M. 2010. Geotechnical engineering handbook. J. Ross publishing, Fort Lauderdale, FL, USA.

Das, G., Razakamanantsoa, A., Herrier, G., Saussaye, L., Lesueur, D., and Deneele, D. 2021. Evaluation of the long-term effect of lime treatment on a silty soil embankment after seven years of atmospheric exposure: Mechanical, physicochemical, and microstructural studies. Engineering Geology, **281**: 105986. doi:10.1016/j.enggeo.2020.105986.

Dash, S.K., and Hussain, M. 2012. Lime stabilization of soils: Reappraisal. Journal of Materials in Civil Engineering, **24**(6): 707–714. doi:10.1061/(ASCE)MT.1943-5533.0000431.

Dassault Systèmes. 2016. Abaqus theory manual. Simulia.

Di Sante, M. 2020. On the compaction characteristics of soil-lime mixtures. Geotechnical and Geological Engineering, **38**(2): 2335–2344. doi:10.1007/s10706-019-01110-w.

Diamond, S., and Kinter, E.B. 1965. Mechanism of soil-lime stabilization. Highway Research Record, (92): 83–101.

Doré, G., Niu, F., and Brooks, H. 2016. Adaptation methods for transportation infrastructure built on degrading permafrost. Permafrost and Periglacial Processes, **27**(4): 352–364. doi:10.1002/ppp.1919.

Doré, G., and Zubeck, H.K. 2009. Cold regions pavement engineering. ASCE Press ; McGraw-Hill, Reston, VA : New York.

Eades, J.L., and Grim, R.E. 1960. Reaction of hydrated lime with pure clay minerals in soil stabilization. Highway Research Board Bulletin, (262).

Esmaeili-Falak, M., Katebi, H., and Javadi, A. 2018. Experimental study of the mechanical behavior of frozen soils - A case study of tabriz subway. Periodica Polytechnica Civil Engineering, **62**(1): 117–125. doi:10.3311/PPci.10960.

Esmaeili-Falak, M., Katebi, H., and Javadi, A.A. 2020. Effect of freezing on stress–strain characteristics of granular and cohesive soils. Journal of Cold Regions Engineering, **34**(2): 05020001. American Society of Civil Engineers. doi:10.1061/(ASCE)CR.1943-5495.0000205.

Evirgen, B., and Tuncan, M. 2019. A physical soil freezing model for laboratory applications. Cold Regions Science and Technology, **159**: 29–39. doi:10.1016/j.coldregions.2018.12.005.

Fang, H.Y., and Chen, W.F. 1971. New method for determination of tensile strength of soils. (345): 62–68.

Fang, H.-Y., Daniels, J., and Daniels, J.L. 2006. Introductory geotechnical engineering: an environmental perspective. Taylor & Francis, London.

Fang, H.-Y., and Daniels, J.L. 2017. Introductory geotechnical engineering. *In* 1st edition. CRC Press.

Federico, A., Vitone, C., and Murianni, A. 2015. On the mechanical behaviour of dredged submarine clayey sediments stabilized with lime or cement. Canadian Geotechnical Journal, **52**(12): 2030–2040. NRC Research Press. doi:10.1139/cgj-2015-0086.

Fei, W., and Yang, Z.J. 2019. Modeling unconfined compression behavior of frozen Fairbanks silt considering effects of temperature, strain rate and dry density. Cold Regions Science and Technology, **158**: 252–263. doi:10.1016/j.coldregions.2018.09.002.

Fortier, R., LeBlanc, A.-M., and Yu, W. 2011. Impacts of permafrost degradation on a road embankment at Umiujaq in Nunavik (Quebec), Canada. Canadian Geotechnical Journal, **48**(5): 720–740. NRC Research Press. doi:10.1139/t10-101.

Gelder, C., and Fowmes, G.J. 2016. Mixing and compaction of fibre- and lime-modified cohesive soil. Proceedings of the Institution of Civil Engineers - Ground Improvement, **169**(2): 98–108. doi:10.1680/grim.14.00025.

GhavamShirazi, S., and Bilsel, H. 2021. Characterization of volume change and strength behavior of micro-silica and lime-stabilized Cyprus clay. Acta Geotechnica, **16**(3): 827–840. doi:10.1007/s11440-020-01060-1.

Ghazavi, M., and Roustaei, M. 2013. Freeze–thaw performance of clayey soil reinforced with geotextile layer. Cold Regions Science and Technology, **89**: 22–29. doi:10.1016/j.coldregions.2013.01.002.

Ghazavi, M., Roustaei, M., Safaei, V., and Kalhor, A. 2023. Effect of freeze–thaw cycles on consolidation behavior of two plastic fine soils. Geotechnical and Geological Engineering, **41**(2): 1473–1483. doi:10.1007/s10706-022-02348-7.

Ghobadi, M.H., Abdilor, Y., and Babazadeh, R. 2014. Stabilization of clay soils using lime and effect of pH variations on shear strength parameters. Bulletin of Engineering Geology and the Environment, **73**(2): 611–619. doi:10.1007/s10064-013-0563-7.

Ghoreishian Amiri, S.A., and Grimstad, G. 2017. Constitutive model for long-term behavior of saturated frozen soil. : 1005–1012. American Society of Civil Engineers. doi:10.1061/9780784480779.125.

Girgis, N., Li, B., Akhtar, S., and Courcelles, B. 2020. Experimental study of rate-dependent uniaxial compressive behaviors of two artificial frozen sandy clay soils. Cold Regions Science and Technology, **180**: 103166. doi:10.1016/j.coldregions.2020.103166.

Goldberg, I., and Klein, A. 1953. Some effects of treating expansive clays with calcium hydroxide. *In* Symposium on Exchange Phenomena in Soils. ASTM International. pp. 53–71.

Gruber, S., and Haeberli, W. 2007. Permafrost in steep bedrock slopes and its temperature-related destabilization following climate change. Journal of Geophysical Research: Earth Surface, **112**(F2). doi:10.1029/2006JF000547.

Güllü, H. 2015. Unconfined compressive strength and freeze–thaw resistance of fine-grained soil stabilised with bottom ash, lime and superplasticiser. Road Materials and Pavement Design, **16**(3): 608–634. Taylor & Francis. doi:10.1080/14680629.2015.1021369.

Guo, J., Jia, L., Wei, Z., and Zhang, L. 2022. Evaluation on the mechanical performance of lime–ground granulated blast-furnace slag stabilized loess. Arabian Journal of Geosciences, **15**(15): 1361. doi:10.1007/s12517-022-10654-w.

Haynes, F.D., Karalius, J.A., and Kalafut, J. 1975. Strain rate effects on the strength of frozen silt.US army cold regions research and engineering laboratory. CRREL research report. International Journal of Rock Mechanics and Mining Sciences & Geomechanics Abstracts,. doi:10.1016/0148-9062(77)90588-5.

Helwany, S. 2007. Applied soil mechanics: with ABAQUS applications. John Wiley & Sons, Hoboken, N.J.

Herrier, G., Lesueur, D., Puiatti, D., Auriol, J.-C., Chevalier, C., Haghighi, I., Cuisinier, O., Bonelli, S., and Fry, J.-J. 2012. Lime treated materials for embankment and hardfill dam. Kyoto.

Herrin, M., and Mitchell, H. 1961. Lime-soil mixtures. *In* Highway Research Board Proceedings. Washington, D.C. pp. 99–138.

Hjort, J., Karjalainen, O., Aalto, J., Westermann, S., Romanovsky, V.E., Nelson, F.E., Etzelmüller, B., and Luoto, M. 2018. Degrading permafrost puts arctic infrastructure at risk by mid-century. Nature Communications, **9**(1): 5147. Nature Publishing Group. doi:10.1038/s41467-018-07557-4.

Hou, F., Lai, Y., Liu, E., Luo, H., and Liu, X. 2018. A creep constitutive model for frozen soils with different contents of coarse grains. Cold Regions Science and Technology, **145**: 119–126. doi:10.1016/j.coldregions.2017.10.013.

Hu, X., Wang, J., and Yu, R. 2013. Uniaxial compressive and splitting tensile tests of artificially frozen soils in tunnel construction of Hong Kong. Journal of Shanghai Jiaotong University (Science), **18**(6): 688–692. doi:10.1007/s12204-013-1450-x.

Hussain, M., and Dash, S.K. 2014. The influence of lime on the compaction behaviour of soils. Environmental Geotechnics, **3**(5): 346–352. doi:10.1680/envgeo.14.00015.

Ishikawa, T., Tokoro, T., and Seiichi, M. 2015. Geohazard at volcanic soil slope in cold regions and its influencing factors. Japanese Geotechnical Society Special Publication, **1**(1): 1–20. doi:10.3208/jgssp.KEY-1.

Ismeik, M., and Shaqour, F. 2020. Effectiveness of lime in stabilising subgrade soils subjected to freeze–thaw cycles. Road Materials and Pavement Design, **21**(1): 42–60. Taylor & Francis. doi:10.1080/14680629.2018.1479289.

Ji, Y., Zhou, G., and Hall, M.R. 2019. Frost heave and frost heaving-induced pressure under various restraints and thermal gradients during the coupled thermal–hydro processes in freezing soil. Bulletin of Engineering Geology and the Environment, **78**(5): 3671–3683. doi:10.1007/s10064-018-1345-z.

Jia, L. (n.d.). Experimental investigation on shear strength parameters of lime stabilized loess.

Jin, H., Wei, Z., Wang, S., Yu, Q., Lü, L., Wu, Q., and Ji, Y. 2008. Assessment of frozen-ground conditions for engineering geology along the Qinghai–Tibet highway and railway, China. Engineering Geology, **101**(3): 96–109. doi:10.1016/j.enggeo.2008.04.001.

Johnson, A.M. 1949. Laboratory experiments with lime-soil mixtures. Highway Research Board Proceedings, **28**: 496–507.

Kadivar, M., and Manahiloh, K.N. 2019. Revisiting parameters that dictate the mechanical behavior of frozen soils. Cold Regions Science and Technology, **163**: 34–43. doi:10.1016/j.coldregions.2019.04.005.

Kamei, T., Ahmed, A., and Shibi, T. 2012. Effect of freeze–thaw cycles on durability and strength of very soft clay soil stabilised with recycled Bassanite. Cold Regions Science and Technology, **82**: 124–129. doi:10.1016/j.coldregions.2012.05.016.

Kan, K., and François, B. 2023. Triaxial tension and compression tests on saturated lime-treated plastic clay upon consolidated undrained conditions. Journal of Rock Mechanics and Geotechnical Engineering, **15**(12): 3328–3342. doi:10.1016/j.jrmge.2023.03.017.

Kanchi, G.M., Neeraja, V.S., and Sivakumar Babu, G.L. 2015. Effect of anisotropy of fibers on the stress-strain response of fiber-reinforced soil. International Journal of Geomechanics, **15**(1): 06014016. American Society of Civil Engineers. doi:10.1061/(ASCE)GM.1943-5622.0000392.

Kavak, A. 1996. The behavior of lime stabilized clays under cyclic loading. PhD dissertation, Boğaziçi University, Istanbul, Turkey.

Kavak, A., and Akyarlı, A. 2007. A field application for lime stabilization. Environmental Geology, **51**(6): 987–997. doi:10.1007/s00254-006-0368-0.

Kelley, C.M. 1988. A long range durability study of lime stabilized bases at military posts in the southwest. National Lime Association, **1**.

Keuper, F., van Bodegom, P.M., Dorrepaal, E., Weedon, J.T., van Hal, J., van Logtestijn, R.S.P., and Aerts, R. 2012. A frozen feast: thawing permafrost increases plant-available nitrogen in subarctic peatlands. Global Change Biology, **18**(6): 1998–2007. doi:10.1111/j.1365-2486.2012.02663.x.

Keuper, F., Dorrepaal, E., van Bodegom, P.M., van Logtestijn, R., Venhuizen, G., van Hal, J., and Aerts, R. 2017. Experimentally increased nutrient availability at the permafrost thaw front selectively enhances biomass production of deep-rooting subarctic peatland species. Global Change Biology, **23**(10): 4257–4266. doi:10.1111/gcb.13804.

Khajeh, A., Chenari, R.J., MolaAbasi, H., and Payan, M. 2022. An experimental investigation on geotechnical properties of a clayey soil stabilised with lime and zeolite in base and subbase courses. Road Materials and Pavement Design,. Taylor & Francis.

Khajeh, A., Ebrahimi, S.A., MolaAbasi, H., Jamshidi Chenari, R., and Payan, M. 2021. Effect of EPS beads in lightening a typical zeolite and cement-treated sand. Bulletin of Engineering Geology and the Environment, **80**(11): 8615–8632. doi:10.1007/s10064-021-02458-1.

Khajeh, A., Jamshidi Chenari, R., and Payan, M. 2020. A simple review of cemented non-conventional materials: soil composites. Geotechnical and Geological Engineering, **38**(2): 1019–1040. doi:10.1007/s10706-019-01090-x.

Khajeh, A., Jamshidi Chenari, R., Payan, M., and MolaAbasi, H. 2023. Assessing the effect of lime-zeolite on geotechnical properties and microstructure of reconstituted clay used as a subgrade soil. Physics and Chemistry of the Earth, Parts A/B/C, **132**: 103501. doi:10.1016/j.pce.2023.103501.

Khajeh, A., Jamshidi Chenari, R., Payan, M., and MolaAbasi, H. 2024. Application of expanded polystyrene beads inclusion in lightening lime-zeolite treated clays: strength and stiffness assessment. Environment, Development and Sustainability, **26**(8): 21369–21397. doi:10.1007/s10668-023-03535-z.

Khattab, S.A., Al-Mukhtar, M., and Fleureau, J.-M. 2007. Long-term stability characteristics of a lime-treated plastic soil. Journal of Materials in Civil Engineering, **19**(4): 358–366. American Society of Civil Engineers. doi:10.1061/(ASCE)0899-1561(2007)19:4(358).

Khoury, N.N., and Zaman, M.M. 2007. Environmental effects on durability of aggregates stabilized with cementitious materials. Journal of Materials in Civil Engineering, **19**(1): 41–48. American Society of Civil Engineers. doi:10.1061/(ASCE)0899-1561(2007)19:1(41).

Konrad, J.-M. 1989. Physical processes during freeze-thaw cycles in clayey silts. Cold Regions Science and Technology, **16**(3): 291–303. doi:10.1016/0165-232X(89)90029-3.

Ladanyi, B. 1972. An engineering theory of creep of frozen soils. Canadian Geotechnical Journal, **9**(1): 63–80. NRC Research Press. doi:10.1139/t72-005.

Ladanyi, B., and Benyamina, M.B. 1995. Triaxial relaxation testing of a frozen sand. Canadian Geotechnical Journal, **32**(3): 496–511. NRC Research Press. doi:10.1139/t95-052.

Lai, Y., Xu, X., Dong, Y., and Li, S. 2013. Present situation and prospect of mechanical research on frozen soils in China. Cold Regions Science and Technology, **87**: 6–18. doi:10.1016/j.coldregions.2012.12.001.

Lasledj, A. 2009. Traitement des sols argileux à la chaux: processus physico-chimique et propriétés géotechniques. PhD thesis, University of Orléans, France.

Le, T.M.H., Depina, I., Guegan, E., and Sinitsyn, A. 2018. Thermal regime of permafrost at Varandey Settlement along the Barents Sea Coast, North West Arctic Russia. Engineering Geology, **246**: 69–81. doi:10.1016/j.enggeo.2018.09.026.

Lee, W., Bohra, N.C., Altschaeffl, A.G., and White, T.D. 1995. Resilient modulus of cohesive soils and the effect of freeze–thaw. Canadian Geotechnical Journal, **32**(4): 559–568. NRC Research Press. doi:10.1139/t95-059.

L'Heureux, J.-S., Locat, A., Leroueil, S., Demers, D., and Locat, J. 2014. Landslides in sensitive clays – from geosciences to risk management. *In* Landslides in Sensitive Clays: From Geosciences to Risk Management. *Edited by* J.-S. L'Heureux, A. Locat, S. Leroueil, D. Demers, and J. Locat. Springer Netherlands, Dordrecht. pp. 1–12.

Li, B., and Akhtar, S. 2022. Characterizations of tensile yield and failure processes of frozen clay soils: laboratory testing and numerical modeling. Bulletin of Engineering Geology and the Environment, **81**(10): 429. doi:10.1007/s10064-022-02942-2.

Li, B., Min, F., Zhang, N., Ma, J., Li, Z., Yao, Z., and Zhang, L. 2023. Experimental study on water transfer mechanism of quicklime modified centrifugal dewatering clay. Construction and Building Materials, **408**: 133492. doi:10.1016/j.conbuildmat.2023.133492.

Li, B., Norouzi, E., Zhu, H.-H., and Wu, B. 2024. A thermo-poromechanical model for simulating freeze–thaw actions in unsaturated soils. Advances in Water Resources, **184**: 104624. doi:10.1016/j.advwatres.2024.104624.

Li, B., and Wong, R.C.K. 2016. Quantifying structural states of soft mudrocks. Journal of Geophysical Research: Solid Earth, **121**(5): 3324–3347. doi:10.1002/2015JB012454.

Li, H., Lai, Y., Wang, L., Yang, X., Jiang, N., Li, L., Wang, C., and Yang, B. 2019a. Review of the state of the art: interactions between a buried pipeline and frozen soil. Cold Regions Science and Technology, **157**: 171–186. doi:10.1016/j.coldregions.2018.10.014.

Li, H., Zhu, Y., Zhang, J., and Lin, C. 2004. Effects of temperature, strain rate and dry density on compressive strength of saturated frozen clay. Cold Regions Science and Technology, **39**(1): 39–45. doi:10.1016/j.coldregions.2004.01.001.

Li, H.-D., Tang, C.-S., Cheng, Q., Li, S.-J., Gong, X.-P., and Shi, B. 2019b. Tensile strength of clayey soil and the strain analysis based on image processing techniques. Engineering Geology, **253**: 137–148. doi:10.1016/j.enggeo.2019.03.017.

Li, X., Liu, E., Song, B., and Liu, X. 2018. An improved nishihara model for frozen loess considering the influence of temperature. Advances in Materials Science and Engineering, **2018**(1): 9073435. doi:10.1155/2018/9073435.

Little, D.N. 1995. Stabilization of pavement subgrades and base courses with lime. Kendall/Hunt Publishing Company, Dubuque, Iowa.

Liu, B., Crooks, J., Nixon, J.F. (Derick), and Zhou, J. 2008a. Experimental studies of pipeline uplift resistance in frozen ground. In international pipeline conference. Calgary, Canada. pp. 2407–2413.

Liu, B., Moffitt, K., Nixon, J.F. (Derick), Zhou, J., and Xiao, Y. 2008b. Numerical studies of pipeline uplift resistance in frozen ground.

Liu, J., Wang, T., and Tian, Y. 2010. Experimental study of the dynamic properties of cement- and lime-modified clay soils subjected to freeze–thaw cycles. Cold Regions Science and Technology, **61**(1): 29–33. doi:10.1016/j.coldregions.2010.01.002.

Liu, X., Liu, E., Zhang, D., Zhang, G., Yin, X., and Song, B. 2019. Study on effect of coarse-grained content on the mechanical properties of frozen mixed soils. Cold Regions Science and Technology, **158**: 237–251. doi:10.1016/j.coldregions.2018.09.001.

Lu, M., Sun, J., Wen, M., Yang, K., and Li, K. 2024. Insight into nonlinear thermal consolidation of saturated clay under coupled thermo-mechanical loading: a unified one-dimensional model. Acta Geotechnica,. doi:10.1007/s11440-024-02382-0.

Ma, J., Huang, K., Zou, B., Li, X., and Deng, Y. 2023. The influence of tunnel insulation measures on the temperature spatiotemporal variation of frozen soil during artificial ground freezing. Cold Regions Science and Technology, **214**: 103942. doi:10.1016/j.coldregions.2023.103942.

Mahedi, M., Cetin, B., and Cetin, K.S. 2019. Freeze-thaw performance of phase change material (PCM) incorporated pavement subgrade soil. Construction and Building Materials, **202**: 449–464. doi:10.1016/j.conbuildmat.2018.12.210.

McCaustland, D.E.J. 1925. Lime dirt in roads. *In* National Lime Association. pp. 12–18.

McDowell, C. 1959. Stabilization of soils with lime, lime-flyash, and other lime reactive materials. Highway Research Board Bulletin, (231).

Meziani, B., and Gadouri, H. 2023. Swelling suppressing by using polypropylene fibre as reinforcement in natural pozzolana-lime-stabilised expansive grey clayey soil artificially contaminated by sulphates. Multiscale and Multidisciplinary Modeling, Experiments and Design, **6**(4): 477–504. doi:10.1007/s41939-023-00157-w.

Miner, K.R., Turetsky, M.R., Malina, E., Bartsch, A., Tamminen, J., McGuire, A.D., Fix, A., Sweeney, C., Elder, C.D., and Miller, C.E. 2022. Permafrost carbon emissions in a changing Arctic. Nature Reviews Earth & Environment, **3**(1): 55–67. Nature Publishing Group. doi:10.1038/s43017-021-00230-3.

Ming, F., Li, D., Zhang, M., and Zhang, Y. 2017. A novel method for estimating the elastic modulus of frozen soil. Cold Regions Science and Technology, **141**: 1–7. doi:10.1016/j.coldregions.2017.05.005.

Minsley, B.J., Pastick, N.J., James, S.R., Brown, D.R.N., Wylie, B.K., Kass, M.A., and Romanovsky, V.E. 2022. Rapid and Gradual Permafrost Thaw: A Tale of Two Sites. Geophysical Research Letters, **49**(21): e2022GL100285. doi:10.1029/2022GL100285.

Mitchell, J.K., and Hooper, D.R. 1961. Influence of time between mixing and compaction on properties of a lime-stabilized expansive clay. *In* Highway Research Board Bulletin. Washington, DC, USA.

Mitchell, J.K., and Soga, K. 2005. Fundamentals of soil behavior. *In* 3. ed. Wiley, Hoboken, NJ.

MolaAbasi, H., Jamshidi Chenari, R., and Payan, M. 2024. An experimental study on the effect of disposable COVID-19 face masks on the mechanical properties of cement-stabilized sand. Environment, Development and Sustainability,. doi:10.1007/s10668-024-04519-3.

Na, S., and Sun, W. 2017. Computational thermo-hydro-mechanics for multiphase freezing and thawing porous media in the finite deformation range. Computer Methods in Applied Mechanics and Engineering, **318**: 667–700. doi:10.1016/j.cma.2017.01.028.

Nassr, A., Esmaeili-Falak, M., Katebi, H., and Javadi, A. 2018. A new approach to modeling the behavior of frozen soils. Engineering Geology, **246**: 82–90. doi:10.1016/j.enggeo.2018.09.018.

Natural Resources Canada. 2017. Supporting airport infrastructure in Canada's north. Available from https://natural-resources.canada.ca/stories/simply-science/supporting-airport-infrastructure-canada-s-north. [accessed 28 February 2025].

Nelson, F.E., Anisimov, O.A., and Shiklomanov, N.I. 2001. Subsidence risk from thawing permafrost. Nature, **410**(6831): 889–890. Nature Publishing Group. doi:10.1038/35073746.

Nixon, J., and Burgess, M. 1999. Norman Wells pipeline settlement and uplift movements. Canadian Geotechnical Journal, **36**(1): 119–135. NRC Research Press. doi:10.1139/t98-092.

Nixon, J.F. 1991. Discrete ice lens theory for frost heave in soils. Canadian Geotechnical Journal, **28**(6): 843–859. NRC Research Press. doi:10.1139/t91-102.

Nixon, J.F. (Derick). 1992. Discrete ice lens theory for frost heave beneath pipelines. Canadian Geotechnical Journal, **29**(3): 487–497. NRC Research Press. doi:10.1139/t92-053.

Norouzi, E., and Li, B. 2024. Finite element modeling of thermal-hydro-mechanical coupled processes in unsaturated freezing soils considering air-water capillary pressure and cryosuction. International Journal for Numerical and Analytical Methods in Geomechanics, **48**(11): 2944–2970. doi:10.1002/nag.3761.

Notman, C.F. 2011. Durability testing of fine grained stabilised soils. Thesis (University of Nottingham only), University of Nottingham. Available from https://eprints.nottingham.ac.uk/12060/. [accessed 5 February 2025].

Obu, J., Westermann, S., Bartsch, A., Berdnikov, N., Christiansen, H.H., Dashtseren, A., Delaloye, R., Elberling, B., Etzelmüller, B., Kholodov, A., Khomutov, A., Kääb, A., Leibman, M.O., Lewkowicz, A.G., Panda, S.K., Romanovsky, V., Way, R.G.,

Westergaard-Nielsen, A., Wu, T., Yamkhin, J., and Zou, D. 2019. Northern hemisphere permafrost map based on TTOP modelling for 2000–2016 at 1 km2 scale. Earth-Science Reviews, **193**: 299–316. doi:10.1016/j.earscirev.2019.04.023.

Ozdemir, M.A. 2016. Improvement in bearing capacity of a soft soil by addition of fly ash. Procedia Engineering, **143**: 498–505. doi:10.1016/j.proeng.2016.06.063.

Padmaraj, D., and Arnepalli, D.N. 2024. Comprehensive evaluation of carbonation and leaching reactions in lime-stabilised soils. Environmental Geotechnics,: 1–13. doi:10.1680/jenge.24.00011.

Parameswaran, V.R., and Jones, S.J. 1981. Triaxial testing of frozen sand. Journal of Glaciology, **27**(95): 147–155. doi:10.3189/S0022143000011308.

Park, D., and Michalowski, R.L. 2017. Three-dimensional stability analysis of slopes in hard soil/soft rock with tensile strength cut-off. Engineering Geology, **229**: 73–84. doi:10.1016/j.enggeo.2017.09.018.

Parsons, R.L., and Milburn, J.P. 2003. Engineering behavior of stabilized soils. Transportation Research Record, **1837**(1): 20–29. SAGE Publications Inc. doi:10.3141/1837-03.

Petry, T.M., and Little, D.N. 2002. Review of stabilization of clays and expansive soils in pavements and lightly loaded structures—history, practice, and future. Journal of Materials in Civil Engineering, **14**(6): 447–460. American Society of Civil Engineers. doi:10.1061/(ASCE)0899-1561(2002)14:6(447).

Pousette, K., Mácsik, J., Jacobsson, A., Andersson, R., and Lahtinen, P. 1999. Peat soil samples stabilised in laboratory – Experiences from manufacturing and testing. *In* Dry Mix Methods for Deep Soil Stabilization. Routledge.

Prusinski, J.R., and Bhattacharja, S. 1999. Effectiveness of portland cement and lime in stabilizing clay soils. Transportation Research Record, **1652**(1): 215–227. SAGE Publications Inc. doi:10.3141/1652-28.

Puswewala, U.G.A., and Rajapakse, R.K.N.D. 1990. Numerical modeling of structure-frozen soil/ice interaction. Journal of Cold Regions Engineering, **4**(3): 133–151. American Society of Civil Engineers. doi:10.1061/(ASCE)0887-381X(1990)4:3(133).

Puzrin, A.M. 2012. Constitutive Modelling in Geomechanics: Introduction. Springer, Berlin, Heidelberg.

Qi, J., Vermeer, P.A., and Cheng, G. 2006. A review of the influence of freeze-thaw cycles on soil geotechnical properties. Permafrost and Periglacial Processes, **17**(3): 245–252. doi:10.1002/ppp.559.

Rogers, C.D.F., and Glendinning, S. 2000. Lime requirement for stabilization. Transportation Research Record, **1721**(1): 9–18. SAGE Publications Inc. doi:10.3141/1721-02.

Rosone, M., Celauro, C., and Ferrari, A. 2020. Microstructure and shear strength evolution of a lime-treated clay for use in road construction. International Journal of Pavement Engineering, **21**(9): 1147–1158. Taylor & Francis. doi:10.1080/10298436.2018.1524144.

Royer, M.-J.S. 2016. Introduction. *In* Climate, Environment and Cree Observations: James Bay Territory, Canada. *Edited by* M.-J.S. Royer. Springer International Publishing, Cham. pp. 1–6.

Saffer, D.M., and Marone, C. 2003. Comparison of smectite- and illite-rich gouge frictional properties: application to the updip limit of the seismogenic zone along subduction megathrusts. Earth and Planetary Science Letters, **215**(1): 219–235. doi:10.1016/S0012-821X(03)00424-2.

Salehi, M., and Sivakugan, N. 2009. Effects of lime-clay modification on the consolidation behavior of the dredged mud. Journal of Waterway, Port, Coastal, and Ocean Engineering, **135**(6): 251–258. American Society of Civil Engineers. doi:10.1061/(ASCE)WW.1943-5460.0000004.

Selvadurai, A.P.S., Hu, J., and Konuk, I. 1999a. Computational modelling of frost heave induced soil–pipeline interaction: II. Modelling of experiments at the Caen test facility. Cold Regions Science and Technology, **29**(3): 229–257. doi:10.1016/S0165-232X(99)00029-4.

Selvadurai, A.P.S., Hu, J., and Konuk, I. 1999b. Computational modelling of frost heave induced soil–pipeline interaction: I. Modelling of frost heave. Cold Regions Science and Technology, **29**(3): 215–228. doi:10.1016/S0165-232X(99)00028-2.

Shastri, A., Sánchez, M., Gai, X., Lee, M.Y., and Dewers, T. 2021. Mechanical behavior of frozen soils: Experimental investigation and numerical modeling. Computers and Geotechnics, **138**: 104361. doi:10.1016/j.compgeo.2021.104361.

Shukla, S., Sivakugan, N., and Das, B. 2009. Fundamental concepts of soil reinforcement — an overview. International Journal of Geotechnical Engineering, **3**(3): 329–342. Taylor & Francis. doi:10.3328/IJGE.2009.03.03.329-342.

Simonsen, E., and Isacsson, U. 1999. Thaw weakening of pavement structures in cold regions. Cold Regions Science and Technology, **29**(2): 135–151. doi:10.1016/S0165-232X(99)00020-8.

Song, Z., Zhang, D., Mao, Y., Mu, Y., Zhang, K., and Zhang, Q. 2020. Behavior of lime-stabilized red bed soil after cyclic wetting-drying in triaxial tests and SEM analysis. Advances in Materials Science and Engineering, **2020**(1): 4230519. doi:10.1155/2020/4230519.

Staszewska, K., Niemunis, A., and Cudny, M. 2024. Experimental observations on the creep behaviour of frozen soil. Acta Geotechnica, **19**(5): 2445–2466. doi:10.1007/s11440-024-02253-8.

Streletskiy, D.A., Sherstiukov, A.B., Frauenfeld, O.W., and Nelson, F.E. 2015. Changes in the 1963–2013 shallow ground thermal regime in Russian permafrost regions. Environmental Research Letters, **10**(12): 125005. IOP Publishing. doi:10.1088/1748-9326/10/12/125005.

Suh, H.S., and Sun, W. 2022. Multi-phase-field microporomechanics model for simulating ice lens growth and thaw in frozen soil. International Journal for Numerical and Analytical Methods in Geomechanics, **46**(12): 2307–2336. doi:10.1002/nag.3408.

Svensson, P.D., and Hansen, S. 2010. Freezing and thawing of montmorillonite — A time-resolved synchrotron X-ray diffraction study. Applied Clay Science, **49**(3): 127–134. doi:10.1016/j.clay.2010.04.015.

Sweidan, A.H., Niggemann, K., Heider, Y., Ziegler, M., and Markert, B. 2022. Experimental study and numerical modeling of the thermo-hydro-mechanical processes in soil freezing with different frost penetration directions. Acta Geotechnica, **17**(1): 231–255. doi:10.1007/s11440-021-01191-z.

Szendefy, J. 2008. Impact of soil stabilization with lime to the structure and bearing capacity of internal soils. In 18th International Conference on Soil Mechanics and Geotechnical Engineering. Paris.

Tanaka, H., Locat, J., Shibuya, S., Soon, T.T., and Shiwakoti, D.R. 2001. Characterization of Singapore, Bangkok, and Ariake clays. Canadian Geotechnical Journal, **38**(2): 378–400. doi:10.1139/t00-106.

Tang, C.-S., Pei, X.-J., Wang, D.-Y., Shi, B., and Li, J. 2015. Tensile strength of compacted clayey soil. Journal of Geotechnical and Geoenvironmental Engineering, **141**(4): 04014122. American Society of Civil Engineers. doi:10.1061/(ASCE)GT.1943-5606.0001267.

Tang, Y., Zhou, J., Hong, J., Yang, P., and Wang, J. 2012. Quantitative analysis of the microstructure of Shanghai muddy clay before and after freezing. Bulletin of Engineering Geology and the Environment, **71**(2): 309–316. doi:10.1007/s10064-011-0380-9.

Tebaldi, G., Orazi, M., and Orazi, U.S. 2016. Effect of freeze—thaw cycles on mechanical behavior of lime-stabilized soil. Journal of Materials in Civil Engineering, **28**(6): 06016002. American Society of Civil Engineers. doi:10.1061/(ASCE)MT.1943-5533.0001509.

Thompson, M.R. 1968. Lime stabilization of soils for highway purposes. Ill Univ Hwy Res Lab Civil Eng Studies,.

Triantafyllidis, Th., and Kimmig, I. 2019. A simplified model for vibro compaction of granular soils. Soil Dynamics and Earthquake Engineering, **122**: 261–273. doi:10.1016/j.soildyn.2018.12.008.

Vasiliev, A.A., Drozdov, D.S., Gravis, A.G., Malkova, G.V., Nyland, K.E., and Streletskiy, D.A. 2020. Permafrost degradation in the western Russian arctic. Environmental Research Letters, **15**(4): 045001. IOP Publishing. doi:10.1088/1748-9326/ab6f12.

Verbrugge, J.-C., Bel, R., Correia, A., Duvigneaud, P.-H., and Herrier, G. 2011. Strength and micro observations on a lime treated silty soil.

Vitel, M., Rouabhi, A., Tijani, M., and Guérin, F. 2015. Modeling heat transfer between a freeze pipe and the surrounding ground during artificial ground freezing activities. Computers and Geotechnics, **63**: 99–111. doi:10.1016/j.compgeo.2014.08.004.

Vorobieff, G., and Murphy, G. 2003. A new approach to pavement design using lime stabilised subgrades. *In* Publication of: ARRB Transport Research, Limited.

Wang, B., Paudel, B., and Li, H. 2016. Behaviour of retrogressive thaw slumps in northern Canada—three-year monitoring results from 18 sites. Landslides, **13**(1): 1–8. doi:10.1007/s10346-014-0549-y.

Wang, D., Abriak, N.E., Zentar, R., and Chen, W. 2013. Effect of lime treatment on geotechnical properties of Dunkirk sediments in France. Road Materials and Pavement Design, **14**(3): 485–503. Taylor & Francis. doi:10.1080/14680629.2012.755935.

Wang, D., Ma, W., Niu, Y., Chang, X., and Wen, Z. 2007. Effects of cyclic freezing and thawing on mechanical properties of Qinghai–Tibet clay. Cold Regions Science and Technology, **48**(1): 34–43. doi:10.1016/j.coldregions.2006.09.008.

Wang, F., Li, G., Ma, W., Wu, Q., Serban, M., Vera, S., Alexandr, F., Jiang, N., and Wang, B. 2019a. Pipeline–permafrost interaction monitoring system along the China–Russia crude oil pipeline. Engineering Geology, **254**: 113–125. doi:10.1016/j.enggeo.2019.03.013.

Wang, P., Liu, E., Song, B., Liu, X., Zhang, G., and Zhang, D. 2019b. Binary medium creep constitutive model for frozen soils based on homogenization theory. Cold Regions Science and Technology, **162**: 35–42. doi:10.1016/j.coldregions.2019.03.019.

Wang, Q., Wang, H., Zhang, J., Wu, D., Zhao, R., Wang, Q., Wang, H., Zhang, J., Wu, D., and Zhao, R. 2023. Mechanical behavior of an FGM-type frozen soil wall: Theory and numerical analysis. Mathematical Biosciences and Engineering, **20**(9): 15544–15567. doi:10.3934/mbe.2023694.

Wang, S., and Liu, F. 2015. A hypoplasticity-based method for estimating thaw consolidation of frozen sand. Geotechnical and Geological Engineering, **33**(5): 1307–1320. doi:10.1007/s10706-015-9902-8.

Wang, S., Qi, J., and Yao, X. 2011. Stress relaxation characteristics of warm frozen clay under triaxial conditions. Cold Regions Science and Technology, **69**(1): 112–117. doi:10.1016/j.coldregions.2011.06.015.

Wang, S., Qi, J., Yin, Z., Zhang, J., and Ma, W. 2014. A simple rheological element based creep model for frozen soils. Cold Regions Science and Technology, **106–107**: 47–54. doi:10.1016/j.coldregions.2014.06.007.

Wang, Y., Guo, P., Li, X., Lin, H., Liu, Y., and Yuan, H. 2019c. Behavior of fiber-reinforced and lime-stabilized clayey soil in triaxial tests. Applied Sciences, **9**(5): 900. Multidisciplinary Digital Publishing Institute. doi:10.3390/app9050900.

Wei, J., Wei, J., Huang, Q., Zainal Abidin, S.M.I.B.S., and Zou, Z. 2023. Mechanism and engineering characteristics of expansive soil reinforced by industrial solid waste: A review. Buildings, **13**(4): 1001. Multidisciplinary Digital Publishing Institute. doi:10.3390/buildings13041001.

Wei, L., Chai, S., Xue, M., Wang, P., and Li, F. 2022. Structural damage and shear performance degradation of fiber–lime–soil under freeze–thaw cycling. Geotextiles and Geomembranes, **50**(5): 845–857. doi:10.1016/j.geotexmem.2022.04.005.

Wen, H., Bhusal, S., and Li, X. 2013. Double punch test: Simple performance test to evaluate the fatigue and rutting potential of asphalt concrete. Journal of Materials in Civil Engineering, **25**(5): 645–652. American Society of Civil Engineers. doi:10.1061/(ASCE)MT.1943-5533.0000628.

Wilkinson, A., Haque, A., Kodikara, J., Adamson, J., and Christie, D. 2010. Improvement of problematic soils by lime slurry pressure injection: Case study. Journal of Geotechnical and Geoenvironmental Engineering, **136**(10): 1459–1468. American Society of Civil Engineers. doi:10.1061/(ASCE)GT.1943-5606.0000359.

Woo, H.-J., and Go, G.-H. 2024. Mechanical behavior assessment of retaining wall structure due to frost heave of frozen ground. International Journal of Geo-Engineering, **15**(1): 7. doi:10.1186/s40703-024-00210-8.

Xu, G., Peng, C., Wu, W., and Qi, J. 2017a. Combined constitutive model for creep and steady flow rate of frozen soil in an unconfined condition. Canadian Geotechnical Journal,. NRC Research Press. doi:10.1139/cgj-2016-0139.

Xu, P., Han, S., and Xing, Y. 2022. Analysis of influencing factors of temperature field in freezing construction of metro connecting passage. Geotechnical and Geological Engineering, **40**(3): 1331–1343. doi:10.1007/s10706-021-01966-x.

Xu, X., Li, Q., Lai, Y., Pang, W., and Zhang, R. 2019. Effect of moisture content on mechanical and damage behavior of frozen loess under triaxial condition along with different confining pressures. Cold Regions Science and Technology, **157**: 110–118. doi:10.1016/j.coldregions.2018.10.004.

Xu, X., Wang, Y., Yin, Z., and Zhang, H. 2017b. Effect of temperature and strain rate on mechanical characteristics and constitutive model of frozen Helin loess. Cold Regions Science and Technology, **136**: 44–51. doi:10.1016/j.coldregions.2017.01.010.

Yang, Y., Wei, Z., Yin, G., Wang, J.G., Wang, W., and Chen, Y. 2016. Uniaxial compression test of frozen tailings. Cold Regions Science and Technology, **129**: 60–68. doi:10.1016/j.coldregions.2016.06.007.

Yang, Z. (Joey), Still, B., and Ge, X. 2015. Mechanical properties of seasonally frozen and permafrost soils at high strain rate. Cold Regions Science and Technology, **113**: 12–19. doi:10.1016/j.coldregions.2015.02.008.

Yao, M., Wang, Q., Ma, B., Liu, Y., Yu, Q., and Han, Y. 2020. Effect of freeze-thaw cycle on shear strength of lime-solidified dispersion soils. Civil Engineering Journal, **6**(1): 114–129. doi:10.28991/cej-2020-03091457.

Ying, Z., Cui, Y.-J., Benahmed, N., and Duc, M. 2022. Changes in microstructure and water retention property of a lime-treated saline soil during curing. Acta Geotechnica, **17**(1): 319–326. doi:10.1007/s11440-021-01218-5.

Yıldız, M., and Soğancı, A.S. 2012. Effect of freezing and thawing on strength and permeability of lime-stabilized clays. Scientia Iranica, **19**(4): 1013–1017. doi:10.1016/j.scient.2012.06.003.

Young, N.L., Lemieux, J.-M., Delottier, H., Fortier, R., and Fortier, P. 2020. A conceptual model for anticipating the impact of landscape evolution on groundwater recharge in degrading permafrost environments. Geophysical Research Letters, **47**(11): e2020GL087695. doi:10.1029/2020GL087695.

Yugui, Y., Feng, G., Yuanming, L., and Hongmei, C. 2016. Experimental and theoretical investigations on the mechanical behavior of frozen silt. Cold Regions Science and Technology, **130**: 59–65. doi:10.1016/j.coldregions.2016.07.008.

Zhang, D., Zhu, Z., and Liu, Z. 2016a. Dynamic mechanical behavior and numerical simulation of frozen soil under impact loading. Shock and Vibration, **2016**(1): 3049097. doi:10.1155/2016/3049097.

Zhang, M., Yang, W., Lai, Y., Pei, W., Zhou, Y., and Bai, M. 2023. Field investigation on the spatiotemporal thermal-deformation characteristics of a composite embankment with two-phase closed thermosyphons on a permafrost slope. Acta Geotechnica, **18**(10): 5427–5439. doi:10.1007/s11440-023-01878-5.

Zhang, W., Ren ,Zhoupeng, Yao ,Ling, Zhou ,Chenghu, and and Zhu, Y. 2016b. Numerical modeling and prediction of future response of permafrost to different climate change scenarios on the Qinghai–Tibet Plateau. International Journal of Digital Earth, **9**(5): 442–456. Taylor & Francis. doi:10.1080/17538947.2015.1041431.

Zhang, Y., Daniels, J.L., Cetin, B., and Baucom, I.K. 2020. Effect of temperature on pH, conductivity, and strength of lime-stabilized soil. Journal of Materials in Civil Engineering, **32**(3): 04019380. American Society of Civil Engineers. doi:10.1061/(ASCE)MT.1943-5533.0003062.

Zhao, X., Zhou, G., Wei, C., and Li, X. 2009. Effects of temperature gradients on elastic modulus and compression strength of the saturated frozen clay. Procedia Earth and Planetary Science, **1**(1): 420–424. doi:10.1016/j.proeps.2009.09.067.

Zheng, F., Shao, S., and Wang, S. 2021. Effect of freeze-thaw cycles on the strength behaviour of recompacted loess in true triaxial tests. Cold Regions Science and Technology, **181**: 103172. doi:10.1016/j.coldregions.2020.103172.

Zhongyan, S., Wanwei, P., Yongzhi, L., and Xiaoxiao, C. 1995. Preliminary research on axial splitting method for determining tensile strength of frozen soil. **17**(1): 33–39.

Zhou, G., Hu, K., Zhao, X., Wang, J., Liang, H., and Lu, G. 2015. Laboratory investigation on tensile strength characteristics of warm frozen soils. Cold Regions Science and Technology, **113**: 81–90. doi:10.1016/j.coldregions.2015.02.003.

Zhou, J., and Li, D. 2012. Numerical analysis of coupled water, heat and stress in saturated freezing soil. Cold Regions Science and Technology, **72**: 43–49. doi:10.1016/j.coldregions.2011.11.006.

Zhou, Z., Ma, W., Zhang, S., Mu, Y., and Li, G. 2018. Effect of freeze-thaw cycles in mechanical behaviors of frozen loess. Cold Regions Science and Technology, **146**: 9–18. doi:10.1016/j.coldregions.2017.11.011.

Zhou, Z., Ma, W., Zhang, S., Mu, Y., and Li, G. 2020. Experimental investigation of the path-dependent strength and deformation behaviours of frozen loess. Engineering Geology, **265**: 105449. doi:10.1016/j.enggeo.2019.105449.

Zhu, Y., and Carbee, D.L. 1984. Uniaxial compressive strength of frozen silt under constant deformation rates. Cold Regions Science and Technology, **9**(1): 3–15. doi:10.1016/0165-232X(84)90043-0.